STRUCTURAL AND FUNCTIONAL DYNAMICS OF SEROTONIN TRANSPORTER GENE VARIANTS

By

Meagan Anne Quinlan

Dissertation

Submitted to the Faculty of the

Graduate School of Vanderbilt University

In partial fulfillment of the requirements

for the degree of

DOCTOR OF PHILOSOPHY

in

Pharmacology

May 10, 2019

Nashville, Tennessee

Approved:

Brian Wadzinski, PhD

Heidi Hamm, PhD

Kevin Schey, PhD

Randy Blakely, PhD

ACKNOWLEDGEMENTS

The completion of this dissertation would not be possible without the unwavering support of several people that have helped me immensely along the way. I first must give my greatest acknowledgment to my Ph.D. mentor Dr. Randy Blakely, without whom this accomplishment would not be possible. Being able to research the serotonin transporter, the protein he cloned back in 1989, has been the highest honor. His depth of knowledge and his unwavering support was unmatched during all the experiments I thought failed. He did always find that silver lining in the blank blots. The enthusiasm he gleaned when I would have exciting new data and even the countless hours we discussed the nuances of serotonin transporter kinetics as we trialed our way through data that didn't always make sense, will definitely not be forgotten. Needless to say, there was not a better mentor that could have taken me through this journey.

I was also lucky to have a supportive thesis committee. To Dr. Brain Wadzinski, Dr. Heidi Hamm, Dr. Ana Carnerio, and Dr. Kevin Schey, all this work definitely would have not been possible without all your insightful questions and constructive critiques. Thank you all for your encouragement and help over the past years.

Another enormous thank you must go to the lab members of the Blakely lab, both at Vanderbilt and Florida Atlantic University. I was fortunate enough to have several post-doctoral fellows that took me under their wing as I made my way through graduate school. My first mentor in the lab was Dr. Ran Ye, who showed me everything I know about protein biochemistry and really encouraged me in my early years of graduate school. Dr. Nicole Baganz was always there for a listening ear and a shoulder to cry on during times when it seemed none of my experiments were working. Last, but certainly not least, Dr. Matthew Robson who humored my unbridled optimism and ambition when I was a young grasshopper. He helped with so many of my crazy experimental ideas, including making transparent brains and we danced our way those countless synaptosomes uptakes and head twitch assays.

Then there is the tremendous help of the Blakely lab research assistants, who were not only there for science support, but also all became great friends. A massive shout out to Jane Wright, Chris Svitek

and Qiao Han at Vanderbilt, who were there during my early graduate career as I found stumbled away around in my first year in the lab. An especially big thank you must also go to Rania Katmaish, who I had the greatest pleasure of training while at Florida Atlantic University. She quickly became by far the most productive and helpful person as I was finishing up my Ph.D. Her enthusiasm for science was contagious, and she helped keep my spirits up until the end.

I have to also give an enormous thank you to my family that have been there literally from day one. My parents were there for me every step of the way and without their unwavering support, I would definitely not be here. From encouraging me to participate in Science Fairs and Science Olympiads, to the yearly physic inspired Christmas gifts, and to indulging all my wild interests through the years in everything from astronomy to geology, I truly owe the fostering of my love of science to you two. To my older sister, Erin, who I always looked up to since a young age. Even if it seemed like I was always copying everything she did, I really must admit she is the one that initially inspired me to pursue science after see her win the science fair herself in elementary school. She has always been there and has always had faith in my ability. And last, but certainly not least, to my countless friends from around the world that supported me along the way. I am so lucky to have numerous friends in various places that kept in contact with me through the years and many moves. My friends always seem to know when to call or text me when I needed it most during this process.

I am eternally grateful for all that I have and know that none of this would have been possible without the help of a number of people. It is not lost on me that a central theme of my dissertation is that the proteins do not act alone, but require a complex set of networks of other proteins to function properly in various states. The completion of my dissertation would not be possible without the immense help of several people that played various roles of support throughout this process. For this reason, I am incredibly thankful to everyone that helped me along the way.

TABLE OF CONTENTS

LIST OF TABLES

Table **Page**

LIST OF FIGURES

Figure **Page**

LIST OF ABBREVIATIONS

5-HT	5-Hydroxytraptamine (serotonin)
AADC	Aromatic acid decarboxylase
ASD	Autism Spectrum Disorder
aCSF	Artificial cerebrospinal fluid
Ala	Alanine
Arg	Arginine
Asn	Asparagine
Asp	Aspartic acid
AP-MS/MS	Affinity purified tandem mass spectrometry
ASD	Autism Spectrum Disorder
BSA	Bovine serum albumin
C-terminal	Carboxy-terminal
CaMKII	Calcium/calmodulin-dependent protein kinase II
CFP	Cyan fluorescence protein
CHO cells	Chinese hamster ovarian cells
CNS	Central nervous system
Cys	Cysteine
DA	Dopamine
DAT	Dopamine transporter
FC	Frontal Cortex
FLOT1	Flotillin-1
FRET	Förster (fluorescence) resonance energy transfer
FST	Forced swim test

GAT	GABA transporter
Glu	Glutamic acid
Gly	Glycine
GST	Glutathione S-transferase
GTP	Guanosine triphosphate
HEK cells	Human embryonic kidney cells
HeLa cells	Henrietta Lacks cells
HET	Heterozygous
Hip	Hippocampus
HPLC	High performance liquid chromatography
ICL	Intracellular Loop
Ile	Isoleucine
IP	Immunoprecipitation
KI	Knock-in
KO	Knock-out
KRH	Krebs-Ringer HEPES buffer
KRB	Krebs-Ringer bicarbonate buffer
Leu	Leucine
LPS	Lipopolysaccharide
Lys	Lysine
MacMARCKs	Myristoylated alanine-rick protein kinase C substrate related protein
MAGE	Melanoma-associated antigen
MAO	Monoamine oxidase
MB	Midbrain
MDD	Major depressive disorder

MDMA	(3,4-methylenedioxy) methamphetamine
MTS	Methanethiosulfonate
MTSEA	2-Aminoethyl methanethiosulfonate
MTSES	Sodium (2-sulfonatoethyl) methanethiosulfonate
MTSET	2-(Trimethylammonium) ethyl methanethiosulfonate
N-terminal	Amino-terminal
NE	Norepinephrine
NET	Norepinephrine transporter
NLGN2	Neuroligin 2
nNOS	Neuronal nitric oxide synthase
NSF	N-ethylmaleimide sensitive fusion protein
OCT	Organic cation transporter
p38 MAPK	p38 mitogen-activated protein kinase
PAGE	Polyacrylamide gel electrophoresis
PCA	Para-chloroamphetamine
PCR	Polymerase chain reaction
Phe	Phenylalanine
PKA	Protein kinase A (cyclic AMP-dependent protein kinase)
PKC	Protein kinase C
PKG	Protein kinase G (cyclic GMP-dependent protein kinase)
PM	Plasma membrane
PP2A	Protein phosphatase 2A
PP2B	Protein phosphatase 2B (calcineurin)
Rab4-GTP	Ras-related protein-GTP
SCAM	Substituted cysteine accessibility method

SCAMP-2	Secretory carrier membrane protein 2
SDS	Sodium dodecyl sulfate
Ser	Serine
SERT	Serotonin transporter
SLC	Solute carrier
SNARE	Soluble N-ethylmaleimide-sensitive factor attachment protein receptors
SSRI	Selective serotonin reuptake inhibitor
Thr	Threonine
TMD	Transmembrane domain
Tph1 & 2	Tryptophan hydroxylase 1 & 2
TST	Tail suspension test
Ub	Ubiquitin
Val	Valine
VAMP2	Vesicle-associated membrane protein 2
VMAT	Vesicular monoamine transporter
WT	Wild type
YFP	Yellow fluorescence protein

CHAPTER 1

INTRODUCTION

The overall goal of this dissertation, presented in partial fulfillment of a doctoral degree in Pharmacology, is to characterize the structural, post-translational, and protein-protein mediated regulation of antidepressant-sensitive serotonin (5-HT, 5-hydroxytryptamine) transporter (solute carrier 6a4; *SLC6A4,* SERT) variants associated with neuropsychiatric disorders. Herein, I will provide an overview of 5-HT and SERT and their contribution to neuropsychiatric disorders. I will focus largely on structural conformations that support the activity of members of the *SLC6* family, including the dopamine (DA) transporter (DAT) and the norepinephrine (NE) transporter (NET), their transport cycles, and how the amino-(N) and carboxyl-(C) termini are impacted by post-translational modifications and protein-protein interactions. Overall, I seek to investigate the hypothesis that wildtype (WT) SERT can be regulated by endogenous signaling pathways as well as disease-associated variants that alter post-translational modifications and structural conformational states, ultimately changing SERT transport kinetics *in vitro* and *in vivo*.

5-HT synthesis and expression

5-HT is a chemical synthesized in both the brain and periphery, deriving its name from the word *serum* as a consequence of gut synthesis and secretion into the bloodstream, and tone, referring to the impact of 5-HT on the vasculature (Rapport et al., 1948). 5-HT is widely produced in many tissues from its precursor, tryptophan, with ~90% of the whole body 5-HT synthesized in intestinal enterochromaffin cells from the amino acid tryptophan in a two-step enzymatic process involving, tryptophan hydroxylase 1 (Tph1) and aromatic amino acid decarboxylase (AADC) (Gershon and Tack, 2007). Once released in response to physical stretch of the intestine, 5-HT supports peristaltic contractions of the intestinal smooth muscle. Appreciable quantities of 5-HT move into the bloodstream where the molecule is actively accumulated into blood platelets by the 5-HT transporter (*SLC6A4,* SERT), the same gene product that is

produced in the brain to support efficient synaptic 5-HT clearance (Blakely et al., 1991; Lesch et al., 1993; Ramamoorthy et al., 1993).

In the periphery, besides its role in the gut and vasculature, 5-HT also plays a vital role in systemic energy homeostasis (Namkung, Kim, & Park, 2015). In the brain, 5-HT exerts important modulatory control over a number of circuits that regulate sleep, appetite, libido, mood, anxiety and social behavior (Frazer and Hensler, 1999). In the CNS, synthesis of 5-HT utilizes tryptophan hydroxylase 2 (Tph2) rather than Tph1 (Walther et al., 2003).

5-HT is packaged for release by platelets and neurons into an acidic (pH ~5.5) cytoplasmic vesicle by the vesicular monoamine transporter 2 (*Slc18a2*; VMAT2). VMAT2, a H^+/monoamine$^+$ antiporter is energized by the transvesicular proton gradient established by an ATP-driven proton pump, leading to transport of one molecule of 5-HT for each effluxed proton (Eiden and Weihe, 2011). At synapses, the release of 5-HT is stimulated by membrane depolarization that leads to opening of voltage-gated Ca^{2+} channels. The rapid elevation of cytosolic Ca^{2+} leads to binding to, and conformational changes in, the Ca^{2+}-sensing protein, synaptotagmin, preassembled with SNARE proteins on synaptic vesicles that are docked at the plasma membrane. Ca^{2+}-dependent conformational changes in synaptotagmin promote changes in associations of the SNARE complex with the lipid bilayer that overcome the energy barrier needed for fusion of vesicle and plasma membranes, resulting in the release of neurotransmitters into the synaptic cleft (Jahn and Scheller, 2006).

5-HT receptors

With the pervasive and varied function of 5-HT, it is no surprise that there is widespread and diverse expression of 5-HT receptors to support the assorted roles of 5-HT. There are 18 different types of 5-HT receptors subdivided into 7 families (5-HT_{1-7}) containing a total of 14 distinct receptors (Nichols and Nichols, 2008). All 5-HT receptors are G-protein coupled receptors (GPCRs), except for the 5-HT_3 subtype, which is a ligand-gated ion channel (Nichols and Nichols, 2008). The most well-studied of these receptors are the 5-HT_1 and 5-HT_2 receptor subtypes, highlighted in greater detail below.

The 5-HT_1 family of receptors are both autoreceptors, located on the cell soma of 5-HT secreting neurons, and classical post-synaptic receptors (Azmitia et al., 1996; Drago et al., 2008). Both types of 5-HT_1 receptors inhibit the cyclic adenosine monophosphate (cAMP) signaling pathway, being specifically coupled to heterotrimeric G proteins containing $G_{\alpha i/o}$. When these receptors bind 5-HT, conformational changes lead to disassociation of $G_{\alpha i/o}$ which then inhibits the enzyme adenylyl cyclase, leading to a reduction of cAMP levels. There are 5 types of 5-HT_1 receptors: 5-HT_{1A}, 5-HT_{1B}, 5-HT_{1D}, 5-HT_{1E}, and 5-HT_{1F} (Nichols and Nichols, 2008). Elucidation of 5HT_{1A} receptor signaling, and the receptor's role in physiology was facilitated by identification of the brain-penetrant, full 5-$HT1_A$ agonist 8-hydroxy-2-(di-n-propylamino)tetralin (8-OH-DPAT). Administration of 8-OH-DPAT to rodents leads to a number of physiological responses, including a reduction in 5-HT neuron firing (Evard et al., 1999) and a decrease in core body temperature (Martin et al., 1992). The activation of somatodendritic 5-HT_{1A} autoreceptors provides a negative feedback reduction in 5-HT neuron firing via G protein-mediated activation of K^+ channels, an action that has been linked to the delayed actions of a class of antidepressants, the selective 5-HT reuptake inhibitors (SSRIs). Increased extracellular 5-HT caused by blockade of SERT within the midbrain, where cell bodies of 5-HT neurons originate, leads to increased activation of 5-HT_{1A} autoreceptors, decreased 5-HT neuron firing, and a reduction of 5-HT release in target regions (Artigas, 1993). In support of this model, co-administration of an SSRI with the partial 5-HT_{1A} antagonist (Pindolol) has been shown to accelerate SSRI-induced responses (Ballesteros and Callado, 2004). 5-HT_{1B} receptors are primarily expressed on axon terminals (Boschert et al., 1994) and act in a negative feedback loop to limit the vesicular release of 5-HT (Sari, 2004). 5-HT_{1B} receptors can also lead to decreased 5-HT concentration in the synapse by increasing 5-HT uptake through SERT (Daws et al., 2000). Whether the mechanism of SERT regulation involves changes in SERT activity or surface trafficking, or both, has yet to be explored in depth. Hagan and colleagues have provided evidence for a reduction in 5-HT transport K_M in synaptosomes from 5-HT_{1B} KO mice, suggesting kinetic versus trafficking effects that lead to enhanced 5-HT uptake (Hagan et al., 2012). Another GPCR, the kappa opiate receptor, acts presynaptically

as a heteroreceptor to elevate SERT function, in this case by increasing transporter trafficking (Sundaramurthy et al., 2017).

5-HT_2 receptors, which are generally expressed post-synaptically, activate the phosphatidylinositol transduction pathway (Roth, 2011) via the $G_{\alpha q/11}$ subunit stimulate phospholipase C, leading to cleavage of phosphatidylinositol 4,5-bisphosphate (PIP_2) from the membrane into inositol (1,4,5) triphosphate (IP3) and diacylglycerol (DAG). These second messengers act downstream to increase cytosolic levels of Ca^{2+} that leads to activation of protein kinase C (PKC) and Ca^{2+}/calmodulin activated protein kinase (CaMK) isoforms and phosphorylation of membrane, cytosolic and nuclear targets. 5-HT_2 receptors of the $5HT_{2A/2C}$ family are the target of hallucinogenic drugs, such as lysergic acid diethylamide (LSD) and 2,5-dimethoxy-4-iodoamphetamine (DOI) (Nichols and Sanders-Bush, 2001). In keeping with this idea, the hallucinogenic potency of a drug positively correlates with the affinity for $5HT_2$ type receptors (Glennon et al., 1984).

SERT: Critical determinant of 5-HT accumulation and clearance

After 5-HT is released into the extracellular space, the capacity for signaling may need to be constrained in space and time. As noted above, 5-HT neurons express a high-affinity, low capacity transporter, SERT, to achieve rapid clearance of 5-HT from the extracellular environment, maintaining low extracellular 5-HT levels in the nM range. Neurons and glia also express low affinity, high capacity monoamine transporters, known as organic cation transporters (*Slc22A*; OCTs) that also play a role in clearing 5-HT, particularly with high volume transmission and most evident in the context of pharmacological SERT blockade or genetic elimination (Couroussé and Gautron, 2015). Once 5-HT has been transported back into the presynaptic terminal, the neurotransmitter can either be degraded by mitochondrial monoamine oxidase (MAO) isoforms (MAO_A and MAO_B) or 5-HT can be recycled back into secretory vesicles for future release (Shih et al., 1999; Eiden and Weihe, 2011; Yaffe et al., 2018). An analogous process allows for platelets to capture 5-HT by SERT and store 5-HT in secretory granules (Rudnick, 1977; Rudnick and Nelson, 1978; Anderson et al., 1987). Storage and stabilization of 5-HT in

platelets established the major reservoir of 5-HT in the bloodstream as free 5-HT in the blood is rapidly eliminated (Anderson et al., 1987).

Within the nervous system, SERT is most commonly depicted as residing pre-synaptically in axon terminals of serotonergic neurons (**Figure 1**), though somatodendritic SERT has been well documented (Lau et al., 2010; Ye et al., 2016). 5-HT neurons originating in midbrain raphe nuclei send diffuse projections to a number of brain regions, including the basal lateral amygdala, hippocampus basal ganglia, hypothalamus, olfactory tubercle, medial septum, substantia nigra, ventral tegmental area, periaqutal gray, superficial layer of the superior colliculus and locus coeruleus (Jacobs and Azmitia, 1992; Charnay and Léger, 2010). Brainstem 5-HT neurons are involved in the regulation of autonomic responses and send axons to the spinal cord where they gait the flow of pain information to higher brain centers (Jacobs and Azmitia, 1992). Midbrain 5-HT neurons are innervated by 5-HT secreting axons to mediate negative feedback control of neuronal firing via somatodendritic 5-HT receptors, as noted above. SERT protein is translated like all membrane proteins, in the cell bodies of the neuron and then translocated to synaptic terminals or varicosities or dendrites (Hensler et al., 1994; Qian et al., 1995b; Lau et al., 2010; Colgan et al., 2012) in transport vesicles for eventual insertion into the plasma membrane. Although most of the research on SERT has focused on the role of the transporter in neurons, evidence also exists that SERT is expressed by glia (Kimelberg and Katz, 1985; Inazu et al., 2001; Kubota et al., 2001; Malynn et al., 2013), though the level of expression is low and functional importance is unclear.

Considering that 90% of 5-HT is located peripherally, it is no surprise that SERT is also widely expressed in several different tissues. SERT has been found in blood platelets (Mercado and Kilic, 2010), lymphoblasts (Faraj et al., 1994), enterochromaffin cells of the gastrointestinal tract (Wade et al., 1996; Gershon and Tack, 2007), epithelial cells of the intestine (Gill et al., 2007), adrenal gland (Schroeter and Blakely, 1996; Brindley et al., 2018), pulmonary endothelium (Strum and Junod, 1972), placenta (Balkovetzs et al., 1989), and the immune system (Baganz and Blakely, 2013). Given the broad expression of SERT and utilization in several different physiological functions, it is no surprise that genetic elimination

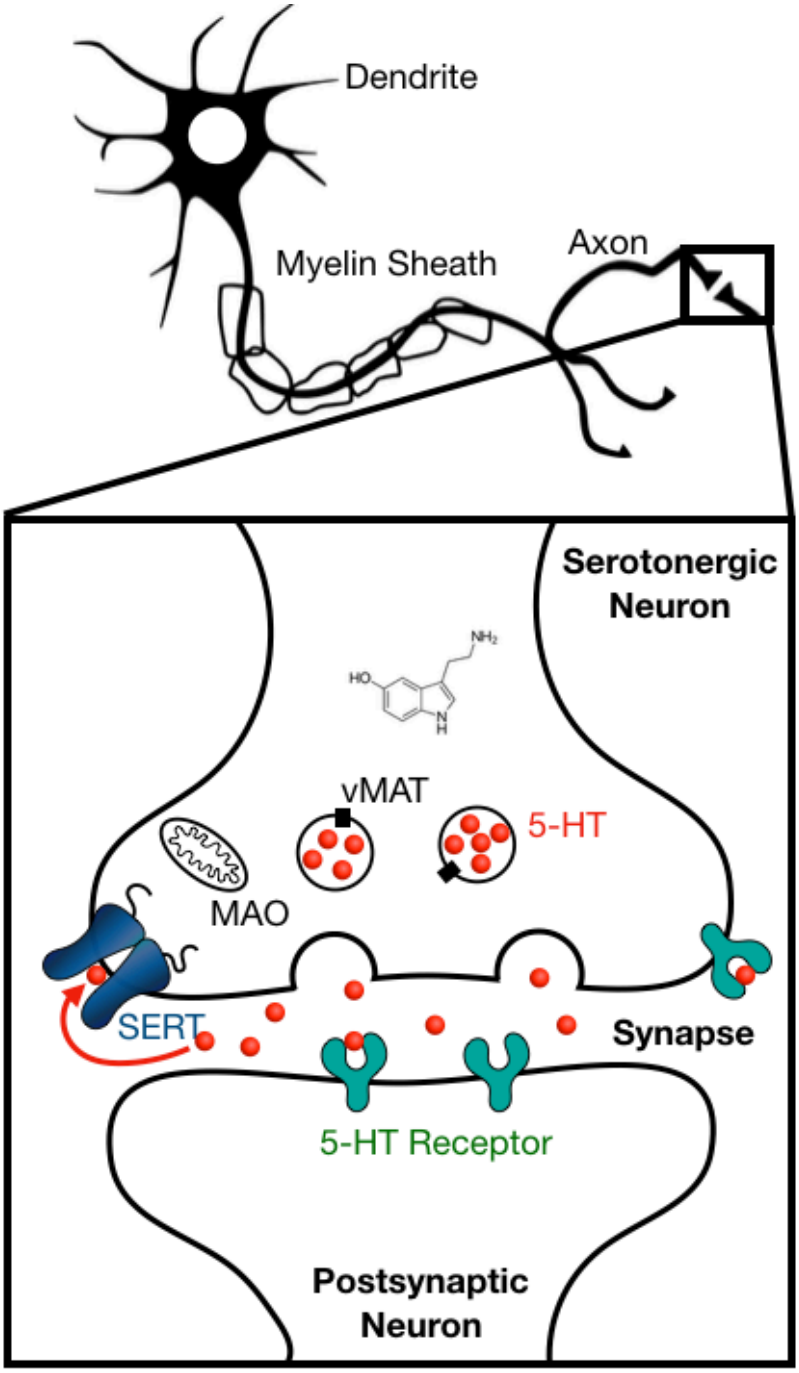

Figure 1. Diagram of 5-HT neuron synapse

of the transporter (SERT KO; $SERT^{-/-}$), leads to a number of behavioral and physiological changes. SERT KO mice exhibit anxiety-like behavior, abnormal response to inescapable stress, hyperactive 5-HT receptors, decreased home cage activity, increased REM sleep, GI dysfunction and a hyperactive neuroendocrine system (Holmes et al., 2003). Many of the phenotypes exhibited by SERT KO mice were recapitulated in SERT KO rats, highlight the conserved role of SERT across species (Kalueff et al., 2010). However, it is important to note that SERT KO animals are viable and do not express any obvious physical abnormalities, indicating that SERT is not necessary for survival, growth, and reproduction, but play essential roles in regulating and modulating responses to environmental and synaptic stimuli. Tolerance of loss of SERT is also not surprising as genetic elimination of the rate-limiting enzymes that produce 5-HT, *Tph1* and *Tph2*, similarly does not result in overt phenotypes (Savelieva et al., 2008), further supporting the role of 5-HT as a modulatory molecule.

Structural characterization of SERT

The SERT gene lacks alternative splicing of coding exons and thus the brain and periphery contain the same SERT protein. SERT was first cloned independently by both Blakely from rat brain (Blakely et al., 1991) and by Hoffman in RBL cells (Hoffman et al., 1991). Soon after, SERT was cloned from the rat spinal cord (Mayser et al., 1991) and intestine (Wade et al., 1996). SERT comprises 630 amino acids that form 12 transmembrane (TM) domains with a long cytoplasmic N-terminus (81 amino acids) and shorter C-terminus (30 amino acids).

In 2005, a bacterial homologue of the monoamine transporters, the *Aquifex aeolicus* Leucine Transporter (LeuT), was crystallized (Yamashita et al., 2005). Initiating a structural era of study of the SLC6 family, work that has formed the basis for many of our hypotheses regarding SERT function, dynamics and drug binding. One key finding of this initial study was that SLC6 transporters consist of two repeated, inverted bundles that bring the residues forming the binding site for ions and organic substrates together. The initial LeuT structure reported by Yamashita and colleagues was of a transporter in a

substrate-bound state with both external and internal states closed (occluded state). Additional structures of LeuT and mammalian SLC6 members have provided structures in outward facing and inward facing configurations (Krishnamurthy and Gouaux, 2012) to aid in the modeling of the transport cycle.

In 2013, a *Drosophila melanogaster* DAT (dDAT), which has a 45% sequence homology with SERT, was crystallized at a 3.0 Å resolution (Yamashita et al., 2005). In 2016, the human SERT (hSERT) was crystallized in the absence and presence of the antidepressant, S-citalopram (Coleman et al., 2016). All these crystal structures validated and supported many previous biochemical studies that detailed structure-function relationships of the SLC6 transporters. It is important to note that a major caveat of crystallization experiments is the need to stabilize the structure of the transporter to promote crystal growth, where highly mobile and unstructured regions of the N- & C-termini had to be cleaved, and the introduction of mutants to make the transporter thermostable, making the transporter unable to properly function. One way to assess the structure of the N-& C-termini is through homology modeling, based on amino acid sequence. Fenollar-Ferrer et al. (2014) accomplished this effort utilizing several modeling techniques including the bioinformatics program PSIPRED to predict the secondary structure of the N- and C-termini, supported by nuclear magnetic resonance (NMR), circular dichroism (CD), and FRET assays. From these studies, these investigators were able to predict multiple models of SERT in different conformational states (Fenollar-Ferrer et al., 2014). While these studies predicted the N-terminus of SERT to be comprised of a few alpha helical sections, many models predict a more undefined structure, suggesting that interactions with one or more proteins may impose structure.

Alternating access model of transport by SERT

SERT is able to overcome the inability of 5-HT to cross the plasma membrane by secondary active transport, tapping into the Na^+ gradient generated by the Na^+/K^+ ATPase, an enzyme also utilized to set the cell's resting membrane potential. Kinetic analysis of SERT uptake shows that for 5-HT to bind, 1 or 2 Na^+ ions must first bind along with a Cl^- ion. Ion binding poises the transporter in a state where the binding pocket is available for 5-HT to bind with high-affinity. 5-HT binding leads to a large structural transition

of a four-helix bundle TM1, TM2, TM6 and TM7 (scaffold by TM3-5 and TM8-10) to close extracellular gates and the opening of intracellular gates to allow the Na^+ ions and 5-HT to be released into the cytoplasm (Rudnick, 2006). For SERT, but not with other SLC6 transporters studied to date, return to an outward-facing state requires binding of 1 K^+ ion (**Figure 2**) (Nelson and Rudnick, 1979). Because the amine group of 5-HT is protonated at physiological pH, the transport of all substrates across the transport cycle results in an electroneutral model of 5-HT transport across SERT, for which direct evidence is available (Rudnick and Nelson, 1978). Interestingly, SERT transport of 5-HT can be accompanied by net, uncoupled current flow (Mager et al., 1994; Lin et al., 1996; Adams and DeFelice, 2003; Schicker et al., 2012) that is dependent on interactions of the presynaptic SNARE protein syntaxin 1A (Quick, 2003).

The cyclic structural movements of the transmembrane domain inverted repeat bundles is a modern elaboration of the schematized "alterrnating access model of transport", sometimes referred to as the "rocking bundle mechanism of transport" due to modeling studies that predict the inverted repeat of helices to allow four helices forming the 5-HT binding site to move against other, relatively stable helices (Forrest et al., 2008; Forrest and Rudnick, 2009). This is in contrast to other transporters, such as the glutamate transporter, which involves the upward and downward moving of substrate-bound helices, a so-called "elevator" mechanism (Ruan et al., 2017).

There are several gating residues that form interactions to occlude the extracellular milieu from the cytosolic space as the transporter moves from the outward-facing to an inward facing state (**Figure 3**). These residues have been identified from x-ray crystal structures of SLC6 transporters in different states, mutagenesis studies, and studies utilizing the substituted cysteine accessibility method (SCAM). Ile179 in TM3 is thought to be an extracellular gating residue, which is just 6 residues from Ile172, which is critical for 5-HT binding and transportation (Chen and Rudnick, 2000). Try176 in TM3 forms the lower portion of the extracellular gate, with Phe335 (extracellular loop 4; ECL4) and a salt-bridge between Arg104 (ECL1) and Glu493 (TM10) shielding 5-HT from the extracellular milieu after binding (Coleman et al., 2016). For intracellular gating, residues Arg79 (N-terminus) and Asp452 (TM10) form an ionic bond while Tyr350 (TM6) forms and hydrogen bond with Glu444 (TM3) of hSERT (Koldsø et al., 2013).

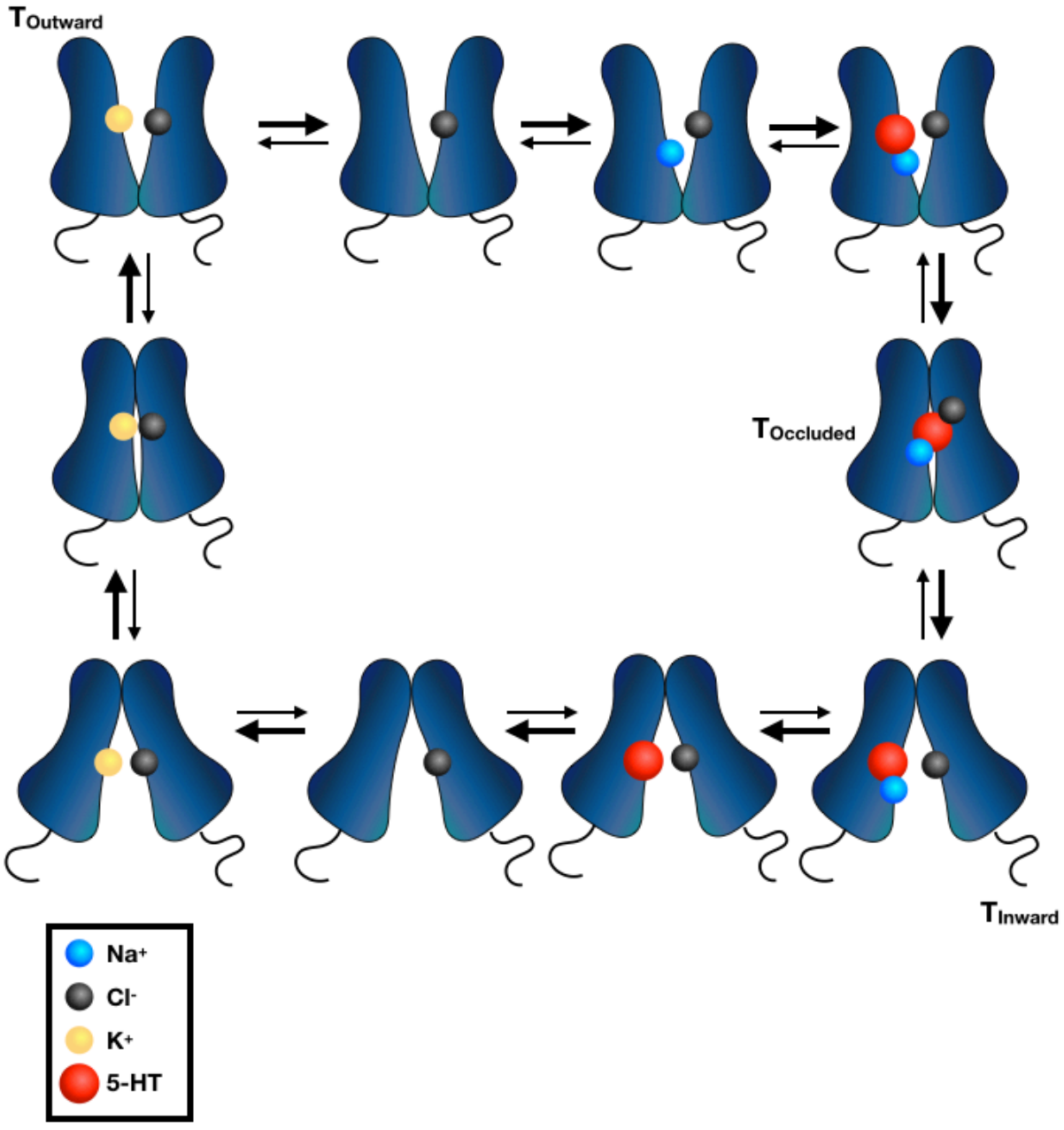

Figure 2. Alternating access model of 5-HT transport

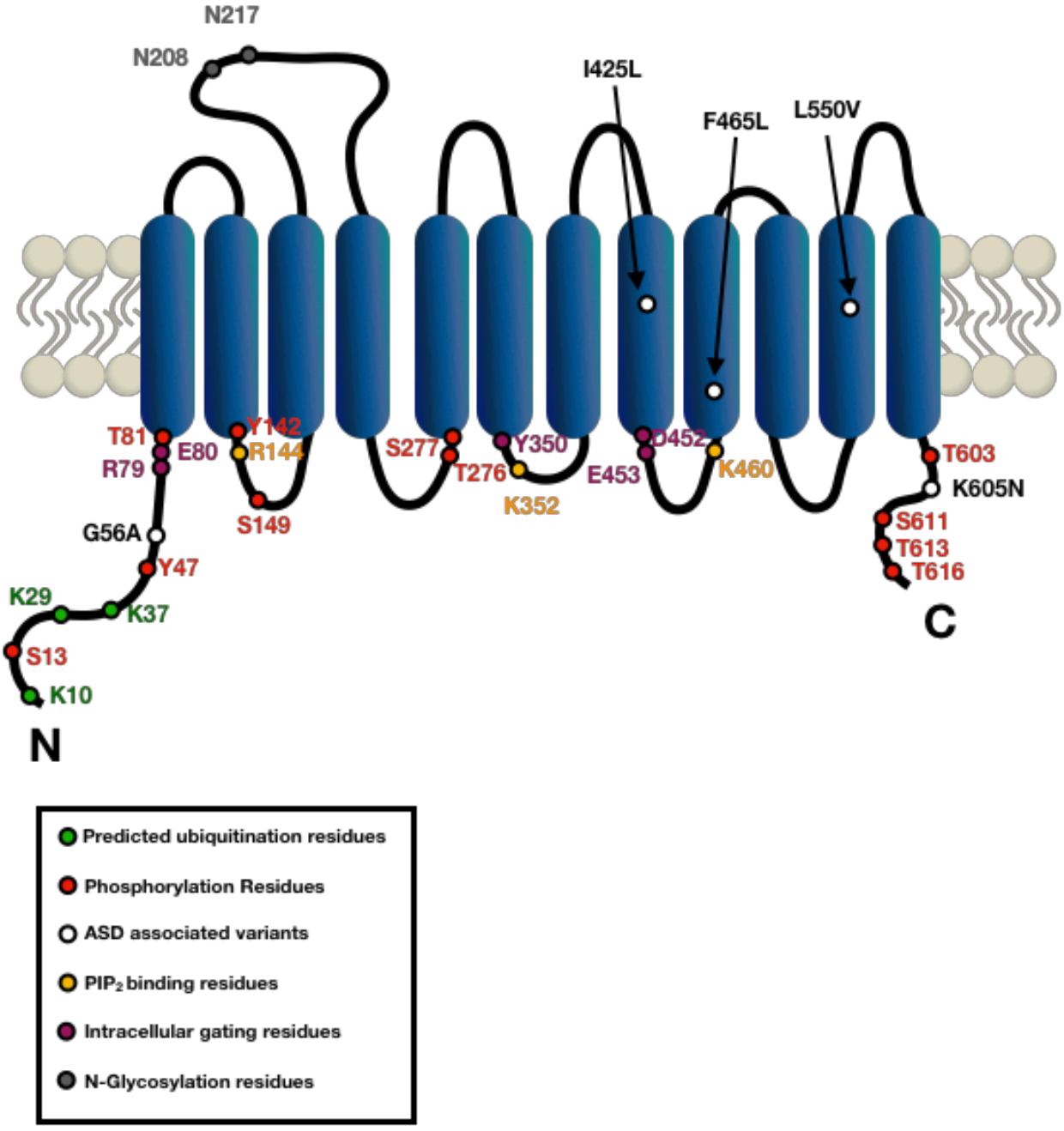

Figure 3. Important SERT residues

For Cl^- ion binding, residues Tyr121, Ser336, Asn368, and Ser 372 were found to be critical (Forrest et al., 2007). Evidence suggests that Cl^- remains bound during the entire transport cycle (Hasenhuetl et al., 2016). Interestingly, Cl^- binding is also critical for the binding of some antidepressants, specifically imipramine, citalopram, sertraline, and fluoxetine, but does not affect cocaine or paroxetine binding (Tavoulari et al., 2009). There are two Na^+ ion binding sites within the transporter, however, evidence suggests that 5-HT uptake is only coupled to the influx of one Na^+ ion (Sneddon, 1969) and the Na1 and Na2 are shown to have separate functions (Felts et al., 2014; Tavoulari et al., 2016). Tavoulari and colleagues found that the occupation of Na^+ in the Na2 site supports an outward facing conformation while Na1 binding induces the conformational shift in the transporter (Tavoulari et al., 2016). Molecular dynamic simulation reveal that 5-HT binding destabilized Na^+ binding to the Na2 site (Felts et al., 2014), potentially suggesting that Na^+ binding in the Na2 site only primes the transporter in an outward facing conformation for substrate binding and then once 5-HT is bound, Na^+ is released from the Na2 site, allowing for transport but is not translocated. Although K^+ has been shown to be required for SERT, inferred to be involved in reconfiguring transition of the inward to outward facing conformation (Nelson and Rudnick, 1979; Schicker et al., 2012), there is currently a lack of knowledge regarding which residues mediate K^+ binding and the full functional importance of this coupling.

Although the N- and C-termini are positioned far away from the substrate and ionic binding sites, and are not present in the crystalized SLC6 family member structures, these regions are well established to play a critical role in regulating transport kinetics and mode of transport (influx vs efflux), as well as specificity of substrate binding to the transporter (Sucic et al., 2010; Fenollar-Ferrer et al., 2014; Sweeney et al., 2017). During the transport cycle, molecular dynamic simulation studies suggest that as the transporter moves from the outward to inward facing conformation, the termini move farther apart, with most of the movement suggested to arise from movement of the N-terminus (Fenollar-Ferrer et al., 2014). The unstructured aspect of the N-& C-termini may allow for dynamic regulation of protein-protein interactions and post-translational modifications (PTMs) that ultimately lead to changes in SERT activity.

Kinase-dependent regulation of SERT

As 5-HT neuron activity and the need for serotonergic modulation depend on multiple variables, including both intrinsic and extrinsic stimuli, SERT uptake kinetics would also be predicted by environmental demands (Blakely and Bauman, 2000; Steiner et al., 2008; Ramamoorthy et al., 2011). Indeed, the transporter is highly regulated by several protein kinases that are sensitive to various stimuli, such as stress or immune activation. These kinases can either act directly on the transporter to facilitate phosphorylation of the transporter (discussed in more detail below) or indirectly by activating a downstream protein that can then interact with the transporter to affect the structural conformation and/or PTM.

An extensive review from the Blakely lab highlights the similarities and differences in the kinase-mediated regulation of monoamine transporters (SERT, DAT, and NET) (Bermingham and Blakely, 2016). Below I will focus mainly on SERT-dependent regulation by three kinases: protein kinase C (PKC), cGMP-dependent protein kinase (PKG), and p38 mitogen-activated protein kinase (p38 MAPK). CaMKII has also been shown to directly interact with SERT and to regulate amphetamine-induced substrate efflux, but will be discussed in later sections. I will also provide a brief overview of SERT modulation by cAMP-dependent protein kinase (PKA), ERK1/2, phosphatidylinositol 3-kinase (PI3K)/Akt, and tyrosine kinases. **Table 1** outlines the main role of each kinase in mediating SERT function and potential phosphorylation sites if known.

Protein Kinase C (PKC)

The classical protein kinase C (PKC) isoforms are activated by the second messengers Ca^{2+} and diacylglycerol (DAG). The canonical signaling cascade triggered by PKC activation begins with stimulation of a GPCR that leads to the release of the $G_{\alpha q}$ subunit to activate phospholipase C (PLC), which cleaves the membrane lipid PIP_2 into inositol 1,4,5-triphosphate (IP3) and DAG. IP3 is released into the cytosol to release Ca^{2+} from intracellular stores. The Ca^{2+} and membrane-bound DAG to activate PKC, which can then act on downstream targets to affect protein function.

Kinase	SERT Phosphorylation (Ref)	SERT Regulation (Ref)
p38 MAPK	Thr276 (unpublished data) Thr616 (Sørensen et al. 2014)	↑ 5-HT Uptake (Zhu et al. 2005, 2006; Prasad 2005, 2009) ↑ SERT surface (Samuvel et al. 2005; Lau et al. 2009; Bruchas et al. 2011) No change in surface expression (Zhu 2005; Prasad 2005, Steiner et al. 2008) Downstream of PKG activation (Zhu et al. 2004) ↑ Lateral mobility (Change et al.2012)
PKG	Thr276 (Ramamoorthy et al. 2007)	↑ 5-HT Uptake and ↑surface trafficking (Miller and Hoffman, 1994, Zhu et al. 2004, 2007, 2011) ↑ Lateral mobility (Change et al., 2012)
PKC	Ser149, Ser277, Thr603 (Sørensen et al. 2014)	↓ 5-HT uptake followed by decrease in surface expression Activation ↓ PP2Ac and Syntaxin 1A interaction, but ↑ Hic-5 interaction
PKA	Phosphorylation of N and C termini (Sørensen et al. 2014)	↑ SERT uptake (Cool et al. 1991; Awtry et al., 2006) ↑ Protein levels, = mRNA, ↓ degradation (Yammamoto et al., 2013)
CaMKII	Ser13 (Sørensent et al. 2014)	↑Amphetamine mediated efflux (Steinkellner et al., 2015) ↑ Surface levels and SERT mediated currents (Ciccone et al., 2008)
PI3K/Akt	No data	Inhibition ↓ 5-HT Vmax and ↓ surface trafficking (Rajamanickam et al., 2015)
ERK1/2	No data	Inhibition blocked estradiol-induced ↓ in 5-HT clearance (Benmansour et al., 2014)
Tyrosine Kinase (Src and Syk)	Y47 and Y142 (Annamalia et al. 2012)	Src - ↑ 5-HT uptake & ↑ SERT surface and protein expression (Annamalia et al., 2012) Syk - ↑ 5-HT uptake and ↑ SERT surface expression (Pavanetto et al. 2011)

Table 1. Kinase Dependent Regulation of SERT Activity

PKC was first shown to phosphorylate SERT domains in 1995 by the Blakely lab using purified rat SERT N-& C-termini fused to glutathione S-transferase (GST) fusion proteins (Qian et al., 1995a). In 1997, the same group showed that activation of PKC by β-PMA in HEK293 cells transfected with rat SERT (rSERT) resulted in a decrease in the maximal velocity (Vmax) of 5-HT transport as well as decreased SERT-mediated currents (Qian et al., 1997). Moreover, PKC activation led to a decrease in SERT surface expression, consistent with the loss of 5-HT transport capacity (Ramamoorthy et al., 1998; Ramamoorthy and Blakely, 1999). Jayanthi and colleagues subsequently found that PKC affects SERT in a time-dependent manner, by first rapidly decreasing SERT uptake independent of surface expression (5 minutes), followed by internalization of SERT (30 minutes) (Jayanthi et al., 2005). Conversely, inhibition of PKC has been shown to modulate SERT-mediated 5-HT efflux (Buchmayer et al., 2013). Mutation of a PKC consensus site at Thr81to Ala or Asp in the transporter N-terminus eliminated the ability of SERT to exhibit amphetamine-induced efflux (Sucic et al., 2010). Several studies have reported that PKC activation increases phosphorylation of serine residues on SERT. By utilizing purified peptides of the intracellular regions of hSERT Sørensen et al. nominated Ser149, Ser277, and Thr603 as hSERT PKC sites (Sørensen et al., 2014).

PKC activation also impacts SERT interacting proteins. Activation of PKC has been shown to reduce interaction of hSERT with both the catalytic subunit of protein phosphatase 2A (PP2Ac) in transiently transfected HEK-293 cells (Bauman et al., 2000) and syntaxin 1A in both transiently transfected HEK-293 cells and cultured rat thalamocortical neurons and synaptosomes (Haase et al., 2001; Quick, 2002a, 2003; Samuvel et al., 2005), but increased interaction with Hic-5, studies performed in human blood platelets (Carneiro and Blakely, 2006).

cGMP-Dependent Protein Kinase (PKG)

Another kinase that regulates SERT is the 3',5'-cyclic guanosine monophosphate (cGMP) dependent protein kinase (PKG). PKG is activated upon the binding of two cGMP molecules that are produced from guanosine triphosphate (GTP) by guanylyl cyclase (GC). Guanylyl cyclase produces cGMP

in response to gaseous membrane-permeant nitric oxide (NO) which is produced from L-arginine by nitric oxidase synthase (NOS) dependent on Ca^{+}/calmodulin binding. NO production can be stimulated by a number of receptors such as the A3 adenosine receptor (A3AR) (Miller and Hoffman, 1994; Zhu et al., 2004, 2007, 2011) discussed more in the next section, and the $5HT_{2B}$ receptor (Launay et al., 2006). Both receptors have also been linked to PKG-mediated SERT modulation as well (Miller and Hoffman, 1994; Zhu et al., 2004; Launay et al., 2006).

Evidence exists that PKG activation drives enhanced 5-HT uptake through an elevation of transporter surface expression in RBL-2H3 cells (Miller and Hoffman, 1994; Zhu et al., 2004), however, another study found in rat synaptosomes PKG increased SERT kinetics in a trafficking-independent manner (Ramamoorthy et al., 2007). The lateral mobility of SERT within the plasma membrane has also been shown to increase after PKG stimulation (Chang et al., 2012). Activation of PKG in transfected cells leads to increased SERT phosphorylation (Ramamoorthy et al., 1998), specifically at residue Thr276 (Ramamoorthy et al., 2007), discussed more in detail in "*SERT phosphorylation*" section below.

Steiner and colleagues found that PKGIα isoform, but not PKGII, forms a complex with SERT (Steiner et al., 2009; Zhang and Rudnick, 2011). The main difference between the PKG isoforms is that PKGII is anchored to the membrane by myristylation whereas PKGIα is cytoplasmic where it can interact with membrane proteins in a regulated fashion. PKGII lipid modification precludes it from forming a functional complex with SERT, as disruption of PKGII myristylation domain allowed PKGII dependent regulation of SERT (Zhang and Rudnick, 2011), consistent with PKGIα as the major isoform regulating SERT endogenously. Despite evidence of a SERT:PKG interaction, later studies showed that PKGIα does not directly phosphorylate SERT transporter in cultured heterologous cells (Wong et al., 2012), suggesting that other kinases may act downstream of, or in parallel with PKG. to phosphorylate and regulate SERT.

p38 Mitogen-Activated Protein Kinase (p38 MAPK)

Isoforms of the p38 MAPK family (p38α, β, ɣ, *δ*) are activated by the MAPK kinases MKK3/6, enzymes that lie downstream of a complex signaling cascade activated by cellular stress that can be induced by reactive oxygen species or inflammatory cytokines (Huang et al., 2009b). One example of a cytokine that leads to activation of p38 MAPKs and that regulates SERT activity is interleukin-1β, acting through the interleukin 1 receptor (IL1R) (Zhu et al., 2006; Baganz et al., 2015) and described in more detail below. Activation of kappa opioid receptor (KOP) (Bruchas et al., 2011; Schindler et al., 2012) and A3AR (Zhu et al., 2004) have also been shown to stimulate p38 MAPK isoforms to modulate SERT function, discussed in more detail in the next section.

Activation of p38α MAPK has been shown to increase SERT activity in both trafficking and trafficking-independent mechanism in various sample preparations: the rat basophilic leukemia cell (RBL-2H3 cells) that endogenously express SERT (Zhu et al., 2005), in rat serotonergic RN46A cells (Zhu et al., 2005), transfected HeLa cells with hSERT (Prasad et al., 2005, 2009), mouse synaptosomes (Zhu et al., 2006), human platelets (Zhu et al., 2005), and human lymphoblast cells (Sutcliffe et al., 2005). The trafficking-independent mechanism of p38 MAPK regulation of SERT is supported by an increase in 5-HT affinity (decreased 5-HT K_M) and labeled the SERT* state (Quinlan et al., 2019). Consistent with this model, a decreased 5-HT K_i for displacement of surface antagonist binding RTI-55 is observed after p38 MAPK-dependent SERT regulation (Zhu et al., 2005). Inhibition of p38 MAPK pathway also appears to affect SERT protein interactions, leading to a loss of PP2Ac and syntaxin 1A associations (Samuvel et al., 2005), discussed more in detail in the "*SERT Interacting Protein*" section.

The expression of p38α MAPK in serotonergic neurons was found by Baganz and colleagues to be essential for the depressive effects of acute immune activation by intraperitoneal injection (IP) of lipopolysaccharide (Baganz et al., 2015), as well as by stress (Bruchas et al., 2011; Schindler et al., 2012). These data suggest the possibility of p38 MAPK as a therapeutic target in disorders that show SERT hyperfunction. In this regard, the use of brain-penetrant p38α MAPK inhibitors (MW108 and MW150) was shown to reverse autism spectrum disorder (ASD)-like behaviors in adult mice that express the

hyperactive SERT variant Ala56 (Robson et al., 2018), a mutant shown previously to be hyperphosphorylated *in vitro* and *in vivo* in a p38 MAPK dependent manner (Prasad et al., 2005; Veenstra-VanderWeele et al., 2012). These findings are described in more detail in the section *Role of 5-HT and SERT in Neuropsychiatric Disorders* below.

SERT Regulation by Other Kinases

Other serine/threonine kinases reported to impact SERT function are PKA (Cool et al., 1991; Yammamoto et al., 2013), ERK 1/2 (Benmansour et al., 2014), and PI3K/Akt (Rajamanickam et al., 2015). The functional role of each of these kinases is briefly outlined in **Table 1** and in the detailed review on kinase-dependent regulation of monoamine transporter (Bermingham and Blakely, 2016). All the kinases discussed above are serine/threonine kinases, however, it should also be noted that there are a number of tyrosine residues in SERT that are the target of tyrosine kinases, such as Srk (Annamalai et al., 2012) and Syk (Pavanetto et al., 2011).

Receptor-dependent regulation of SERT function

Kinase/phosphatase signaling cascades that regulate protein function are downstream of autoreceptor and heteroreceptor activation. It is well known that a number of receptors activate downstream kinases, such as those described in the above section, and act to modulate SERT function, These include 5-HT_{1B} receptors (Daws et al., 2000), adenosine receptors (Miller and Hoffman, 1994; Zhu et al., 2004, 2007), α2-adrenergic receptors (Ansah et al., 2003), atypical histamine receptors (Launay et al., 1994), Tropomyosin-related kinase B receptors (TrkB) (Benmansour et al., 2008), interleukin 1 receptors (IL1R) (Zhu et al., 2006, 2010) and kappa opioid receptors (KOP) (Sundaramurthy et al., 2017). Below I highlight three important receptors that are linked to kinase-dependent regulation SERT function.

Interleukin 1 Receptor (IL1R)

There is a strong link between immune dysfunction and neuropsychiatric diseases including major depressive disorder (MDD), known as the sickness hypothesis of MDD (Charlton, 2000). Increased serum levels of proinflammatory cytokines, IL-1β, IL-6, and TNF-α have been found in depressed patients (Maes, 1999). Activation of the immune system by lipopolysaccharide (LPS) in healthy human volunteers causes depressive-like phenotypes that positively correlate with TNF-α and IL-1β levels (Yirmiya et al., 2000). The major treatment for MDD is SSRIs, which specifically target SERT (Goodnick and Goldstein, 1998). Thus, it is possible that elevations of some cytokines, such as IL-1β, IL-6, TNF-α, may produce their effects by increasing SERT activity.

Proinflammatory cytokines, like IL-1β and TNF-α, activate p38 MAPK (Clerk et al., 1999; Pantouli et al., 2005), and activation of the p38 MAPK pathway has been shown to rapidly enhance SERT-mediated 5-HT uptake (see above). In 2006, Zhu and colleagues showed that IL-1β in a dose- and time-dependent manner, over the course of minutes, increased SERT function as measured by a decrease in 5-HT K_M with no change in Vmax (Zhu et al., 2006). IL-1β also was also shown to increase surface SERT lateral mobility within the plasma membrane (Chang et al., 2012). Inhibition of the IL1R and p38 MAPK both eliminated the IL-1β mediated increase in 5-HT uptake (Zhu et al., 2006). To link the regulation of SERT within the CNS driven by a peripheral immune response to behavioral changes, the Blakely lab employed a low dose LPS intraperitoneally injection (0.2 mg/kg) to avoid sickness induced changes in behaviors. LPS induced an increase in synaptosomal 5-HT uptake, as well as depressive-like phenotypes, 1-hour post injection. However, these effects were lost in IL1R constitutive KO mice (Zhu et al., 2010). It was also found that the LPS induced depression and increased 5-HT uptake was due to the serotonergic expression of p38α MAPK (Baganz et al., 2015). It is postulated that LPS increases IL-1β (either peripherally or centrally) to act on IL1Rs expressed in 5-HT neurons. IL-1R stimulation triggers singling cascaded to activate p38α MAPK which then acts on SERT to increased 5-HT clearance and diminished 5-HT receptor activation to elicit depressive-like phenotypes. To elucidate whether serotonergic IL1R expression is necessary for

modulating both SERT function and LPS induced depressive-like effects, the Blakely lab recently generated an *IL1R*$^{flx/flx}$ mouse line (Robson et al., 2016) that has been crossed with ePET1 Cre mice to selectively eliminate IL1R within serotonergic neurons. Conversely, the lab plans to utilize "IL1R restore mice", where IL-1Rs are selectively expressed in specific neurons in an otherwise IL-1R KO background (Liu et al., 2015), to assess if IL1R expression in 5-HT neurons is sufficient for these biochemical and behavioral effects.

Kappa Opioid Receptor (KOP)

Kappa opioid receptors belong to the G-protein coupled receptor (GPCR) family and are expressed in nerve terminals of serotonergic neurons (Berger et al., 2006; Kalyuzhny & Wessendorf, 1999). These studies show that treatment with KOR antagonists has antidepressant-like effects, while KOR agonist produced depressive-like phenotypes in rodent models. One of the links between KOR and depressive behavior has been suggested to be SERT since activation of KOR with the KOR agonists U69,593 or U50,488 in transfected cells decreases 5-HT uptake, specifically by decreasing SERT Vmax with no change in K_M (Sundaramurthy et al., 2017). This decrease in Vmax is due to lower SERT surface levels caused by decreased trafficking and increased internalization of SERT from the plasma membrane. This decrease in SERT function is dependent on protein kinase B (PKB)/Akt and CaMKII, as inhibition of these kinases blocked KOP agonist-mediated decrease in 5-HT uptake (Sundaramurthy et al., 2017). SERT regulation by KOP also extended to *ex vivo* ventral and dorsal striatal synaptosomes preparations (Sundaramurthy et al., 2017).

Stimulation of KOR has also been shown to produce enhanced SERT phosphorylation (Sundaramurthy et al., 2017). Interestingly, in addition to PKB/Akt and CaMKII, KOR activation has also been linked to p38 MAPK pathways. For example, Bruchas and colleagues found that social defeat (Bruchas et al., 2011) and forced swim stress (Schindler et al., 2012) lead to an increased surface trafficking of SERT in a p38α MAPK dependent manner and that this effect could be blocked the KOR antagonist, norBNI (Bruchas et al., 2011; Schindler et al., 2012). The authors propose that stress-related behaviors are

induced by an increase in dynorphin release that acts through the KOR/p38α MAPK pathway to upregulate SERT surface levels and thus reduce extracellular 5-HT availability. The intersection of KOR and IL-1R mediate effects will likely be a fascinating chapter in the story of SERT regulation-dependent behaviors.

A3 Adenosine Receptor (A3AR)

In 1994, Miller and Hoffman showed that addition of the adenosine receptor (AR) agonist, NECA, rapidly increased SERT mediated 5-HT uptake in RBL-2H3. This AR-mediated increase in uptake was blocked by inhibition of PKG (H8), suggesting AR stimulation is acting through a PKG pathway (Miller and Hoffman, 1994). Zhu and colleagues later showed that the A3 subtype of the AR (A3AR) mediated NECA increases in 5-HT uptake and that receptor activation induced both a trafficking-dependent (PKG pathway) and independent mechanism (PKG-p38 MAPK pathways) (Zhu et al., 2004). The A3AR-PKG pathway regulation leads to an increase in SERT Vmax, with no change in 5-HT K_M, and was recapitulated *in vivo* (Zhu et al., 2007). Interestingly, Zhao et al. reported that the LPS induced increase in 5-HT uptake seen in RBL-2H3 cells was blocked by A3AR inhibition (Zhao et al., 2015), though a specific mechanism for this effect has not been identified. Finally, the A3 adenosine receptor has been shown to form a functional complex with SERT *in vivo*, which increases upon A3AR stimulation (Zhu et al., 2011).

In 2013, the laboratory of James Sutcliff identified two ASD-associated rare coding variations in the A3AR gene: Leu90Val and Val171Ile. In collaboration with the Blakely lab this group showed that A3AR Val90 activation more strongly increased cGMP levels and increased SERT function than WT A3AR (Campbell et al., 2013), mimicking the enhanced uptake shown in the ASD-associated SERT variants (Sutcliffe et al., 2005), further supporting that variation in genes that are part of the SERT regulome may impact ASD risk.

Reverse transport of SERT by amphetamine and amphetamine-like derivatives

Although transporters are most commonly known for their role in uptake, transporters can also act in the reverse to efflux neurotransmitter from the cytoplasm to the extracellular space. Mutant transporters have been shown to exhibit anomalous transmitter efflux, such as in the case for the ADHD and ASD associated DAT variant, DAT Val559 (Mazei-Robison et al., 2008). However, efflux of neurotransmitters from transporters is mostly studied in the context of amphetamine analogs. In this regard, there are many derivatives of D-amphetamine, the active isomer, that vary in selectivity across the various monoamine transporters. D-amphetamine, also known as "speed" has a higher affinity for DAT and NET compared to SERT, whereas SERT has a higher affinity for 3,4-methylenedioxymethamphetamine (MDMA, "ecstasy") and fenfluramine (Green et al., 2003).

Amphetamines are psychostimulants that act as competitive substrates for DAT, NET, and SERT as well as VMAT2. Once amphetamine enters the cytoplasm either through the transporter or through passive diffusion through the membrane, the intracellular concentration of monoamines rapidly rises, as VMAT2 uptake of amine can no longer package monoamines into vesicles and outward leak of transmitter from vesicles is not attenuated by vesicle uptake (Heal, Smith, Gosden, & Nutt, 2013). Amphetamines also induce a Na^+ inward current across the plasma membrane (Schicker et al., 2012). This increase in Na^+ and monoamine levels leads to the reverse transport of monoamines, causing excess neurotransmitter in the synapse (Heal et al., 2013). The mechanism by which monoamine transporters switch from uptake mode to an efflux capacity is still not well-elucidated.

Some evidence suggests that amphetamine actions require an oligomeric state of the transporter, in which each transporter of the complex acts in distinct modes: one transporter functions in the forward transport whereas the other acts in the reverse or efflux state (Seidel et al., 2005). Many other interacting proteins and lipid moieties have also been implicated in amphetamine's ability to trigger reverse transport. For example, PIP_2 has been shown to interact with SERT and to be required for amphetamine action, but has no effect on 5-HT uptake (Buchmayer et al., 2013). More mechanistic detail for DAT:PIP_2 has been determined showing that PIP_2 interacts with DAT N-terminus to coordinates N-terminal interactions with

intracellular loop 4 (ICL4) leading to a conformational transition to an inward facing state (Khelashvili et al., 2015), a state required for substrate efflux. These ideas support a model whereby amphetamines impact the ability of the N-terminus of monoamine transporters to interact with intracellular loops governing the direction of substrate flux, effects that may be mimicked by N-terminal mutations.

As noted above, the phosphorylation of the DAT N-terminus, most likely through the C-terminal interacting CaMKII protein, is required for amphetamine-induced efflux (Khoshbouei et al., 2004; Fog et al., 2006). CaMKIIα has been shown to interact with the C-terminus of SERT and modulate reverse transport (Steinkellner et al., 2015). A sperate experiment demonstrates that CaMKII phosphorylates the N-terminus (Ser13) (Sørensen et al., 2014) although it has yet to be determined if phosphorylation at this site is required for amphetamine-induced efflux. That being said, we know that truncation of the first 32 amino acids of SERT (which includes the putative CaMKII phosphorylation site Ser13) significantly diminishes the ability to efflux substrate (Kern et al., 2017). It is thought that the N-terminus acts as a lever to support amphetamine function, as tethering the N-terminus to the plasma membrane inhibits the ability of SERT to support the efflux mode (Sucic et al., 2010). This data supports that idea the N-terminus plays a critical role in modulating amphetamine-induced efflux.

Interestingly, syntaxin 1A stabilizes DAT phosphorylation (Cervinski et al., 2010) and amphetamine increases DAT:syntaxin 1A interaction in a CaMKII-dependent manner (Binda et al., 2008), therefore suggesting syntaxin1 1A:DAT:CaMKII form an important functional complex in mediating reversal of DA transport. Similarly, syntaxin 1A also form a complex with SERT N-terminus as well, however, in contrast to DAT, syntaxin 1A decreases amphetamine-induced 5-HT efflux in murine catecholaminergic cells (CAD cells) (Montgomery et al., 2011). This discrepancy between DAT and SERT in the requirement of syntaxin 1A in mediating amphetamine-induced efflux may be useful in targeting amphetamine actions in either a DAT or SERT specific manner.

Intriguingly, amphetamine has been shown to increase SERT phosphorylation in a p38 MAPK dependent manner (Samuvel et al., 2005). However, p38 MAPK inhibition destabilizes SERT:syntaxin 1A interactions in rat midbrain synaptosomes (Samuvel et al., 2005), suggesting that p38 MAPK activation

may stabilize or enhance SERT:syntaxin 1A interaction, which was previously found to prevent SERT mediated efflux (Montgomery et al., 2011). This may be due to the various sample preparations or indicative of a complex SIP network of SERT mediated efflux that requires further investigation.

Finally, Ca^{2+}-dependent PKCβ also enhances amphetamine-induced efflux for both SERT (Buchmayer et al., 2013) and DAT (Johnson et al., 2005). A novel inhibitor of PKC has even been found to be effective in eliminating amphetamine-induced DA efflux and amphetamine mediated increase in locomotion behavior (Newman, 2017). Interestingly, both PKC and amphetamine increase phosphorylation of the N-terminal amino acid 53 (Thr53 in mouse DAT and Ser53 in hDAT) and mutation of this residue blocks amphetamine-induced efflux (Foster et al., 2012; Challasivakanaka et al., 2017). However, Thr53 is followed by Pro54, indicating PKC is the not the substrate, but instead the target of the proline-directed kinase, such as p38 MAPK, however, this has yet to be determined (Foster et al., 2012; Challasivakanaka et al., 2017). It was also shown that when a potential PKC phosphorylation site (Thr81) located at the juxtaposition between the N-terminus and TM1, when mutated to alanine, the transporter favored an inward facing conformation, but also significantly decreased amphetamine-induced efflux (Sucic et al., 2010).

While the exact mechanism of amphetamine-induced efflux is still under active investigation, the evidence suggests reversal of transport involves the orchestration of several SERT interacting protein, kinases, phosphorylation, and the N- and C-termini.

Protein-protein interactions with SERT

Another means by which the SERT function is regulated is through interaction with neighboring proteins (SERT-interacting proteins, SIPs). Over the past 20 years, a number of SIPs have been reported to modulate both SERT function and/or surface expression (**Table 2)** (Haase et al., 2001; González and Robinson, 2004; Sung et al., 2005; Sager and Torres, 2011; Zhong et al., 2012). A recent publication detailed a full proteomic analysis of rat SIPs via affinity-purification tandem mass spectrometry (AP-MS/MS) from total rat brain lysate, yeast two-hybrid screen and GST-pulldown method with rSERT N- and C-termini.

Protein Name	Interaction Domain	SERT Activity/Expression	Reference
Neuronal Nitric Oxide Synthase (nNOS)	PDZ domain of C-terminus: aa 628-630 (NAV)	↓ Activity and Surface (↓ trafficking); 5-HT uptake stimulated nNOS activity	Chanrion et al., 2007
Protein Phosphatase A (PP2Ac)	Destabilized by PKC activation	Inhibition blocks p38 MAPK mediated upregulation	Bauman et al., 2000; Zhu, Carneiro, Dostmann, Hewlett, & Blakely, 2005
Calcineurin (PP2B)	C-term of SERT with catalytic and regulatory subunit of	↑ Activity and surface, prevents PKC mediated phosphorylation and decrease 5HT uptake	Seimandi et al., 2013
Syntaxin 1A	SERT N-term; destabilized by PKC activation; enhanced by CaMKII	Regulated Na^+ transport stoichiometry, trafficking transporter to membrane	Ciccone, Timmons, Phillips, & Quick, 2008; Quick, 2002
Hic-5	C-terminus of SERT	Cytoskeleton and PM localization of SERT	Carneiro & Blakely, 2006
Integrin βIII	Directly with C-term	↑ 5-HT Uptake and Surface	Carneiro, Cook, Murphy, & Blakely, 2008
MacMARCKs	C-term of SERT	↓ Vmax 5-HT uptake; reduced down-regulation mediated by PKC	Jess, El Far, Kirsch, & Betz, 2002
α/ɣ Synuclein	?	↓ 5HT uptake (↓ Vmax; = Km)	Wersinger & Sidhu, 2009
N-ethylmaleimide-sensitive Factor (NSF)	Both N- and C-term of SERT	NSF KD decreases SERT surface expression and uptake	Iwata et al., 2014
A3 Adenosine Receptor	Activation of A3AR enhances interaction	Activation of A3AR ↑ surface expression and activity mediated by PKG and p38 MAPK	Zhu et al., 2011
Secretory Carrier Membrane Protein 2 (SCAMP2)	N-term of SERT	Subcellular redistribution and ↓ surface expression and activity	Müller, Wiborg, & Haase, 2006
14-3-3	N-term of SERT and 14-3-3	↓ Vmax (no effect on Km); possible involvement of PKC	Haase, Killian, Magnani, & Williams, 2001

Table 2. SERT Interacting Proteins

Protein Name	Interaction Domain	SERT Activity/Expression	Reference
Ca^{2+}/Calmodulin Dependent Protein Kinase (CaMKII)	C-term on SERT	↑ amphetamine mediated 5-HT efflux; Predicted to phosphorylate N-terminus	Steinkellner et al., 2015
Melanoma Associated Antigen D1 (MAGE-D1)	MAGE Homology Domain	↓ SERT expression (via ↑ SERT-Ub) and activity	Mouri et al., 2012
Rab4-GTP	C-terminus (aa 616-624); enhanced interaction in presence of extracellular 5-HT	Retrains SERT intracellularly	Ahmed et al., 2008
Vesicle-Asssociated Membrane Protein 2 (VAMP2)	C-terminus of VAMP2	SNARE-independent; PC12 ↑ SERT activity, HEK293 ↓ surface expression and activity	Müller, Kragballe, Fjorback, & Wiborg, 2014
Flotillin 1 (FLOT1)	?	↑ SERT expression after chronic corticosterone admiration in FLOT1 KO compared to WT	Reisinger et al., 2018
Neuroligin 2 (NLGN2)	?	Midbrain specific interaction; NLGN2 KO mice have ↓ SERT expression compared to WT	Ye et al., 2016
Sec23A/24C	C-terminus	Export of SERT from Endoplasmic Reticulum	Sucic et al., 2011; Chanrion et al. 2007
Myosin IIA	?	Disruption of N-glycosylation of SERT ↓ interaction	Ozaslan et al. 2003
Calnexin/Calreticulin	?	Chaperone proteins; Calnexin interaction dependent on N-glycosylation	Tate et al. 1999
Neutral Amino Acid Transporter (ASCT2)	?	↓ 5-HT V_{max} and $K_{M;}$ ↓ Surface expression; ↓ Glycosylation	Seyer et al. 2016
Protein Kinase C-Alpha Binding Protein (PICK1)	PDZ domain of C-terminus: aa 628-630 (NAV)	Weaker interaction than DAT and NET:PICK1 interaction; ↑DA uptake and DAT surface expression	Torres et al. 2001; Chanrion et al. 2007
Channel Interacting PDZ Protein	PDZ domain of C-terminus: aa 628-630 (NAV)	?	Chanrion et al. 2007

(Haase et al., 2017). A few SIPs identified in this screen were previously identified to interact with SERT, verifying the method employed. Many novel SIPs were also found, including many mitochondrial-associated proteins

It is important to note that in general where SIPs interact at different stages of translation, trafficking and endocytosis and activity regulation is not well characterized for most SIPs. As SIP identification is an effort pursued in my thesis studies, I outline below the methods that are utilized to identify and verify SIPs. I will also highlight a few SIPs that have been shown to affect SERT function in relation to kinase of interest to our lab, p38 MAPK, PKG, and PKC.

Methods to Identify and Verify SIPs

There are several starting points in the identification of SERT interacting proteins. First, one initiate studies via a candidate approach, in which one identifies likely interactors based on knowledge of a specific protein that regulates SERT (e.g. a kinase), that it is co-expressed with SERT (Ye et al., 2014, 2016), and/or has been known to interact and regulate other members of the *SLC* family. A second way to identify novel SERT interacting proteins is through an unbiased approach, such as through a yeast two-hybrid screen or through transporter purification approaches, followed by identification of partners by mass spectrometry-based approaches. The most common of the latter strategies is via transporter co-immunoprecipitation (co-IP) based approaches, in which the protein of interest is purified from a native or transfected cell sample via an antibody against the primary protein (or against an engineered tag). Alternatively, as in the AP-MS/MS approach noted above, the protein can be purified by binding to a drug with high affinity and specificity, such as with SERT using citalopram-conjugated to beads. One must of course deal with the possibility of identifying false positives interacting proteins bind non-specifically to the beads utilized in the assay. To control for this, it is important to use a negative control, such as the use of a KO mouse from which to repeat interaction studies. There is also the possibility that co-IPs lead to false negatives, as can be seen in proteins that only interacts with the target of interest transiently or the interactors are of low abundance, are unstable or aggregate in detergents, and thus are not detectable by this

method. Low-affinity interactions may be stabilized by chemical cross-linking approaches and the use of detergents that are known to permit structural studies or support other protein interactions may also give confidence that false negatives are being avoided.

Another way to detect and verify protein-protein interactions is through imaging techniques such as fluorescence resonance energy transfer (FRET) or bioluminescence resonance energy transfer (BRET) analysis. In these studies, SERT and SIP of interest are tagged with compatible fluorophores where the emission wavelength of one fluorophore is the excitation wavelength of the other fluorophore (Brzostowski et al., 2009). The excitation of the latter fluorophore is thus dependent on the orientation and proximity of the former fluorophore, which typically occurs at ~10 nm or closer. For example, excitation of cyan fluorescent protein (CFP; donor fluorophore) at ~430 nm leads to an emission of ~500 nm which can excite yellow fluorescent protein (YFP; acceptor fluorophore) to emit a ~530 nm wavelength. Therefore, if SERT and SIP are in close enough proximity, excitation of CFP will lead to the detection of a YFP signal (Brzostowski et al., 2009). BRET is a similar concept, except instead of utilizing donor fluorescent proteins, a bioluminescence donor protein is used to excite an acceptor fluorophore, avoiding the problems of photobleaching and autofluorescence (Dimri et al., 2016).

Syntaxin 1A and CaMKII

Syntaxin 1A is most well known as a member of the SNARE complex which mediates vesicular fusion and release of neurotransmitters (Bennett et al., 1993). Syntaxin 1A has also been shown to interact and regulate a number of other members of the neurotransmitter transporters, including SERT (Quick, 2002a), such as the GABA transporter type 1 (*SLC6A1*,GAT1) (Quick, 2002b), NET (*SLC6A2*, Sung et al., 2003) and DAT (*SLC6A3*, Binda et al., 2008).

Syntaxin 1A was first shown to interact with SERT in 2002 via a candidate-based co-IP strategy using thalamocortical neuron cultures (note SERT is expressed by neurons of the embryonic thalamus whereas in the adult SERT is restricted to raphe serotonergic neurons). Cleavage of syntaxin 1A by treatment of in thalamocortical cultures with botulinum toxin C1 led to a decreased surface expression of

SERT and reduced the capacity for 5-HT uptake, as measured by a lower SERT Vmax for 5-HT but equivalent K_M (Quick, 2002a). The interaction with syntaxin 1A may be relevant to PKC mediated downregulation of SERT uptake, as activation of PKC has been reported to decrease SERT:syntaxin 1A interactions (Haase et al., 2001; Quick, 2002a, 2003; Samuvel et al., 2005). Interestingly, inhibition of p38 MAPK by PD169316 has also been reported to diminish SERT:syntaxin 1A interactions in rat midbrain synaptosomes (Samuvel et al., 2005), and thus conditions that elevate SERT activity may involve stabilization of SERT:syntaxin 1A interactions. The syntaxin 1A interaction also dictates the presence or absence of uncoupled ion conduction by SERT, revealing that syntaxin 1A couples Na^+ flux to substrate uptake and eliminates the ability of SERT to support substrate independent Na^+ flux (Quick, 2003). The syntaxin 1A interaction appears to be dependent on CaMKII activity, as inhibition of CaMKII promotes SERT-mediated Na^+ currents and prevents SERT:syntaxin 1A interaction (Ciccone et al., 2008). CaMKIIα was also shown to interact with SERT and modulated amphetamine-induced efflux (Steinkellner et al., 2014, 2015), effects that are known to require the SERT N-terminus (Sucic et al., 2010; Kern et al., 2017). Syntaxin 1A physically interacts with the N-terminus of SERT (specifically Ser13-Glu23) (Quick, 2003) whereas CaMKII interacts with the C-terminus (Steinkellner et al., 2015), but is predicted to phosphorylate the N-terminus of SERT (Ser13) (Sørensen et al., 2014). As noted above, modeling studies indicate that the N- and C-termini of SERT approach each other during the transport cycle, which could facilitate CaMKII phosphorylation of the N-terminus.

Similar CaMKII, amphetamine, and syntaxin 1A-dependent interactions and regulation of transporter surface expression and efflux propensity also appear with the other monoamine transporters. For example, syntaxin 1A was also shown to interact with the NET N-terminus, but here appears to play a contradictory role as syntaxin 1A supports the trafficking of NET to the plasma membrane, but also limits NE uptake, suggesting that stages of the transporter:syntaxin 1A interactions may have different functional consequences. PKC activation disrupts syntaxin 1A:NET interaction to downregulate NET uptake (Sung et al., 2003). Interestingly, amphetamine appears to rapidly increase NET:syntaxin 1A interaction at the surface in a CaMKII dependent manner (Dipace et al., 2007). Syntaxin 1A also interacts with DAT N-

terminus (Lee et al., 2004), specifically the first 33 amino acids, and amphetamine also promotes DAT:syntaxin 1A interaction at the cell surface, also in a CaMKII manner (Binda et al., 2008). As described for SERT above, CaMKII also has been shown to interact with the C-terminus of DAT and mediate amphetamine-induced efflux and modulate N-terminal phosphorylation (Fog et al., 2006). Moreover, syntaxin 1A stabilizes DAT phosphorylation levels as cleavage of syntaxin 1A by botulinum toxin C decreased basal DAT phosphorylation levels (Cervinski et al., 2010). However, the residues supporting syntaxin 1A-sensitive DAT phosphorylation are unknown. Similar to SERT and NET, DAT interaction with syntaxin 1A suppress channel activity of Caenorhabditis elegans (C. elegans) DAT (Carvelli et al., 2008). However, in contrast to SERT, cleavage of syntaxin by botulinum toxin C in rat striatal tissue led to increased DAT activity, and co-expression with syntaxin 1a in heterologous expression systems decreased DAT surface expression, consequently decreasing DAT Vmax (Cervinski et al., 2010). Also, unlike NET, DAT regulation by PKC is not controlled by syntaxin 1a (Cervinski et al., 2010). The opposing effects of syntaxin 1a on DAT and SERT mediated uptake and surface expression might be due to the divergences in sequences of the N-and C-terminus. Additionally, the effect of syntaxin 1A on SERT phosphorylation levels has also not been determined.

Protein Phosphatase 2A (PP2A)

Inhibition of protein phosphatases by okadaic acid (OA) and calyculin A, increases SERT phosphorylation levels and leads to a decrease in SERT function, suggesting that phosphorylation of SERT dictates transporter activity (Ramamoorthy et al., 1998). In 2000, Bauman and colleagues found that SERT formed a functional complex with the active catalytic subunit of PP2A (PP2Ac) in transiently transfected HEK-293 cells (Bauman et al., 2000). PP2Ac:SERT interaction was disrupted by activation of PKC by phorbol ester, an effect that could be prevented by co-incubation with PKC inhibitor or 5-HT. Inhibition of PP2A by OA or calyculin A also prevented PP2Ac:SERT interaction increased SERT phosphorylation levels and decreased surface expression and 5-HT uptake (Bauman et al., 2000; Blakely and Bauman,

2000). The PP2Ac interaction is not limited to SERT, as co-IP studies with NET and DAT also shows PP2Ac:transporter association (Bauman et al., 2000).

PP2Ac:SERT associations have been linked to p38 MAPK dependent regulation of the transporter. PP2A can be activated by p38 MAPK (Westermarck et al., 2001) and inhibition of PP2A by calyculin A and fostriecin prevents the anisomycin-dependent increase in 5-HT uptake (Zhu et al., 2005). Conversely, inhibition of p38 MAPK disrupts the association between PP2Ac and SERT in transfected cells (Samuvel et al., 2005). Interesting, hyperfunctional SERT variants are insensitive to regulation by p38 MAPK, PKG, and PP2Ac, and show alteration in PP2Ac:SERT interactions (Prasad et al., 2009). Thus, PP2A plays an important role both in maintaining SERT phosphorylation levels and in mediating kinase-dependent regulation of 5-HT uptake, where p38 MAPK may lead to activation of PP2Ac, stimulating SERT:PP2Ac interaction to maintain SERT at the surface, while PKC activation disrupts this association, leading to internalization and decreased uptake.

Calcineurin/PP2B

Inhibitors of the Ca^{2+}-activated protein phosphatase calcineurin (CaN; PP2B), such as Tacrolimus (FK506) and cyclosporine A (CsA), are used clinically in transplant patients as immunosuppressants to prevent organ rejection. Interestingly, transplant patients are at an increased risk of developing mood disorders and approximately 60% of organ transplant patients develop depression (Corbett et al., 2013). Both FK506 and CsA have been shown to cause a number of neuropsychiatric side effects that reduce the patient's quality of life and negatively influence their clinical outcome (Corbett et al., 2013). Transplant patients are commonly prescribed SSRIs to combat depressive symptoms that develop after organ graft (Corbett et al., 2013), providing evidence that targeting SERT is effective in treating immunosuppressant-induced depression. Seimandi et al have identified a possible molecular cause for this immunosuppressant-induced depression – an interaction between CaN and SERT (Seimandi et al., 2013).

Characterization of the SERT:CaN interaction via GST-pull down and MS analysis revealed that both the catalytic (CaNA) and regulatory (CaNB) subunits of CaN interact with the C-terminus of SERT from whole mouse brain lysates. Seimandi and colleagues (2013) identified four residues of SERT required for CaN binding: R595-IIT600. These amino acids reside on the intracellular C- terminal tail of SERT at the interface of the plasma membrane. This motif is similar to the CaN binding site of other protein partners, such as the transcription factor, nuclear factor of activated T cell, NFAT (Takeuchi et al., 2007). However, the specific residues of CaN that are required for these interactions with SERT have not been determined. Knowledge of the protein motif located within CaN responsible for SERT:CaN interactions may reveal amino acid sequences important for interactions of other protein partners with SERT.

Although the CaN motif necessary to interact with SERT is unknown, Seimandi et al. (2013) presented evidence that the activity of CaN regulates the SERT/CaN interaction. A constitutively active CaNA (CA-CaNA) mutant resulted in an increase in SERT:CaN association as compared to a phosphatase-dead CaNA (PD-CaNA) mutant, assessed *in vitro* by co-IP (Seimandi et al., 2013). This finding provides evidence that CaN activity may act either through post-translational modifications or protein associations to alter the transport capacity of SERT, an effect that could have profound implications on serotonergic signaling and behaviors.

As noted, the SERT:CaN interaction occurs on the transporter C-terminus, which is crucial to the activity state and localization of SERT (Larsen et al., 2006). Co-expression of SERT and CA:CaNA in HEK-293 cells significantly increased the velocity of 5-HT uptake and the surface expression of SERT. Pharmacological inhibition of CA:CaNA with increasing concentrations of FK506 was found to decrease 5-HT uptake in a dose-dependent manner (Seimandi et al., 2013). This revealed that the SERT:CaN interaction is functional in nature, with the enzymatic activity of CaN regulating SERT trafficking.

Interestingly, the active state of CaN has also been linked to the mechanism of action of SSRIs (Crozatier et al., 2007), suggesting that CaN-mediated dephosphorylation may play a role in modulating SERT activity. Although expression of CA-CaNA was found to increase SERT activity in HEK-293 cells, it did not alter the phosphorylation state of SERT. Yet, activation of PKC with β-phorbol 12-myristate 13-

acetate (PMA) in the presence CA-CaNA reduces N- terminal phosphorylation of a serine residue (Ser48 or Ser52) on SERT (Seimandi et al., 2013) This provides evidence that a C-terminal interaction can affect the state of the distal N-terminus of the protein; an effect that may have significant implications for the regulation of SERT transport activity.

This functional SERT:CaN interaction was confirmed *in vivo* using mice that expressed inducible CA-CaNA in forebrain neurons. Consistent with *in vitro* experiments, synaptosomes from these mice exhibit an increase in 5-HT uptake and surface expression of SERT (Seimandi et al., 2013). Interestingly, mice that express inducible CA-CaNA not only in the forebrain, but also in the Dentate gyrus of the hippocampus, are more sensitive to SSRI-induced antidepressant-like effects (Crozatier et al., 2007). Behavioral studies in mice suggest that the activation of CaN results in antidepressant-like effects, which is congruent with the increased incidence of depression observed in patients receiving CaN inhibitors for immunosuppressive therapy. Further investigation of CaN:SERT interaction role in modulating depressive-like phenotypes may reveal a mechanism by which immunosuppressant drug therapy elicit the adverse side effect of depression.

Neuronal Nitric Oxide Synthase (nNOS)

It has been well established that the gaseous second messenger NO, produced by neuronal nitric oxide synthase (nNOS), regulates the release of 5-HT in different brain regions (Prast and Philippu, 2001). NO has been shown to activate guanylyl cyclase to produce cGMP, which can then bind to PKG and act on SERT to increase 5-HT surface expression and uptake (Miller and Hoffman, 1994; Zhu et al., 2004). Interestingly nNOS has been reported to be a critical SIP in modulating SERT activity (Chanrion et al., 2007). Despite the fact that PKG increases SERT trafficking (Steiner et al., 2008), it was found that co-expression of nNOS with SERT in transfected cells led to a decrease in SERT surface expression and 5-HT uptake, and this effect was blocked if the PDZ-binding domain of SERT (C-terminal NAV sequences; amino acid 628-630) was mutated (Chanrion et al., 2007)., suggesting the C-terminus as the site of interaction. Additionally, a genetic loss of nNOS *in vivo* leads to an increase in 5-HT uptake in

synaptosomes, further supporting the role of nNOS inhibiting SERT activity. Conversely, it was found that 5-HT uptake via SERT stimulated nNOS activity as NO production increased in the presence of 5-HT and this effect was blocked by SERT inhibition (Chanrion et al., 2007). These findings may be indicative of a feed-forward mechanism in which SERT-mediated 5-HT uptake and increased NO production leads to activation of PKG to further increase SERT activity (Garthwaite, 2007).

Flotillin-1 (FLOT1)

Flotillin-1 (FLOT1), a membrane-raft protein, was initially linked to regulation and interaction with DAT (Cremona et al., 2011; Gabriel et al., 2013). DAT, like SERT, partitions between microdomains within the plasma membrane, and it has been found that FLOT1 retains DAT in lipid rafts and is necessary for PKC-dependent endocytosis of the transporter (Cremona et al., 2011; Gabriel et al., 2013). However, other work has indicated that depletion of FLOT1 from the plasma membrane does not affect PKC-mediated endocytosis of DAT, but rather enhances diffusion of DAT in the plasma membrane (Sorkina et al., 2012). The Blakely lab found that the ADHD-associated DAT variant (R615C), which exhibits disrupted localization to membrane microdomains and constitutive endocytosis, demonstrates decreased interactions with Flot-1 compared to WT DAT (Sakrikar et al., 2012). FLOT1 interaction with DAT has also been linked to amphetamine action. DAT R615C variant with disrupted FLOT1 interaction was also differentially regulated by amphetamine (Sakrikar et al., 2012). Finally, FLOT1 expression in *Drosophila* DA neurons was also found to be required for amphetamine-enhanced locomotion (Pizzo et al., 2013).

Recently, FLOT1 was reported shown to interact with SERT (Reisinger et al., 2018). Genetic knock out of *Flot1* in mice did not affect SERT expression or function. However, the loss of FLOT1 in the depressogenic chronic corticosterone paradigm increased depressive behavior, as measured in the tail suspension test. Chronic corticosterone also led to a significant decrease in SERT mRNA production, however, in FLOT1 KO mice, this effect was blunted, leading to increased SERT expression relative to WT under this stress paradigm (Reisinger et al., 2018).

Post-translational modifications of SERT

PTMs of proteins are direct and often reversible means by which to alter the conformational state of a protein, thus impacting functional kinetics and/or protein trafficking or compartmentation. Major PTMs that have been studied in relation to SERT are N-glycosylation, ubiquitination, and phosphorylation.

SERT N-Glycosylation

Most PTM studied are predicted to occur on intracellular residues of SERT. However, the large second extracellular loop (ECL2) plays a critical role in regulating SERT function and expression and is known to undergo N-linked glycosylation (Tate and Blakely, 1994). Glycosylation of both human and rodent SERT as Asn208 and Asn217 (**Figure 3**), by high-mannose-type oligosaccharides, occurs in the endoplasmic reticulum (ER) shortly after SERT is translated and appropriately folded. SERT is then trafficked to the Golgi apparatus where it can undergo mature-glycosylation, followed by export to the plasma membrane. N-glycosylation of SERT is tissue-dependent, as revealed in studies of brain and platelet SERT (Qian et al., 1995b). It is thought that proper glycosylation of the transporter facilitates chaperone binding, a sign that the transporter is properly folded and ready to be targeted to the cell surface. Tate and Blakely reported that N-glycosylation of SERT is required to maintain the stability and steady-state levels of the protein, but does not affect SERT function (Tate and Blakely, 1994). N-glycosylation can be further modified by that addition of sialic acid. Mutations of rSERT Asn208Gln/Asn217Gln to disrupt N-linked glycosylation on SERT, impairs SERT interaction with myosin IIA, functional oligomerization, 5-HT uptake, and the ability of SERT to be regulated by PKG (Ozaslan et al., 2003). Surprisingly, Nobukuni and colleagues have reported that the C-terminus of SERT can modulate N-glycosylation of the rat, human and mouse SERT (Nobukuni et al., 2009), most likely through protein-protein interactions that are important in the trafficking of SERT from the ER to Golgi apparatus and finally to the plasma membrane.

SERT Ubiquitination

Ubiquitination refers to the addition of the protein ubiquitin to the amino group of lysine residues or the N-terminal methionine residue. Ubiquitination of a protein can target the protein for degradation by the proteasome, alter the structural conformation and function of a protein and/or localization of the protein within the cell (Schnell and Hicke, 2003; Mukhopadhyay and Riezman, 2007). Two studies have appeared within the past five years that have highlighted the potential roles of SERT ubiquitination. The first study reports an interaction of the E3 ubiquitin ligase melanoma antigen D1 (MAGE-D1) with SERT that evidence suggests increases SERT ubiquitination and decreases SERT protein levels, suggesting that SERT ubiquitination may target the transporter for increased degradation (Mouri et al., 2012). MAGE-D1 KO mice exhibit depressive phenotypes, suggested by the authors to be due to increases in SERT expression levels, though many other explanations are possible. The same lab then explored the role of SERT ubiquitination in lymphoblasts derived from MDD patients and found that samples originating from fluvoxamine-resistant patients had lower levels of ubiquitinated SERT, suggesting that SERT ubiquitination (or SERT protein levels) may be utilized a biomarker for antidepressant efficacy in MDD (Mouri et al., 2016). It is currently unknown which residues of SERT are ubiquitinated. The UbPred (www.ubpred.org) website (Radivojac et al., 2010), a software that predicts ubiquitinated residues based on protein sequence, nominates K10 (0.91 score), K29 (0.89 score), and K37 (0.89 score) in hSERT with high confidence (**Figure 3**). Interestingly, three N-terminal lysine residues of DAT (Lys19, Lys27, and Lys3) have been identified as ubiquitination sites that are involved in PKC mediated endocytosis (Miranda et al., 2005, 2007).

There are two studies within the past five years that have highlighted potential roles of SERT ubiquitination. The first study linking the E3 ubiquin ligase melanoma antigen D1 (MAGE-D1) interacts with SERT and increases SERT ubiquitination and decreases SERT expression. MAGE-D1 KO mice exhibited depressive phenotypes, thought to be due to increase in SERT expression levels, suggesting that SERT ubiquitination may target it for more rapid degradation and turnover (Mouri et al., 2012). The same lab then explored the role of SERT ubiquitination in lymphoblasts derived MDD patients and found that

samples originating from fluvoxamine-resistant patients had lower levels of ubiquitinated SERT and thus higher SERT protein levels compared to fluvoxamine-responsive samples, suggesting that SERT ubiquitination or SERT protein levels may be utilized a biomarker for antidepressant efficacy in MDD patients (Mouri et al., 2016).

SERT Phosphorylation

It is now well established that phosphorylation of monoamine transporters regulates transport kinetics (Ramamoorthy et al., 2011). The first defined phosphorylation site in SERT is Thr276, a residue located in the second intracellular loop (ICL2) between TM4 and TM5. This residue derives from work by Ramamoorthy et al. 2007 in an effort to identify mouse SERT residues that are phosphorylated in synaptosomes and transfected cells upon PKG activation, which at the time had been reported to increase SERT mediated 5-HT uptake. SERT phosphorylation levels were determined by an autoradiogram of 8-Br-cGMP treated mouse midbrain synaptosomes subjected to metabolic labeling with [^{32}P]orthophosphate followed by SERT immunoprecipitation. SERT was found to be basally phosphorylated with the addition of 8-Br-cGMP leading to increased SERT phosphorylation (Ramamoorthy et al., 2007). PKG is a serine/threonine kinase, so to determine which residue was phosphorylated, a phosphoamino acid analysis was performed by subjecting metabolically labeled SERT to acid hydrolysis and high voltage thin layer chromatography. Under these conditions, the phosphorylation induced by 8-Br-cGMP was found to be derived from the labeling of a threonine residue. Each of the 18 intracellular threonine residues located in SERT was then mutated to alanine, and only the Thr276Ala mutant lost the ability to be regulated by PKG in transfected CHO cells (Ramamoorthy et al., 2007). More recently, a Thr276 phospho-specific antibody has been developed. This antibody has been used to establish that phosphorylation at Thr276 is conformationally-sensitive, with evidence that phosphorylation of IL2 increases when the residue becomes solvent exposed in an inward-facing conformation (Zhang et al., 2016). Additionally, Rosenthal's lab reported that human SERT Thr276 phosphorylation depends on the lipid membrane environment, showing that depletion of cholesterol by MβCD and mevastatin increased the abundance of SERT p-Thr276 (Bailey

et al., 2018). This is in line with previous work also showing that cholesterol depletion promotes SERT to an inward facing conformation (Laursen et al., 2018), the conformation required for SERT phosphorylation of Thr276 (Zhang et al., 2016). In addition, loss of cholesterol decreases SERT activity (Scanlon et al., 2001), perhaps due to an increase in transporters in the inward facing conformation. A cholesterol binding site was found to be located in a hydrophobic grove between TM1a, TM5 and TM7 (Laursen et al., 2018), potentially stabilizing SERT into specific conformational states that regulates SERT PTMs and function.

Since the identification of Thr276, there has been increasing efforts to identify the other phospho-residues within in SERT. In 2014, Sørensen and colleagues performed a comprehensive analysis of potential SERT phosphorylated residues. To accomplish this, the authors synthesized peptides of all the intracellular regions of SERT and incubated the peptides *in vitro* with various purified kinases known to regulate SERT: PKG, p38 MAPK, PKA, CaMKII, and PKC (specific isoforms of kinases were not noted in this study). They then subjected each peptide to LC-MS/MS analysis, efforts that revealed 5 novel SERT phosphorylation sites: Ser13 (CaMKII), Ser149 (PKC), Ser277 (PKC), Thr603 (PKC), Thr616 (p38 MAPK). Interestingly PKG was not found to phosphorylate any residue, which supports Wong et al. findings that PKG does not directly phosphorylate SERT (Wong et al., 2012). While the use of peptides allowed for the identification of novel phosphorylation sites, one of the major drawbacks to this approach is the lack of structural restriction imposed by interaction with other domains and residues of the transporter and the lack of other proteins and lipids that interact with the full-length transporter in the membrane that can expose or mask these residues (or others) during the transport cycle. This idea is highlighted in the 2016 paper by Zhang et al. noted above in which Thr276 is part of the second intracellular loop that forms an alpha-helical loop in the outward facing conformation and then unwinds as the transporter moves to the inward-facing state, making Thr276 accessible at that point to modification by protein kinases for phosphorylation (Zhang et al., 2016).

There is also evidence of tyrosine phosphorylation in SERT: specifically, hSERT Y47 (N-terminus) and Y142 (ICL1) (Annamalai et al., 2012) (**Figure 3**). Mutation of these tyrosine residues to phenylalanine (F; to maintain aromaticity) reduces basal phospho-tyrosine levels in human trophoblast cells. These

residues are thought to be the target of the tyrosine kinase, Src, as co-expression of Src with these hSERT tyrosine mutants, unlike wildtype SERT, did not show an increase in tyrosine phosphorylation. Interestingly, phosphorylation of these residues was linked to SERT protein stability, as activation of Src led to reduced protein levels. Moreover, the hSERT Y47F and Y142F mutants demonstrated increased total and surface levels, despite a decrease in 5-HT uptake (Annamalai et al., 2012). This discrepancy may be explained by epitope unmasking due to PTM changes as a result of the Y47F and Y142F mutations.

Role of 5-HT and SERT in neuropsychiatric disorders

5-HT and SERT have been linked to a number of neuropsychiatric diseases, especially disorders that affect mood, such as major depressive disorder (MDD) (Plaznik et al., 1989; Meltzer, 1990). Additionally, anxiety (Iversen, 1984), aggression (Francesco Ferrari et al., 2005; Duke et al., 2013)), suicidal behavior (Mann et al., 1990), obsessive-compulsive disorder (OCD) (Sinopoli et al., 2017), schizophrenia (Blelch et al., 1988; Meltzer, 1999), and autism spectrum disorder (ASD) (Muller et al., 2016) have been considered to involve changes in CNS serotonergic signaling.

Major Depressive Disorder (MDD)

The most common disorder associated with 5-HT and SERT is MDD, which impacts as many as 20% of individuals during their lifetime. Indeed, a tenet of the monoamine hypothesis for MDD states that a key underlying biological basis for depression involves diminished 5-HT and/or NE signaling (Hirschfeld, 2000), in large part, but not exclusively, based on major antidepressant medications acting through their chronic targeting of SERT and NET, respectively.

SSRIs, including fluoxetine (Prozac), citalopram (Celexa) and paroxetine (Paxil), act to rapidly block SERT activity, and are often the first line of treatment for MDD (Goodnick and Goldstein, 1998). To test the efficacy of drugs for the treatment of depression, two behavioral tests in rodent models have been implemented, the forced swim test (FST) and the tail suspension test (TST) (Castagné et al., 2011).

While these tests are sensitive to acute SSRI treatment, in human populations there is a two or more week delayed onset of antidepressant effects (Wong and Licinio, 2001). Additionally, SSRIs have a number of off-target effects (Carrasco and Sandner, 2005) and so the necessity of SERT blockade in antidepressant efficacy has been questioned. However, utilizing a model that is insensitive to SSRI mediated SERT blockade, Nackenoff and colleagues demonstrated that the SERT Met172 mouse, shows that SERT inhibition is necessary for the antidepressant effect of fluoxetine and citalopram in both the acute models noted above, as well as in tests of novelty-suppressed feeding and hippocampal stem cell density and survival, which require chronic SSRI administration (Nackenoff et al., 2016). Interestingly, this research also demonstrates that SERT antagonism is dispensable, at least in the mouse, for the antidepressant-like actions of vortioxetine (Trintellix), which not only blocks SERT but also targets a number of 5-HT receptors (Nackenoff et al., 2017). The SERT Ile172Met variant was identified as a consequence of the pharmacological difference in SSRI potency exhibited between hSERT (Ile172) and Drosophila *melanogaster* SERT (dSERT; Met167). Substitution to convert Ile172 (located in TM2) to Met172 in hSERT or mSERT induced a 100-to 1,000-fold reduction in potency for a number of SERT inhibitors, including SSRIs and cocaine, both *in vitro* (Henry et al., 2006) and *in vivo* (Thompson et al., 2011; Simmler et al., 2017).

It is reasonable, based on the findings with the SERT Ile172Met substitution, to wonder whether SERT coding variants contribute to treatment-resistant depression. However, to date, all coding variants identified in SERT are rare and no coding variants in SERT have been associated with depression, although these have been associated with OCD and ASD (see below). That being said, there has been a link to a common functional polymorphism in the promotor region of *Slc6a4* (5-HTTLPR) has also been linked to depression and stressful life events (Caspi et al., 2003). The 5-HTTLPR is a 44-base pair insertion or deletion sequence located in the promoter that gives rise to a long (*l)* or short (s) allele, respectively (Heils et al., 2002). The *s* allele has been reported to confer lower transcriptional activity of the *SLC6A4* gene and consequently reduced SERT protein expression, compared to the *l* allele (Lesch et al., 1996). Differences in brain function observed in patients with 5-HTTLPR polymorphism, for example with cortico-amygdala

interactions, could contribute to depression (Pezawas et al., 2005). The contribution of 5-HTTLPR status to depression risk suggests that carriers of the s allele (*s/l* or *s/*s) have an increased risk for developing depression in response to stressful life events compared to carries 5HTLPR *l/l* individuals (Caspi et al., 2003). Interestingly the *s* allele has been reported to lead to a reduced response to SSRIs (Rausch, 2005).

Obsessive Compulsive Disorder (OCD)

OCD is a neuropsychiatric syndrome characterized by repetitive thoughts that manifest into obsessions and ritualistic like behaviors that are meant to decrease stress. One of the strongest links to serotonergic involvement in OCD is the ability of SSRIs, selectively, in improving OCD symptoms, with a lack of therapeutic response to norepinephrine reuptake inhibitors and dopamine agonists (Kellner, 2010) as well as a more rapid onset of action than for SSRIs and depression. A number of serotonergic genes variants have also been associated with OCD, including *Slc6a4* (SERT), *Htr2a* (5-$HT2_A$ receptor), *Htr1b* (5-HT_{2B} receptor), and *Htr2c* (5-HT_{2C} receptor) (Sinopoli et al., 2017).

Importantly, a non-synonymous SNP in *SLC6A4* was identified in a subset of patients with OCD, anorexia nervous, and Asperger syndrome that changes an isoleucine at residue 425 to valine in TM5 (Ozaki et al., 2003; Delorme et al., 2005). Subsequently, Kilic and colleagues found that the Ile425Val substitution 5-HT transport with no change in surface expression (Kilic et al., 2003). Interestingly, another variation at this site, Ile425Leu, was identified in ASD and found to also increase 5-HT uptake, but through increases in SERT surface expression (Sutcliffe et al., 2005; Prasad et al., 2009). The differences here may reflect differences in the cell model for heterologous expression (COS-7 vs HeLa as the latter cells confer much less protein expression after transfection, less likely to saturate trafficking mechanisms). Additionally, the Ile425Val variant was found to be insensitive to further increase in 5-HT uptake upon PKG activation, however inhibition of PKG decreases the naturally elevated 5-HT uptake, suggesting that Val425 is stabilized in a conformation that allows for phosphorylation and constitutive activation by PKG and/or an inability of protein phosphatases such as PP2A to dephosphorylate the transporter. In this regard, Zhang and colleagues examined the contribution of Thr276, the site required for PKG modulation of SERT

activity, mutating this site to alanine or aspartic acid, and found that Thr276 was critical for SERT Val425 uptake activity to be down-regulated by PKG inhibitors (Zhang and Rudnick, 2005a).

Autism Spectrum Disorder (ASD)

5-HT and SERT are well known to be expressed early in development, studies first shown by *in situ* hybridization studies in the mid-gestation mouse embryo (Schroeter and Blakely, 1996). Therefore, it is no surprise that disruptions in 5-HT signaling have been linked to increasing the risk of developing neurodevelopmental disorders, such as ASD. The first link to ASD and 5-HT dates back to 1961, in which elevated 5-HT was found in blood platelets in a subset of ASD patients (Schain and Freedman, 1961). Decreased plasma levels of a 5-HT metabolite, melatonin, has also been identified in a group of ASD patients, thought to be due to disruptions in the serotonin-N-acetyl serotonin-melatonin pathway (Pagan et al., 2014). In 1996, it was also found that depletion of the 5-HT precursor, tryptophan, in the diet worsen ASD symptoms (McDougle et al., 1996a). In PET images, boys with ASD demonstrated decreased [^{11}C]methyl-tryptophan levels in both the frontal cortex and thalamus compared to their male sibling counterpart, indicating that altered 5-HT synthesis may be associated with ASD (Chugani et al., 1997). Below, I present an in-depth review on ASD and its link to SERT coding variants.

ASD and autism-associated SERT coding variants

ASD was first described by Leo Kanner in 1943 in a paper published in *Pathology* entitled "Autistic Disturbances of Affective Contact." In this paper, Kanner presented 11 cases of children with what he labeled "infantile autism" which was a term originally used to depict a phenotype in schizophrenic patients that were withdrawn from the outside world (Leo Kanner, 1943). Since the first description of autism, the American Psychiatric Association has classified autism in the Diagnostic and Statistical Manual of Mental Disorders (DSM). Today, the most recent DSM (DSM-V) describes ASD by two major behavioral characterizations: deficits in both social communication and interaction, and repetitive restricted behaviors.

Over the past few years, there has been a rapid increase in the prevalence, with estimates now indicating 1 in 59 children in the United States are diagnosed with ASD with a skewed 4:1 male dominance (Baio et al., 2018).

While there is no biomarker that encompasses everyone diagnosed with ASD, the oldest biochemical feature found in a significant proportion of ASD subjects (about 25-30%) is elevated 5-HT in blood platelets, called hyperserotonemia (Hanley et al., 1977; Mulder et al., 2004; Kolevzon et al., 2010). As mentioned above, blood platelets do not express the necessary machinery to produce 5-HT, but instead take up 5-HT, produced by gut enterochromaffin cells, through SERT (Lesch et al., 1993). Therefore, a few means by which patients with ASD may exhibit hyperserotonemia is through increased expression of hyperactivity SERT, or through a decreased release of 5-HT from blood platelets.

Interestingly, SSRIs are often prescribed off-label to ASD patients and found to be effective in treating repetitive behaviors (McDougle et al., 1996b; Hollander et al., 2012; Williams et al., 2013; Ji and Findling, 2015). In 2005, the Blakely lab, in collaboration with James Sutcliff at Vanderbilt University, identified 5 nonsynonymous single nucleotide polymorphisms (SNPs) within the *SLC6A4* gene from 120 families with multiple children affected with ASD, specifically in male-only affected families (**Figure 3)** (Sutcliffe et al., 2005). Four of these variants (Gly56Ala, Ile425Leu, Phe465Leu, and Leu550Val) conferred enhanced 5-HT uptake when transfected into cells while the C-terminal Lys605Asn showed no effect on SERT activity (Prasad et al., 2005, 2009). The Ile425Leu, Phe465Leu, and Leu550Val SERT variants caused an increase in V_{max} relative to WT SERT which could be explained by the enhanced surface expression of these variant transporters. On the other hand, Gly56Ala (SERT Ala56 here on out) did not impact V_{max} or surface expression, yet did decrease SERT K_M compared to WT SERT (Prasad et al., 2009), suggesting a possible increase in 5-HT affinity as the explanation for elevated initial rates of 5-HT uptake. Interestingly, SERT Ala56 was also insensitive to stimulation by activators of p38 MAPK and PKG, yet had increased sensitivity to PKC-mediated downregulation. Although the Lys605Asn variant did not affect 5-HT uptake, it did prove insensitive to p38 MAPK and PKG-mediated increase in 5-HT uptake (Prasad et

al., 2005) suggesting that the mutation may impose common structural changes as seen with the Gly56Ala variant.

Characterization of SERT Ala56 Knock-In Mouse Model

Moving forward, our lab decided to focus its efforts on understanding the basis of the SERT Ala56 hyperfunction, as it may provide insight into SERT regulation. Furthermore, SERT Ala56 is the most common variant, existing in about 1% of the US population, is highly conserved across mammalian species, was over-transmitted 3:1 to subjects with ASD, and displayed a male gender bias (Veenstra-VanderWeele et al., 2009). We, therefore, developed a knock-in (KI) mouse model expressing the SERT Ala56 variant to study the effects of the variant *in vivo* (Veenstra-VanderWeele et al., 2009).

SERT Ala56 KI mice exhibit the core ASD-like behaviors: decreased communication as assessed through ultrasonic vocalizations, increased repetitive behaviors as measured by bouts of wire hanging in the home cage, and decreased social behaviors as assessed by the tube test of social dominance and the three-chamber social assay (Veenstra-VanderWeele et al., 2012). As mentioned above there are a number of comorbid disorders associated with ASD, including altered sensory processing. SERT Ala56 KI mice showed no defects in learning behavioral responses to auditory and visual cues independently, however, showed deficits in multisensory processing (Siemann et al., 2017). Thus, the SERT Ala56 KI mouse model provided a new avenue for investigation of the functional impact of a hypermorphic SERT variant on the manifestations of ASD-like behavior.

Mimicking the enhanced uptake seen *in vitro*, SERT Ala56 KI mice display elevated 5-HT clearance rates compared to WT mice in the CA3 region of the hippocampus as measured by *in vivo* chronoamperometry (Veenstra-VanderWeele et al., 2012; Robson et al., 2018). Elevated 5-HT in the blood, or hyperserotonemia, was also found in the SERT Ala56 KI mice. The increased 5-HT clearance could be hypothesized to lead to decreased extracellular 5-HT levels (later confirmed in Quinlan et al. 2019 by microdialysis measures), leading to hypersensitive 5-HT receptors, which was evident by SERT Ala56 KI mice heightened response to DOI-induced head twitch (hallucinogenic 5-$HT2_A$ receptor agonist) and 8-OH-DPAT induced hypothermia (5-HT_{1A} receptor agonist). It is important to note that these mice display

no difference in total tissue levels of 5-HT nor changes in other neurotransmitter levels relative to WT mice. No differences were detected in total SERT expression (Veenstra-VanderWeele et al., 2009, 2012), though it is unknown if SERT Ala56 affects *in vivo* surface expression that could account as well for increased rates of clearance, though changes in surface expression were not seen *in vitro*.

Considering that 5-HT and SERT play important roles in gut motility and gastrointestinal distress, and is a comorbid disorder with ASD, we examined the gut health of the SERT Ala56 KI mice and found disruption in GI transit, hypoplasia of the enteric nervous system, reduced peristaltic reflex activity, and proliferation of crypt epithelial cells (Margolis et al., 2016). Moreover, the GI phenotypes are prevented by administration of a 5-HT_4 agonist *in utero* (Margolis et al., 2016). These findings suggest that the SERT Ala56 mutation confers both brain and peripheral phenotypes, and some of these may be initiated during early development.

SERT is hyperphosphorylated in a p38 MAPK dependent manner in the SERT Ala56 KI mice (Veenstra-VanderWeele et al., 2012). Thus, we wanted to test the hypothesis that SERT Ala56 traits can be reversed through inhibition of p38 MAPK, specifically focusing on the alpha isoform as past studies have revealed SERT regulation by p38α MAPK (Baganz et al., 2015). Chronic (5 mg/kg 1-week once daily (QD) I.P. injection), but not acute (one 5 mg/kg injection) treatment with the p38α MAPK inhibitor (MW150) reversed the social deficits and GI distress in adult (8-10 weeks) mice (Robson et al., 2018). Due to SERT being present throughout the body, it is possible that behavioral manifestations of the mutant mice could arise peripherally. In this regard, Robson and colleagues reported that genetic deletion of p38α MAPK from CNS serotonergic neurons (p38α MAPK flx/flx::ePet1 Cre) also reversed the social deficits in these mice (Robson et al., 2018), suggesting that CNS SERT plays a role in mediating at least some of the SERT Ala56 phenotypes.

It is important to note that all the above studies were performed with homozygous SERTAla56 mice derived from heterozygous breeding (Het X Het) breeding. Since SERT is expressed in the placenta and 5-HT is essential to normal fetal development, there is also the possibility that the heterozygous SERT Ala56 could alter 5-HT signaling between dam and embryos, though these mothers also gave rise to the

homozygous Gly56 tested in parallel. However, Muller and colleagues found that if the mother was homozygous for the SERT Ala56 allele, placental mRNA related to immune and metabolic-related pathways are altered and there are decreased levels of 5-HT in the placenta and embryonic forebrain at E14.5 which may contribute to a broadening of 5-HT sensitive thalamocortical axonal projections (Muller et al., 2017).

Finally, all the experiments noted above with the SERT Ala56 mice were performed on a mixed, but predominantly 129S6/S4 background. Some of the SERT Ala56 behavioral phenotypes (except for social deficits) are altered when the mutation was placed on a C57BL/6 background (Kerr et al., 2013). Unfortunately, the mechanism for this strain-dependent difference remains elusive, although it supports the idea that genetic variations such as Ala56 impose risk as opposed to acting deterministically, and will thus manifest their effects in the context of a permissive genetic background or under specific environmental conditions.

Summary

As described above, SERT-mediated 5-HT uptake and clearance dictates a number of physiological responses by tightly controlling the levels of extracellular 5-HT available to signal. SERT is regulated by multiple signaling pathways that can either act directly or indirectly to modulate SERT surface levels and/or activity. These regulatory influences are thought to be imposed transiently as a consequence of receptor activation that activates signaling cascades, including PKG and p38 MAPK, that can act on the transporter to alter PTMs and SIPs, ultimately affecting SERT function. The changes in surface trafficking and activity arising from regulatory signaling pathways can be mimicked by engineered and inherited mutations that change SERT coding sequences. Several of the ASD-associated inherited variants, including SERT Ala56 and SERT Asn605, modulate function and/or regulation in the absence of apparent changes in surface trafficking. Engineered mutations to eliminate or mimic SERT phosphorylation at Thr276 also alters the regulation of SERT by kinase-dependent pathways (**Figure 4**).

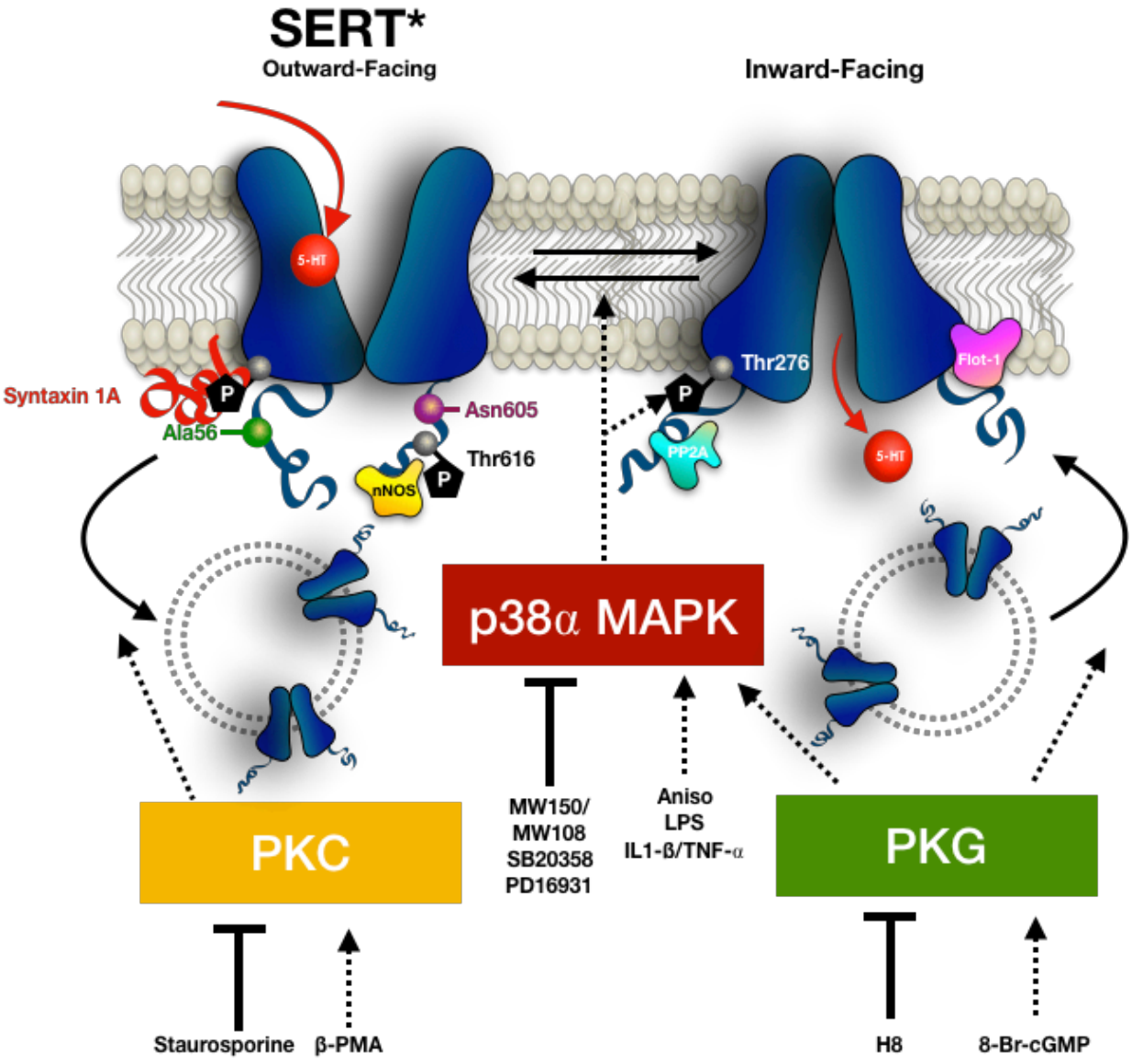

Figure 4. Structural and functional dynamics of SERT coding and engineered variants

My hypothesis is that these mutations impose structural constraints that shift the conformational equilibrium and affects SIPs and PTM, which results in altered SERT function . To test this hypothesis, I propose the following Specific Aims:

Aim 1: Determine whether SERT coding variants identified in ASD subjects alter transporter conformational equilibrium that leads to changes in SERT function *in vitro* and *in vivo*.

Aim 2: Determine whether SERT Ala56 alters protein associations compared to WT SERT.

Aim 3: Establish a novel *in vivo* model that precludes phosphorylation of Thr276 *in vivo* and determine initial biochemical and behavioral phenotypes.

CHAPTER 2

BIASED CONFORMATIONAL STATE OF ASD-ASSOCIATED SERT CODING VARIANTS

Adapted with permission from:

Quinlan MA, Krout D, Katamish R, Robson MJ, Nettesheim C, Gresch PJ, Mash D, Henry K, Blakely RD (2019) Human Serotonin Transporter Coding Variation Establishes Conformational Bias with Functional Consequences. ACS Chem Neurosci 14:acschemneuro.8b00689.

Introduction

ASD, a neurobehavioral condition with high prevalence and significant, but heterogeneous genetic contributions (Waye and Cheng, 2018), has been linked to disruptions in 5-HT signaling (Muller et al., 2016). More than 50 years ago, Schain and Freedman (Schain and Freedman, 1961) reported elevated whole blood 5-HT levels (hyperserotonemia) in subjects with ASD. Multiple studies since this time have demonstrated hyperserotonemia in a subset (25-30%) of ASD subjects, primarily derived from elevated 5-HT stores in platelets (Schain and Freedman, 1961; Cook et al., 1993). These stores of 5-HT arise from platelet SERT accumulation of enterochromaffin cell-derived 5-HT (Lesch et al., 1993). Genetic studies of multiplex ASD families identified a region centered over 17q11.2 that harbors *SLC6A4*, the SERT gene (Stone et al., 2004; Cantor et al., 2005; Sutcliffe et al., 2005), as bearing significant linkage to ASD. Since ASD has been associated with hyperserotonemia, and the coding sequence of human SERT is identical in the brain and platelets (Lesch et al., 1993), we hypothesized that the linkage signal might reflect the transmission of ASD-associated SERT coding variants that could elevate risk for ASD. Indeed, our efforts revealed multiple, rare functional SERT coding variants (Sutcliffe et al., 2005), as well as multiple, novel noncoding variants. Remarkably, a common feature of the SERT coding variants in both subject lymphoblasts and transfected cells was a capacity to confer elevated 5-HT transport activity as compared to 5-HT transport conferred by the reference (WT) alleles at the respective position (Prasad et al., 2005;

Sutcliffe et al., 2005; Prasad et al., 2009). Further studies revealed that the most common of these variants, SERT Ala56, induces elevated 5-HT transport (Prasad et al., 2005; Sutcliffe et al., 2005) in the absence of changes in either total or surface SERT protein (Prasad et al., 2005, 2009). Rather, SERT Ala56 demonstrates a reduction in 5-HT K_M compared to SERT Gly56, the WT allele (Prasad et al., 2005), suggesting an increased efficiency for 5-HT uptake at sub-saturating 5-HT concentrations. Importantly, the stimulatory impact of the SERT Ala56 variant on 5-HT transport has been demonstrated in the brain of SERT Ala56 KI mice *in vivo* (Veenstra-VanderWeele et al., 2009, 2012). Moreover, these mice exhibited hyperserotonemia, consistent with a model where the variant imposes a peripheral biochemical trait that correlates with the presence of behavioral and comorbid physiological changes arising from the variant expressed elsewhere (Veenstra-VanderWeele et al., 2012; Margolis et al., 2016; Robson et al., 2018).

Mechanistic studies of SERT Ala56 hyperfunction indicates that the variant may exist constitutively in a conformation normally transiently induced by activation of protein kinase G (PKG) (Ramamoorthy et al., 2007) and p38α MAPK (Zhu et al., 2004, 2005). Consistent with this hypothesis, SERT Ala56 demonstrates no further increase in 5-HT uptake activity when expressed heterologously (Prasad et al., 2005) or natively (Prasad et al., 2009) and treated with activators of PKG or p38 MAPK. SERT Ala56 is also hyperphosphorylated under basal conditions in these preparations in a p38 MAPK-dependent manner (Veenstra-VanderWeele et al., 2009, 2012). Finally, the elevated 5-HT clearance observed in SERT Ala56 mice, as well as multiple physiological and behavioral phenotypes, can be reversed by treatment of these animals with the p38α MAPK inhibitors, MW108 and MW150 (Robson et al., 2018). Another SERT missense variant identified in the 2005 ASD study that promoted the study of SERT Ala56, the C-terminal variant SERT Asn605, also displays reduced PKG/p38 MAPK sensitivity (Prasad et al., 2005). A structural basis, however, for the kinetic and regulatory changes of either SERT Ala56 or SERT Asn605 has not been established.

SERT, like other members of the Na^+/Cl^- dependent neurotransmitter transporter family (SLC6) (Kristensen et al., 2011), translocates substrates across the membrane via an alternating access mechanism (Forrest et al., 2008; Adhikary et al., 2017). In this model, 5-HT and co-transported ions bind to SERT

when bindings sites become exposed to the extracellular space via an "outward-facing conformation" Upon the binding of substrates, the transporter changes conformation such that the substrate binding sites are shielded from the extracellular space, yielding a "substrate-occluded conformation". Further conformational changes lead to exposure of the substrate binding sites to the cytoplasm and release of 5-HT and co-transported ions, a state termed the "open-inward conformation" (Forrest et al., 2008). Following 5-HT release intracellularly, and the binding of a single K^+ ion, the 5-HT unbound carrier reorients to reestablish the outward-facing conformation, preparing the transporter for the next transport cycle. High resolution structure and modeling studies (Chen and Rudnick, 2000; Forrest et al., 2008; Fenollar-Ferrer et al., 2014; Coleman et al., 2016) suggest that during the transport cycle, the transporter undergoes a conformational shift of sets of helices, referred to as a "rocking bundle" mechanism (Forrest et al., 2008). In this model, transmembrane (TM) segments 1-5 and 6-10, which form two inverted repeat bundles, move in relation to each other to open and close internal and external gates that grant or occlude access to the substrate binding site. Whereas residues within SERT transmembrane domains comprise sites of substrate binding, residues within the transporter's intracellular N- and C-termini appear to contribute to the regulation of transporter trafficking and function. Moreover, these domains have become increasingly recognized as determinants of substrate binding affinity, the directionality of transport (i.e. influx versus efflux), and the rate of substrate translocation (Khoshbouei et al., 2004; Sucic et al., 2010; Khelashvili et al., 2015; Kern et al., 2017; Sweeney et al., 2017; Razavi et al., 2018). Herein, I report functional and structural evidence that the N-terminal SERT Ala56 coding variant imposes conformations that, with greater probability than seen with the WT transporter, orients SERT in an outward-facing state. Somewhat similar findings are evident for the C-terminal Asn605 variant, indicating that modest structural changes in either cytoplasmic tails can result in both local and global changes in conformation that for some individuals may impact disease risk.

Results

Conformational Bias of SERT Ala56 Evaluated by Studies of Fenfluramine-Mediated 5-HT Efflux In Vitro and In Vivo.

The alternation of conformations that drives neurotransmitter uptake from the extracellular space also participates (Fischer and Cho, 1979; Sulzer et al., 2005), with qualifications (Sitte et al., 2001; Kern et al., 2017), in the ability of transporters to support movement of elevated intracellular substrate (efflux) from the cytoplasm to the extracellular space (Sulzer et al., 2005). The mutually sequential nature of the alternating access model predicts that alterations in conformational stability that enhance outward-facing conformations and 5-HT uptake rates will reduce the population of inward-facing conformations, and reduce transporter-mediated 5-HT efflux. Moreover, amphetamines are well known to enhance efflux of substrates by monoamine transporters, including SERT (Sulzer et al., 2005), with D-fenfluramine being relatively SERT-selective (Rothman et al., 2001) and commonly used to drive SERT-mediated 5-HT efflux *in vitro* (Rudnick and Wall, 1992; Sitte et al., 2001; Hilber et al., 2005) and *in vivo* (Gobbi et al., 1993; Balcioglu and Wurtman, 1998). In this regard, the SERT Ala56 variant lies in the SERT N-terminus, which has been shown to dictate the capacity for SERT-mediated 5-HT efflux induced by amphetamine derivatives (Kern et al., 2017).

To examine whether SERT Ala56 displays altered 5-HT efflux rates, we first loaded CHO cells stably expressing WT or SERT Ala56 to equilibrium with [^{3}H]5-HT (20 nM, 1 hr at 37°C). Both WT and SERT Ala56 cells loaded to equivalent levels **(**Figure 5**A)** in keeping with the equilibrium nature of the incubations and the equivalent surface expression of WT and SERT Ala56. We then rapidly removed external substrate prior to incubation of cells with 10 μM D-fenfluramine for 1, 3, or 5 min, collecting and quantifying radiolabel in the extracellular media, as described in Experimental Procedures. When cells were exposed to D-fenfluramine, WT cells supported significant (~80%) 5-HT efflux that was consistent from 1-5 min (**Figure 6A**). However, at both 1 and 3 min, SERT Ala56 cells supported significantly less 5-HT efflux in response to the D-fenfluramine challenge, amounting to ~60-70% 5-HT efflux, which is 10-20% less than the efflux generated by WT cells (**Figure 6A**). A longer, 5 min incubation with D-fenfluramine,

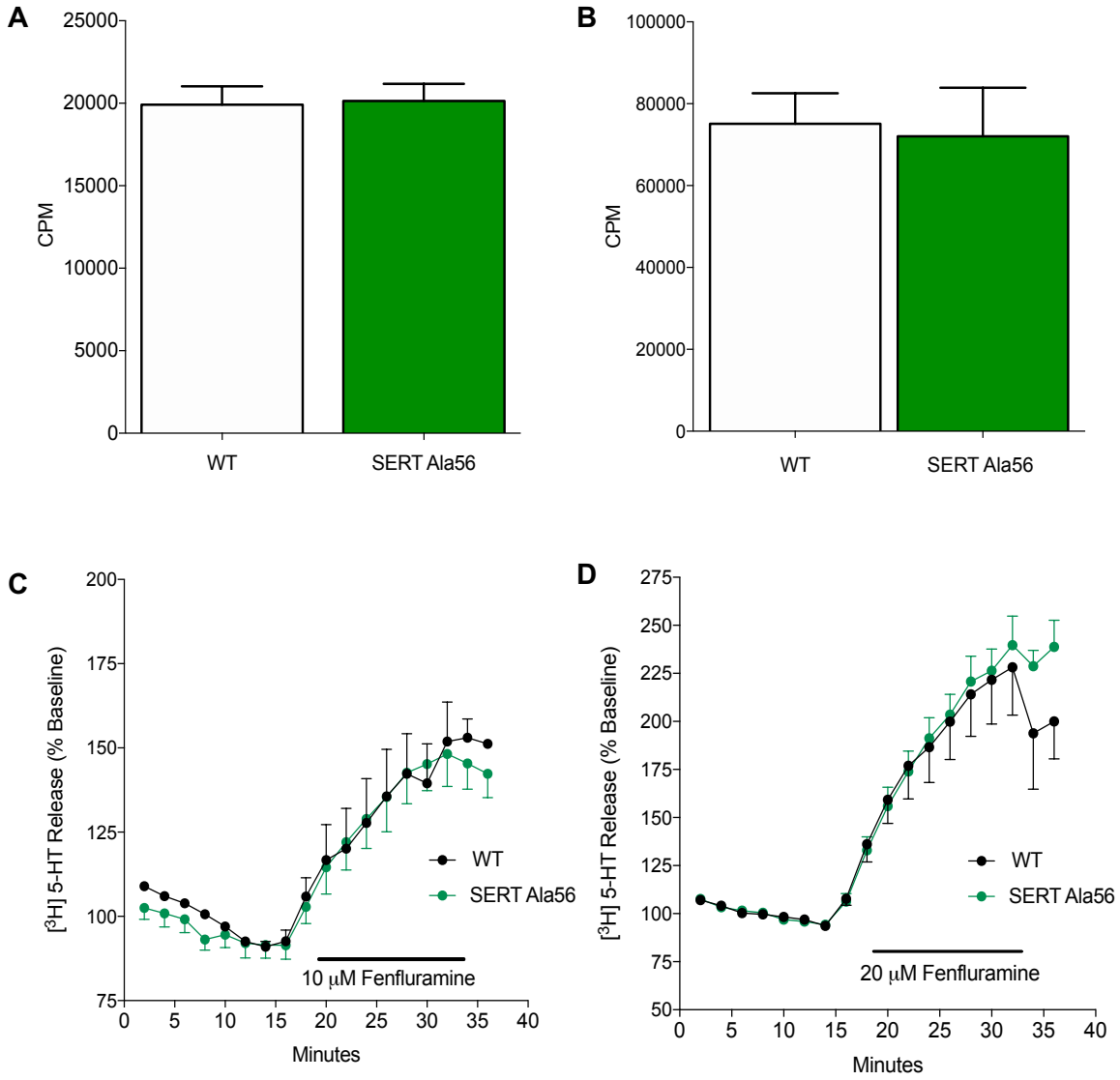

Figure 5. High concentration of D-fenfluramine mediated [^{3}H]5-HT efflux

Equal loading of [^{3}H]5-HT in both (A) Flp-In CHO cells and (B) hippocampal slices (unpaired t-test, n.s., n = 4-5). (C-D) There is also no difference in [^{3}H]5-HT efflux in response to high concentrations, 10 and 20 μM, D-fenfluramine between WT and SERT Ala56 littermate controls (two-way repeated-measures ANOVA; Bonferroni post-hoc test of genotype differences, n.s., n = 4-5).

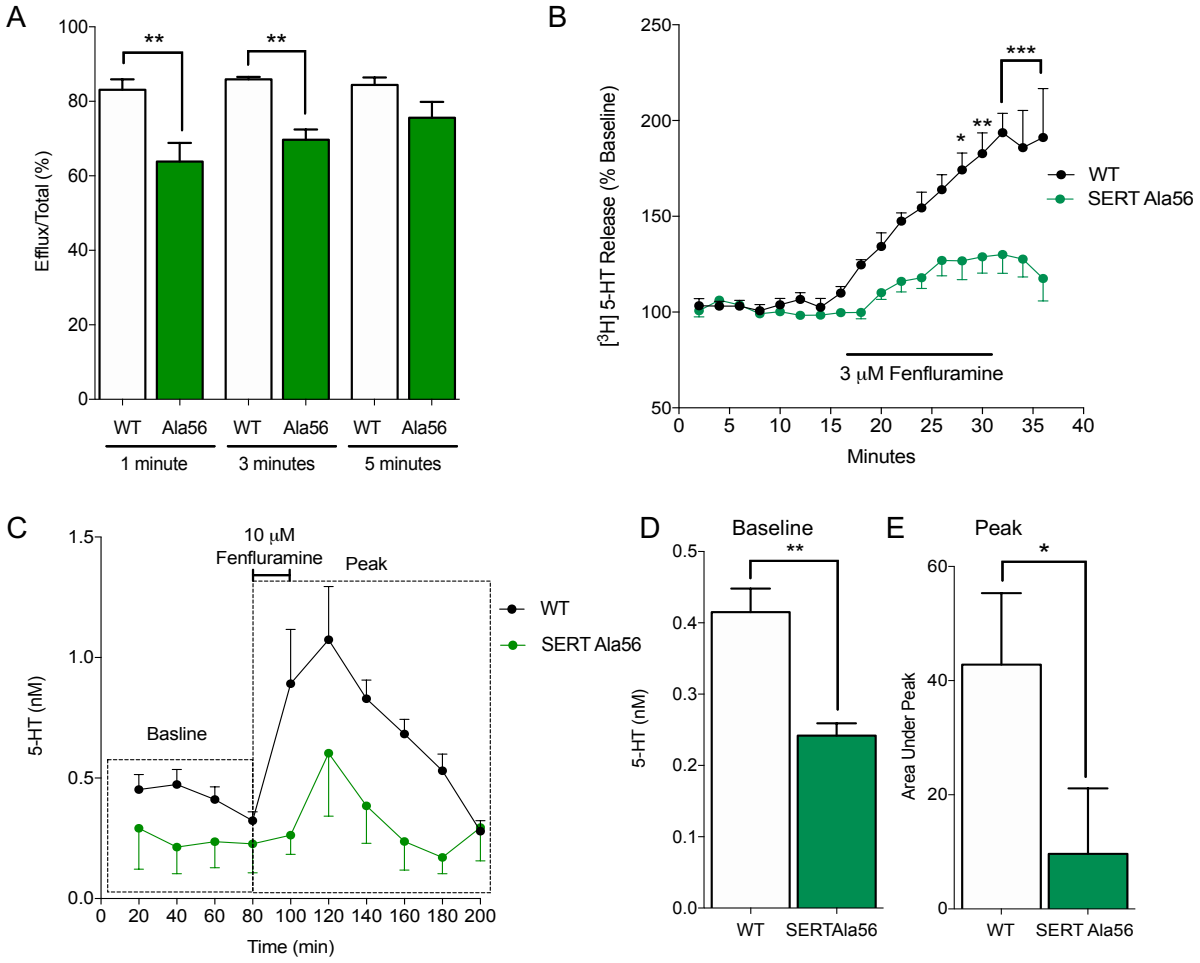

Figure 6. Fenfluramine mediated 5-HT efflux of SERT Ala56

(A) CHO cells stably expressing hSERT (WT) or hSERT Ala56 were loaded for 1 hour with 20 nM [^{3}H]5-HT and then subjected to 10 μM D-fenfluramine for 1,3, or 5 minutes. Cells expressing SERT Ala56 efflux less [^{3}H]5-HT at 1- and 3-min incubation with D-fenfluramine compared to WT expressing cells (two-way repeated-measures ANOVA; Bonferroni post-hoc test of genotype differences, $^{**}P \leq 0.01$; n=4). (B) Hippocampal slices were assessed for D-fenfluramine mediated [^{3}H]5-HT efflux loaded with 400 nM [^{3}H]5-HT for 30 minutes and then perfused with KRB buffer for 15 min to establish baseline followed by 15 min 3 μM D-fenfluramine pulse and then a 15 min wash out with KRB. Slices prepared from SERT Ala56 mice showed a blunted D-fenfluramine mediated [^{3}H]5-HT efflux compared to WT (two-way repeated-measures ANOVA; Bonferroni post-hoc test of genotype differences, $^{*}P \leq 0.05$, $^{**}P \leq 0.01$, $^{***}P \leq 0.001$; n=5). (C) *In vivo* microdialysis data also show SERT Ala56 mice have a significant decrease in extracellular 5-HT levels in response to fenfluramine infusion (10 μM for 20 min at 1mL/min flow rate) compared to WT in CA3 region of the hippocampus. (D) SERT Ala56 shows decreased extracellular 5-HT levels measured at baseline (average from 0-80 minutes, in nM) compared to WT (unpaired t-test; $^{**}P \leq 0.01$; n=7-8). (E) Area under the microdialysis peak from 80-200 min also shows blunted 5-HT efflux in response to D-fenfluramine in SERT Ala56 mice compared to WT (unpaired t-test; $^{*}P \leq 0.05$; n=7-8).

however, resulted in SERT Ala56 efflux reaching WT levels, consistent with reduced kinetic efficiency loading or transporting 5-HT, versus a difference in intrinsic efflux capacity.

To determine whether diminished 5-HT efflux activity is evident in native preparations, we examined the ability of hippocampal slices prepared from WT (SERT Gly56) and SERT Ala56 knock-in (KI) littermate mice to efflux preloaded [^{3}H]5-HT in response to D-fenfluramine. No differences were obtained in total amount of [^{3}H]5-HT accumulated in the cell following our equilibrium loading protocol (**Figure 5B**), consistent with a lack of effect of the SERT Ala56 mutation on transporter protein levels *in vitro* and *in vivo* (Prasad et al., 2005; Veenstra-VanderWeele et al., 2012). At low D-fenfluramine concentrations (3 μM), [^{3}H]5-HT efflux was significantly blunted in slices from SERT Ala56 mice compared to efflux obtained with WT preparations (**Figure 6B**). However, at higher concentrations of D-fenfluramine (10 and 20 μM), equivalent efflux of [^{3}H]5-HT was observed between the WT and variant (Figure 5C-D). These findings are consistent with a biased conformation of SERT Ala56 in the mouse brain slice preparation that is evident at lower substrate concentrations, but negated at higher substrate concentrations. Another explanation for the observed reduced efflux capacity of SERT Ala56 is an altered affinity for fenfluramine, however in a [^{3}H]citalopram competition binding assay from hippocampal membranes, we found no difference between genotypes in fenfluramine affinity (**Figure 7**).

Finally, to test whether genotype differences are evident for D-fenfluramine-induced 5-HT efflux *in vivo*, we assessed extracellular 5-HT levels by microdialysis in the CA3 region of the hippocampus following reverse dialysis of D-fenfluramine *in situ* (Figure 6C). Across the first 80 minutes of collection, we found baseline extracellular 5-HT levels to be decreased in the SERT Ala56 mice, relative to levels in WT mice (**Figure 6D**), consistent with the enhanced basal 5-HT clearance observed in the SERT Ala56 mice in the same brain region (Veenstra-VanderWeele et al., 2012; Robson et al., 2018). It is important to note that past studies have found no difference in total 5-HT levels between genotypes in various brain regions, including the hippocampus (Veenstra-VanderWeele et al., 2012; Robson et al., 2018). At 80 min, we infused 10 μM D-fenfluramine through the dialysis probe, a concentration chosen based on an expectation of ~10% exchange across the dialysis membrane and an effort, established by our *ex vivo*

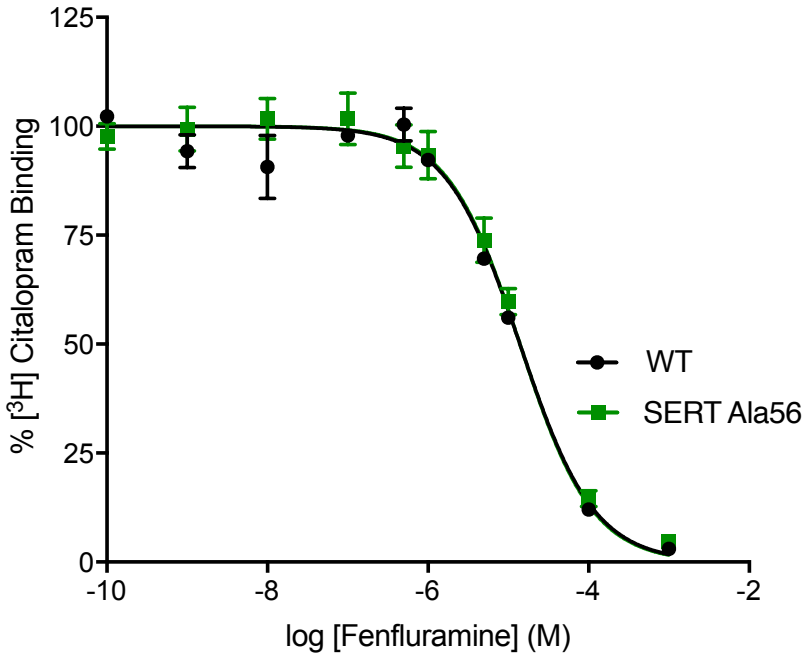

Figure 7. D-fenfluramine competition binding assay with [^{3}H]citalopram
There is no difference between SERT Ala56 and WT mice in fenfluramine (0-1mM) binding as assessed by competition with [^{3}H]citalopram (5nM) binding (two-way repeated-measures ANOVA; Bonferroni post-hoc test of genotype differences, n.s.; n=3).

studies, to deliver a subsaturating D-fenfluramine concentration. As expected (Rocher et al., 1999), we observed a significant time-dependent rise in extracellular 5-HT levels in WT mice. Parallel experiments with SERT Ala56 littermates demonstrated a significantly blunted response to D-fenfluramine compared to WT, analyzed as the area under the peak from 80-200 min, relative to the average baseline calculated for each genotype (**Figure 6E**). These data provide *in vivo* evidence supporting the hypothesis that SERT Ala56 biases transporter conformation, most likely outward-facing, that can promote an enhanced rate of extracellular 5-HT clearance while yielding a reduced rate of D-fenfluramine stimulated 5-HT efflux. These findings are also consistent with prior studies with larger SERT N-terminal deletions revealing that this region is critical in modulating efflux potential (Kern et al., 2017). This observation is further strengthened by studies of the dopamine (DA) and norepinephrine (NE) transporters (DAT and NET, respectively) where findings indicate that amphetamine-induced substrate efflux is influenced by N-terminal residues that can support transporter phosphorylation and or protein interactions (Khoshbouei et al., 2004; Dipace et al., 2007; Binda et al., 2008; Guptaroy et al., 2009).

SERT Ala56 Conformation Assessed through Noribogaine Uptake Inhibition.

Ibogaine, a psychoactive molecule derived from the plant *Tabernathe iboga*, and its active metabolite noribogaine, have been reported to stabilize SERT in an inward-facing conformation (Staley et al., 1996; Jacobs et al., 2007; Bulling et al., 2012). If SERT Ala56 more frequently assumes an outward-facing conformation, the potency of noribogaine could be observed to be reduced. To examine this issue, we determined the potency of noribogaine for inhibition of [^{3}H]5-HT uptake in transporter-transfected CHO cells as described in Experimental Procedures. Since noribogaine is a non-competitive inhibitor of SERT (Koldsø et al., 2013), work by Cheng and Prusoff (Cheng and Prusoff, 1973) indicates that the IC_{50} equals the K_i and is not dependent on the K_M of the transporter, which is important considering that SERT Ala56 demonstrates a decreased 5-HT K_M compared to WT SERT (Prasad et al., 2009). We found that the IC_{50} for noribogaine to block 5-HT uptake from hSERT transfected CHO cells was modestly, but significantly, increased for SERT Ala56 as compared to WT SERT (SERT Ala56 = 0.507 nM; $R^2 = 0.91$; 95% CI [0.37,

0.68]; WT SERT = 0.315 nM; R^2 = 0.87; 95% CI [0.22, 0.45]; $P \leq 0.05$), consistent with the mutant transporter having an increased probability to rest in an outward-facing conformation during noribogaine binding.

SERT Ala56 Impact on Cytoplasmic Domain Apposition Assessed by Fluorescence Resonance Energy Transfer.

Fluorescence resonance energy transfer (FRET) approaches allow for a measurement of the relative distance between proteins or their domains (Piston and Kremers, 2007), with caveats relating to the orientation of fluorophores potentially appearing as changes in distance (Berney and Danuser, 2003). Biochemical and modeling studies indicate that as biogenic amine transporters cycle from inward to outward-facing conformations, the N- and C-termini move closer to each other (Schicker et al., 2012; Fenollar-Ferrer et al., 2014). We hypothesized that if SERT Ala56 biases the transporter toward an outward-facing conformation, the N- and C-termini of SERT should more often lie closer together than with WT SERT, which might be evident with FRET studies of dually-tagged transporters. We, therefore, transfected CHO cells individually with either WT or SERT Ala56 constructs that were tagged with a cyan fluorescent protein (CFP) and a yellow fluorescent protein (YFP), on the N- and C-termini, respectively. The dual addition of CFP and YFP (C-SERT-Y) did not compromise the ability of Ala56 to elevate 5-HT uptake (**Figure 8A**), nor alter protein expression levels, as assessed by western blot analysis (**Figure 9**). Unfortunately, we were not able to verify equivalent surface expression of the tagged mutant and WT SERT constructs due to, we believe, the low levels of expression or loss of antibody epitope at the surface. However, past studies did reveal that untagged SERT Ala56 did not alter SERT surface expression compared to WT SERT in transfected cells (Sutcliffe et al., 2005). Also, the total protein of C-SERT-Y constructs detected in cells migrated as expected of mature, glycosylated SERT, so we do not believe that the tagged constructs are misfolded, although we cannot rule out that a greater propensity for this leads to more of the transporter being degraded. As predicted, cells transfected with C-Ala56-Y demonstrated a

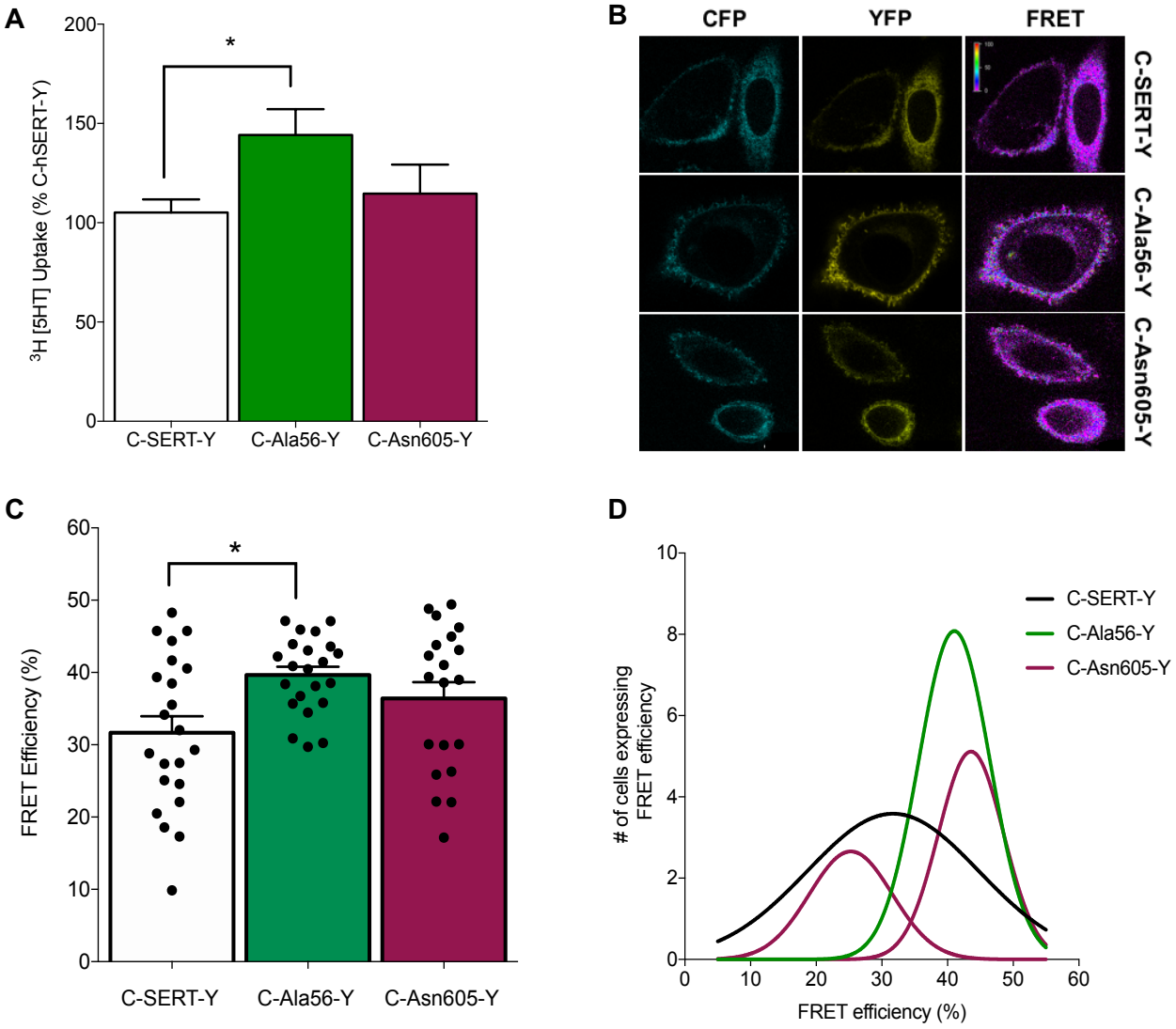

Figure 8. FRET efficiency of SERT N- and C-terminal proximity

(A) The addition of CFP and YFP tag to the N & C-terminus respectively, does not impact the ability to SERT Ala56 to enhance [^{3}H]5-HT uptake (20 nM for 10 min at 37°C in transfected CHO cells), one-way ANOVA followed by Tukey's post-hoc test, *$P \leq 0.05$, n= 6-9; Error bars represent ± SEM. (B) Representative FRET images of transfected CHO cells with indicated CFP-YFP dual tagged constructs with CFP excitation/emission, YFP excitation/emission, calculated FRET efficiency (CFP excitation/YFP emission). (C) FRET efficiency, calculated as described in Methods. (Error Bars ± SEM, One-way ANOVA followed by Tukey's post hoc test, *$P \leq 0.05$, n=22). (D) Histogram of FRET efficiency show C-Ala56-Y distribution is significantly shifted to the right compared to WT (Kruskal-Wallis ANOVA followed by Dunn's post hoc analysis, $P \leq 0.05$, n=22) and C-Asn605-Y split into two Gaussian's curves.

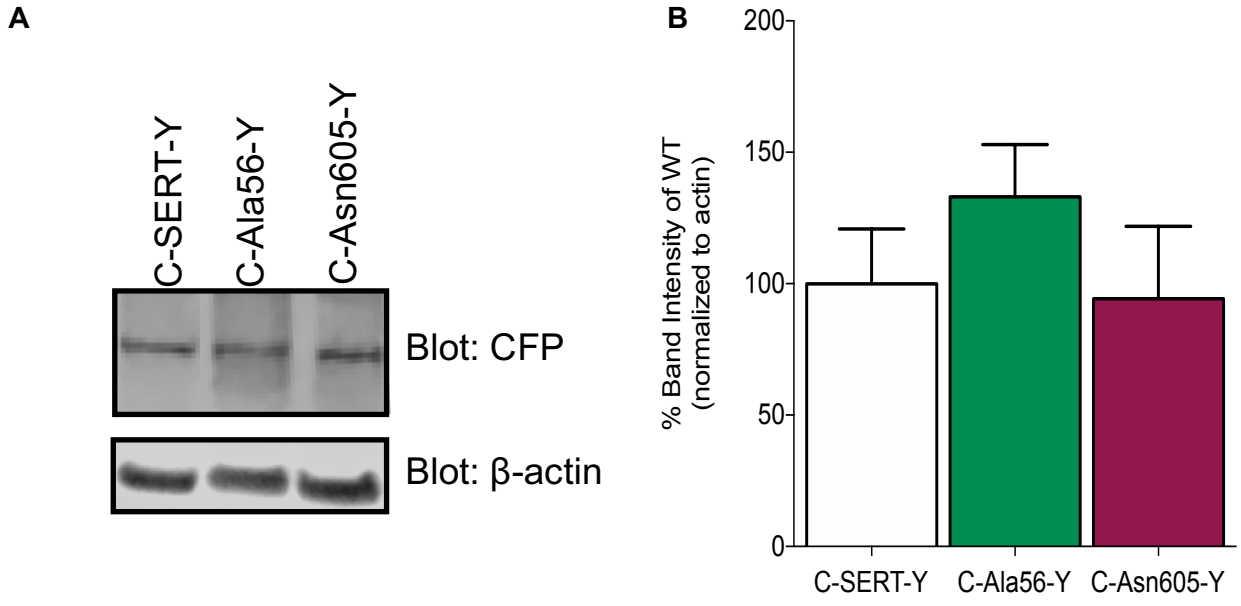

Figure 9. Western blot of total C-SERT-Y and variant constructs

(A) Representative immunoblot of C-SERT-Y constructs probed with CFP antibody. (B) No difference between C-SERT-Y, C-Ala56-Y, and C-Asn605-N total protein expression as assess by densitometry of western blot bands normalized to β-actin levels (ordinary one-way ANOVA, followed by Dunnett's post-hoc analysis, n.s., P>.05, n= 4-7)

significant increase in FRET efficiency compared to cells transfected with WT C-SERT-Y (**Figure 8B-C**). Moreover, a population analysis of the distribution of FRET efficiency from C-Ala56-Y transfected cells revealed a much tighter distribution than observed for C-SERT-Y (**Figure 8D**).

The naturally-occurring, C-terminal SERT coding substitution Lys605Asn (SERT Asn605) was also found to be transmitted to affected probands in our prior ASD study (Sutcliffe et al., 2005). As shown in our previous work, this variant demonstrates normal 5-HT uptake activity in transfected cells, but like the Ala56 variant, exhibits a complete insensitivity to PKG and p38 MAPK stimulation (Prasad et al., 2005). When the C-SERT-Y construct bearing the Lys605Asn substitution was transfected into CHO cells, we detected no difference from C-SERT-Y in resulting 5-HT uptake (**Figure 8A**) nor did we observe an increase in the average FRET signal (**Figure 8B-C**). However, the sum of two Gaussians better fit the distribution of C-Asn605-Y FRET efficiencies (**Figure 8D**) than a single distribution (two-tailed unpaired t-test; $P \leq 0.001$), with the distribution associated with greater FRET efficiencies underlying the distribution that fits the C-Ala56-Y data. These findings suggest that SERT Asn605 may populate one of two distinct conformations, either outward-facing or inward facing, with a limited population of intermediate states, unlike WT SERT. We do not know whether the conformations that these ASD associated variants confer are mimicked in FRET assays using WT SERT treated with compounds that alter SERT conformation and activity, such as fenfluramine or noribogaine, but consider this an important future study.

Sensitivity of 5-HT Transport to Methanethionsulfonates Supports an Increased Propensity for both SERT Ala56 and SERT Asn605 to Reside in an Outward-facing Conformation.

The Substituted Cysteine Accessibility Method (SCAM) (Karlin et al., 1998), where the aqueous exposure of cysteine (Cys) residues of functional relevance are queried using inactivating methanethiosulfonate (MTS) reagents, has been commonly used to infer conformation of transporter domains, including those belonging to SERT (Sato et al., 2004; Zhang and Rudnick, 2005b; Henry et al., 2006, 2011; Rudnick, 2011). In SERT, the rate of transport inactivation achieved by a membrane permeant MTS reagent such as MTSEA, at an engineered Cys (Ser277Cys) in intracellular loop 2 (ILC2) (substituted

on an otherwise reactive Cys depleted transporter (SERT X5C)), provides a quantitative estimate of transporters present in inward-facing conformations (Zhang and Rudnick, 2005b, 2006). When we compared the sensitivity of SERT X5C to SERT X5C/Cys277 to MTSEA in transfected HEK-MSR cells, we found the expected increase in transport inactivation for the latter construct due to the addition of solvent exposed Cys277 in a loop critical for conformational cycling (**Figure 10A and D**). On the X5C/Cys277 background, substitution of either Ala56 or Asn605 for their WT counterparts rendered the Cys277 residue on these transporters less sensitive to MTSEA than SERT X5C/Cys277 (**Figure 10A and D**), consistent with the terminal variants having a reduction in the population of inward-facing conformations. Inactivation of 5-HT uptake at the endogenous residue Cys109 by a membrane impermeant MTS reagent, such as MTSET or MTSES, has been used successfully to indicate the fraction of transporters in an outward-facing state (Chen et al., 1997). When the sensitivity to MTSES or MTSET of WT SERT (containing Cys109) was compared to SERT Ala56 (**Figure 10B-D**), we observed an increased rate of inactivation of the latter construct by both MTS reagents. These findings support an increased propensity for Cys109 in either the Ala56 or the Asn605 constructs to reside in an outward-facing conformation across the duration of the assay. Together, the SCAM analysis assessed the exposure of conformationally-sensitive Cys residues and provided evidence that the conformational equilibrium of both naturally-occurring SERT coding variants shifts to favor an outward-facing state.

Evidence from Limited Proteolysis Studies that SERT Ala56 and SERT Asn605 Favor Outward-Facing Conformations.

The data presented thus far suggest that the Ala56 and the Asn605 variant SERT proteins exhibit a global change in structure that favors an open-outward conformation. SERT is a large, 630 amino acid protein, comprised of 12 transmembrane domains and cytoplasmic N- and C-termini (Ramamoorthy et al., 1993). Given the location of SERT Ala56 in the N-terminus, it seemed unlikely to us that, without a local structural alteration, the single methyl group that distinguishes Ala56 from Gly56 (WT) would be able to exert global, conformational effects. Gly56 lies in a region of the N-terminus predicted to be unfolded,

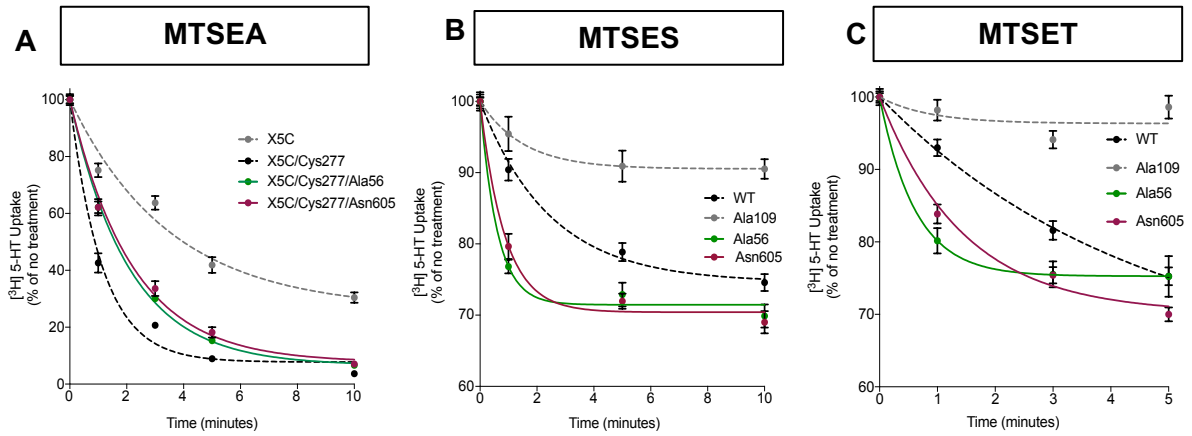

D

MTSEA		MTSES		MTSET	
Construct	**$T_{1/2}$ (min)**	**Construct**	**$T_{1/2}$ (min)**	**Construct**	**$T_{1/2}$ (min)**
X5C/Cys277	0.81± 0.11	Cys109	1.77 ± 0.17	Cys109	3.34 ± 0.44
X5C	2.47± 0.18***	Cys109Ala	2.75 ± 0.19*	Cys109Ala	0.51 ± 0.1***
X5C/Cyc277/Ala56	1.43 ± 0.06**	Ala56	0.43 ± 0.05***	Ala56	0.52 ± 0.12***
X5C/Cyc277/Asn605	1.56 ± 0.18**	Asn605	0.64 ± 0.12**	Asn605	1.02 ± 0.13**

Figure 10. Sensitivity of N and C termini ASD SERT variants to MTS inactivation of uptake supports outward-facing conformation

(A) To determine accessibility of the cytoplasmic permeation pathway HEK-MSR cells expressing terminal ASD-associated mutants (SERT Ala56 and Asn605) in the S277C/X5C background were treated with 2 mM MTSEA for the indicated time. Following treatment, cells were assayed for [^{3}H]5-HT uptake (50 nM for 10 min at 37°C). Remaining activity is plotted as a percent of untreated cells and the values represent the mean ± SEM from four or more independent experiments. SERT Ala56 and Asn605 were less sensitive to MTSEA inactivation, suggesting that Cys277 was less accessible. (B&C) Cys109, located on the extracellular end of TM1, is an extracellular probe for the membrane impermeant thiol-reactive reagent, MTSES (B) and MTSET (C). Both the terminal ASVs (SERT Ala56 and Asn605) are more sensitive to MTSES and MTSET inactivation, suggesting that Cys109 is more accessible in these mutants compared to control cells. (D) Table with time for MTS reagent to decrease total 5-HT uptake in each mutant by 50% ($t_{1/2}$). One-way ANOVA, Dunnett's, *$P \leq 0.05$, **$P \leq 0.01$, ***$P \leq 0.001$, n=8.

possibly allowing conformational alterations of this domain during and throughout the transport cycle (Fenollar-Ferrer et al., 2014). Alternatively, N-terminal interacting proteins could stabilize conformations locally and globally by differentially interacting with the Ala56 substituted domain. To examine mutation-induced changes in local N-terminal conformation, we implemented a trypsin accessibility protocol (Fontana et al., 2004) using membranes from CHO cells transfected with either WT or mutant SERTs. An N-terminal HA tag was present in WT and mutant constructs to allow us to monitor exposure and trypsin digestion of the N-terminus as a function of time. Importantly, the N-terminus of SERT has been reported to demonstrate differential sensitivity to trypsin cleavage as a result of ionic, substrate or antagonist interactions (Kern et al., 2017), with the N-termini of outwardly-oriented transporters being relatively protected against trypsin digestion. As shown in **Figure 11A**, HA-tagged SERT Ala56 demonstrated a greater degree of trypsin resistance as compared to HA-tagged WT SERT. Interestingly, the HA-tagged SERT Asn605 variant also displayed significantly reduced N-terminal trypsin sensitivity (**Figure 11B**).

Whether a global change in conformation impacts the structure of the N-terminus or vice-versa, cannot be assessed from the trypsin sensitivity data noted above. However, previous studies (Kern et al., 2017) have demonstrated that the presence or absence of NaCl alters N-terminus trypsin sensitivity in a manner that might be useful to distinguish whether the SERT Ala56 exerts conformational effects independent of changes in global structure. In support of this idea, the N-terminus of WT SERT exhibits reduced trypsin sensitivity when Na^+ in the buffer is substituted with impermeant cations, presumably due to a requirement for Na^+ interactions at the intramembrane substrate binding site to stabilize transporters in an open-outward conformation (Kern et al., 2017). We, therefore, evaluated the trypsin sensitivity of WT HA-SERT and HA-SERT Ala56 in media where Na^+ was substituted by choline chloride (ChCl). In these studies, we found that the N-terminus of HA-SERT Ala56 remained less trypsin-sensitive than WT HA-SERT, despite the absence of Na^+ (**Figure 11C**). These findings indicate that the Ala56 substitution imposes local changes in conformation of the SERT N-terminus and/or the differential binding of associated proteins to this domain, in addition to the more global conformational changes revealed by measures of 5-HT uptake/efflux, FRET or transporter functional inactivation by MTS reagents.

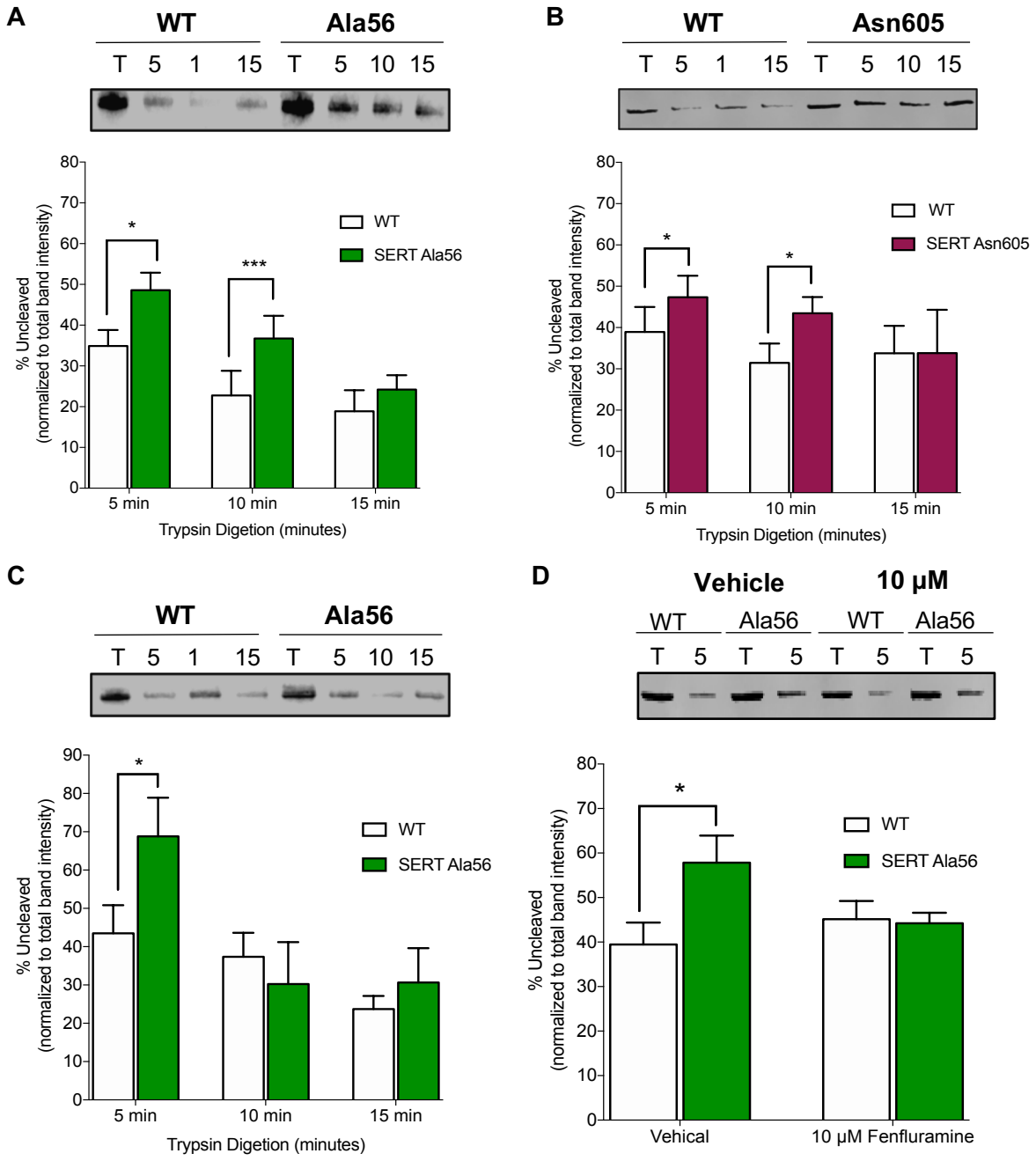

Figure 11. Tryptic digestion of the N-terminus of terminal ASD SERT coding variants

Membranes (50 µg total) isolated from CHO cells expressing (A) HA-SERT or HA-SERT Ala56 or (B) HA-SERT Asn605 were incubated in buffer containing 150 mM NaCl. Trypsin (4 µg) was added at room temperature for 5, 10, or 15 minutes. Samples were subjected to western blot analysis of HA tag. Percentage of SERT cleaved by trypsin was calculated by dividing the band density of the trypsin sample by the total (labeled as "T" on blot). (Error bars indicate ± SEM Paired t-test. $*P \leq 0.05$, $**P \leq 0.01$, n=6-9). (C) Ionic substitution of NaCl with 150 mM ChCl did not affect the increased protection of SERT Ala56 N-terminal tryptic digestion at 5 min. Paired t-test. $*P \leq 0.05$, n=6-9. (D) Addition of 10 µM D-fenfluramine to membranes normalized SERT Ala56 digestion to WT levels at 5 min (Paired t-test. $*P \leq 0.05$, n =10).

Finally, we explored the effects of D-fenfluramine at saturating concentrations on the protection of the SERT N-terminus to tryptic digestion (in the presence of NaCl). We found that the addition of 10 μM D-fenfluramine to membrane preparations had no effect on proteolysis of WT SERT (**Figure 11D**), consistent with findings of Kern and colleagues using the SERT-targeted amphetamine, *p*-chloroamphetamine (Kern et al., 2017). However, D-fenfluramine incubation with HA-SERT Ala56 expressing membranes increased N-terminal trypsin sensitivity to that seen with WT HA-SERT (**Figure 11D**). These findings indicate that the binding of substrates to SERT is sufficient to relieve N-terminal conformational changes induced by SERT Ala56, suggesting bi-directional communication between the N-terminus and residues forming the substrate binding pocket.

Discussion

Altogether, the studies in our report reveal a remarkable ability of small changes in the sequence of cytoplasmic N- and C-termini to affect both local and global SERT conformations. SERT Ala56 confers elevated 5-HT uptake at sub-saturating substrate concentrations relative to WT SERT, mimicking transient 5-HT transport changes following PKG and p38 MAPK activation (Zhu et al., 2004, 2005). Consistent with this idea, SERT Ala56 (as well as SERT Asn605) interferes with the ability of PKG and p38 MAPK activators to elevate transporter activity further (Prasad et al., 2005, 2009). Ala56 lies in the middle of the N-terminus, which has the potential, based on models, to interact with intracellular loop 2 (ICL2) that lies between transmembrane domains 4 and 5. ICL2 has been shown to be conformationally dynamic and bears a site, Thr276, that becomes phosphorylated following PKG activation (Ramamoorthy et al., 2007; Zhang et al., 2016; Bailey et al., 2018). Thr276 has been shown to be phosphorylated in the inward-facing conformation upon the activation of PKG which leads to enhanced uptake kinetics (Blakely et al., 1998; Ramamoorthy et al., 1998, 2007). Because SERT Ala56 is insensitive to increase 5-HT uptake upon PKG activation, we speculate that the Ala56 substitution alters an N-terminus:ICL2 interaction to bias conformation in a manner similar to that arising from PKG-dependent Thr276 phosphorylation. Such a model can explain the reduction in 5-HT K_M observed with SERT Ala56 (Prasad et al., 2009). The ability

of the Ala56 substitution to induce N-terminal conformational changes, along with the ability of p38α MAPK inhibition to reduce SERT Ala56 hyperphosphorylation and hyperactivity (Prasad et al., 2005; Veenstra-VanderWeele et al., 2012; Robson et al., 2018), suggests that the phosphorylation of one or more sites, such as Thr276, arises following changes in either N-terminal conformation or kinase activation. Further studies are needed to identify these sites and examine their responsiveness to changes in N-terminus structure.

Surprisingly, the Asn605 substitution of the SERT C-terminus impacts both the sensitivity of the N-terminus to trypsin and biases the transporter globally to an outward-facing conformation as seen with the Ala56 variant, without increasing 5-HT uptake. Our FRET studies indicate that the C-terminal mutation may stabilize SERT in either outward-facing or inward-facing conformations, though this results in no net gain in 5-HT uptake. Nonetheless, the Asn605 mutation imparts, like Ala56, an insensitivity of SERT to activators of both PKG and p38 MAPK. A putative p38 MAPK site has been identified in the SERT C-terminus at Thr616 (Sørensen et al., 2014). Interestingly, Asn605 lies in a critical alpha helical loop which interacts with ICL1 to promote proper folding of SERT in an inward-facing conformation ready to traffic to the surface (Koban et al., 2015).

A model worth exploring further is that SERT Ala56 facilitates transporter phosphorylation, such as at Thr276, that stabilizes an outward-facing conformation whereas the Asn605 substitution has bimodal conformational effects, one that enhances N- and C-terminal interactions to stabilize an outward-facing conformation, and another that disrupts p38 MAPK phosphorylation of the C-terminus, stabilizing an inward-facing conformation. Clearly, additional biochemical, structural and modeling studies are needed to clarify these possibilities. Regardless, our findings reveal a capacity for relatively small changes in SERT cytoplasmic domains to drive alterations in transporter conformation, underlying functional and regulatory changes.

Methods

Animals and Materials

All experiments using animal subjects were conducted according to the National Institutes of Health Guide for the Care and Use of Laboratory Animals. All experiments involving animal subjects were conducted as pre-approved by the Vanderbilt University and Florida Atlantic University Institutional Animal Care and Use Committees. SERT Ala56 and SERT Gly56 (WT) littermate males (129/sv background) 8-12 weeks old were generated from heterozygous breeding. Mouse genotyping was conducted as previously described (Veenstra-VanderWeele et al., 2012). All reagents, salts and buffers, unless otherwise specified, were obtained from Sigma-Aldrich (St. Louis, MO, USA).

CHO Cell Culture and Transfection

Chinese hamster ovary (CHO) cells used for transfection of human SERT (hSERT) constructs were obtained from the American Type Culture Collection (ATCC, Manassas, VA, USA) maintained in Dulbecco's Modified Eagle's Medium (DMEM, Invitrogen, Carlsbad, CA, USA), 10% fetal bovine serum (FBS; Thermo Fisher, Waltham, MA, USA) 2 mM L-glutamine, 100 units/mL penicillin and 100 µg/mL streptomycin at 37°C in a 5% CO_2 humidified incubator.

Culture of the stably expressing Flp-In^{TM}-Cho hSERT and hSERT Ala56 were used as described in Prasad et al. 2009. However, to overcome the lower total and surface expression of SERT Ala56 compared to WT, which is believe to be due to 5-HT levels in the FBS in the media (although not shown directly), cells were grown as described above except the DMEM was supplemented with dialyzed FBS (Cat # F0392, Millipore Sigma, Burlington, MA, USA).

D-fenfluramine-Mediated [^{3}H]5-HT Efflux

In vitro D-fenfluramine release, Flp-In^{TM}-CHO-stable cell lines expressing SERT Ala56 or WT SERT, previously described,(Prasad et al., 2009) were plated at 100,000 cells per well on a 24 well poly-D

lysine coated plate. At 24-48 hrs after plating, cells were washed 2X with warmed Krebs-Ringers-HEPES (KRH) assay buffer (130 mM NaCl, 1.3 mM KCl, 2.2 mM $CaCl_2$, 1.2 mM $MgSO_4$, 1.2 mM KH_2PO_4, 10 mM HEPES, 10 mM glucose, 100 µM pargyline, 100 µM ascorbic acid, pH 7.4) and then loaded with 20 nM [^{3}H]5-HT (Hydroxytryptamine Creatinine Sulfate; Specific activity 28 Ci·mmol^{-1}; Perkin-Elmer, NET498, Waltham, MA, USA) for 1 hr at 37ºC followed by 2X wash with warmed KRH to remove excess [^{3}H]5-HT. Cells were then subjected to 500 µL total volume of 10 µM D-fenfluramine or vehicle for the indicated time. The supernatant was then collected and 0.1% SDS was added to the wells to lyse the cells to account for unreleased [^{3}H]5-HT. 250 µL of EcoScint XR scintillation fluid (National Diagnostics, Atlanta, GA, USA) was added to the supernatant and the cell lysates and counted using a TriCarb 2900TR scintillation counter (Perkin-Elmer, Waltham, MA, USA). Efflux was calculated by the counts in supernatant divided by the total number of counts (supernatant + cell lysis) in both the presence and absence of D-fenfluramine. To obtain D-fenfluramine mediated efflux, efflux in the absence of D-fenfluramine was subtracted from efflux in the presence D-fenfluramine. Data were analyzed by an ordinary one-way ANOVA followed by Sidak's multiple comparison test of genotype differences.

Ex vivo D-fenfluramine induced [^{3}H]5-HT efflux was conducted as previously described (Ansah et al., 2003). Briefly, the hippocampus of a mouse was dissected after rapid decapitation and chopped on a cold plate into ~300 µm slices with a razor blade. Slices were placed in 300 µL of oxygenated Krebs' Ringer Bicarbonate (KRB) buffer (126 mM NaCl, 2.5 mM KCl, 2.4 mM $CaCl_2$ 1.2 mM $MgCl_2$, 1.2 mM NaH_2PO_4, 10 mM D-glucose, and 21.4 mM $NaHCO_3$, pH 7.4) supplemented with 50 µM pargyline, 50 µM ascorbic acid, and 10 nM nisoxetine and 100nM nomifensine to block NET and DAT, respectively. The slices were incubated with 400 nM [^{3}H]5-HT for 30 minutes at 37°C. The slices were then loaded into the perfusion chamber of the Brandel SF-12 Suprafusion system (Brandel, Gaithersburg, MD, USA), sandwiched between GF/B glass fiber filter discs (Whatman, Maidstone, UK). Chambers containing filter-immobilized brain slices were perfused at a flow rate of 0.7 mL/min with oxygenated KRB buffer for 45 min to remove unloaded [^{3}H]5-HT. Then samples were collected every 2 minutes, with the first 16 min used to establish baseline release, followed by a 16 min perfusion with the indicated concentration of D-fenfluramine, and

then an 8 min wash out with KRB buffer. At the end of the experiment, the filters and tissue were collected and lysed in 2 mL of 20% SDS. Five mL of EcoScint XR scintillation fluid (National Diagnostics, Atlanta, GA, USA) was added to each fraction and radioactivity was counted using a TriCarb 2900TR scintillation counter (Perkin-Elmer, Waltham, MA, USA). Data for release is presented as a fraction of the total [^{3}H]5-HT loaded into each sample (amount released + amount remaining in the tissue), normalized as a percent of baseline. Two-way repeated measure ANOVA followed by Bonferroni post-hoc test of genotype differences was used to analyze statistical significance.

D-fenfluramine Competition Binding Assay with [^{3}H]Citalopram

Hippocampal membrane samples from SERT Ala56 mice and their WT littermate controls were prepared as previously described (Veenstra-VanderWeele et al., 2012). Briefly, after rapid decapitation, the hippocampus was extracted and homogenized utilizing a Teflon-glass homogenizer in 3 mL of 50 mM Tris, pH 7.4 followed by a 20-minute centrifugation at 15,000 X *g*. The resulting pellet was washed again in 50 mM Tris, pH 7.4 and re-centrifuged for 20 minutes at 15,000 X *g*. The supernatant was discarded and the pellet was resuspended in 50 mM Tris with 120 mM NaCl, pH 7.4. 200 µg of membranes were preincubated with various concentrations of fenfluramine (0.1 nM, 1 nM, 10 nM, 100 nM, 500 nM, 1 µM, 5 µM, 10 µM,100 µM, 1 mM) for 10 min at 37°C followed by the addition of 5 nM [^{3}H]citalopram (Perkin Elmer, Specific activity 74.5 Ci·mmol^{-1}, NET1039, Waltham, MA, USA) for 1 hr at room temp. Samples were then harvested using a Brandel 48-sample Harvester (Brandel, Gaithersburg, MD, USA) onto GF/B Whatman filters (Whatman, Maidstone, UK). The filters were washed three times with ice-cold PBS buffer and then placed into 7 mL of EcoScint H scintillation fluid (National Diagnostics, Atlanta, GA, USA) overnight. Radioactivity was counted using a TriCarb 2900TR scintillation counter (Perkin-Elmer, Waltham, MA, USA). Binding was calculated and the non-linear fit of log IC_{50} inhibition was calculated using Prism 7.

In Vivo Microdialysis Assessment of D-fenfluramine Mediated 5-HT Efflux

Mice were anesthetized with isoflurane and placed in a stereotaxic frame using mouse-specific ear bars (Kopf Instruments, Tujunga, CA, USA). A guide cannula (Synaptech, Marquette, MI, USA) was placed 1 mm above the dorsal hippocampus (-1.94 AP from Bregma, ± 2.0 ML and -1.0 DV from dura and secured to the skull with glass ionomer cement (Instech Solomon, Plymouth Meeting, PA, USA). After recovery from surgery, animals were placed in individual dialysis chambers. A microdialysis probe (Synaptech, Marquette, MI, USA) with the active length of 1 mm was inserted into the guide cannula. One end of the tether was attached to the headpiece and the other end attached to a liquid swivel (Instech Solomon, Plymouth Meeting, PA, USA) that was mounted on a counterbalanced arm above the dialysis chamber. The probe was perfused at a flow rate of 1.0 µL/min with artificial cerebral spinal fluid (aCSF) containing 149 mM NaCl, 2.8 mM KCl, 1.2 mM $CaCl_2$, 1.2 mM $MgCl_2$, pH 7.2 at a flow rate of 1.0 µL/min overnight. On the day of the experiment, four baseline dialysis fractions (20 min each) were collected. After the 4th baseline, sample the aCSF was switched to aCSF containing 10 µM D-fenfluramine for 20 min. Dialysate samples were stored at -80°C and analyzed by HPLC-EC for 5-HT levels. After the dialysis session, animals were overdosed with sodium pentobarbital, brains removed and post-fixed in 4% paraformaldehyde in 0.1 M phosphate buffer, sectioned, stained, and examined for acceptable probe placement. Extracellular 5-HT levels from 0-80 min at the beginning of the experiment are reported as "Baseline Levels" and reported in nM concentration. The area under the peak was calculated utilizing Prism 7 "Area Under the Curve" function taking the mean from 0-80 min as the baseline for each genotype.

5-HT Transport Assay in SERT Transiently-Transfected CHO Cells

CHO cells were plated on clear bottom 96 well poly-D lysine coated plates at 20,000 cells per well. The next day, cells were transfected with 0.1 µg of DNA per well utilizing TransIT®-LT1 (Mirus, Madison, WI, USA). Forty-eight hours later, cell culture media was removed and plates were washed 3X with 300 µL warmed phosphate buffered saline (PBS) with an ELX microplate washer (Biotek, Winooski, VT, USA). [^{3}H]5-HT uptake assays were performed in 200 µL final volume of KRH assay buffer. Inhibitors

were added and incubated at 37ºC for 10 min followed by the addition of 20 nM (final concentration) [^{3}H]5-HT. For the uptake inhibition studies, noribogaine HCL was custom manufacture under cGMP conditions performed by Ajimoto Omnichem (Lot number: 606950001). Eight serial dilutions of noribogaine from 10 mM to 1 nM were used. After 10 min at 37°C, transport assays were stopped by rapid wash 3X with ice-cold PBS using the ELX microplate washer. MicroScint scintillation cocktail (200 µL) was added to each well and agitated for 1 hr. Counts representing total and non-specific 5-HT uptake were measured using a MicroBeta2 Microplate counter (Perkin-Elmer, Waltham, MA, USA). Specific uptake was determined by subtracting the counts from wells incubated with 10 µM paroxetine for 10 min at 37°C prior to the addition of [^{3}H]5-HT. The non-linear fit of log IC_{50} inhibition was calculated using Prism 7 to determine statistical significance.

Assessment of SERT N- and C-termini Apposition using Fluorescence Resonance Energy Transfer (FRET)

CFP, YFP, CFP-YFP, and CFP-SERT-YFP constructs were generously provided by Sonja Sucic and Harald Sitte, Medical University of Vienna. CFP-Ala56-YFP and CFP-Asn605-YFP constructs were generated from these vectors using the Q5 site-directed mutagenesis kit (New England Biolabs, Ipswich, MA, USA). Each construct was individually transfected into CHO cells plated (20,000 cells per dish) onto 35 mm MatTek poly-d-lysine coated dishes (No. 1.5 cover glass, Ashland, MA, USA). Cells were washed 2X with warmed PBS and then imaged in KRH buffer over 5 min in a Tokai Hit Stage top incubator set to 37ºC and 5% CO_2. We used a 60X oil immersion objective (Plan Apo Lambda, NA 1.4) on an A1R confocal Ti inverted microscope at the Florida Atlantic University Cell Imaging Core. All FRET images were captured utilizing the FRET plugin of NIS Elements Imaging Software (Nikon, Tokyo, Japan). The scan head dichroic mirror optical configurations were set up to acquire the donor alone (Dd: excite CFP at 440nm and dichromatic mirror set to capture CFP 485/35 nm), acceptor alone (Aa; excite YFP at 514 and dichromatic mirror set to capture YFP at 538/33 nm), FRET (Da; excite CFP at 440 nm and dichromatic mirror set to capture YFP at 538/33nm) and bleed through (Ad; excite YPF at 514 nm and dichromatic mirror set to capture CFP 485/35 nm). Negative controls of CFP and YFP constructs were imaged alone to

acquire CoA (Acceptor in FRET or $Da_{ACCEPTOR}$) and CoB (Donor in FRET or Da_{DONER}). As a positive FRET control, a fused CFP-YFP construct was also imaged. Images were thresholded manually to regions of interest that were defined by the membrane of the cells and the corrected FRET (Corr FRET) and FRET efficiency (FRET eff) for each image was averaged over the 5 min by the FRET plugin in NIS Elements as followed:

$$\text{Corr FRET} = [Da_{FRET} - Dd_{FRET} \text{ X } (Da_{Doner}/Dd_{Doner}) - Aa_{FRET} \text{ X } (Da_{ACEPTOR}/Aa_{ACEPTOR})] / Dd_{FRET}$$

$$\text{FRET Eff} = \text{Corr FRET} / Dd_{FRET} * 100$$

Total expression of C-SERT-Y and variant constructs were assessed by western blot analysis. Briefly, CHO cells were lysed in RIPA buffer (50 mM Tris, pH 7.4, 150 mM NaCl, 1 mM EDTA, 1% Triton X-100, 1% sodium deoxycholate, 0.1% SDS) for 1 hr at 4° C and then centrifuged for 20 min at 17,000 X *g*. 50 µg of the resulting supernatant was incubated with 4X Laemmle buffer (Bio-Rad Laboratories, Hercules, CA, USA) at room temp for 30 min and then separated on a NuPAGE 10% Bis-Tris protein gel (Invitrogen, Carlsbad, CA, USA) and transferred to Immobilon-FL PVDF membrane (Millipore Sigma, Burlington, MA, USA). Protein was visualized by immunoblotting with a rabbit-CFP antibody (BioRad, Hercules, CA, USA) then probed with IRDye 680RD secondary antibody (LI-COR Biosciences, Lincoln, NE, USA). Immunoreactive bands were imaged using the Odyssey Fc (LI-COR Biosciences, Lincoln, NE, USA). Actin levels were measured as a loading control using an HRP-labeled β-actin antibody (Sigma-Aldrich (St. Louis, MO, USA). Densitometry was performed using Image Studio software (LI-COR Biosciences, Lincoln, NE USA).

Sensitivity to Transport Inactivation by Methanethiosulfonate Reagents

ASD variants were introduced into native or cysteine-reduced SERT backgrounds of pcDNA3-hSERT using the Stratagene QuikChange® kit (Agilent Technologies, Santa Clara, CA, USA) and verified by sequencing (Eurofins MWG Operon, Huntsville, AL, USA). Analysis of the intracellular Cys277 probe

required introduction of the ASDs into the X5C background (C15A, C21A, C109A, C357I, and C622A) (Sato et al., 2004) prior to transient expression in HEK-MSR cells (Thermo Fisher, Waltham, MA, USA) using TransIT®-LT1 (1 µl per 200 ng of DNA; Mirus, Madison, WI, USA). Cells were maintained in a humidified chamber with 5% CO2 at 37°C in DMEM supplemented with 10% FBS and 600 µg/ml G418. HEK-MSR cells were plated at a density of 10,000 or 50,000 cells/well in 24-well culture plates, allowed to settle and attach for 24 hrs, and then transfected with the mutant plasmids. After 24 hr, cells were washed with 37°C PBS/CM buffer (137 mM NaCl, 2.7 mM KCl, 10.1 mM Na_2HPO_4, 1.8 mM KH_2PO_4, 0.1 mM $CaCl_2$, 1.0 mM $MgCl_2$, pH 7.4) or NMDG-Cl buffer (120 mM NMDG-Cl, 5.4 mM KCl, 1.2 mM $CaCl_2$, 10 mM glucose, 7.5 mM HEPES, pH 7.4) and incubated with 1 mM MTSET, 10 mM MTSES, or 2 mM MTSEA (Biotium, Fremont CA, USA) for 1-10 min at room temp. Post-treatment, cells were washed with PBS/CM or NMDG-Cl buffer and assayed for transport activity by incubation with 50 nM [^{3}H]5-HT for 5 min at 37°C in MKRHG buffer (5 mM Tris, 7.5 mM HEPES, 120 mM NaCl, 5.4 mM KCl, 1.2 mM $CaCl_2$, 1.2 mM $MgSO_4$, 10 mM glucose, pH 7.4). Cells were dissolved in MicroScint™-20 (Perkin-Elmer, Waltham, MA, USA) scintillation fluid and counts/min of radioactivity were determined using a TopCount NXT scintillation counter (Perkin-Elmer, Waltham, MA, USA). Specific uptake was determined by subtracting uptake observed in non-transfected cells. All experiments were repeated in three or more separate assays and data fit to a one-phase decay curve. Half-life values estimated from inactivation were analyzed using a one-way ANOVA followed by a post-hoc Dunnett's test (GraphPad Software Prism 5).

Limited Proteolysis of SERT N-terminus

CHO cells transfected with HA-tagged SERT constructs were washed with PBS to remove media and then scraped in 1 mL of Trypsin Homogenization Buffer (20 mM HEPES, 2 mM $MgCl_2$, 0.5 M EDTA, pH 7.4). Cells were incubated on ice for 30 min followed by five, 1-sec sonication pulses using a Q125 Sonicator (Fisher Scientific, Waltham, MA, USA). Samples were centrifuged for 10 minutes at 17,000 X *g* and the resulting pellet was resuspended in trypsin homogenization buffer substituted with 150 mM NaCl or ChCl. For digestion assays, 50 µg of protein was incubated with 4 µg of trypsin (Promega, Madison, WI,

USA) for 5, 10 or 15 min on ice. The reaction was stopped by the addition of 8 µg of soybean inhibitor (Sigma-Aldrich, St. Louis, MO, USA). Then, 2X Laemmle buffer (Bio-Rad Laboratories, Hercules, CA, USA) was added to the sample and boiled at 95°C for 3 min. Samples were separated using a NuPAGE 10% Bis-Tris protein gel (Invitrogen, Carlsbad, CA, USA) and transferred to Immobilon-FL PVDF membrane (Millipore Sigma, Burlington, MA, USA). HA-tagged SERT protein was visualized using a mouse anti-HA antibody (BioLegend, San Diego, CA, USA) probed with IRDye 680RD secondary antibody (LI-COR Biosciences, Lincoln, NE, USA). Immunoreactive bands were imaged using the Odyssey Fc (LI-COR Biosciences, Lincoln, NE, USA) and densitometry was performed using Image Studio software (LI-COR Biosciences, Lincoln, NE USA). Tryptic digestion efficiency was determined by calculating the percent uncleaved as the band intensity of tryptic digestion divided by the total band intensity. If there was a 2-fold difference in total SERT expression across genotypes or less than 90% of the protein remained after digestion, the blot was not analyzed. To account for variation in band intensity across blots, paired Student's t-tests at each time point were used for statistical analysis.

Statistical and Graphical Analyses

Data from experiments were analyzed and graphed using Prism 7.0 (GraphPad Software, Inc., La Jolla, CA, USA). For all analyses, a $P \leq 0.05$ was used to infer statistical significance. Specific details of statistical tests are given in each figure legend.

CHAPTER 3

PROTEOMIC ANALYSIS OF HYPERACTIVE SERT INTERACTING PROTEINS

Ran Ye, Matthew J. Robson, Kristie Rose, and Randy D. Blakely
contributed to the studies reported in this chapter

Introduction

Disruptions in serotonergic signaling have been implicated in a wide array of neurological disorders, including depression (Plaznik et al., 1989; Meltzer, 1990), ASD (Cook et al., 1997; Muller et al., 2016) and OCD (Sinopoli et al., 2017), among others. The primary regulator of the termination of 5-HT signaling is the high-affinity 5-HT transporter SERT, which rapidly clears 5-HT from the extracellular space. Evidence suggests that SERT responds to environmental demands of the system to modulate 5-HT uptake activity, ultimately to regulate the availability, in space and time, of extracellular 5-HT. For example, activation of the interleukin 1 receptor (IL-1R), signaling through p38 MAPK pathway elevates SERT activity (SERT*), decreasing extracellular 5-HT levels (Zhu et al., 2010). Interestingly, stimulation of kinase pathways linked to increase SERT activity, such as p38 MAPK and PKG (Zhu et al., 2004) has also been shown to modulate SERT interacting proteins (SIPs) (Bauman et al., 2000; Samuvel et al., 2005; Zhu et al., 2011). Thus, it is hypothesized SERT exists in multiple activity states, defined and mediated by distinct SIP complexes. Clearly defining the protein complexes of the different SERT conformational states will be useful in identifying possible novel drug targets beyond SERT to manage 5-HT associated disorders, particularly as therapeutic targeting of SERT has delayed efficacy and is achieved only with relatively complete transporter blockade. More subtle therapeutics that alter or overcome the actions of SIPs may allow for a restoration of SERT activity versus a complete blockade. However, identifying these macromolecular complexes is technically challenging, as SERT does not exist in a static state with a defined and constitutive set of proteins (Steiner et al., 2008). Were we to have SERT stabilized in a distinct

conformation, one particularly associated with medical complications, we could hope to identify complexes that interact only transiently with WT SERT and that might be of disease relevance to explore. In this regard, the Blakely lab identified a gain-of-function, autism-associate coding variant, SERT Ala56 (Prasad et al., 2005, 2009; Sutcliffe et al., 2005), which our evidence from Chapter 2 indicates to be stabilized in a state distinct from WT SERT and associated with increased activity (SERT*). The availability of this SERT Ala56 knock-in mouse model (Veenstra-VanderWeele et al., 2009, 2012) provides a natively-expressed pool of stabilized SERT* from which we can search for proteins that prefer (or not) the SERT* state.

I present here my efforts to pursue candidate and proteomic analyses of SIPs differentially associated with a functional SERT coding variant. This data provides insight into novel pathways and proteins that may mediate SERT activity state.

Results

Identification of SERT Complexes by Immunoprecipitation

In order to identify novel SIPs using an unbiased approach, we optimized a SERT affinity-purification (AP) protocol of midbrain synaptosomes from male WT, SERT Ala56 and SERT KO mice. Importantly, we decided to only focus on male mice for this study as the past characterization of these mice has been exclusively done in males (Veenstra-VanderWeele et al., 2012; Robson et al., 2018), mostly due to the fact that that there is a 4:1 male bias found in ASD (Baio et al., 2018) . However, future studies would clearly benefit from understanding sex difference in SERT functional regulation, which may provide evidence to explains the male dominates exhibited by ASD. We also selected the midbrain region to identify SERT complexes as the midbrain has the highest expression of SERT and also contains SERT in both somatodendritic and axonal compartments (Ye et al., 2016). However, it is thought that SERT protein complexes vary in target brain areas, such as the hippocampus or prefrontal cortex, which act to modulate the distinct regulation of the transporter required of each brain region. Differences in transporter proteins interactions in various brain regions has been previously been reported in our lab for both SERT (Ye et al.,

2016) and DAT (Gowrishankar et al., 2018). Mapping the SERT interactome in various brain regions will be critical to understand SERT function in different contexts.

SERT was immunoprecipitated from midbrain synaptosomes utilizing a C-terminal SERT anti-serum #48 (epitope developed against amino acid 596-622 of rat SERT and detects both hSERT and rodent SERT; (Qian et al., 1995b)) that was covalently cross-linked to magnetic protein A beads, as described in Methods (**Figure 12**). Since the SERT Ala56 mutation is located within the N-terminus, we wanted to avoid using an antibody directed against the N-terminus, as the mutation may affect antibody recognition. This approach allows us to isolate and characterize SERT complexes from native tissue and identify both direct and indirect protein-protein interactions.

SERT-associated protein complexes were determined by using Multi-dimensional Protein Identification Technology (MudPIT) (Wolters et al., 2001), an application that allows for increased detection of peptides from LC-MS/MS. The resulting peptides match to a total of 1050 proteins. To quantify the amount of protein interacting with SERT in the different conditions, two label-free quantifying techniques were employed, normalized spectral counts and precursor ion intensity. To eliminate non-specific proteins, proteins that were only identified in samples from SERT KO midbrain, as well as proteins with a 1.5-fold enrichment in SERT KO compared to WT or SERT Ala56 by either normalized spectral counts or precursor ion intensity, were removed from final analysis, narrowing the list of specific SIPs to 459 proteins (**Table 7**). Importantly, SERT was identified only in WT SERT and SERT Ala56 samples and there was no difference in SERT levels estimated between these samples in ion intensity or normalized spectral counts, indicating the utility of our methods for identifying and quantifying proteins in our immunocomplexes. Also, several proteins that were previously described SIPs were identified in by this study (noted by * in **Table 7**) as well as proteins found in a separate proteomic analysis from another lab (noted by ** in **Table 7)** (Haase et al., 2017), further supporting the utility of our methods. In order to uncover SIPs that differentially interact with WT SERT compared to SERT Ala56, the $\log_2$ fold change in SIP levels from the WT/Ala56 ratio was calculated for both normalized spectral counts and precursor ion intensity (fold change < -1 means increased interaction with SERT Ala56, fold change > 1 means decreased

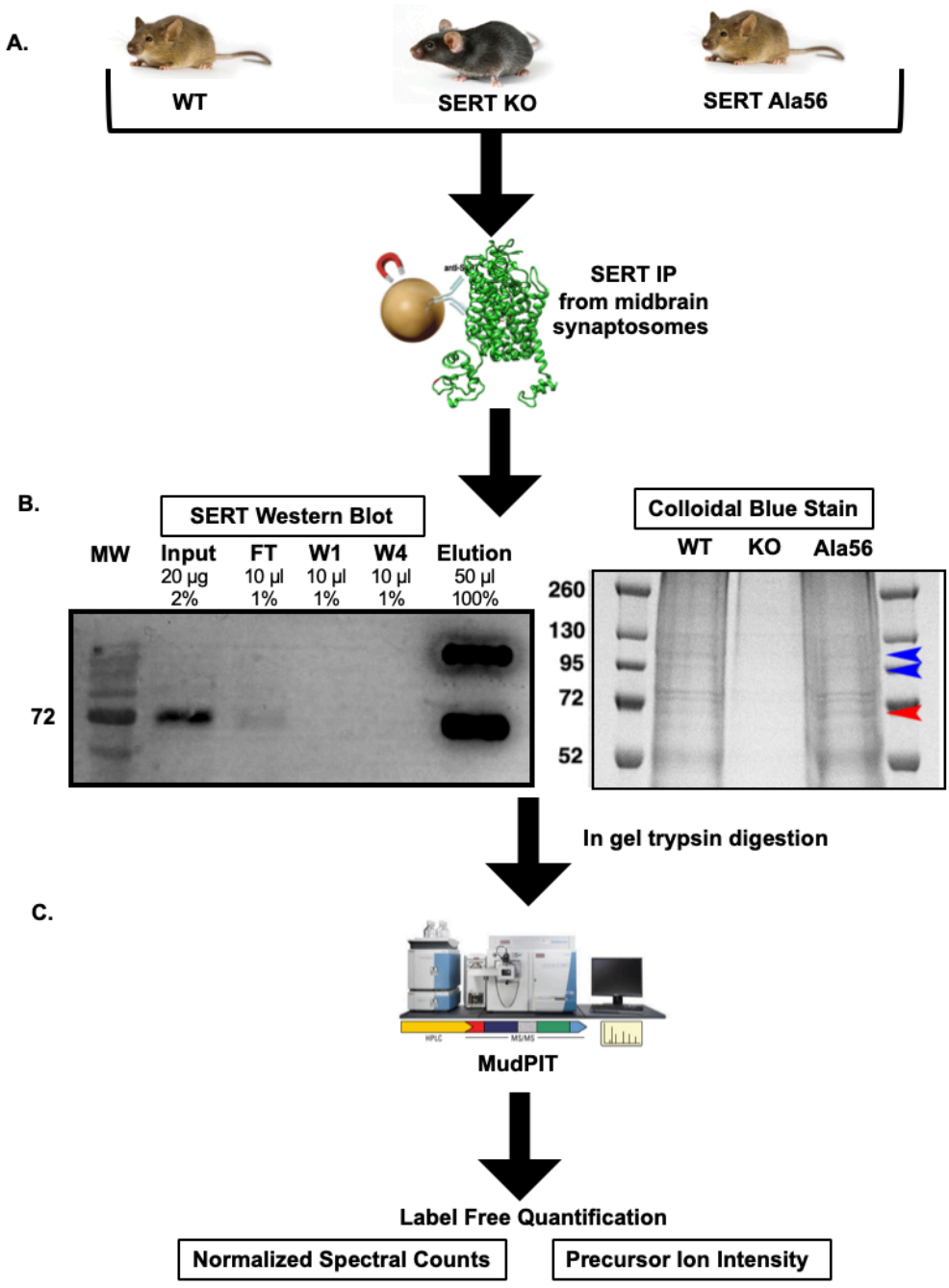

Figure 12. SERT co-immunoprecipitation followed by LC-MS/MS
(A) Midbrain synaptosomes from WT, SERT KO (negative control), and SERT Ala56 mice were affinity purified for SERT (n=3). Western blot confirms efficient SERT IP. (B) Coomassie-blue stain of eluate from SERT IP confirms altered protein association profiles (red and blue arrow indicate increase and decrease, respectively, protein band intensities in SERT Ala56 compared to WT). (C) In gel tropic digestion was followed by an 8 step MudPIT. Eluting peptides were mass analyzed on an LTQ Orbitrap Velos (Thermo Scientific). Scaffold (version 4.7.3) was used to validate MS/MS based peptide and protein identifications.

interaction with SERT Ala56 and fold change between -1 and 1 means no difference between genotype; **Table 7**). Due to the exploratory nature of our effort, and the complementary aspects of these methods of quantification, we only required differences in only one of the two approaches to consider for further analysis. As seen in **Figure 13** most proteins show overlap between normalized spectral count and precursor ion intensity in quantifying differential SIPs across conditions, with only a few exceptions.

For example, CaMKIIβ by normalized spectral count analysis shows $\log_2$ fold-change of 2.57 indicating decreased interaction with SERT Ala56, but by ion intensity, the $\log_2$ fold-change WT/SERT Ala56 is -0.37 indicating no differences between genotypes. Previous studies identified CaMKIIβ and CaMKIIα as a SIP and found that CaMKIIα played an important in mediating D-amphetamine-induced 5-HT efflux, with no further follow up on the role of CaMKIIβ (Steinkellner et al., 2015). This is of interest considering that SERT Ala56 was shown to blunt efflux in response to the D-amphetamine derivative, D-fenfluramine (Quinlan et al., 2019), potentially suggesting that SERT Ala56:CaMKII association is also affected.

Interestingly, significantly more proteins were nominated as SIPs with WT SERT (302 proteins; 65.8%) compared to SERT Ala56 (66 proteins; 14.38%) based on the $\log_2$ fold change of precursor ion intensity (Chi-square test $P < 0.01$). To provide some clarity on the association of the proteins within this list of 459 proteins, network and functional clustering analysis was performed based on $\log_2$ fold change of precursor ion intensity proteins with increased and decreased interaction with SERT Ala56 as well as with proteins that showed no difference in interaction between genotypes (91 proteins; 19.83%), and all proteins combined (459 proteins).

Network Analysis of SIPs with Increased Interaction with SERT Ala56

There were 66 proteins with increased interaction with SERT Ala56 compared to WT SERT as defined by $\log_2$ ion intensity of WT/Ala56 of less than -1. Functional annotation clustering from DAVID bioinformatics resource identified enrichment in proteins assigned to the cytoskeleton (GO:0005856), GTP

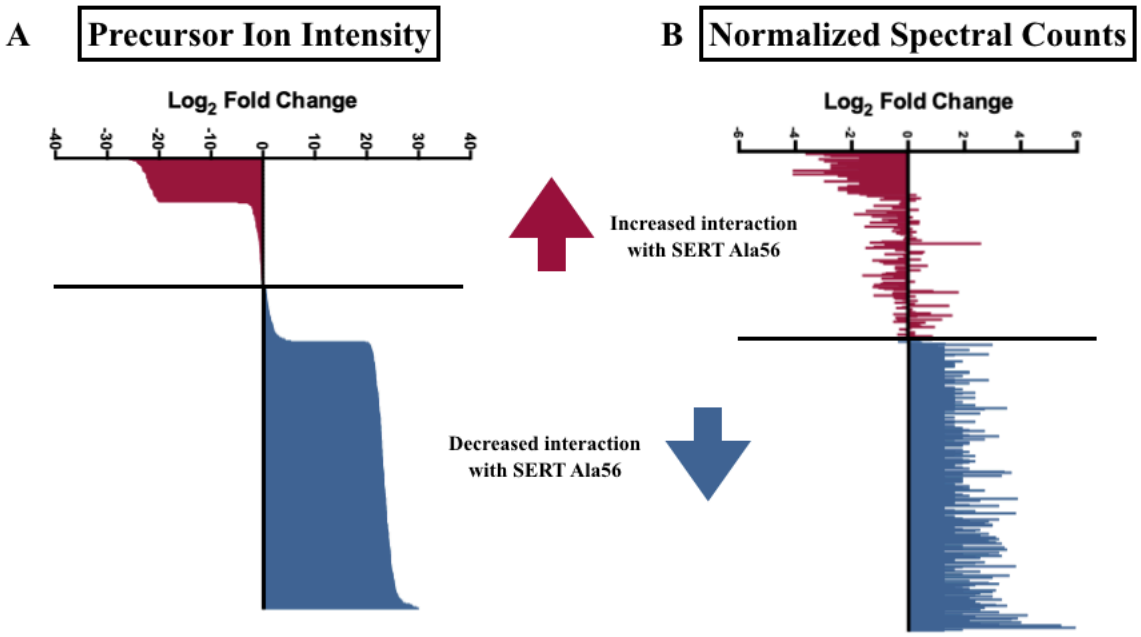

Figure 13. Log_2 fold change of SIPs between SERT Ala56 and WT SERT

(A) Log_2 fold change of **(A)** precursor ion intensity and **(B)** normalized spectral counts. Proteins in red indicated proteins increased interaction with SERT Ala56 compared to WT and blue labeled proteins show increased association with WT SERT compared to SERT Ala56 based on precursor ion intensity.

binding (GO:0005525) and cell-cell adherens junction (GO:0005913) (**Table 3**). The input of these proteins into the STRING program found this network has significantly more interactions than expected (protein-protein enrichment, Fisher's exact test $P = 0.00827$) (**Figure 14**).

Three proteins that have been previously identified as SIPs were included in this list of proteins with increased interaction with SERT Ala56 compare to WT SERT: serine/threonine protein phosphatase 2A (PP2A) regulatory subunit B (Ppp2r2c), protein transport protein Sec23a, and 14-3-3η.

PP2A is a holoenzyme consisting of a catalytic "C" subunit coupled to "A" scaffolding subunit and a regulatory "B" subunit (Kremmer et al., 2015). The catalytic subunit of PP2A (PP2Ac) has been previously shown to form a functional interaction with SERT (Bauman et al., 2000). Interestingly, the "C" subunit interacted less with SERT Ala56 compared to WT SERT, discussed more below. One possibility to explain the differential binding of the "B" subunit versus the "C" subunit is that the "B" regulatory subunit of PP2A binds to SERT Ala56 in a conformation that does not allow PP2Ac to bind.

Sec23A/24C, PDZ containing proteins, are members of coat protein complex II (COPII) that bind to the C-terminus of SERT at amino acids Arg607-Iso608 (Chanrion et al., 2007; Sucic et al., 2011), and have been reported to mediate SERT transport from the endoplasmic reticulum (ER) to the membrane surface (Sucic et al., 2011). SERT Ala56 in transfected cells does not affect SERT surface expression (Prasad et al., 2009), and thus no effort has been expended to assess changes in membrane trafficking that could arise from heterologous expression of SERT Ala56. There may be cause to revisit this idea given that the DAT Cys615 coding variant associated with ADHD has been found to undergo a different mode of membrane recycling once transferred to the cell surface (Sakrikar et al., 2012). It should also be noted that SERT surface levels from SERT Ala56 KI mice have yet to be determined and may be different from *in vitro* studies, a phenomenon seen with another ADHD-associated DAT variant, DAT Val559 (Gowrishankar et al., 2018), where surface expression is not altered in transfected cells, but is impacted *in vivo*.

Annotation Cluster	Enrichment Score	Protein #	Protein IDs	p Value
Cytoskeleton	3.05	12	Mark1, Mark2, Add3, Capza1, Cep131, Coro1c, Cro2b, Pitpnm2, Sept11, Sept5, Sept8, Spta1	2.2E-04
GTP Binding	1.72	4	Agap1, Sept11, Sept5, Sept8	1.5E-01
Cell-Cell Adherens Junction	3.05	7	Mark2, Arglu1, Capza1, Dlg1, Eef1g, Hspa5, Puf60	4.7E-04

Table 3. DAVID Functional Analysis of SIPs Increased with SERT Ala56

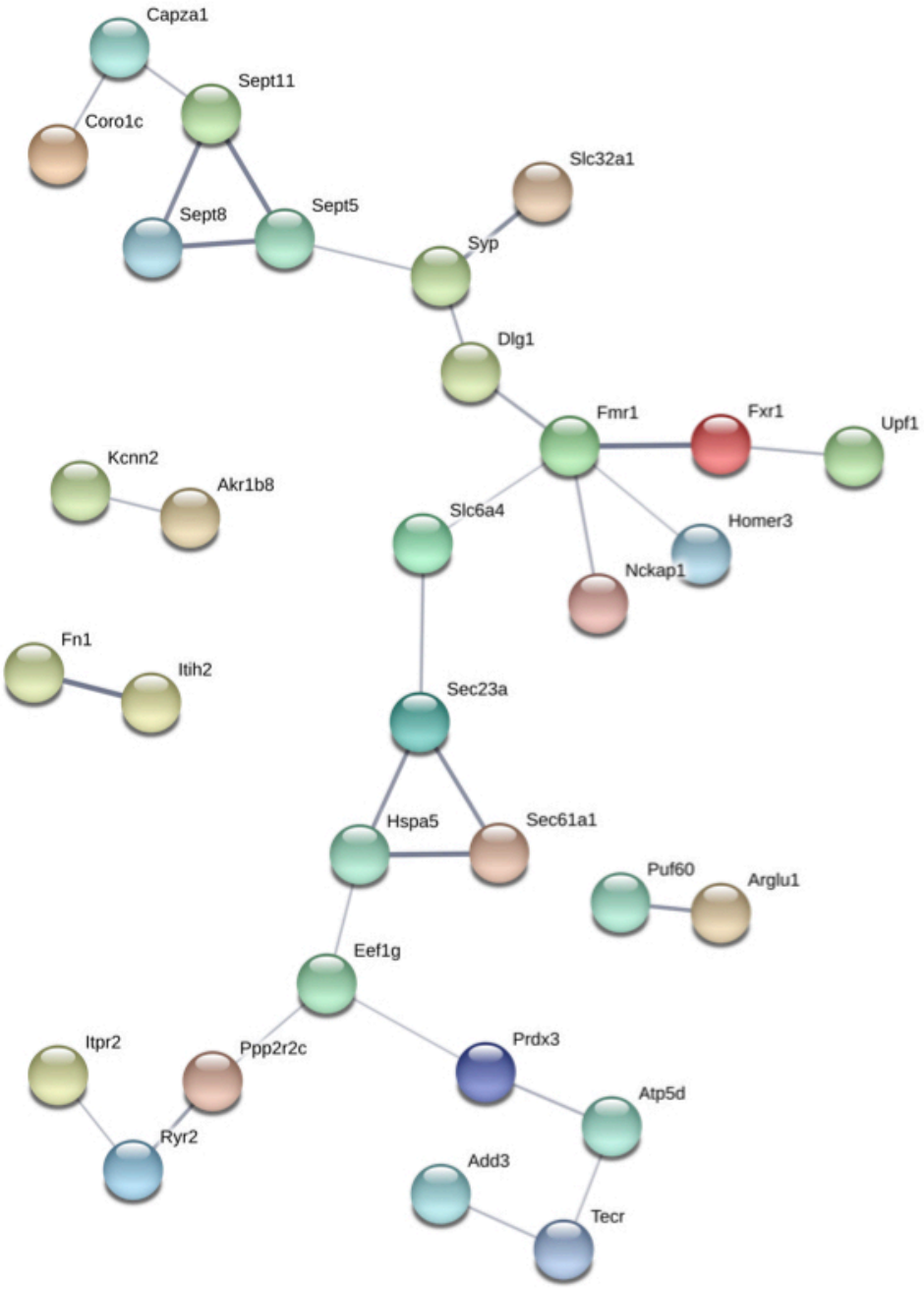

Figure 14. STRING network analysis of SIPs increased with SERT Ala56

14-3-3 are adaptor proteins that stabilize a number of protein-protein interactions (Aitken et al., 2004). 14-3-3τ has been shown to interact with the N-terminus of SERT and decreased SERT Vmax potentially through a PKC dependent pathway (Haase et al., 2001). However, there are multiple isoforms of 14-3-3 and two other 14-3-3 isoforms (α/β and ɣ) were shown to have increased interaction with WT SERT while 14-3-3η showed increased interaction with SERT Ala56. These findings, if confirmed, may indicate the use of 14-3-3 isoforms in different cellular compartments of 5-HT neurons (i.e. soma, dendrites, axons). Further studies will be needed to tease apart the complexity of the interactions of the various 14-3-3 isoforms with SERT, which may play very different roles in regulating SERT activity.

One novel family of proteins shown to interact with SERT Ala56 are the septin family. Septins are a cytoskeletal GTPases which play a role in vesicle trafficking and compartmentalization of the plasma membrane. Some studies suggest that septins may regulate exocytosis (Tokhtaeva et al., 2015). Interestingly, Sept5 interacts with Sept11 (Bläser et al., 2010), which was also identified as a SIP and Sept5 (also referred to as CDCrel-1) which has been shown to bind to syntaxin 1A and inhibit exocytosis (Beites et al., 1999). Syntaxin 1A has been shown to form a functional complex with SERT (Quick, 2002a), so potentially these findings may suggest the presence of a Sep5:Sep11:Syntaxin 1A:SERT macromolecular complex. As to the broader relevance of this work, it is interesting that Sept5 has been implicated in a number of diseases, including ASD (Harper et al., 2012; Hiroi et al., 2012).

Haase and colleagues found in their proteomic analysis of SIPs an enrichment in synaptic vesicle proteins (Haase et al., 2017). We identified two vesicular proteins, synaptophysin (Syp) and synaptotagmin-11 (Syt11) in the list of proteins which have increased interaction with SERT Ala56. However, synaptic vesicles proteins were not found enriched in our specific network analysis, though it is well known that vesicle protein complexes are dynamic interactors and some components may simply not have been assembled in the extracts analyzed. Nonetheless, it seems reasonable to speculate that associations of a more active SERT Ala56 might enhance proximity of the transporter to synaptic vesicles as a means of enhancing the repacking of 5-HT. In this regard, a close association of DAT with the vesicle protein

synaptogyrin-3 protein has been described by Egana et al. and suggested to play a role in DAT-dependent refilling of DA synaptic vesicles (Egana et al., 2009).

Another novel interesting SIP shown to interact with SERT Ala56 is the fragile X mental retardation 1 protein (FMR1). We also identified the fragile X-related protein (Fxr1). Fragile X syndrome (FXS), a single gene disorder that results in the silencing of *Fmr1,* has considerable overlap in symptomology with ASD (Belmonte and Bourgeron, 2006) and has been linked to 5-HT dysregulation (Hanson and Hagerman, 2015). Treatment with the SSRI sertraline has been found to be beneficial for some patients with FSX (Hanson and Hagerman, 2015). FMR1 proteins are known to be RNA binding proteins that tightly regulate the translation of proteins at an active synapse (Dockendorff and Labrador, 2019), such as the metabotropic glutamate receptor mGlur5 (Bear et al., 2004). Since the function of FMR1/FXR1 is most often considered in relation to post-synaptic compartments where translational control of protein expression can be manifested, it may be necessary to consider a somatodendritic site of SERT expression and functions therein for the SIPs.

Network Analysis of SIPs with Decreased Interactions with SERT Ala56

Of the 459 proteins nominated from my studies as SIPs, 302 (or 66% of total proteins recovered) were shown to have decreased interactions with SERT Ala56 compared to WT SERT. Functional annotation clustering from DAVID online resource tool identified enrichment of proteins in this network that are assigned to kinase activity (GO:0016301), specifically serine/threonine kinases (GO:0004674), amphetamine addition (KEGG pathway) and Arp2/3 protein complex (GO:0005885) (**Table 4**). The input of these proteins into the STRING program found this network has significantly more interactions than expected (protein-protein enrichment, Fisher's exact test $P < 1.0e\text{-}16$) (**Figure 15**).

In support of the findings related to kinase networks, several serine/threonine kinases were identified to demonstrate a decreased association with SERT Ala56, including Mapk3, also known as the extracellular signal-regulated kinase 1 (ERK-1). Not much is known about ERK-1 regulation of SERT,

Annotation Cluster	Enrichment Score	Protein #	Protein IDs	p Value
Kinase Activity	5.41	28	Araf, Cdc42bpb, Mark3, Mark4, Tnik, Agk, Cask, Csn1d, Csnk1d, Csnk2a1, Cerk, Cdk18, Cdkl5, Dgkz, Dgkb, Ddr1, Fn3k, Gk, Gsk3b, Magi3, Mast1, Mapk3, Mapk8ip2, Map2k1, Map3k13, Pfkl, Phkg1, Prkg2, Pdk3	7.4E-06
Ampehtamine Addiction	3.66	6	Gria1, Gria2, Gria3, Gria4, Crin2a, Ppp1ca	9.4E-03
Arp2/3 Protein Complex	3.62	5	Actr3, Arpc2, Arpc3, Arpc4, Arpc5l	1.5E-05
Serine/ Threonine Protein Kinase	3.08	17	Araf, Cdc42bpb, Mark3, Mark4, Tnik, Cask, Csnk1d, Csnk2a1, Cdk18, Cdkl5, Gsk3b, Mast1, Mapk3, Map3k13, Phkg1, Prkg2	1.1E-04

Table 4. DAVID Functional Analysis of SIPs Decreased with SERT Ala56

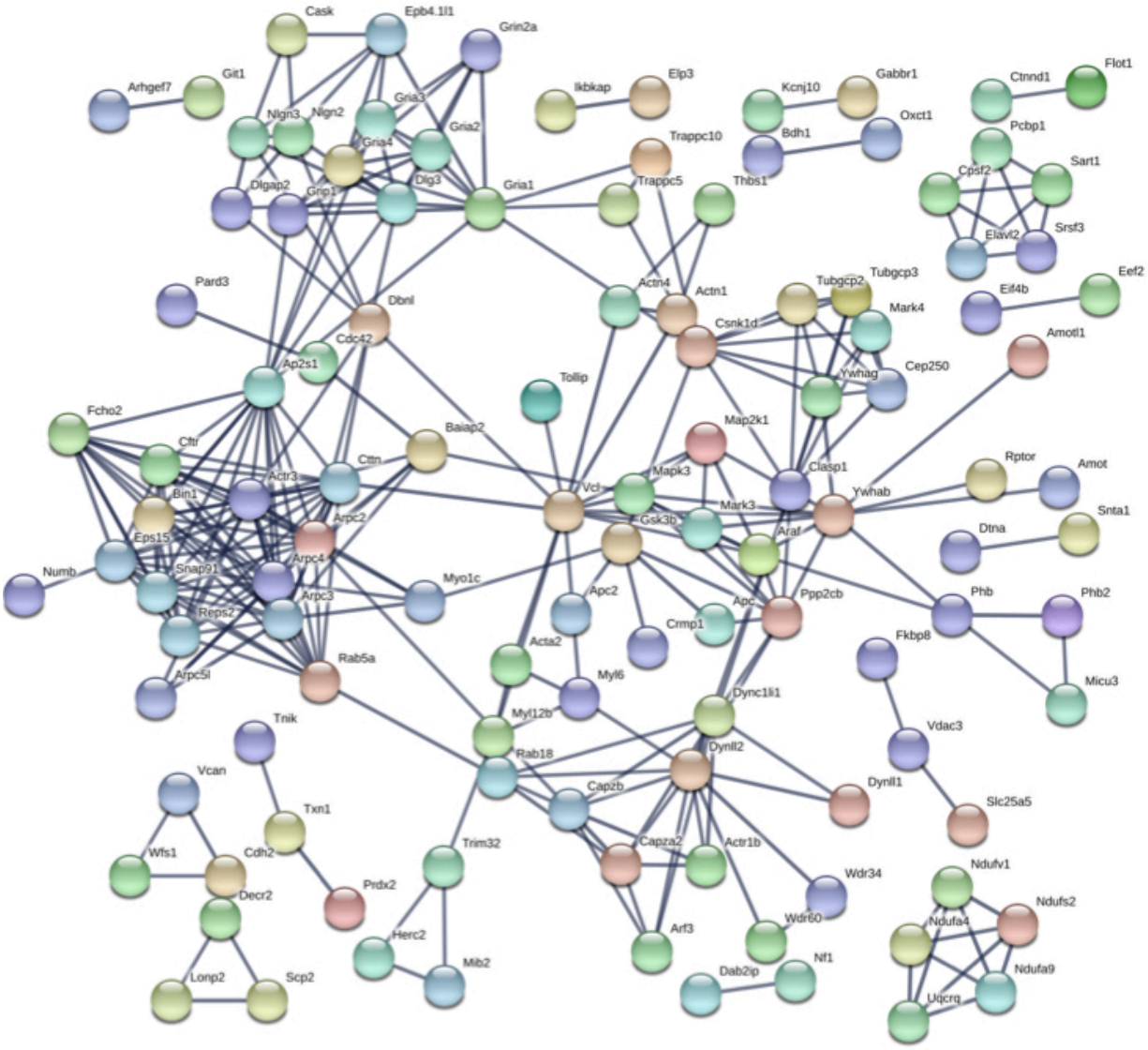

Figure 15. STRING network analysis of SIPs decreased with SERT Ala56

except for one study that reported that inhibition of ERK-1 prevented an estradiol-induced decrease in 5-HT clearance in the rat hippocampus (Benmansour et al., 2014). However, the role of ERK-1 in regulating DAT activity, surface expression and N-terminal phosphorylation have been well studied (Moron et al., 2003; Bolan et al., 2007; Foster et al., 2012; Owens et al., 2012). Given that SERT is regulated by other MAPK family members, specifically p38α MAPK, further studies are warranted to validate and determine the functional significance of this association.

The Arp2/3 protein complex regulates and binds to the intricate branched actin network that plays an important role in the maturation of dendritic spines (Korobova and Kvitkina, 2010), especially during development (Chou and Wang, 2016). Disruptions in actin cytoskeleton networks may be involved in some of the mechanisms purported to contribute to neuropsychic disorders (Yan et al., 2016), specifically spine morphology has been found to be disrupted in ASD (Martínez-Cerdeño, 2017) and schizophrenia (Datta et al., 2017). Given the presence of SERT in somatodendritic compartments, and our own work indicating a physical association with NLGN2 in this compartment (Ye et al., 2016), the Arp3/3 protein complex is worth further study as a potential determinant of SERT localization or trafficking in this compartment.

Interestingly, a significant number of proteins that are involved in a KEGG pathway ascribed to amphetamine addiction were also identified to be less associated with SERT Ala56 compared to WT SERT. Our finding of a decreased fenfluramine (a SERT-specific amphetamine) induced 5-HT efflux in cells expressing SERT Ala56 vs WT SERT (Quinlan et al., 2019) may relate to an inability of proteins in this network to properly regulate the process of transporter-mediated 5-HT efflux.

Many previously described SIPs are also found in this list, including PP2Ac, PKG, NLGN2 and FLOT1, which are described in more detail below.

PP2Ac was also shown to have decreased interaction with SERT Ala56, despite increased interactions of the mutant SERT with the regulatory subunit B (Ppp2r2C). Although this converse profile for two subunits of the same complex are unclear, since PP2A is a Ser/Thr protein phosphatase that has already been implicated in the control of SERT phosphorylation (Bauman et al., 2000), the decreased

interaction of PP2Ac may speak to the hyperphosphorylation of SERT Ala56 seen *in vivo* (Veenstra-VanderWeele et al., 2012).

PKGII was also identified to be reduced in SERT Ala56 complexes. Interestingly, past studies have shown that PKGII does not interact with SERT due to the myristoylation domain that anchors PKGII to the membrane (Zhang and Rudnick, 2011). However, these studies were performed *in vitro* (HeLa cells) and perhaps *in vivo* SERT may localize to different lipid raft domains that allow SERT to engage in PKGII-dependent regulation. The reduced interaction seen with SERT Ala56 may relate to the inability to further activate the mutant transporter with PKG activators.

As noted above, NLGN2 forms a functional interaction with SERT in somatodendritic compartments, specifically within the midbrain (Ye et al., 2016), most likely at dendritic sites that support GABAergic synapses. Interestingly *Nlgn*2 KO mice exhibit social deficits that are mimicked in SERT Ala56 mice (Ye et al., 2016), suggesting that NLGN2 may exhibit some of its perturbations of social behavior through SERT and 5-HT-dependent mechanism. We have speculated that SERT, 5-HT_{1A} receptors, NLGN2 and GABA receptors may form a complex to spatially co-organize inhibitory control mechanisms that regulate 5-HT neuron excitability.

The protein that demonstrates the greatest reduction in associations with SERT Ala56, based on precursor ion intensity, is FLOT1, which has been previously shown to interact with DAT (Cremona et al., 2011; Sorkina et al., 2012) and SERT (Reisinger et al., 2018). Flotillin has been identified as a risk gene for MDD (Zhong et al., 2019), though the wide distribution of the protein makes it difficult to attribute specific behavioral changes to simply a serotonergic site of expression. In regard to DAT, our lab found that an ADHD-associated DAT variant (Arg615Cys) also showed decreased interaction with Flot-1 and this change coincided with altered DAT localization within membrane lipid rafts (Sakrikar et al., 2012). SERT Ala56 has been found to localize to lipid raft compartments and to exhibit dynamic, regulated mobility within these domains (Magnani et al., 2004). Interestingly, FLOT1 interaction with DAT is also necessary for amphetamine-induced changes in DAT function (Sakrikar et al., 2012; Pizzo et al., 2013). Considering SERT Ala56 shows a blunted fenfluramine-induced 5-HT efflux (Quinlan et al., 2019), SERT

Ala56:FLOT1 interactions may be constitutively diminished, supporting changes in transporter functional states. Altogether, these studies in the context of our proteomic findings support the need for further analysis of mutation-induced alterations in FLOT1:SERT Ala56 associations.

Network Analysis of SIPs that Shown Similar Interaction with Both WT SERT and SERT Ala56

In the proteomic analysis, 91 of the 459 proteins identified showed no difference in interaction with WT SERT and SERT Ala56, though these proteins were assessed to have some degree of SERT specificity since they were not present in SERT KO samples. Functional annotation clustering of these proteins utilizing the online DAVID platform showed enrichment in proteins assigned to Src Homology 3 (SH3) domain contacting proteins (UniProt keyword), GTPase activation (UniProt keyword), ATP binding (GO: 0005524), PDZ domain binding (GO: 0030165), and kinase activity (GO:0016301) (**Table 5**). Analysis of the network by the online STRING platform showed significantly more interactions than expected (protein-protein enrichment, Fisher's exact test $P = 2.8e-08$) (**Figure 16**).

Proteins within the PDZ domain network represent scaffolding proteins that regulate multiprotein complexes within the plasma membrane of both presynaptic active and postsynaptic density zones (Garner et al., 2000; Nourry et al., 2003). The very C-terminal end of SERT contains a conserved, nonclassical PDZ binding motif (NAV; amino acids 628-630), and thus it is not a surprise that a number PDZ domain binding proteins were found to interact with SERT, including nNOS, PICK1, and the channel interacting PDZ protein (Chanrion et al., 2007). PDZ domain is also referred to as the *Drosophila* discs-large (DLG) homology domain as genetic disruptions of these proteins in *Drosophila* have been found to cause significant changes to the morphology of synapses (Budnik, 1996). Interestingly, a number of variants of the Dlg and Dlg associated protein (Dlgap) have been found in ASD patients (Li et al., 2014). Genetically elimination of Dlgap1 from mice decreases sociability (Coba et al., 2018). Considering 5-HT plays a critical role in modulating social behavior (Muller et al., 2016; Walsh et al., 2018), perhaps some of the behavioral effects of Dlgap mutations involves disruptions in SERT function. Often, PZD domains are found in

Annotation Cluster	Enrichment Score	Protein #	Protein IDs	p Value
SH3 Domain	6.51	11	Arhgap26, Arhgap32, Shank3, Srgap3, Yes1, Dlg2, Dlg4, Macf1, Sorbs1, Tjp2, Tnk2	1.0E-08
GTPase Activation	4.81	8	Agap2, Arhgap21. Arhgap23, Arhgap26, Arhgap32,Srgap3, Myo9a,Sipa1l1	3.9E-06
ATP Binding	4	19	Actr2, Abcd3, Atp9a, Agap2, Bmp2k, Yes1, Adck1, Acsl6, Camk2b, Csnk1a1, Csnk1d, Gak, Dgke, Mthfd1, Myo9a, Myo18a, Pcx, Stk39, Tnk2	1.1E-04
Guanylate Kinase/ PDZ Domain Binding	3.16	4	Dlg2, Dlg4, Magi2, Tjp2	1.1E-04
Kinase Activity	2.28	11	Bmp2k, Yes1, Adck1, Camk2b, Csn1a1, Csnk1e, Gak, Dgke, Prkar2a, Stk39,Tnk2	9.0E-04

Table 5. DAVID Functional Analysis of SIPs of Similar Interaction with WT SERT and SERT Ala56

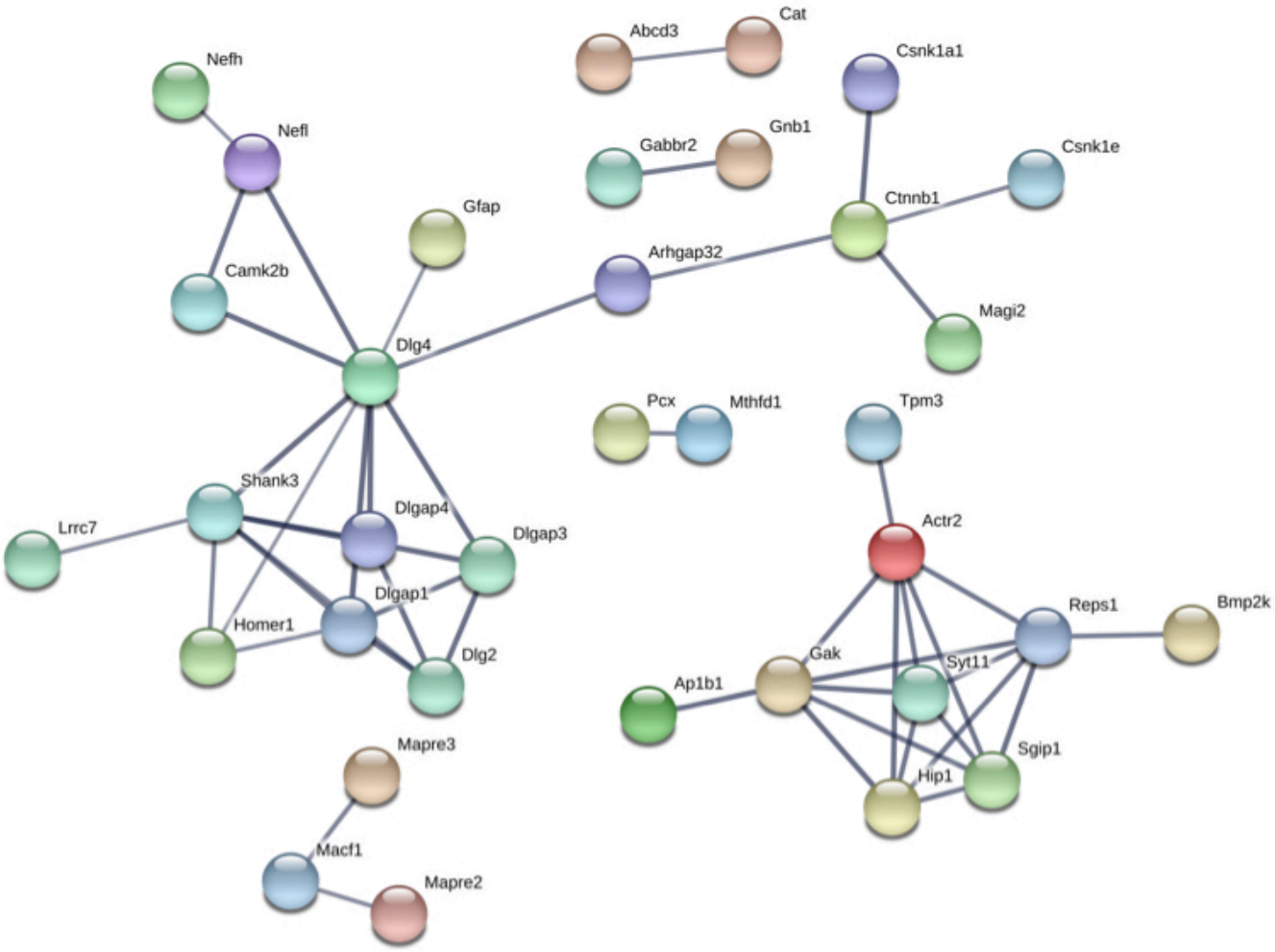

Figure 16. STRING network analysis of SIPs that show no difference between WT SERT Ala56 and SERT Ala56

combination with other interaction domains, including SH3 (Nourry et al., 2003), features of another network shown to be enriched in our SIP analysis.

There is only one SH3 domain (PXXP) (Kurochkina and Guha, 2013) located within the C-terminus of SERT, amino acids 614-617 (PETP). Interestingly, Thr616 has been shown to support SERT phosphorylation *in vitro* by p38α MAPK (Sørensen et al., 2014). The role of this SH3 domain is currently unknown, however, could function as a scaffold for protein binding. Such a role has been suggested for the SH3 domain located in the DAT N-terminus, which also contains a MAPK phosphorylation site (Thr53) (Vaughan and Foster, 2013) that our lab has shown to be phosphorylated in response to D2 autoreceptor activation (Gowrishankar et al., 2018).

One protein identified as unaffected by the Ala56 mutation that contains both an SH3 domain and PDZ domain is the membrane scaffolding protein Shank3, another gene where mutations have been associated with ASD (Moessner et al., 2007). Shank3 is expressed post-synaptically in excitatory synapses and binds with neuroligins (another protein associated with ASD (Singh and Eroglu, 2013) and found on this list), and accumulating evidence suggests that ASD is in part due to dysfunction of glutamatergic synapses (Arons et al., 2012; Rojas, 2014). A number of other proteins in this list are found at excitatory synapses including a glutamate receptor (Gria1,2,3,4), glutamate receptor-interacting protein 1 (Grip1), NMDA receptor 2 (Grin2a) and a glutamate transporter (Slc1a3) isoform (**Table 7**) that has been implicated in amphetamine action on DA neurons (Underhill et al., 2014). 5-HT is a modulatory molecular and forms tripartite synapses with glutamatergic synapses (Belmer et al., 2017). Potentially SERT Ala56 differentially interacts with scaffolding proteins linked to glutamatergic synapses that may at least partially explain some of the ASD-linked effects exhibited by these mice. Additionally, the presence of SERT in somatodendritic compartments where glutamate synapses are formed on 5-HT neurons may better explain these findings since the extracts used for proteomic studies were taken from the midbrain where 5-HT neuron cell nodes are localized. In this regard, the Amara lab has implicated SLC1A3 glutamate transporters in amphetamine action through a somatodendritic site of action (Underhill et al., 2014).

Network Analysis of All Identified SIPs

Functional annotation clustering of these proteins utilizing the online DAVID platform showed enrichment in proteins assigned to SH3 domain-containing proteins (UniProt keyword), PDZ domain (UniProt sequence feature), kinase activity (GO:0016301) and receptor clustering (GO:0043113) (**Table 6**). Input of these proteins into the STRING program found this network has significantly more interactions than expected (protein-protein enrichment, Fisher's exact test $P < 1.0e\text{-}16$ (**Figure 17**).

STRING analysis also identifies reference publications that contain genes or proteins that show a significant overlap with the input list. Interestingly, three reviews on ASD showed significant overlap of cited proteins and SIPs identified in the study: review of ionotropic glutamate receptors in ASD and FXS (Uzunova et al., 2014) found that 20 of the 65 proteins listed overlapped with SIPs identified in the study (FDR= 8.35e-11), and a review on monogenic mouse models of ASD (Hulbert and Jiang, 2016) reported 16 of 39 genes mentioned were found in our proteomic analysis (FDR = 9.88e-10). Together, these studies point to the possibility that the finding of rare mutations in SERT in association with ASD may point to many other protein complexes, some linked to and affected by SERT mutations, that also drive risk for ASD, at least in part, through disruptions in 5-HT signaling.

Additionally, considering genes that are associated with structural connectivity of neurons (Lin et al., 2016), 16 of 73 genes mentioned overlap with proteins identified in my study (FDR = 4.45e-07). This suggests that several ASD related proteins with SERT regulation and activity may lead to a broader impact than simple single synapse considerations, and may provide novel targets for a more circuit level treatment of disorders associated with serotonergic dysfunction.

Annotation Cluster	Enrichment Score	Protein #	Protein IDs	p Value
SH3 Domain	9.36	25	Caskin1, Arhgap26, Arhgap32, Arhgap42, Arhgef7, Shank3, Srgap3, Yes1, Baiap2, Bin1, Cask, Cttn, Dlg1, Dlg2, Dlg3, Dlg4, Dbnl, Macf1, Mapk8ip2, Myo1f, Sorbs1, Sorbs2, Spta1, Tjp2, Tnk2	6.6E-12
PDZ Domain	8.83	11	Dlg1, Dlg2, Dlg3, Dlg4, Grip1, Magi1, Magi2, Magi3, Pard3, Ptpn13, Tjp2	1.2E-10
Kinase	6.72	42	Araf, Bmp2k, Cdc42bpb, Mark1, Mark2, Mark3, Mark4, Tnik, Yes1, Adck1, Agk, Camk2b, Cask, Csnk1a1, Csnk1d, Csnk1e, Csnk2a1, Cerk, Gak, Cdk18, Cdkl5, Dgkz, Dgkb, Dgke, Ddr1, Fn3k, Gk, Gsk3b, Magi3, Mast1, Mapk3, Mapk8ip2, Map2k1, Map3k13, Pfkl, Phkg1, Prpf4b, Prkar2a, Prkg2, Pdk3, Stk39, Tnk2	1.6E-09
Receptor Clustering	3.75	5	Dlg1, Dgl2, Dlg3, Dlg4, Magi2	3.8E-03

Table 6. DAVID Functional Analysis of All Identified SIPs

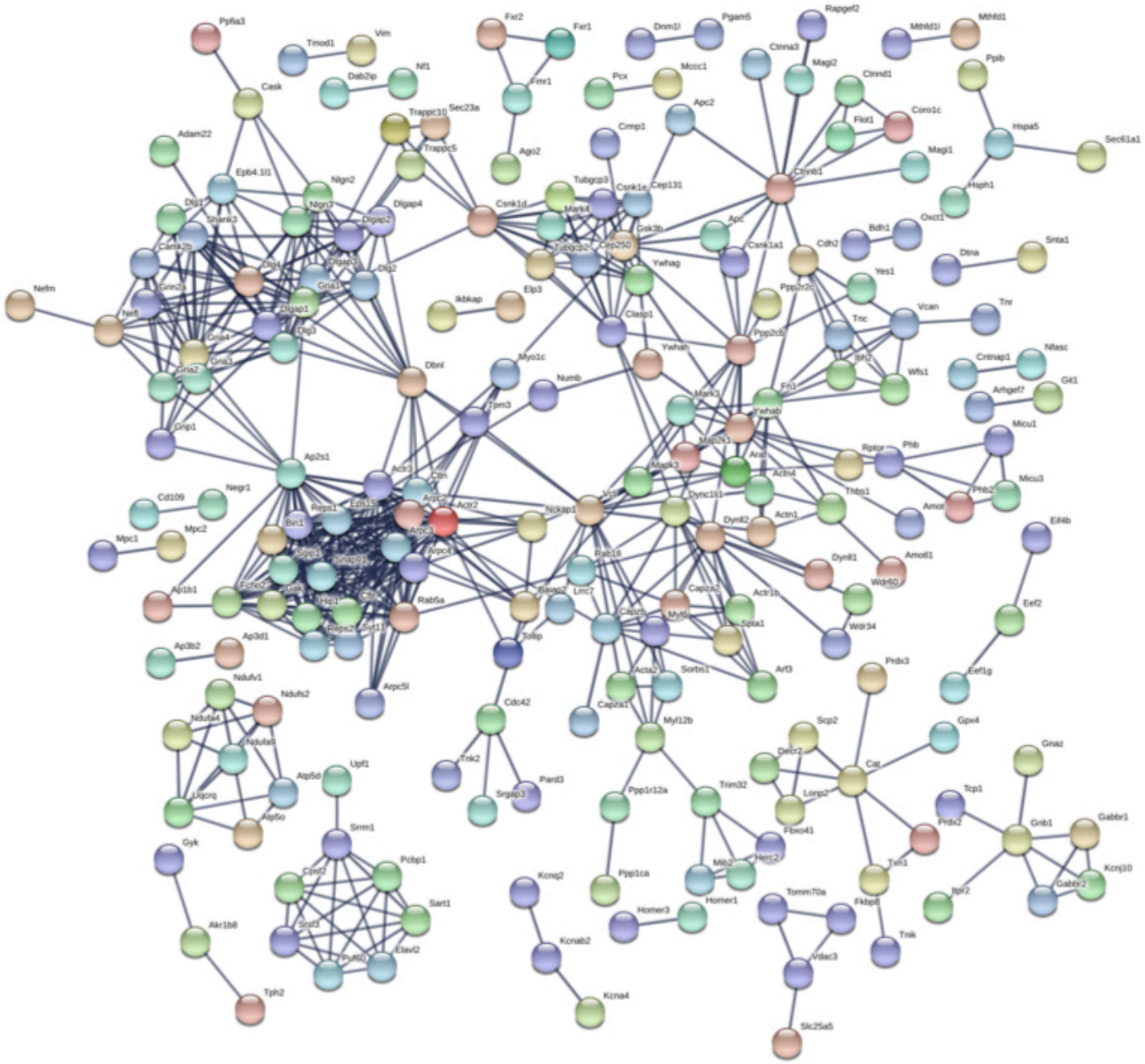

Figure 17. STRING network analysis of all identified SIPs

Discussion

SERT is a dynamically regulated protein that relies on a growing list of SIPs to traffic, stabilize and functionally regulate the transporter. Past studies have identified several SIPs that regulate SERT function. However, the identification of large molecular complexes that mediate SERT function and that are impacted by functional mutations has yet to be identified.

In our analysis of SIPs, a number of previously described proteins, such as CaMKII (Steinkellner et al., 2015), FLOT1 (Reisinger et al., 2018), PP2Ac (Bauman et al., 2000), and NLGN2 (Ye et al., 2016) were identified in this proteomic analysis of SIPs (*proteins in **Table 7**). Additionally, a number novel interacting proteins, many of which have been linked to ASD, such as septin proteins (Harper et al., 2012; Hiroi et al., 2012), DLGN (Li et al., 2014; Coba et al., 2018), FMR1 (Belmonte and Bourgeron, 2006), NLGN3 (Singh and Eroglu, 2013) and SHANK3 (Moessner et al., 2007) were also identified in this proteomic analysis of SIPs.

It was clear from this study that several SIPs associated with synapse and membrane localization were identified, which is no surprise considering SERT functions at the synapse. However, how SERT in different activity states compartmentalizes into different raft domains within the plasma membrane is still not well elucidated. Of interesting note, a peptide targeted against the C-terminus of SERT, disrupting SIPs (Chanrion et al., 2007), increases SERT lateral mobility within the membrane, an effect mimicked by activation of p38 MAPK and PKG (Chang et al., 2012). It is believed that increased mobility is due to an untethering of SERT from scaffolding proteins, increasing SERT motility (Chang et al., 2012). One hypothesis that emerges from this observation is that SERT Ala56 has enhanced membrane lateral mobility, which is supported by the decreased number of proteins that interact with SERT Ala56 compared to WT SERT.

This study provides novel insights into proteins that may regulate SERT activity state, and future studies aim to verify differential interaction with SERT and the role of these proteins in regulating SERT functional state. Importantly, this list also provides potential novel targets that might act in a network to

regulate SERT and thus may be useful in generating therapeutics for diseases that exhibit serotonergic dysfunction, such as ASD.

Methods

Animal Usage

All experiments conducted using animal subjects were conducted according to the National Institutes of Health Guide for the Care and Use of Laboratory Animals. All experiments involving animal subjects were conducted as pre-approved by the Vanderbilt University and Florida Atlantic University Institutional Animal Care and Use Committees. SERT Ala56 and WT littermate males (129/sv background) 8-12 weeks old generated from heterozygous breeding while SERT KO mice on a C57BL/6J background were breed from homozygous breeding. Mouse genotyping was conducted as previously described (Veenstra-VanderWeele et al., 2012).

Antibodies

SERT: guinea pig anti-5-HTT (#HTT-GP-Af1400, Frontier Institute, Japan; 1:2,000 for western blots); SERT anti-serum #48 (for co-immunoprecipitation (Qian et al., 1995b)); HRP-labeled β-actin antibody (Sigma-Aldrich (St. Louis, MO, USA).

Serotonin Transporter Co-Immunoprecipitation and Western Blot

To increase SERT pull down for proteomic analysis, freshly dissected midbrain tissue from 4 mice were homogenized in 10% (w/v) of 0.32 M sucrose, 10 mM HEPES, 2 mM EDTA utilizing a Teflon-glass tissue homogenizer. The resulting midbrain homogenate was centrifuged for 10 minutes at 800 X g and the supernatant was then subjected to 10,000 x g spin for 10 min. Pellets were lysed for 1 hr rotating in PBS + 0.7% n-Dodecyl-beta-Maltoside (DDM; Thermo Fisher Waltham, MA, USA) detergent containing protease inhibitors (P8340, 1:100; Sigma, St. Louis, MO, USA) at 4°C. Protein lysates were centrifuged

for 15 min at 16,060 × *g* to obtain soluble material. Protein concentrations were determined by the BCA method (Thermo Fisher, Waltham, MA, USA). 1 mg of supernatant was then added to 50 µL protein A Dynabeads (Invitrogen, Carlsbad, CA) that were previously cross-linked with an anti-SERT serum #48 using dimethyl pimelimidate (DMP) (Schneider et al., 1982). Briefly, beads were washed 3X in PBS at room temp followed by incubation with #48 anti-SERT serum at 4°C for 1 h. Antibody-bound beads were then incubated with 6.5 mg/mL DMP in 0.2 M Triethylamine (TEA) buffer for 30 min at room temperature. The incubation step was repeated 3X with freshly made DMP buffer each time. Cross-linked beads were then quenched in 50 mM ethanolamine (EA) buffer for 5 min at room temp, washed 2X in 1 M glycine (pH = 3) buffer, and then 3X in PBS (10 min, room temp) and then stored at 4C until use. Immunocomplexes were eluted by incubating beads with 2X Laemmli sample buffer at 70°C for 10 min. Eluted samples were subjected were separated by 10% SDS-PAGE, blotted to PVDF (Millipore, Billerica, MA) membrane and then incubated with primary and secondary antibodies at dilutions noted above. Immunoreactive bands were identified by band visualization and quantitation by enhanced chemiluminescence (BioRad Clarity ECL, Hercules, CA) using an ImageQuant LAS 4000 imager (GE Healthcare Life Sciences, Chicago, IL) or an Odyssey FC imager (Li-Cor Biosciences, Lincoln, NE).

Liquid Chromatography-Tandem Mass Spectrometry

Proteomic analysis was performed in the Vanderbilt Proteomics Core Facility of the Mass Spectrometry Research Center. SERT immunocomplexes eluted from the antibody-conjugated Dynabeads were first resolved for 6 cm using a 10% Novex® precast gel. Protein bands were excised from the gel and cut into 1 mm^3 pieces. The gel pieces were then treated with 45mM DTT for 30 minutes, and available Cys residues were carbamidomethylated with 100mM iodoacetamide for 45 minutes. After destaining the gel pieces with 50% MeCN in 25 mM ammonium bicarbonate, proteins were digested with trypsin (10 ng/µL) in 25 mM ammonium bicarbonate overnight at 37°C. Peptides were extracted by gel dehydration (60% MeCN, 0.1% TFA), the extract was dried by speed vacuum centrifugation, and peptides were reconstituted in 0.1% formic acid. The peptide solutions were then loaded onto a capillary reverse phase analytical

column (360 μm O.D. x 100 μm I.D.) using an Eksigent NanoLC Ultra HPLC and autosampler. The analytical column was packed with 20 cm of C18 reverse phase material (Jupiter, 3 μm beads, 300Å, Phenomenox), directly into a laser-pulled emitter tip. Peptides were gradient-eluted at a flow rate of 500 nL/min, and the mobile phase solvents consisted of 0.1% formic acid, 99.9% water (solvent A) and 0.1% formic acid, 99.9% acetonitrile (solvent B). A 90 min gradient was performed, consisting of the following: 0-15 min (sample loading via autosampler onto column), 2% B; 15-65 min, 2-40% B; 65-74 min, 40-90% B; 74-75 min, 90% B; 75-76 min 90-2% B; 76-90 min (column equilibration), 2% B. Eluting peptides were mass analyzed on an LTQ Orbitrap Velos mass spectrometer (Thermo Scientific), equipped with a nanoelectrospray ionization source. The instrument was operated using a data-dependent method with dynamic exclusion enabled. Full scan (m/z 300-2000) spectra were acquired with the Orbitrap (resolution 60,000), and the top 16 most abundant ions in each MS scan were selected for fragmentation via collision-induced dissociation (CID) in the LTQ. An isolation width of 2 m/z, activation time of 10 ms, and 35% normalized collision energy were used to generate MS2 spectra. Dynamic exclusion settings allowed for a repeat count of 1 within a repeat duration of 10 sec, and the exclusion duration time was set to 15sec. For identification of peptides, tandem mass spectra were searched with Sequest (Thermo Fisher Scientific) against a mouse subset database created from the UniProtKB protein database (www.uniprot.org). Variable modifications of +57.0214 on Cys (carbamidomethylation) and +15.9949 on Met (oxidation) were included for database searching. Search results were assembled using Scaffold 3.6.4 (Proteome Software).

Sequest and Mascot Protein Identification

Charge state deconvolution and deisotoping were not performed. All MS/MS samples were analyzed using Mascot (Matrix Science, London, UK; version 1.4.1.14) and Sequest (Thermo Fisher Scientific, San Jose, CA, USA; version 1.4.1.14) by The Scripps Research Institute, Jupiter Florida. Mascot was set up to search Mouse2016_08_BSA (16918 entries) assuming the digestion enzyme trypsin. Sequest was set up to search Mouse2016_08_BSA.fasta (16918 entries) also assuming trypsin. Mascot was searched with a fragment ion mass tolerance of 20 PPM and a parent ion tolerance of 10.0 PPM. Sequest was searched

with a fragment ion mass tolerance of 0.020 Da and a parent ion tolerance of 10.0 PPM. Carbamidomethyl of cysteine was specified in Mascot and Sequest as a fixed modification. Deamidated ion of asparagine and glutamine and oxidation of methionine were specified in Mascot and Sequest as variable modifications. Scaffold (version Scaffold_4.7.3, Proteome Software Inc., Portland, OR) was used to validate MS/MS based peptide and protein identifications. Peptide identifications were accepted if they could be established at greater than 89.0% probability to achieve an FDR less than 1.0% by the Scaffold Local FDR algorithm. Protein identifications were accepted if they could be established at greater than 99.0% probability to achieve an FDR less than 1.0% and contained at least 2 identified peptides. Protein probabilities were assigned by the Protein Prophet algorithm (Nesvizhskii et al., 2003). Proteins that contained similar peptides and could not be differentiated based on MS/MS analysis alone were grouped to satisfy the principles of parsimony. A total of 1050 proteins were identified.

Label-Free Quantification by Precursor Ion Intensity and Normalized Spectral Counts

Spectral counts or the number of peptides observed per protein have been found to correlate with protein abundance and therefore has been utilized a label-free quantification method (Wong and Cagney, 2009). However, there are many factors that can skew the number of spectral counts, including protein length, protein abundance and variation across sample MS analyses (Miteva et al., 2013). Therefore normalization of spectral counts has been developed as previously described (Paoletti et al., 2006; Tsai et al., 2012). Briefly, normalized spectral abundance factor (NSAF) is calculated by dividing by the number of spectra for each protein +1 (to avoid 0 spectral counts) by the length of the protein and the total number of spectra from all proteins identified in the sample then multiplying by 100. This NSAF value is divided the estimated proteome abundance (PAX) value from the PAX Database (www.pax-db.org) to assess the relative enrichment of proteins within an isolated complex correcting for the possible bias resulting from highly abundant proteins. This forms the normalized spectral count.

Another label-free quantification method is the measurement of the precursor ion intensity of the MS1 spectra (Wong and Cagney, 2009). Scaffold Q+ (version Scaffold_4.7.3, Proteome Software Inc.,

Portland, OR) was used to quantitate. Normalization was performed iteratively (across samples) on intensities. Medians were used for averaging. Spectra data were log-transformed, pruned of those matched to multiple proteins, and weighted by an adaptive intensity weighting algorithm. Of 22133 spectra in the experiment at the given thresholds, 5672 (26%) were included in quantitation. Differentially expressed proteins were determined by applying Mann-Whitney Test with unadjusted significance level $p < 0.05$. To enrich for specific protein interactions, any protein only identified in SERT KO samples or were 1.5 times greater normalized spectral counts or precursor ion intensity of SERT KO compared to either WT or SERT Ala56 samples were eliminated. Also, all ribosomal proteins were removed from the list to eliminate proteins that are involved in the translation of SERT, which was not of interest for this analysis. This narrowed the final list of SERT interacting proteins from 1050 proteins to 459 proteins. To determine differential protein interactions, the $\log_2$ fold change of WT/Ala56 was calculated for both spectral counts and precursor ion intensity.

Functional Clustering Analysis of SIPs by DAVID and STRING

Functional clustering was broken up into 4 lists of proteins: Increased interaction with SERT Ala56 ($\log_2$ ion intensity less than -1); Decreased interaction with SERT Ala56 ($\log_2$ ion intensity greater than 1); Similar interaction between WT SERT and SERT Ala56 ($\log_2$ ion intensity between -1 and 1); and all identified proteins.

The **D**atabase for **A**nnotation, **V**isualization and **I**ntegrated **D**iscovery (DAVID v.6.8; https://david.ncifcrf.gov/) is a platform that allows for the identification of biological themes and gene ontology terms from a list of genes (Huang et al., 2009a). The mouse genome was selected as the population background. Functional Annotation Clustering was performed as described in Haase et al. 2017 with a few exceptions. For the list of proteins with increased interaction with SERT Ala56 medium-stringency classification stringency were utilized. For the other three lists, high stringency was used.

The **S**earch **T**ool for the **R**etrieval of **IN**teracting **G**enes/Proteins (STRING; https://string-db.org) analysis was utilized to build functional networks of known and predicted interacting proteins. Interaction

networks were generated using all five sources: genomic context predictions, high-throughput lab experiments, co-expression, automated text mining, and previous knowledge in databases. The protein-protein enrichment analysis is based on the number of edges detected compared to the expected number edges based on the number of nodes presented (Fisher's exact test followed by a correction for multiple testing) (Szklarczyk et al., 2017). Network edges depict confidence with the line thickness indicating the strength of data support.

Statistical and Graphical Analyses

Data from experiments were analyzed and graphed using Prism 7.0 (GraphPad Software, Inc., La Jolla, CA, USA). For all analyses, a $P < 0.05$ was taken to infer statistical significance. Specific details of statistical tests are given in Figure Legends.

Proteomic Analysis of SERT Interacting Proteins

Protein	Gene	Uniprot Accession #	WT		SERT KO		SERT Ala56		Log_2 (WT/Ala56)	
			Precursor Ion Intensity	Spectral Count	Precursor Ion Intensity	Spectral Count	Precursor Ion Intensity	Spectral Count	Precursor Ion Intensity	Spectral Count
CD109 antigen	Cd109	Q8R422	0	0	0	0	25.6	4.4968	-25.6	-2.45859
Rho GTPase-activating protein 42	Arhgap4	B2RQE8	0	0	0	0	24.94	3.3726	-24.94	-2.12849
Serine/threonine-protein phosphatase 2A 55 kDa regulatory subunit B*	Ppp2r2c	Q8BG02	0	0	0	0	24.23	11.242	-24.23	-3.61376
Centrosomal protein of 131 kDa	Cep131	Q62036	0	0	0	0	24.15	6.7451	-24.15	-2.95328
Inter-alpha-trypsin inhibitor heavy chain H2	Itih2	Q61703	0	0	0	0	23.93	5.621	-23.93	-2.72704
Metastasis-associated protein MTA2	Mta2	Q9R190	0	0	0	0	23.66	2.2484	-23.66	-1.69972
Complement C1q subcomponent subunit C	C1qc	Q02105	0	0	0	0	23.28	2.2484	-23.28	-1.69972
Glutathione S-transferase P 1	Gstp1	P19157	0	0	0	0	23.27	7.8693	-23.27	-3.14882
Tolloid-like protein 1	Tll1	Q62381	0	0	0	0	23.09	2.2484	-23.09	-1.69972
Aldose reductase-related protein 2	Akr1b8	P45377	0	0	0	0	23.09	6.7451	-23.09	-2.95328
Carbonic anhydrase 12	Ca12	Q8CI85	0	0	0	0	22.98	4.4968	-22.98	-2.45859
ATP synthase subunit delta, mitochondrial	Atp5d	Q9D3D9	0	0	0	0	22.97	4.4968	-22.97	-2.45859
Protein transport protein Sec23A*	Sec23a	Q01405	0	0	0	0	22.66	5.621	-22.66	-2.72704
Coronin-2B	Coro2b	Q8BH44	0	0	0	0	22.49	3.3726	-22.49	-2.12849
Golgi-associated plant pathogenesis-related protein 1	Glipr2	Q9CYL5	0	0	0	0	22.38	5.621	-22.38	-2.72704
Protein transport protein Sec61 subunit alpha isoform 1	Sec61a1	P61620	0	0	0	0	22.32	3.3726	-22.32	-2.12849
Synaptophysin	Syp	Q62277	0	0	0	0	22.32	5.621	-22.32	-2.72704
SPATS2-like protein	Spats2l	Q91WJ7	0	0	0	0	22.31	2.2484	-22.31	-1.69972
78 kDa glucose-regulated protein	Hspa5	P20029	0	0	0	0	22.15	15.739	-22.15	-4.06514
Thioredoxin-dependent peroxide reductase, mitochondrial	Prdx3	P20108	0	0	0	0	22.09	6.7451	-22.09	-2.95328
Septin-5	Sept5	Q9Z2Q6	0	0	0	0	22.03	2.2484	-22.03	-1.69972
14-3-3 protein eta *	Ywhah	P68510	0	0	0	0	22.02	15.739	-22.02	-4.06514
Homer protein homolog	Homer3	Q99JP6	0	0	0	0	21.88	4.4968	-21.88	-2.45859
Tetratricopeptide repeat protein 25	Ttc25	Q9D4B2	0	0	0	0	21.69	4.4968	-21.69	-2.45859
Acrosin-binding protein	Acrbp	Q3V140	0	0	0	0	21.67	3.3726	-21.67	-2.12849
Calcium uptake protein 1, mitochondrial	Micu1	Q8VCX5	0	0	0	0	21.65	2.2484	-21.65	-1.69972
Tudor and KH domain-containing protein	Tdrkh	Q80VL1	0	0	0	0	21.57	3.3726	-21.57	-2.12849
Membrane-associated phosphatidylinositol transfer protein 2	Pitpnm2	Q6ZPQ6	0	0	0	0	21.48	2.2484	-21.48	-1.69972

Table 7. SERT Interacting Proteins from Midbrain WT and SERT Ala56 KI Mice

Protein	Gene	Uniprot Accession #	WT		SERT KO		SERT Ala56		Log_2 (WT/Ala56)	
			Precursor Ion Intensity	Spectral Count	Precursor Ion Intensity	Spectral Count	Precursor Ion Intensity	Spectral Count	Precursor Ion Intensity	Spectral Count
Mitochondrial import receptor subunit TOM70	Tomm70a	Q9CZW5	0	0	0	0	21.28	6.7451	-21.28	-2.95328
Lipoprotein lipase	Lpl	P11152	0	0	0	0	21.05	2.2484	-21.05	-1.69972
Ubiquitin-associated domain-containing protein 2	Ubac2	Q8R1K1	0	0	0	0	20.99	2.2484	-20.99	-1.69972
Oxysterol-binding protein-related protein 3	Osbpl3	Q9DBS9	0	0	0	0	20.93	2.2484	-20.93	-1.69972
Elongation factor 1-gamma	Eef1g	Q9D8N0	0	0	0	0	20.93	3.3726	-20.93	-2.12849
Ral GTPase-activating protein subunit beta	Ralgapb	Q8BQZ4	0	0	0	0	20.88	2.2484	-20.88	-1.69972
Serine/threonine-protein kinase PRP4 homolog	Prpf4b	Q61136	0	0	0	0	20.81	4.4968	-20.81	-2.45859
UPF0258 protein KIAA1024	Kiaa1024	Q8K3V7	0	0	0	0	20.45	3.3726	-20.45	-2.12849
Ryanodine receptor 2	Ryr2	E9Q401	0	0	0	0	20.35	4.4968	-20.35	-2.45859
PH and SEC7 domain-containing protein 1	Psd	Q5DTT2	0	0	0	0	20.31	3.3726	-20.31	-2.12849
Inactive ubiquitin carboxyl-terminal hydrolase 54	Usp54	Q8BL06	0	0	0	0	20.23	2.2484	-20.23	-1.69972
Small conductance calcium-activated potassium channel protein	Kcnn2	P58390	0	0	0	0	19.98	3.3726	-19.98	-2.12849
Arginine and glutamate-rich protein 1	Arglu1	Q3UL36	20.71	3.4791	0	0	25.4	13.49	-4.69	-1.69377
Disintegrin and metalloproteinase domain-containing protein 22	Adam22	Q9R1V6	22.38	11.133	23.05	4.4555	25.08	8.9935	-2.7	0.279874
Leucine zipper protein 1	Luzp1	Q8R4U7	20.8	5.5666	0	0	23.26	16.863	-2.46	-1.44375
Retinol dehydrogenase 13	Rdh13	Q8CEE7	21.64	2.0875	0	0	23.81	4.4968	-2.17	-0.83215
F-actin-capping protein subunit alpha-1	Capza1	P47753	22.98	12.525	0	0	24.93	8.9935	-1.95	0.436566
Disks large homolog 1	Dlg1	Q811D0	22.23	22.962	23.28	16.337	24.15	46.092	-1.92	-0.97473
Regulator of nonsense transcripts 1	Upf1	Q9EPU0	21.63	5.5666	0	0	23.45	4.4968	-1.82	0.256554
Double zinc ribbon and ankyrin repeat-containing protein 1	Dzank1	Q8C008	21.06	5.5666	20.79	2.9703	22.85	6.7451	-1.79	-0.23813
Septin-11 **	Sep11	Q8C1B7	22.62	22.962	22.01	8.9109	24.39	23.608	-1.77	-0.03837
Serine/threonine-protein kinase MARK2	Mark2	Q05512	21.95	11.829	23.03	5.9406	23.72	14.614	-1.77	-0.28343
Septin-8	Sept8	Q8CHH9	24.59	31.312	25.22	17.822	26.35	37.098	-1.76	-0.23764
Vesicular inhibitory amino acid transporter	Slc32a1	O35633	21.5	1.3917	0	0	23.12	4.4968	-1.62	-1.20055
Fragile X mental retardation syndrome-related protein 1	Fxr1	Q61584	22.71	14.612	22	2.9703	24.23	16.863	-1.52	-0.19431
Very-long-chain enoyl-CoA reductase	Tecr	Q9CY27	23.01	9.7416	22.35	5.9406	24.41	14.614	-1.4	-0.53963
Arf-GAP with GTPase, ANK repeat and PH domain-containing	Agap1	Q8BXK8	23.19	18.091	22.27	7.4258	24.58	19.111	-1.39	-0.07509
Coronin-1C	Coro1c	Q9WUM4	23.58	14.612	23.65	4.4555	24.93	11.242	-1.35	0.350816
Mitochondrial pyruvate carrier 1	Mpc1	P63030	21.57	1.3917	0	0	22.91	5.621	-1.34	-1.46901
Fibronectin	Fn1	P11276	22.04	6.2624	22.84	4.4555	23.34	10.118	-1.3	-0.61437

Protein	Gene	Uniprot Accession #	WT		SERT KO		SERT Ala56		Log_2 (WT/Ala56)	
			Precursor Ion Intensity	Spectral Count	Precursor Ion Intensity	Spectral Count	Precursor Ion Intensity	Spectral Count	Precursor Ion Intensity	Spectral Count
Sulfide:quinone oxidoreductase, mitochondrial	Sqrdl	Q9R112	22.55	10.437	0	0	23.76	17.987	-1.21	-0.73130
Inositol 1,4,5-trisphosphate receptor type 2	Itpr2	Q9Z329	23.34	1.3917	0	0	24.51	7.8693	-1.17	-1.89078
Fragile X mental retardation protein 1 homolog	Fmr1	P35922	22.16	7.6541	0	0	23.32	10.118	-1.16	-0.36144
Poly(U)-binding-splicing factor PUF60	Puf60	Q3UEB3	23.13	9.7416	22.61	7.4258	24.28	24.732	-1.15	-1.26035
Gamma-adducin	Add3	Q9QYB5	22.93	12.525	21.96	5.9406	24.08	11.242	-1.15	0.143789
Nck-associated protein 1	Nckap1	P28660	22.07	13.221	22.56	5.9406	23.17	16.863	-1.1	-0.32895
Spectrin alpha chain, erythrocytic 1 O	Spta1	P08032	22.06	18.787	0	0	23.1	35.974	-1.04	-0.90195
Serine/threonine-protein kinase MARK1	Mark1	Q8VHJ5	22.14	14.612	21.04	5.9406	23.15	23.608	-1.01	-0.65647
Protein phosphatase 1 regulatory subunit 12A	Ppp1r12a	Q9DBR7	21.92	7.6541	0	0	22.85	5.621	-0.93	0.386334
Single-stranded DNA-binding protein, mitochondrial	Ssbp1	Q9CYR0	20.91	2.0875	0	0	21.81	6.7451	-0.9	-1.32684
Casein kinase I isoform epsilon	Csnk1e	Q9JMK2	22.6	9.0457	0	0	23.42	6.7451	-0.82	0.375222
RalBP1-associated Eps domain-containing protein 1	Reps1	O54916	23.86	13.917	23.13	5.9406	24.66	17.987	-0.8	-0.34805
ATP synthase subunit O, mitochondrial	Atp5o	Q9DB20	24.4	9.0457	22.96	4.4555	25.18	10.118	-0.78	-0.14631
Catalase	Cat	P24270	22.37	2.0875	0	0	23.12	7.8693	-0.75	-1.52238
Gamma-aminobutyric acid type B receptor subunit 2	Gabbr2	Q80T41	22.34	6.9583	22.14	2.9703	23.06	10.118	-0.72	-0.48236
WD repeat-containing protein 47	Wdr47	Q8CGF6	21.08	6.2624	0	0	21.7	5.621	-0.62	0.133397
Rho GTPase-activating protein 32	Arhgap32	Q811P8	21.26	8.3499	0	0	21.88	10.118	-0.62	-0.24987
Centrosomal protein of 170 kDa protein B	Cep170b	Q80U49	21.44	9.7416	0	0	22.03	14.614	-0.59	-0.53963
Tropomyosin alpha-3 chain	Tpm3	P21107	21.52	8.3499	19.44	2.9703	22.08	6.7451	-0.56	0.271667
Spermatogenesis-associated serine-rich protein 2	Spats2	Q8K1N4	21.19	4.8708	0	0	21.72	6.7451	-0.53	-0.39972
TNF receptor-associated factor 3	Traf3	Q60803	24.57	50.795	23.75	29.703	25.09	60.706	-0.52	-0.25259
Leucine-rich repeat-containing protein 7	Lrrc7	Q80TE7	22.2	17.396	21.48	5.9406	22.71	15.739	-0.51	0.136178
Disks large homolog 4	Dlg4	Q62108	24.26	60.537	24.17	28.218	24.75	59.582	-0.49	0.022564
Brain-enriched guanylate kinase-associated protein	Begain	Q68EF6	22.6	12.525	0	0	23.07	13.49	-0.47	-0.09942
Disks large-associated protein 4	Dlgap4	B1AZP2	22.19	9.7416	0	0	22.65	7.8693	-0.46	0.276316
Voltage-gated potassium channel subunit beta-2	Kcnab2	P62482	24.13	9.0457	23.92	4.4555	24.53	10.118	-0.4	-0.14631
Signal-induced proliferation-associated 1-like protein	Sipa1l1	Q8C0T5	20.89	3.4791	0	0	21.29	2.2484	-0.4	0.463479
Rho GTPase-activating protein 23	Arhgap23	Q69ZH9	22.3	4.8708	20.77	4.4555	22.69	10.118	-0.39	-0.92126
Probable phospholipid-transporting ATPase IIA	Atp9a	O70228	21.07	2.0875	0	0	21.45	6.7451	-0.38	-1.32684
Calcium/calmodulin-dependent protein kinase type II*	Camk2b	P28652	23.65	58.449	23.34	26.733	24.02	8.9935	-0.37	2.572590

Protein	Gene	Uniprot Accession #	WT		SERT KO		SERT Ala56		Log_2 (WT/Ala56)	
			Precursor Ion Intensity	Spectral Count	Precursor Ion Intensity	Spectral Count	Precursor Ion Intensity	Spectral Count	Precursor Ion Intensity	Spectral Count
cAMP-dependent protein kinase type II-alpha regulatory subunit*	Prkar2a	P12367	22.2	2.7833	0	0	22.53	5.621	-0.33	-0.80740
Neurofilament light polypeptide	Nefl	P08551	27.16	179.52	25.14	81.684	27.49	196.73	-0.33	-0.13137
Casein kinase I isoform alpha	Csnk1a1	Q8BK63	22.07	1.3917	0	0	22.4	4.4968	-0.33	-1.20055
PTB domain-containing engulfment adapter protein 1	Gulp1	Q8K2A1	23.37	4.175	22.86	5.9406	23.69	13.49	-0.32	-1.48542
Contactin-associated protein 1 **	Cntnap1	O54991	22.35	5.5666	0	0	22.67	7.8693	-0.32	-0.43367
Vacuolar protein sorting-associated protein 13C	Vps13c	Q8BX70	22.61	39.662	21.33	8.9109	22.93	53.961	-0.32	-0.43472
Rho GTPase-activating protein 26	Arhgap26	Q6ZQ82	23.02	10.437	22.02	4.4555	23.32	11.242	-0.3	-0.09813
Leucine-rich repeat and calponin homology domain-containing protein 1	Lrch1	P62046	23.55	10.437	0	0	23.84	6.7451	-0.29	0.562352
STE20/SPS1-related proline-alanine-rich protein kinase	Stk39	Q9Z1W9	23.56	8.3499	0	0	23.81	5.621	-0.25	0.497901
Microtubule-associated protein RP/EB family member 2	Mapre2	Q8R001	22.34	2.7833	0	0	22.59	5.621	-0.25	-0.80740
Mitochondrial carrier homolog 1	Mtch1	Q791T5	23.31	6.9583	0	0	23.55	7.8693	-0.24	-0.15635
AP-1 complex subunit beta-1	Ap1b1	O35643	23.75	40.358	21.66	19.307	23.99	43.843	-0.24	-0.11671
Tyrosine-protein kinase Yes	Yes1	Q04736	23.73	2.0875	0	0	23.95	2.2484	-0.22	-0.07329
Membrane-associated guanylate kinase, WW and PDZ domain-containing protein 2	Magi2	Q9WVQ1	22.4	6.9583	0	0	22.61	8.9935	-0.21	-0.32852
Disks large-associated protein 1	Dlgap1	Q9D415	23.3	12.525	0	0	23.51	8.9935	-0.21	0.436566
Activated CDC42 kinase 1	Tnk2	O54967	23.45	4.175	0	0	23.6	11.242	-0.15	-1.24220
Serine/threonine-protein phosphatase PGAM5, mitochondrial	Pgam5	Q8BX10	22.64	3.4791	0	0	22.79	7.8693	-0.15	-0.98561
Tight junction protein ZO-2	Tjp2	Q9Z0U1	22.94	14.612	21.76	2.9703	23.08	17.987	-0.14	-0.28235
Actin-binding LIM protein 3	Ablim3	Q69ZX8	22.23	7.6541	0	0	22.35	14.614	-0.12	-0.85138
F-box only protein 41	Fbxo41	Q6NS60	21.76	4.175	0	0	21.87	4.4968	-0.11	-0.08703
SH3 and multiple ankyrin repeat domains protein 3	Shank3	Q4ACU6	22.74	13.221	21.84	5.9406	22.84	7.8693	-0.1	0.681130
Catenin beta-1	Ctnnb1	Q02248	24.16	36.879	23.67	22.277	24.25	50.589	-0.09	-0.44566
Unconventional myosin-XVIIIa	Myo18a	Q9JMH9	22.78	40.358	22.04	5.9406	22.85	51.713	-0.07	-0.34999
2-oxoisovalerate dehydrogenase subunit alpha, mitochondrial	Bckdha	P50136	22.11	1.3917	0	0	22.17	2.2484	-0.06	-0.44169
Inter-alpha-trypsin inhibitor heavy chain H1	Itih1	Q61702	23.16	4.8708	0	0	23.2	3.3726	-0.04	0.425065
FERM, RhoGEF and pleckstrin domain-containing protein 1	Farp1	F8VPU2	22.91	6.9583	21.8	2.9703	22.9	8.9935	0.01	-0.32852
Neurofilament heavy polypeptide	Nefh	P19246	25.45	75.149	24.31	43.07	25.43	100.05	0.02	-0.40817
Calcium-binding and coiled-coil domain-containing protein 1	Calcoco1	Q8CGU1	22.21	4.8708	0	0	22.19	8.9935	0.02	-0.76743
Calcium-binding mitochondrial carrier protein SCaMC-2	Slc25a25	A2ASZ8	23.47	5.5666	0	0	23.44	11.242	0.03	-0.89862
Stomatin-like protein 2, mitochondrial	Stoml2	Q99JB2	22.59	4.175	0	0	22.53	14.614	0.06	-1.59320

Protein	Gene	Uniprot Accession	WT		SERT KO		SERT Ala56		Log$_2$ (WT/Ala56)	
			Precursor Ion Intensity	Spectral Count	Precursor Ion Intensity	Spectral Count	Precursor Ion Intensity	Spectral Count	Precursor Ion Intensity	Spectral Count
SLIT-ROBO Rho GTPase-activating protein 3	Srgap3	Q812A2	22.3	4.8708	21.79	2.9703	22.24	6.7451	0.06	-0.39972
Unconventional myosin-IXa	Myo9a	Q8C170	21.42	2.0875	0	0	21.32	3.3726	0.1	-0.50205
Microtubule-actin cross-linking factor 1	Macf1	Q9QXZ0	22.99	69.583	22.13	34.159	22.86	132.65	0.13	-0.92106
Sodium-dependent serotonin transporter	Slc6a4	Q60857	25.73	33.4	24.69	2.9703	25.6	33.726	0.13	-0.01360
Microtubule-associated protein RP/EB family member 3	Mapre3	Q6PER3	22.92	2.0875	0	0	22.77	2.2484	0.15	-0.07329
Protein THEM6	Them6	Q80ZW2	22.37	2.7833	0	0	22.22	2.2484	0.15	0.219915
Rho GTPase-activating protein 21	Arhgap21	Q6DFV3	20.66	1.3917	0	0	20.48	3.3726	0.18	-0.87045
C-1-tetrahydrofolate synthase, cytoplasmic	Mthfd1	Q922D8	22.08	4.175	0	0	21.89	8.9935	0.19	-0.94943
AMP deaminase 3	Ampd3	O08739	22.22	4.8708	0	0	22.01	12.366	0.21	-1.18693
RING finger protein 222	Rnf222	Q8CEF8	23.56	3.4791	0	0	23.33	4.4968	0.23	-0.29538
Actin-related protein 2	Actr2	P61161	23.09	2.7833	0	0	22.86	7.8693	0.23	-1.22917
Synaptotagmin-11 **	Syt11	Q9R0N3	22.26	2.7833	0	0	22.01	6.7451	0.25	-1.03363
Guanine nucleotide-binding protein G(I)/G(S)/G(T) subunit beta-1	Gnb1	P62874	23.01	2.0875	0	0	22.76	4.4968	0.25	-0.83215
Tenascin	Tnc	Q80YX1	21.14	2.0875	0	0	20.82	3.3726	0.32	-0.50205
Myotubularin-related protein 5	Sbf1	Q6ZPE2	21.83	9.0457	0	0	21.5	4.4968	0.33	0.869914
Disks large-associated protein 3	Dlgap3	Q6PFD5	23.94	13.917	22.26	2.9703	23.6	3.3726	0.34	1.770394
Vimentin	Vim	P20152	24.4	22.266	23	13.366	24.04	32.602	0.36	-0.53032
Liprin-alpha-3	Ppfia3	P60469	23.21	12.525	21.63	5.9406	22.81	17.987	0.4	-0.48938
Uncharacterized aarF domain-containing protein kinase 1	Adck1	Q9D0L4	21.03	1.3917	0	0	20.63	4.4968	0.4	-1.20055
Huntingtin-interacting protein 1	Hip1	Q8VD75	21.59	4.175	0	0	21.15	3.3726	0.44	0.243067
SH3-containing GRB2-like protein 3-interacting protein 1	Sgip1	Q8VD37	21.9	2.0875	0	0	21.43	3.3726	0.47	-0.50205
Serine/arginine repetitive matrix protein 1	Srrm1	Q52KI8	21.05	1.3917	0	0	20.56	2.2484	0.49	-0.44169
Protein SCAI	Scai	Q8C8N2	23.39	4.8708	0	0	22.88	5.621	0.51	-0.17349
Disks large homolog 2	Dlg2	Q91XM9	24.13	35.487	23.58	8.9109	23.61	28.105	0.52	0.326115
Sorbin and SH3 domain-containing protein 1	Sorbs1	Q62417	24	18.091	0	0	23.45	19.111	0.55	-0.07509
Pyruvate carboxylase, mitochondrial	Pc	Q05920	23.66	15.308	22.92	8.9109	23.07	21.36	0.59	-0.45534
Long-chain-fatty-acid--CoA ligase 6	Acsl6	Q91WC3	21.5	2.7833	0	0	20.91	2.2484	0.59	0.219915
BMP-2-inducible protein kinase	Bmp2k	Q91Z96	22.43	9.0457	0	0	21.83	8.9935	0.6	0.007516
Arf-GAP with GTPase, ANK repeat and PH domain-containing protein	Agap2	Q3UHD9	22.09	13.917	0	0	21.46	4.4968	0.63	1.440293
Transcriptional activator protein Pur-alpha	Pura	P42669	25.45	26.441	22.55	13.366	24.81	30.353	0.64	-0.19227

Protein	Gene	Uniprot Accession #	WT		SERT KO		SERT Ala56		Log_2 (WT/Ala56)	
			Precursor Ion Intensity	Spectral Count	Precursor Ion Intensity	Spectral Count	Precursor Ion Intensity	Spectral Count	Precursor Ion Intensity	Spectral Count
ATP-binding cassette sub-family D member 3	Abcd3	P55096	23.33	4.8708	0	0	22.6	6.7451	0.73	-0.39972
IQ motif and SEC7 domain-containing protein 1	Iqsec1	Q8R0S2	24.15	28.529	23.57	13.366	23.39	25.856	0.76	0.136888
Homer protein homolog 1	Homer1	Q9Z2Y3	24.14	28.529	22.78	4.4555	23.38	28.105	0.76	0.020865
Diacylglycerol kinase epsilon	Dgke	Q9R1C6	22.49	4.8708	0	0	21.71	4.4968	0.78	0.094965
Pentatricopeptide repeat domain-containing protein 3, mitochondrial	Ptcd3	Q14C51	22.42	4.175	0	0	21.59	3.3726	0.83	0.243067
AP-3 complex subunit beta-2	Ap3b2	Q9JME5	22.7	20.179	21.71	5.9406	21.81	11.242	0.89	0.790795
Cyclin-G-associated kinase	Gak	Q99KY4	22.01	2.0875	0	0	21.11	3.3726	0.9	-0.50205
Tenascin-R	Tnr	Q8BYI9	23.27	11.829	0	0	22.36	3.3726	0.91	1.552845
Glial fibrillary acidic protein	Gfap	P03995	25.13	99.503	22.73	11.881	24.2	80.942	0.93	0.294563
Neurofilament medium polypeptide	Nefm	P08553	26.21	137.77	22.32	49.01	25.2	185.49	1.01	-0.42640
BTB/POZ domain-containing protein KCTD3	Kctd3	Q8BFX3	22.81	4.8708	0	0	21.78	6.7451	1.03	-0.39972
Mitochondrial 2-oxoglutarate/malate carrier protein	Slc25a11	Q9CR62	25.75	32.008	0	0	24.63	13.49	1.12	1.187758
F-actin-capping protein subunit beta	Capzb	P47757	23.85	13.917	23.34	7.4258	22.68	17.987	1.17	-0.34805
MAP/microtubule affinity-regulating kinase 3	Mark3	Q03141	22.25	13.221	0	0	21.04	19.111	1.21	-0.49996
Peripheral plasma membrane protein CASK	Cask	O70589	23.3	9.0457	0	0	22.06	5.621	1.24	0.601457
Peptidyl-glycine alpha-amidating monooxygenase	Pam	P97467	23.53	5.5666	0	0	22.25	4.4968	1.28	0.256554
Rab11 family-interacting protein 2	Rab11fip2	G3XA57	23.06	7.6541	0	0	21.71	5.621	1.35	0.386334
Elongation factor 2	Eef2	P58252	20.86	3.4791	0	0	19.46	2.2484	1.4	0.463479
Cadherin-2	Cdh2	P15116	23.09	18.091	21.26	4.4555	21.59	8.9935	1.5	0.933830
Ral GTPase-activating protein subunit alpha-1	Ralgapa1	Q6GYP7	22.63	4.8708	0	0	21.05	4.4968	1.58	0.094965
ARF GTPase-activating protein GIT1	Git1	Q68FF6	23.3	6.2624	0	0	21.7	7.8693	1.6	-0.28837
14-3-3 protein gamma*	Ywhag	P61982	24.06	18.091	0	0	22.44	19.111	1.62	-0.07509
Junctophilin-3	Jph3	Q9ET77	22.28	3.4791	0	0	20.61	3.3726	1.67	0.034717
WD repeat-containing protein 60	Wdr60	Q8C761	22.34	2.7833	0	0	20.59	2.2484	1.75	0.219915
Serine/threonine-protein kinase MRCK beta	Cdc42bpb	Q7TT50	21.77	2.7833	0	0	19.98	2.2484	1.79	0.219915
Neurabin-2	Ppp1r9b	Q6R891	22.32	4.175	0	0	20.51	5.621	1.81	-0.35549
Partitioning defective 3 homolog	Pard3	Q99NH2	20.76	2.7833	0	0	18.93	2.2484	1.83	0.219915
Paralemmin-1	Palm	Q9Z0P4	22.53	4.8708	0	0	20.53	2.2484	2	0.853827
Epidermal growth factor receptor substrate 15	Eps15	P42567	24.36	29.225	22.42	11.881	22.31	30.353	2.05	-0.05286
Glutamate receptor 2	Gria2	P23819	23.3	9.7416	0	0	21.1	11.242	2.2	-0.18863

Protein	Gene	Uniprot Accession #	WT		SERT KO		SERT Ala56		Log_2 (WT/Ala56)	
			Precursor Ion Intensity	Spectral Count	Precursor Ion Intensity	Spectral Count	Precursor Ion Intensity	Spectral Count	Precursor Ion Intensity	Spectral Count
AP-3 complex subunit delta-1	Ap3d1	O54774	24.05	42.445	23.54	20.792	21.61	23.608	2.44	0.820062
Peripherin	Prph	P15331	23.11	7.6541	0	0	20.4	5.621	2.71	0.386334
Ganglioside-induced differentiation-associated protein 1	Gdap1	O88741	23.85	4.175	0	0	21.02	5.621	2.83	-0.35549
Nuclease EXOG, mitochondrial	Exog	Q8C163	23.56	3.4791	0	0	20.28	2.2484	3.28	0.463479
Mitogen-activated protein kinase kinase kinase 13	Map3k13	Q1HKZ5	23.4	6.9583	0	0	19.59	2.2484	3.81	1.292730
MAP/microtubule affinity-regulating kinase 4	Mark4	Q8CIP4	22.74	6.9583	21.34	2.9703	18.86	0	3.88	2.992460
Peptidyl-prolyl cis-trans isomerase B	Ppib	P24369	23.61	5.5666	0	0	18.68	2.2484	4.93	1.015417
Trafficking protein particle complex subunit 10	Trappc10	Q3TLI0	18.66	1.3917	0	0	0	0	18.66	1.258036
Beta-centractin	Actr1b	Q8R5C5	19.26	1.3917	0	0	0	0	19.26	1.258036
Protein-glutamine gamma-glutamyltransferase 2	Tgm2	P21981	19.41	1.3917	0	0	0	0	19.41	1.258036
Epiplakin	Eppk1	Q8R0W0	19.61	3.4791	0	0	0	0	19.61	2.163208
Cleavage and polyadenylation specificity factor subunit 2]	Cpsf2	O35218	19.63	1.3917	0	0	0	0	19.63	1.258036
Neuronal pentraxin-1	Nptx1	Q62443	19.69	1.3917	0	0	0	0	19.69	1.258036
Neurofibromin	Nf1	Q04690	19.79	1.3917	0	0	0	0	19.79	1.258036
Dihydropyrimidinase-related protein 1	Crmp1	P97427	19.8	6.2624	0	0	0	0	19.8	2.860446
Adenomatous polyposis coli protein 2	Apc2	Q9Z1K7	19.89	2.0875	0	0	0	0	19.89	1.626439
Elongator complex protein 1	Ikbkap	Q7TT37	19.9	1.3917	0	0	0	0	19.9	1.258036
Guanine nucleotide-binding protein-like 3	Gnl3	Q8CI11	20.01	1.3917	0	0	0	0	20.01	1.258036
Coronin-2A	Coro2a	Q8C0P5	20.05	1.3917	0	0	0	0	20.05	1.258036
Alpha-1-syntrophin	Snta1	Q61234	20.09	1.3917	0	0	0	0	20.09	1.258036
ADP-ribosylation factor-like protein 6	Arl6	O88848	20.1	1.3917	0	0	0	0	20.1	1.258036
E3 ubiquitin-protein ligase HERC2	Herc2	Q4U2R1	20.13	2.7833	0	0	0	0	20.13	1.919645
Mitogen-activated protein kinase 3	Mapk3	Q63844	20.19	2.0875	0	0	0	0	20.19	1.626439
La-related protein 1	Larp1	Q6ZQ58	20.2	1.3917	0	0	0	0	20.2	1.258036
Rho GTPase-activating protein 39	Arhgap39	P59281	20.21	2.0875	0	0	0	0	20.21	1.626439
Eukaryotic translation initiation factor 4B	Eif4b	Q8BGD9	20.23	2.0875	0	0	0	0	20.23	1.626439
Traf2 and NCK-interacting protein kinase	Tnik	P83510	20.23	2.0875	0	0	0	0	20.23	1.626439
Angiomotin-like protein 1	Amotl1	Q9D4H4	20.3	1.3917	0	0	0	0	20.3	1.258036
Adhesion G protein-coupled receptor B2	Adgrb2	Q8CGM1	20.33	1.3917	0	0	0	0	20.33	1.258036
Pre-B-cell leukemia transcription factor-interacting protein 1	Pbxip1	Q3TVI8	20.38	1.3917	0	0	0	0	20.38	1.258036

Protein	Gene	Uniprot Accession #	WT		SERT KO		SERT Ala56		Log_2 (WT/Ala56)	
			Precursor Ion Intensity	Spectral Count	Precursor Ion Intensity	Spectral Count	Precursor Ion Intensity	Spectral Count	Precursor Ion Intensity	Spectral Count
Tripartite motif-containing protein 46	Trim46	Q7TNM2	20.41	1.3917	0	0	0	0	20.41	1.258036
CLIP-associating protein 1	Clasp1	Q80TV8	20.41	3.4791	0	0	0	0	20.41	2.163208
Neuroligin-2 *	Nlgn2	Q69ZK9	20.44	3.4791	0	0	0	0	20.44	2.163208
Dehydrogenase/reductase SDR family member 7B	Dhrs7b	Q99J47	20.47	1.3917	0	0	0	0	20.47	1.258036
Fructosamine-3-kinase	Fn3k	Q9ER35	20.48	1.3917	0	0	0	0	20.48	1.258036
D-3-phosphoglycerate dehydrogenase	Phgdh	Q61753	20.48	2.7833	0	0	0	0	20.48	1.919645
Optic atrophy 3 protein homolog	Opa3	Q505D7	20.51	1.3917	0	0	0	0	20.51	1.258036
Long-chain-fatty-acid--CoA ligase ACSBG1	Acsbg1	Q99PU5	20.52	1.3917	0	0	0	0	20.52	1.258036
Probable ubiquitin carboxyl-terminal hydrolase FAF-X	Usp9x	P70398	20.54	2.0875	0	0	0	0	20.54	1.626439
Protein LAP2	Erbb2ip	Q80TH2	20.55	6.2624	0	0	0	0	20.55	2.860446
Lethal(2) giant larvae protein homolog 1	Llgl1	Q80Y17	20.57	1.3917	0	0	0	0	20.57	1.258036
Neurochondrin	Ncdn	Q9Z0E0	20.57	2.0875	0	0	0	0	20.57	1.626439
Catenin delta-1	Ctnnd1	P30999	20.58	3.4791	0	0	0	0	20.58	2.163208
Ceramide kinase	Cerk	Q8K4Q7	20.58	1.3917	0	0	0	0	20.58	1.258036
Collagen alpha-4(VI) chain	Col6a4	A2AX52	20.6	1.3917	0	0	0	0	20.6	1.258036
Synaptotagmin-6 **	Syt6	Q9R0N8	20.63	1.3917	0	0	0	0	20.63	1.258036
Regulatory-associated protein of mTOR	Rptor	Q8K4Q0	20.65	2.0875	0	0	0	0	20.65	1.626439
Ankycorbin	Rai14	Q9EP71	20.69	2.0875	0	0	0	0	20.69	1.626439
Inactive hydroxysteroid dehydrogenase-like protein 1	Hsdl1	Q8BTX9	20.71	2.7833	0	0	0	0	20.71	1.919645
Monofunctional C1-tetrahydrofolate synthase, mitochondrial	Mthfd1l	Q3V3R1	20.72	1.3917	0	0	0	0	20.72	1.258036
Succinyl-CoA:3-ketoacid coenzyme A transferase 1,	Oxct1	Q9D0K2	20.72	2.0875	0	0	0	0	20.72	1.626439
Aggrecan core protein	Acan	Q61282	20.73	4.175	0	0	0	0	20.73	2.371558
Microtubule-associated serine/threonine-protein kinase 1	Mast1	Q9R1L5	20.76	2.7833	0	0	0	0	20.76	1.919645
U4/U6.U5 tri-snRNP-associated protein 1	Sart1	Q9Z315	20.77	1.3917	0	0	0	0	20.77	1.258036
Vesicle-associated membrane protein-associated protein A **	Vapa	Q9WV55	20.84	2.0875	0	0	0	0	20.84	1.626439
Dynamin-1-like protein	Dnm1l	Q8K1M6	20.85	2.0875	0	0	0	0	20.85	1.626439
Tyrosine-protein phosphatase non-receptor type 13	Ptpn13	Q64512	20.87	4.175	0	0	0	0	20.87	2.371558
Glycerol kinase	Gk	Q64516	20.96	2.0875	0	0	0	0	20.96	1.626439
DCC-interacting protein 13-beta	Appl2	Q8K3G9	20.97	2.0875	0	0	0	0	20.97	1.626439
Prickle-like protein 2	Prickle2	Q80Y24	21.01	2.0875	0	0	0	0	21.01	1.626439

Protein	Gene	Uniprot Accession #	WT		SERT KO		SERT Ala56		Log_2 (WT/Ala56)	
			Precursor Ion Intensity	Spectral Count	Precursor Ion Intensity	Spectral Count	Precursor Ion Intensity	Spectral Count	Precursor Ion Intensity	Spectral Count
Gamma-tubulin complex component 2	Tubgcp2	Q921G8	21.02	2.7833	0	0	0	0	21.02	1.919645
Neurofascin	Nfasc	Q810U3	21.03	2.0875	0	0	0	0	21.03	1.626439
Clathrin coat assembly protein AP180	Snap91	Q61548	21.05	1.3917	0	0	0	0	21.05	1.258036
Sn1-specific diacylglycerol lipase alpha	Dagla	Q6WQJ1	21.05	4.175	0	0	0	0	21.05	2.371558
Casein kinase II subunit alpha	Csnk2a1	Q60737	21.06	2.0875	0	0	0	0	21.06	1.626439
Toll-interacting protein	Tollip	Q9QZ06	21.09	2.0875	0	0	0	0	21.09	1.626439
Tubulin alpha chain-like 3	Tubal3	Q3UX10	21.1	10.437	0	0	0	0	21.1	3.515636
Leucine zipper putative tumor suppressor 3	Lzts3	A2AHG0	21.1	5.5666	0	0	0	0	21.1	2.715146
Voltage-dependent R-type calcium channel subunit alpha-1E	Cacna1e	Q61290	21.12	2.0875	0	0	0	0	21.12	1.626439
WD repeat-containing protein 34	Wdr34	Q5U4F6	21.14	1.3917	0	0	0	0	21.14	1.258036
Unconventional myosin-If	Myo1f	P70248	21.14	1.3917	0	0	0	0	21.14	1.258036
CAP-Gly domain-containing linker protein 3	Clip3	B9EHT4	21.15	4.8708	0	0	0	0	21.15	2.553557
C-Jun-amino-terminal kinase-interacting protein 2	Mapk8ip2	Q9ERE9	21.18	1.3917	0	0	0	0	21.18	1.258036
Serine/threonine-protein kinase A-Raf	Araf	P04627	21.19	1.3917	0	0	0	0	21.19	1.258036
Peroxisomal 2,4-dienoyl-CoA reductase	Decr2	Q9WV68	21.21	1.3917	0	0	0	0	21.21	1.258036
Protein argonaute-2	Ago2	Q8CJG0	21.22	2.0875	0	0	0	0	21.22	1.626439
NADH dehydrogenase [ubiquinone] flavoprotein 1, mitochondrial	Ndufv1	Q91YT0	21.24	1.3917	0	0	0	0	21.24	1.258036
Tropomodulin-1	Tmod1	P49813	21.24	1.3917	0	0	0	0	21.24	1.258036
K^+/Na^{2+} hyperpolarization-activated cyclic nucleotide-gated channel	Hcn2	O88703	21.25	2.0875	0	0	0	0	21.25	1.626439
MAP7 domain-containing protein 2	Map7d2	A2AG50	21.28	4.175	0	0	0	0	21.28	2.371558
Non-specific lipid-transfer protein	Scp2	P32020	21.3	2.0875	0	0	0	0	21.3	1.626439
Polypeptide N-acetylgalactosaminyltransferase 16	Galnt16	Q9JJ61	21.38	1.3917	0	0	0	0	21.38	1.258036
Ubiquitin carboxyl-terminal hydrolase 12	Usp12	Q9D9M2	21.39	1.3917	0	0	0	0	21.39	1.258036
NADH dehydrogenase [ubiquinone] 1 alpha subcomplex subunit 9, mitochondrial	Ndufa9	Q9DC69	21.41	2.0875	0	0	0	0	21.41	1.626439
UPF0606 protein KIAA1549	Kiaa1549	Q68FD9	21.43	1.3917	0	0	0	0	21.43	1.258036
Membrane-associated guanylate kinase, WW and PDZ domain-containing protein 3	Magi3	Q9EQJ9	21.43	2.7833	0	0	0	0	21.43	1.919645
Elongator complex protein 3	Elp3	Q9CZX0	21.46	1.3917	0	0	0	0	21.46	1.258036
Gamma-tubulin complex component 3	Tubgcp3	P58854	21.46	3.4791	0	0	0	0	21.46	2.163208
Armadillo repeat-containing X-linked protein 1	Armcx1	Q9CX83	21.47	5.5666	0	0	0	0	21.47	2.715146
Cytoplasmic dynein 1 light intermediate chain 1	Dync1li1	Q8R1Q8	21.48	2.0875	0	0	0	0	21.48	1.626439

Protein	Gene	Uniprot Accession #	WT		SERT KO		SERT Ala56		Log_2 (WT/Ala56)	
			Precursor Ion Intensity	Spectral Count	Precursor Ion Intensity	Spectral Count	Precursor Ion Intensity	Spectral Count	Precursor Ion Intensity	Spectral Count
Calmodulin-regulated spectrin-associated protein 2	Camsap2	Q8C1B1	21.48	2.7833	0	0	0	0	21.48	1.919645
E3 ubiquitin-protein ligase UBR5	Ubr5	Q80TP3	21.49	1.3917	0	0	0	0	21.49	1.258036
Pyruvate dehydrogenase (acetyl-transferring)] kinase isozyme 3, mitochondrial	Pdk3	Q922H2	21.51	3.4791	0	0	0	0	21.51	2.163208
Adenomatous polyposis coli protein	Apc	Q61315	21.51	8.3499	0	0	0	0	21.51	3.224950
TBC1 domain family member 10B	Tbc1d10b	Q8BHL3	21.52	2.7833	0	0	0	0	21.52	1.919645
Peptidyl-prolyl cis-trans isomerase FKBP8	Fkbp8	O35465	21.52	2.0875	0	0	0	0	21.52	1.626439
NACHT and WD repeat domain-containing protein 2	Nwd2	Q6P5U7	21.52	5.5666	0	0	0	0	21.52	2.715146
Signal recognition particle subunit SRP68	Srp68	Q8BMA6	21.54	1.3917	0	0	0	0	21.54	1.258036
Actin-related protein 2/3 complex subunit 5-like protein	Arpc5l	Q9D898	21.55	2.0875	0	0	0	0	21.55	1.626439
Band 4.1-like protein 1	Epb41l1	Q9Z2H5	21.57	3.4791	0	0	0	0	21.57	2.163208
Calmodulin-regulated spectrin-associated protein 3	Camsap3	Q80VC9	21.57	3.4791	0	0	0	0	21.57	2.163208
Protein SERAC1	Serac1	Q3U213	21.59	2.7833	0	0	0	0	21.59	1.919645
Rho guanine nucleotide exchange factor 7	Arhgef7	Q9ES28	21.59	2.7833	0	0	0	0	21.59	1.919645
Calcium uptake protein 3, mitochondrial	Micu3	Q9CTY5	21.61	1.3917	0	0	0	0	21.61	1.258036
Angiomotin	Amot	Q8VHG2	21.62	1.3917	0	0	0	0	21.62	1.258036
Thrombospondin-1	Thbs1	P35441	21.63	1.3917	0	0	0	0	21.63	1.258036
Membrane-associated guanylate kinase, WW and PDZ domain-containing protein 1	Magi1	Q6RHR9	21.64	2.7833	0	0	0	0	21.64	1.919645
Adhesion G protein-coupled receptor L1	Adgrl1	Q80TR1	21.67	2.0875	0	0	0	0	21.67	1.626439
Dimethyladenosine transferase 1, mitochondrial	Tfb1m	Q8JZM0	21.68	3.4791	0	0	0	0	21.68	2.163208
Fumarylacetoacetate hydrolase domain-containing protein 2A	Fahd2	Q3TC72	21.69	2.0875	0	0	0	0	21.69	1.626439
Oxysterol-binding protein-related protein 6	Osbpl6	Q8BXR9	21.69	2.7833	0	0	0	0	21.69	1.919645
Protein flightless-1 homolog	Flii	Q9JJ28	21.7	2.0875	0	0	0	0	21.7	1.626439
Versican core protein	Vcan	Q62059	21.7	4.175	0	0	0	0	21.7	2.371558
T-complex protein 1 subunit alpha	Tcp1	P11983	21.72	1.3917	0	0	0	0	21.72	1.258036
Calcium-independent phospholipase A2-gamma	Pnpla8	Q8K1N1	21.73	1.3917	0	0	0	0	21.73	1.258036
Neuroligin-3	Nlgn3	Q8BYM5	21.73	2.7833	0	0	0	0	21.73	1.919645
Cyclin-dependent kinase-like 5	Cdkl5	Q3UTQ8	21.73	3.4791	0	0	0	0	21.73	2.163208
Protein ELFN1	Elfn1	Q8C8T7	21.74	4.175	0	0	0	0	21.74	2.371558
Caskin-1	Caskin1	Q6P9K8	21.75	3.4791	0	0	0	0	21.75	2.163208
Phytanoyl-CoA dioxygenase, peroxisomal	Phyh	O35386	21.77	2.7833	0	0	0	0	21.77	1.919645

Protein	Gene	Uniprot Accession #	WT		SERT KO		SERT Ala56		Log_2 (WT/Ala56)	
			Precursor Ion Intensity	Spectral Count	Precursor Ion Intensity	Spectral Count	Precursor Ion Intensity	Spectral Count	Precursor Ion Intensity	Spectral Count
MTSS1-like protein	Mtss1l	Q6P9S0	21.77	2.0875	0	0	0	0	21.77	1.626439
Receptor-type tyrosine-protein phosphatase N2	Ptprn2	P80560	21.78	2.0875	0	0	0	0	21.78	1.626439
Peroxiredoxin-2	Prdx2	Q61171	21.78	1.3917	0	0	0	0	21.78	1.258036
Carbonyl reductase family member 4	Cbr4	Q91VT4	21.8	2.7833	0	0	0	0	21.8	1.919645
Profilin-2	Pfn2	Q9JJV2	21.8	3.4791	0	0	0	0	21.8	2.163208
NADH dehydrogenase [ubiquinone] iron-sulfur protein 2, mitochondrial	Ndufs2	Q91WD5	21.83	1.3917	0	0	0	0	21.83	1.258036
Solute carrier family 25 member 46	Slc25a46	Q9CQS4	21.84	1.3917	0	0	0	0	21.84	1.258036
Disabled homolog 2-interacting protein	Dab2ip	Q3UHC7	21.86	9.7416	0	0	0	0	21.86	3.425136
Alpha-actinin-4	Actn4	P57780	21.87	11.829	0	0	0	0	21.87	3.681336
Signal-induced proliferation-associated 1-like protein 2	Sipa1l2	Q80TE4	21.88	2.7833	0	0	0	0	21.88	1.919645
Phosphorylase b kinase gamma catalytic chain, skeletal	Phkg1	P07934	21.89	1.3917	0	0	0	0	21.89	1.258036
Disks large-associated protein 2	Dlgap2	Q8BJ42	21.89	9.0457	0	0	0	0	21.89	3.328506
Vacuolar protein sorting-associated protein 16 homolog	Vps16	Q920Q4	21.91	1.3917	0	0	0	0	21.91	1.258036
Methylcrotonoyl-CoA carboxylase subunit alpha, mitochondrial	Mccc1	Q99MR8	21.92	2.7833	0	0	0	0	21.92	1.919645
Huntingtin-associated protein 1	Hap1	O35668	21.92	2.7833	0	0	0	0	21.92	1.919645
Myc box-dependent-interacting protein 1	Bin1	O08539	21.96	1.3917	0	0	0	0	21.96	1.258036
Vinculin	Vcl	Q64727	21.98	2.7833	0	0	0	0	21.98	1.919645
Cytospin-B	Specc1	Q5SXY1	21.98	2.7833	0	0	0	0	21.98	1.919645
Serine beta-lactamase-like protein LACTB, mitochondrial	Lactb	Q9EP89	22	1.3917	0	0	0	0	22	1.258036
Trafficking protein particle complex subunit 5	Trappc5	Q9CQA1	22.03	2.0875	0	0	0	0	22.03	1.626439
Myosin regulatory light chain 12B	Myl12b	Q3THE2	22.04	2.0875	0	0	0	0	22.04	1.626439
Guanine nucleotide-binding protein G(z) subunit alpha	Gnaz	O70443	22.05	3.4791	0	0	0	0	22.05	2.163208
RalBP1-associated Eps domain-containing protein 2	Reps2	Q80XA6	22.07	2.7833	0	0	0	0	22.07	1.919645
Protein rogdi homolog	Rogdi	Q3TDK6	22.07	3.4791	0	0	0	0	22.07	2.163208
Sphingosine-1-phosphate lyase 1	Sgpl1	Q8R0X7	22.09	2.7833	0	0	0	0	22.09	1.919645
Coiled-coil domain-containing protein 177	Ccdc177	Q3UHB8	22.09	5.5666	0	0	0	0	22.09	2.715146
Cell division control protein 42 homolog	Cdc42	P60766	22.1	2.0875	0	0	0	0	22.1	1.626439
Glutamate receptor-interacting protein 1	Grip1	Q925T6	22.11	2.0875	0	0	0	0	22.11	1.626439
Dual specificity mitogen-activated protein kinase kinase 1	Map2k1	P31938	22.12	1.3917	0	0	0	0	22.12	1.258036
Phospholipid hydroperoxide glutathione peroxidase, nuclear	Gpx4	Q91XR9	22.13	2.7833	0	0	0	0	22.13	1.919645

Protein	Gene	Uniprot Accession #	WT		SERT KO		SERT Ala56		Log_2 (WT/Ala56)	
			Precursor Ion Intensity	Spectral Count	Precursor Ion Intensity	Spectral Count	Precursor Ion Intensity	Spectral Count	Precursor Ion Intensity	Spectral Count
GTP-binding protein Di-Ras2	Diras2	Q5PR73	22.13	3.4791	0	0	0	0	22.13	2.163208
Serine/threonine-protein phosphatase 2A catalytic subunit beta isoform *	Ppp2cb	P62715	22.14	2.0875	0	0	0	0	22.14	1.626439
Diacylglycerol kinase beta	Dgkb	Q6NS52	22.15	2.0875	0	0	0	0	22.15	1.626439
14-3-3 protein beta/alpha	Ywhab	Q9CQV8	22.15	13.917	0	0	0	0	22.15	3.898885
Transmembrane protein 160	Tmem160	Q9D938	22.16	1.3917	0	0	0	0	22.16	1.258036
Ras-related protein Rap-2a	Rap2a	Q80ZJ1	22.18	4.8708	0	0	0	0	22.18	2.553557
Multifunctional protein ADE2	Paics	Q9DCL9	22.23	2.0875	0	0	0	0	22.23	1.626439
Peptidyl-prolyl cis-trans isomerase A **	Ppia	P17742	22.23	2.0875	0	0	0	0	22.23	1.626439
Serine/arginine-rich splicing factor 3	Srsf3	P84104	22.25	1.3917	0	0	0	0	22.25	1.258036
Glutamate receptor 1	Gria1	P23818	22.25	3.4791	0	0	0	0	22.25	2.163208
Glutamate receptor 4	Gria4	Q9Z2W8	22.26	8.3499	0	0	0	0	22.26	3.224950
Ras GTPase-activating protein-binding protein 2	G3bp2	P97379	22.29	1.3917	0	0	0	0	22.29	1.258036
Ras-related protein Rab-5A	Rab5a	Q9CQD1	22.34	1.3917	0	0	0	0	22.34	1.258036
Storkhead-box protein 1	Stox1	B2RQL2	22.36	1.3917	0	0	0	0	22.36	1.258036
F-BAR domain only protein 2	Fcho2	Q3UQN2	22.36	2.0875	0	0	0	0	22.36	1.626439
Heat shock protein 105 kDa	Hsph1	Q61699	22.36	4.175	0	0	0	0	22.36	2.371558
D-beta-hydroxybutyrate dehydrogenase, mitochondrial	Bdh1	Q80XN0	22.38	2.7833	0	0	0	0	22.38	1.919645
ATP-dependent 6-phosphofructokinase, liver type	Pfkl	P12382	22.43	13.221	0	0	0	0	22.43	3.829951
Protein FAM98A	Fam98a	Q3TJZ6	22.43	1.3917	0	0	0	0	22.43	1.258036
Myelin-associated glycoprotein	Mag	P20917	22.45	1.3917	0	0	0	0	22.45	1.258036
LETM1 domain-containing protein 1	Letmd1	Q924L1	22.46	2.0875	0	0	0	0	22.46	1.626439
Serine protease HTRA1	Htra1	Q9R118	22.46	1.3917	0	0	0	0	22.46	1.258036
Centrosome-associated protein CEP250	Cep250	Q60952	22.46	2.7833	0	0	0	0	22.46	1.919645
Neuronal growth regulator 1	Negr1	Q80Z24	22.47	8.3499	0	0	0	0	22.47	3.224950
Long-chain-fatty-acid--CoA ligase 3	Acsl3	Q9CZW4	22.47	3.4791	0	0	0	0	22.47	2.163208
Fragile X mental retardation syndrome-related protein 2	Fxr2	Q9WVR4	22.51	6.2624	0	0	0	0	22.51	2.860446
Carnitine O-palmitoyltransferase 1	Cpt1a	P97742	22.51	2.7833	0	0	0	0	22.51	1.919645
Unconventional myosin-Ic	Myo1c	Q9WTI7	22.54	5.5666	0	0	0	0	22.54	2.715146
CAP-Gly domain-containing linker protein 2	Clip2	Q9Z0H8	22.54	6.9583	0	0	0	0	22.54	2.992460
DnaJ homolog subfamily A member 3, mitochondrial	Dnaja3	Q99M87	22.54	6.9583	0	0	0	0	22.54	2.992460

Protein	Gene	Uniprot Accession #	WT		SERT KO		SERT Ala56		Log_2 (WT/Ala56)	
			Precursor Ion Intensity	Spectral Count	Precursor Ion Intensity	Spectral Count	Precursor Ion Intensity	Spectral Count	Precursor Ion Intensity	Spectral Count
Tryptophan 5-hydroxylase 2*	Tph2	Q8CGV2	22.55	1.3917	0	0	0	0	22.55	1.258036
Solute carrier family 25 member 33	Slc25a33	Q3TZX3	22.55	2.0875	0	0	0	0	22.55	1.626439
Cyclin-dependent kinase 18	Cdk18	Q04899	22.57	2.7833	0	0	0	0	22.57	1.919645
DnaJ homolog subfamily C member 11	Dnajc11	Q5U458	22.57	4.8708	0	0	0	0	22.57	2.553557
Glutamate receptor ionotropic, NMDA 2A	Grin2a	P35436	22.58	4.175	0	0	0	0	22.58	2.371558
Transmembrane and coiled-coil domains protein 3	Tmcc3	Q8R310	22.59	1.3917	0	0	0	0	22.59	1.258036
DnaJ homolog subfamily B member 6	Dnajb6	O54946	22.6	2.0875	0	0	0	0	22.6	1.626439
E3 ubiquitin-protein ligase TRIM32	Trim32	Q8CH72	22.61	6.2624	0	0	0	0	22.61	2.860446
Probable Xaa-Pro aminopeptidase 3	Xpnpep3	B7ZMP1	22.62	4.8708	0	0	0	0	22.62	2.553557
Poly(rC)-binding protein 1	Pcbp1	P60335	22.63	4.8708	0	0	0	0	22.63	2.553557
Sorbin and SH3 domain-containing protein 2	Sorbs2	Q3UTJ2	22.66	7.6541	20.44	2.9703	0	0	22.66	3.113383
Synaptopodin **	Synpo	Q8CC35	22.67	4.175	0	0	0	0	22.67	2.371558
Brain-specific angiogenesis inhibitor 1-associated protein 2	Baiap2	Q8BKX1	22.67	8.3499	0	0	0	0	22.67	3.224950
Acylglycerol kinase, mitochondrial	Agk	Q9ESW4	22.68	5.5666	0	0	0	0	22.68	2.715146
Disks large homolog 3	Dlg3	P70175	22.75	6.2624	0	0	0	0	22.75	2.860446
ELAV-like protein 4	Elavl4	Q61701	22.76	7.6541	0	0	0	0	22.76	3.113383
Glutamate receptor 3	Gria3	Q9Z2W9	22.76	9.0457	0	0	0	0	22.76	3.328506
Protein phosphatase 1 regulatory subunit 29	Elfn2	Q68FM6	22.78	1.3917	0	0	0	0	22.78	1.258036
Protein-L-isoaspartate(D-aspartate) O-methyltransferase	Pcmt1	P23506	22.78	2.7833	0	0	0	0	22.78	1.919645
Carboxypeptidase E	Cpe	Q00493	22.85	2.0875	0	0	0	0	22.85	1.626439
Synaptotagmin-5 **	Syt5	Q9R0N5	22.86	9.7416	0	0	0	0	22.86	3.425136
Dystrobrevin alpha	Dtna	Q9D2N4	22.87	2.7833	0	0	0	0	22.87	1.919645
Alpha-actinin-1	Actn1	Q7TPR4	22.93	10.437	0	0	0	0	22.93	3.515636
Cystic fibrosis transmembrane conductance regulator	Cftr	P26361	22.94	1.3917	0	0	0	0	22.94	1.258036
ELAV-like protein 2	Elavl2	Q60899	22.94	9.0457	0	0	0	3.3726	22.94	1.200014
Protein numb homolog	Numb	Q9QZS3	22.95	8.3499	0	0	0	0	22.95	3.224950
Constitutive coactivator of PPAR-gamma-like protein 2	Fam120c	Q8C3F2	22.95	2.7833	0	0	0	0	22.95	1.919645
BTB/POZ domain-containing protein KCTD8	Kctd8	Q50H33	22.98	6.2624	0	0	0	0	22.98	2.860446
Septin-10	Sep10	Q9DB72	22.98	9.0457	0	0	0	0	22.98	3.328506
BTB/POZ domain-containing protein 17 O	Btbd17	P62814	23.02	4.175	0	0	0	0	23.02	2.371558

Protein	Gene	Uniprot Accession #	WT		SERT KO		SERT Ala56		Log_2 (WT/Ala56)	
			Precursor Ion Intensity	Spectral Count	Precursor Ion Intensity	Spectral Count	Precursor Ion Intensity	Spectral Count	Precursor Ion Intensity	Spectral Count
V-type proton ATPase subunit B, brain isoform	Atp6v1b2	Q9JM76	23.03	4.8708	0	0	0	0	23.03	2.553557
Actin-related protein 2/3 complex subunit 3	Arpc3	P35293	23.04	2.0875	0	0	0	0	23.04	1.626439
Ras-related protein Rab-18	Rab18	Q8CG46	23.04	2.0875	0	0	0	0	23.04	1.626439
Structural maintenance of chromosomes protein 5	Smc5	P55066	23.06	1.3917	0	0	0	0	23.06	1.258036
Neurocan core protein	Ncan	Q61423	23.09	5.5666	0	0	0	0	23.09	2.715146
Potassium voltage-gated channel subfamily A member 4	Kcna4	Q8CHG7	23.1	4.175	0	0	0	0	23.1	2.371558
Rap guanine nucleotide exchange factor 2	Rapgef2	A2AKB4	23.14	1.3917	0	0	0	0	23.14	1.258036
FERM and PDZ domain-containing protein 1	Frmpd1	P29341	23.18	1.3917	0	0	0	0	23.18	1.258036
Polyadenylate-binding protein 1	Pabpc1	Q61410	23.2	13.221	0	0	0	0	23.2	3.829951
cGMP-dependent protein kinase 2*	Prkg2	Q5M8N0	23.21	2.7833	0	0	0	0	23.21	1.919645
CB1 cannabinoid receptor-interacting protein 1	Cnrip1	Q9WV18	23.23	1.3917	0	0	0	0	23.23	1.258036
Gamma-aminobutyric acid type B receptor subunit 1	Gabbr1	Q9CVB6	23.26	2.0875	0	0	0	0	23.26	1.626439
Actin-related protein 2/3 complex subunit 2	Arpc2	Q60605	23.27	1.3917	0	0	0	0	23.27	1.258036
Myosin light polypeptide 6	Myl6	Q65CL1	23.28	4.8708	0	0	0	0	23.28	2.553557
Catenin alpha-3	Ctnna3	Q9D7F7	23.29	1.3917	0	0	0	0	23.29	1.258036
Charged multivesicular body protein 4c	Chmp4c	P10639	23.31	1.3917	0	0	0	0	23.31	1.258036
Thioredoxin	Txn	G5E829	23.32	2.7833	0	0	0	0	23.32	1.919645
Plasma membrane calcium-transporting ATPase 1	Atp2b1	Q80UP3	23.34	11.133	0	0	0	0	23.34	3.600864
Diacylglycerol kinase zeta	Dgkz	P12815	23.35	1.3917	0	0	0	0	23.35	1.258036
Alpha-1,3/1,6-mannosyltransferase ALG2	Alg2	Q9DBE8	23.35	6.9583	0	0	0	0	23.35	2.992460
Mitochondrial fission regulator 1-like	Mtfr1l	Q9CWE0	23.35	1.3917	0	0	0	0	23.35	1.258036
Dynein light chain 1, cytoplasmic	Dynll1	P63168	23.39	1.3917	0	0	0	0	23.39	1.258036
Glycine receptor subunit beta	Glrb	P48168	23.4	3.4791	0	0	0	0	23.4	2.163208
Potassium voltage-gated channel subfamily KQT member 2	Kcnq2	Q9Z351	23.4	1.3917	0	0	0	0	23.4	1.258036
ATP-sensitive inward rectifier potassium channel 10	Kcnj10	Q9JM63	23.41	6.2624	0	0	0	0	23.41	2.860446
Ankyrin repeat and BTB/POZ domain-containing protein	Btbd11	Q6GQW0	23.42	8.3499	0	0	0	0	23.42	3.224950
Serine/threonine-protein phosphatase PP1-alpha catalytic	Ppp1ca	P62137	23.43	4.175	0	0	0	0	23.43	2.371558
Very-long-chain (3R)-3-hydroxyacyl-CoA dehydratase 3	Hacd3	Q8K2C9	23.46	3.4791	0	0	0	0	23.46	2.163208
Glycogen synthase kinase-3 beta	Gsk3b	Q9WV60	23.48	2.0875	0	0	0	0	23.48	1.626439
E3 ubiquitin-protein ligase MIB2	Mib2	Q8R516	23.5	2.7833	0	0	0	0	23.5	1.919645

Protein	Gene	Uniprot Accession #	WT		SERT KO		SERT Ala56		Log_2 (WT/Ala56)	
			Precursor Ion Intensity	Spectral Count	Precursor Ion Intensity	Spectral Count	Precursor Ion Intensity	Spectral Count	Precursor Ion Intensity	Spectral Count
Palmitoyl-protein thioesterase 1	Ppt1	O88531	23.53	3.4791	0	0	0	0	23.53	2.163208
BTB/POZ domain-containing protein KCTD12	Kctd12	Q6WVG3	23.58	7.6541	0	0	0	0	23.58	3.113383
Prohibitin **	Phb	P67778	23.63	2.7833	0	0	0	0	23.63	1.919645
Actin-related protein 3	Actr3	Q99JY9	23.67	6.9583	0	0	0	0	23.67	2.992460
Src substrate cortactin	Cttn	Q60598	23.73	4.8708	0	0	0	0	23.73	2.553557
DDB1- and CUL4-associated factor 7	Dcaf7	P61963	23.75	4.175	0	0	0	0	23.75	2.371558
Rabphilin-3A	Rph3a	P47708	23.81	1.3917	0	0	0	0	23.81	1.258036
Hyaluronan and proteoglycan link protein 1	Hapln1	Q9QUP5	23.81	6.9583	0	0	0	0	23.81	2.992460
LanC-like protein 1	Lancl1	O89112	23.83	3.4791	0	0	0	0	23.83	2.163208
Wolframin	Wfs1	P56695	23.89	2.0875	0	0	0	0	23.89	1.626439
Claudin-11	Cldn11	Q60771	23.94	9.0457	0	0	0	0	23.94	3.328506
Hemoglobin subunit beta-1	Hbb-b1	P02088	23.95	4.175	0	0	0	0	23.95	2.371558
Mitochondrial pyruvate carrier 2	Mpc2	Q9D023	23.99	4.175	0	0	0	0	23.99	2.371558
Lon protease homolog 2, peroxisomal	Lonp2	Q9DBN5	24.03	1.3917	0	0	0	0	24.03	1.258036
Prohibitin-2	Phb2	O35129	24.03	4.8708	0	0	0	0	24.03	2.553557
Casein kinase I isoform delta	Csnk1d	Q9DC28	24.07	7.6541	0	0	0	0	24.07	3.113383
Arf-GAP with GTPase, ANK repeat and PH domain-containing protein 3	Agap3	Q8VHH5	24.14	10.437	0	0	0	0	24.14	3.515636768
Coiled-coil domain-containing protein 15	Ccdc15	Q8C9M2	24.14	2.0875	0	0	0	0	24.14	1.626439
Cytochrome c oxidase subunit NDUFA4	Ndufa4	Q62425	24.19	5.5666	0	0	0	0	24.19	2.715146
Ankyrin repeat and sterile alpha motif domain-containing	Anks1b	Q8BIZ1	24.21	3.4791	0	0	0	0	24.21	2.163208
Actin-related protein 2/3 complex subunit 4	Arpc4	P59999	24.22	4.8708	0	0	0	0	24.22	2.553557
G-protein coupled receptor 98	Gpr98	Q8VHN7	24.27	1.3917	0	0	0	0	24.27	1.258036
Beta-adducin	Add2	Q9QYB8	24.3	8.3499	0	0	0	0	24.3	3.224950
ADP-ribosylation factor 3	Arf3	P61205	24.35	2.7833	0	0	0	0	24.35	1.919645
Metaxin-2	Mtx2	O88441	24.37	1.3917	0	0	0	0	24.37	1.258036
Phosphatidylserine decarboxylase proenzyme	Pisd	Q8BSF4	24.55	18.091	23.92	7.4258	0	0	24.55	4.254820
Syntaxin-binding protein 5 *	Stxbp5	Q8K400	24.7	2.0875	0	0	0	0	24.7	1.626439
RUN domain-containing protein 3A	Rundc3a	O08576	24.71	4.175	0	0	0	0	24.71	2.371558
F-actin-capping protein subunit alpha-2	Capza2	P47754	24.76	13.917	0	0	0	0	24.76	3.898885
Voltage-dependent anion-selective channel protein 3	Vdac3	Q60931	24.79	11.829	22.18	2.9703	0	0	24.79	3.681336

Protein	Gene	Uniprot Accession #	WT		SERT KO		SERT Ala56		Log_2 (WT/Ala56)	
			Precursor Ion Intensity	Spectral Count	Precursor Ion Intensity	Spectral Count	Precursor Ion Intensity	Spectral Count	Precursor Ion Intensity	Spectral Count
Epithelial discoidin domain-containing receptor 1	Ddr1	Q03146	25.04	3.4791	0	0	0	0	25.04	2.163208
AP-2 complex subunit sigma	Ap2s1	P62743	25.17	2.7833	0	0	0	0	25.17	1.919645
Excitatory amino acid transporter 1	Slc1a3	P56564	25.45	15.308	0	0	0	0	25.45	4.027507
Cytochrome b-c1 complex subunit 8	Uqcrq	Q9CQ69	25.5	4.8708	0	0	0	0	25.5	2.553557
Dynein light chain 2, cytoplasmic	Dynll2	Q9D0M5	25.51	8.3499	0	0	0	0	25.51	3.224950
ADP/ATP translocase 2	Slc25a5	P51881	26.06	43.141	0	0	0	0	26.06	5.464047
Drebrin-like protein	Dbnl	Q62418	26.92	1.3917	0	0	0	0	26.92	1.258036
Actin, aortic smooth muscle	Acta2	P62737	27.27	103.68	0	0	0	0	27.27	6.709842
Leukemia inhibitory factor receptor	Lifr	P42703	27.5	1.3917	0	0	0	0	27.5	1.258036
StAR-related lipid transfer protein 9	Stard9	Q80TF6	28.17	2.7833	0	0	0	0	28.17	1.919645
Flotillin-1 *	Flot1	O08917	28.57	1.3917	0	0	0	0	28.57	1.258036

CHAPTER 4

GENETIC MANIPULATION OF MICE TO INTERFERE WITH CONFORMATION AND SIGNALING DEPENDENT SERT REGULATION: CREATION AND ANALYSIS OF THE SERT ALA276 AND SERT GLU276 MOUSE

Krista Paffenroth, Paula A. Kurdziel, Ran Ye, Isabel Stillman, Mathew J. Robson, Fiona Harrison, Sammanda Ramamoorthy, and Randy D. Blakely contributed to the studies reported in this chapter.

Introduction

The transporter is a highly dynamic membrane protein, manipulated by a number of kinases, including p38 MAPK, PKC, PKG and CaMKII signaling pathways (Bermingham and Blakely, 2016). Many of these pathways have also been linked to mediating SERT phosphorylation levels. While there are a number of predicted phosphorylation sites located along the cytoplasmic regions of SERT (Sørensen et al., 2014), Thr276 located on ICL2, was the first SERT phosphorylation site characterized (Ramamoorthy et al., 2007).

SERT Thr276 was first investigated in relation to its role as a key mediator of PKG-dependent regulation of SERT (Ramamoorthy et al., 2007). It was well known that activation of PKG pathways led to both enhanced SERT mediate 5-HT uptake and SERT phosphorylation levels (Ramamoorthy et al., 1998). Moreover, when Thr276 was mutated to Ala, SERT becomes insensitive to PKG activators, such as 8-Br-cGMP, in terms of activity and phosphorylation (Ramamoorthy et al., 2007). This work implicated Thr276 as being the key amino acid required for PKG-dependent regulation of the transporter in both mouse and human SERT. Notably, Wong and colleagues reported that although 8-Br-cGMP treatment of hSERT-transfected cells leads to transporter phosphorylation, PKG is not the direct kinase that phosphorylates SERT, suggesting that a different Ser/Thr kinase is activated through PKG-dependent pathways to phosphorylate SERT Thr276 (Wong et al., 2012).

Data generated by Zhang et al. indicates that SERT Thr276 becomes accessible for phosphorylation when the transporter is cycling through the inward-facing conformation (Zhang et al., 2016), most likely in

the conformation assumed by the transporter as it releases its substrate 5-HT into the cytoplasm. These findings are consistent with ICL2, where Thr276 resides, unwinding and becoming solvent exposed and accessible for modulation as it enters the inward-facing conformation (Zhang and Rudnick, 2005b).

Recently, SERT Thr276 phosphorylation has also been found to be sensitive to membrane lipid environments, with phosphorylation at Thr276 increasing when cholesterol is depleted from the membrane in rat midbrain primary neuronal cultures, which also leads to an enhanced lateral movement of SERT through the membrane (Bailey et al., 2018). Currently the role of phosphorylation at SERT Thr26 *in vivo* is unknown. To investigate this issue, we developed a mouse line that is incapable of phosphorylation at amino acid 276 by mutating the Thr to an Ala using CRISPR/Cas 9 technology, generating a SERT Ala276 KI mouse. We also generated a Thr 276 phosphomimetic line where the Thr at 276 was mutated to encode a Glu residue, although through a currently unknown mechanism, the SERT Glu276 lost both SERT mRNA and protein production. Herein, I describe our initial characterization of the SERT Ala276 mouse, finding that many phenotypes do not appear to be different in comparison with WT animals. However, we identified interesting sex-dependent behavioral changes in the SERT Ala276 KI mice that may indicate that SERT regulation in males and females is different.

Results

Generation of SERT Ala276/Glu276 Mice by CRISPR/Cas9 and Baseline Characterizations

To study the *in vivo* impact of SERT Thr276, we sought to both eliminate the ability of Thr276 to be phosphorylated by mutating the Thr residue to Ala in the native mouse SERT locus and to generate a constitutive mimic of Thr276 phosphorylation by changing the Thr codon to Glu. Using the CRISPR/Cas9 approach, we developed a guide RNA targeted to chromosome 11 of the 6th exon of the *Slc6a4* gene and donor oligonucleotides that possesses sequences leading to change changes of the codon at SERT 276 from Thr (ACG) to Ala (GCG) or Glu (GAG) (**Figure 18A)**. One male SERT Ala276 and one female SERT Glu276 founder mouse was identified via Sanger sequencing (**Figure 18B**) and was used to generate heterozygous (Het)

mice that were subsequently backcrossed to the C57Bl/6J background 4 generations to eliminate any off-target genes affected by CRISPR.

From 25 separate Het breeding pairs of SERT Ala276 of 69 litters across two institutions (Vanderbilt University and Florida Atlantic University), which resulted in 458 pups total, we tabulated offspring genotype and sex. The SERT Ala56 allele knock-in mice exhibited normal Mendelian segregation (**Figure 18C**) when animals of both sexes were examined. Interestingly, we found a significant bias in the sex of offspring from Het breeders, with fewer males recovered than females although genotype distribution within each sex-maintained expectation for Mendelian transmission (**Figure 18C**), suggesting an issue of a Het SERT Ala276 maternal genotype in the generation or growth of male vs female embryos (or that mothers selectively kill males in immediately after birth, which we would miss). The weights between genotypes of both sexes do not differ at any point from weening to adulthood (3-12 weeks of age) **(Figure 18D)**.

Biogenic Amine Levels in SERT Ala276 Mice are Unaltered.

We next assessed if SERT Ala276 affected the levels of 5-HT and other biogenic amines and metabolites in four different brain regions of adult (8-12 weeks) animals: midbrain, hippocampus, forebrain and cerebellum. 5-HT and the main 5-HT metabolite, 5-hydroxyindoleacetic acid (5-HIAA), demonstrated no difference across genotypes **(Table 8A-B).** We also measured catecholamine levels, finding again normal levels across all genotypes in all brain regions assessed for DA and NE and two metabolites of these neurotransmitters, 3,4-dihydroxyphenyl-acetic acid (DOPAC) and homovanillic acid (HVA)**,** respectively. Finally, we evaluated the main excitatory and inhibitory neurotransmitters, Glu and γ-aminobutyric acid (GABA), respectively, and again found no differences between SERT Ala56, heterozygous (Het), and WT littermates for both males and females.

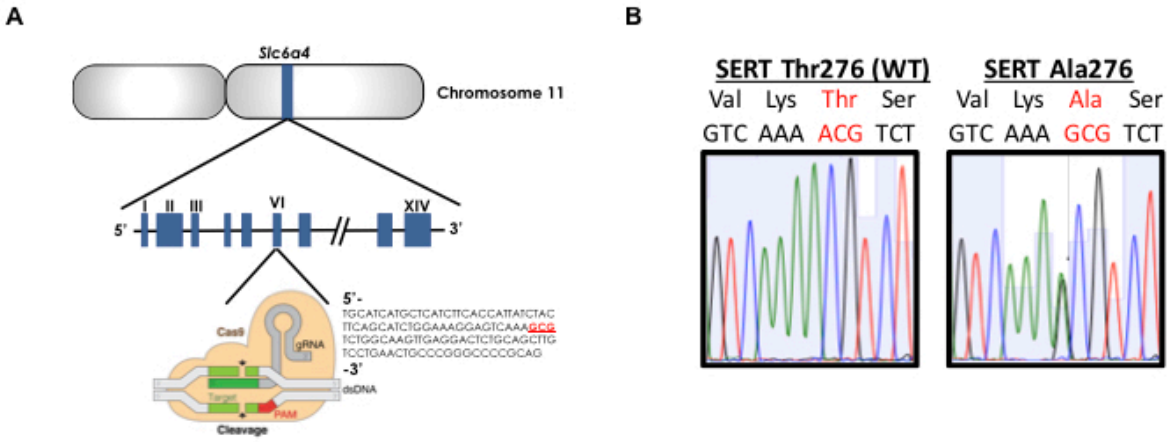

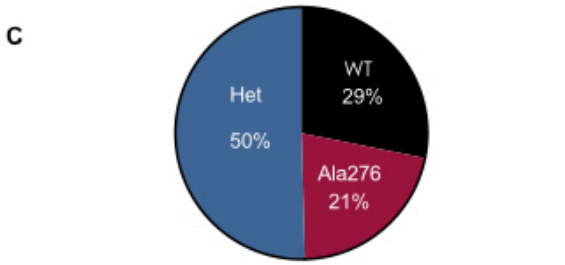

		WT	Het	Ala276	Total
Expected	M	57.25 (12.5%)	114.5 (25%)	57.25 (12.5%)	229 (50%)
	F	57.25 (12.5%)	114.5 (25%)	57.25 (12.5%)	229 (50%)
	Total	114.5 (25%)	229 (50%)	114.5 (25%)	458 (100%)
Observed	M	67 (14.63%)	121 (26.42%)	51 (11.14%)	180 (30.3%)***
	F	62 (13.54%)	110 (24.02%)	47 (10.26%)	278 (60.7%)***
	Total	129 (28.17%)	231 (50.44%)	98 (21.4%)	458 (100%)

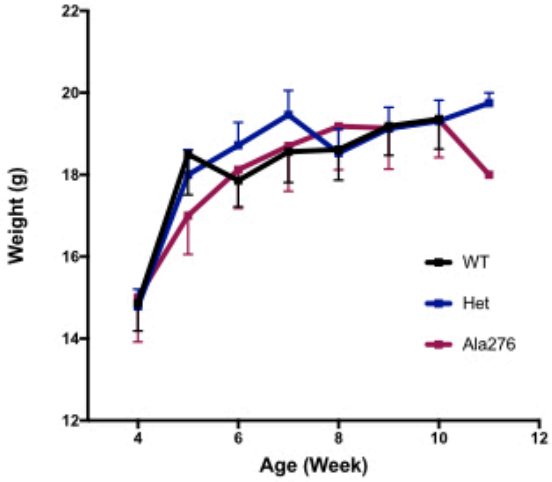

Figure 18. Generation of SERT Ala276 mice and baseline characterizations

(A) SERT Ala276 mice were generated by CRISPR/Cas9 technology utilizing a guide RNA targeted against the 6th exon of SERT on chromosome 11 with a donor oligo that contained the SNP from "ACG" encoding threonine to "GCG" encoding alanine at amino acid 276. **(B)** DNA sequencing of the founder mouse showing threonine mutation (ACG) to alanine (GCG) mutation. **(C)** SERT Ala276 shows normal Mendelian genetics from heterozygous breeders (Chi square, genotypes n.s.; male vs. female ***P<0.001; n=458). **(D)** SERT Ala276 and heterozygous mice show normal body weights compared to WT mice measured from 4 to 12 weeks (Two-way ANOVA, n.s.; n=5-10).

A

		Midbrain				Hippocampus			
		Male		Female		Male		Female	
		WT	KI	WT	KI	WT	KI	WT	KI
	n	7	4	6	4	7	4	6	4
Biogenic Amie (ng/mg of protein)	5-HT	24.64 ± 0.70	25.25 ± 6.398	32.83 ± 1.07	31.12 ± 1.83	19.57 ± 1.04	15.05 ± 3.79	21.01 ± 0.88	22.10 ± 2.11
	5-HIAA	14.24 ± 0.56	15.03 ± 0.54	17.95 ± 0.85	22.00 ± 3.03	7.90 ± 0.39	7.40 ± 0.83	9.11 ± 0.44	11.65 ± 1.60
	DA	1.53 ± 0.10	1.90 ± 0.35	2.37 ± 0.21	1.75 ± 0.27	0.36 ± 0.07	0.26 ± 0.03	0.23 ± 0.02	0.49 ± 0.19
	DOPAC	1.06 ± 0.08	1.25 ± 0.13	1.41 ± 0.13	1.41 ± 0.22	0.32 ± 0.03	0.34 ± 0.08	0.28 ± 0.03	0.49 ± 0.15
	HVA	1.84 ± 0.16	2.19 ± 0.12	2.50 ± 0.13	2.36 ± 0.47	0.76 ± 0.07	0.81 ± 0.19	0.81 ± 0.08	1.29 ± 0.43
	NE	14.8 ± 0.46	16.97 ± 1.25	16.51 ± 0.58	16.93 ± 1.22	11.43 ± 0.57	12.7 ± 0.83	12.16 ± 0.47	14.14 ± 1.13
	GABA	66.81 ± 1.38	69.07 ± 2.35	72.52 ± 11.40	66.52 ± 1.68	34.85 ± 1.87	36.27 ± 1.51	40.09 ± 1.20	49.28 ± 5.98
	Glutamate	184.80 ± 8.51	204.60 ± 6.96	196.4 ± 7.92	210.80 ± 4.21	228.20 ± 20.3	237.50 ± 15.56	268.30 ± 15.25	291.50 ± 32.29

B

		Frontal Cortex				Cerebellum			
		Male		Female		Male		Female	
		WT	KI	WT	KI	WT	KI	WT	KI
	n	7	4	6	4	7	4	6	4
Biogenic Amie (ng/mg of protein)	5-HT	17.56 ± 0.79	14.38 ± 3.02	17.10 ± 0.99	15.00 ± 1.08	5.63 ± 0.54	5.01 ± 1.82	5.38 ± 0.43	12.43 ± 4.16
	5-HIAA	4.43 ± 0.21	4.79 ± 0.63	4.78 ± 0.42	6.04 ± 0.64	3.01 ± 0.31	2.67 ± 0.57	3.45 ± 0.16	7.77 ± 3.13
	DA	53.77 ± 8.22	37.39 ± 9.48	43.88 ± 5.13	26.59 ± 17.77	0.25 ± 0.01	0.23 ± 0.02	0.24 ± 0.03	0.35 ± 0.05
	DOPAC	5.55 ± 0.74	5.46 ± 1.45	4.42 ± 0.53	4.09 ± 2.16	0.23 ± 0.02	0.18 ± 0.04	0.25 ± 0.02	0.39 ± 0.11
	HVA	6.372 ± 0.83	5.98 ± 2.62	6.37 ± 0.83	5.98 ± 2.62	0.34 ± 0.02	0.32 ± 0.04	0.32 ± 0.03	0.69 ± 0.27
	NE	10.1 ± 0.28	12.41 ± 1.37	10.45 ± 0.24	11.37 ± 0.77	10.45 ± 0.32	11.17 ± 0.63	11.65 ± 0.58	15.36 ± 2.31
	GABA	33.02 ± 1.22	28.68 ± 4.74	32.73 ± 1.15	37.70 ± 1.97	29.40 ± 2.72	25.99 ± 0.80	27.29 ± 1.19	31.38 ± 2.27
	Glutamate	248.90 ± 12.48	258.30 ± 10.15	236.70 ± 4.61	274.60 ± 29.65	161.50 ± 32.83	214.50 ± 13.43	211.90 ± 9.66	205.10 ± 10.84

Table 8. Biogenic Amine Levels of SERT Ala276 Mice are Normal

HPLC analysis of biogenic amine levels in WT and SERT Ala276 littermates, both male and female, in the **(A)** midbrain and hippocampus and **(B)** frontal cortex and cerebellum. 5-HT and the main metabolite of 5-HT, 5-hydroxyindoleacetic acid (5-HIAA) were not significantly different between genotypes. Catecholamine levels, like DA and its metabolites, DOPAC and HVA, and NE were also not significantly different between genotypes in all brain regions. Also, the major inhibitory and excitatory neurotransmitters, GABA and Glu, respectively, were also not different between genotypes in all brain regions. Ordinary one-way ANOVA followed by Tukey's multiple comparison test, n.s. (n=4-7).

SERT mRNA, Protein Levels, and Uptake Kinetics in SERT Ala276.

To determine whether SERT Ala276 or SERT Glu276 resulted in any changes in the expression of SERT mRNA or protein, we performed qPCR and Western blot analyses, respectively. In both midbrain and hippocampal extracts, we observed no effect of SERT Ala276 genotype on transporter mRNA expression (**Figure 19A)**. Since mRNA levels do not always directly correlate with protein expression, we also performed Western blot analysis from midbrain detergent (RIPA, see Methods) extracts and again found no differences across genotypes (**Figure 19B)**.

A proxy to measure SERT protein expression, and one that can also reveal conformational changes, is the use of radioligand binding assays with isolated membranes, incubated with a radiolabeled antagonist. We pursued these assays (see Methods), using [^{3}H]citalopram as the radiolabel. Surprisingly, we found a significant, genotype-dependent decrease in SERT Ala276 [^{3}H]citalopram binding compared to WT littermates (Figure 19C). Since total protein levels were found to be normal, these data could mean that either the Ala56 containing transporter adopts a conformation with reduced binding affinity for citalopram, or that the allele impacts membrane trafficking as we may have not recovered intracellular, non-surface trafficked vesicles containing the transporter when isolating membranes. If the latter observation is the case, we would expect to see changes in 5-HT uptake kinetics that reflect the changes in radioligand binding. We expected no change in 5-HT uptake kinetics as a result of the Thr276Ala substitution since *in vitro* studies with transfected hSERT Ala276 showed no difference in SERT-mediated 5-HT uptake (Ramamoorthy et al., 2007), and as expected, SERT Ala276 did not alter the K_M or V_{max} of SERT mediated 5-HT uptake in midbrain synaptosomes **(Figure 19D**). These findings suggest that while the transporter can cycle through transport conformations at normal rates, the binding site for citalopram may be impacted by the allele, reducing antagonist affinity.

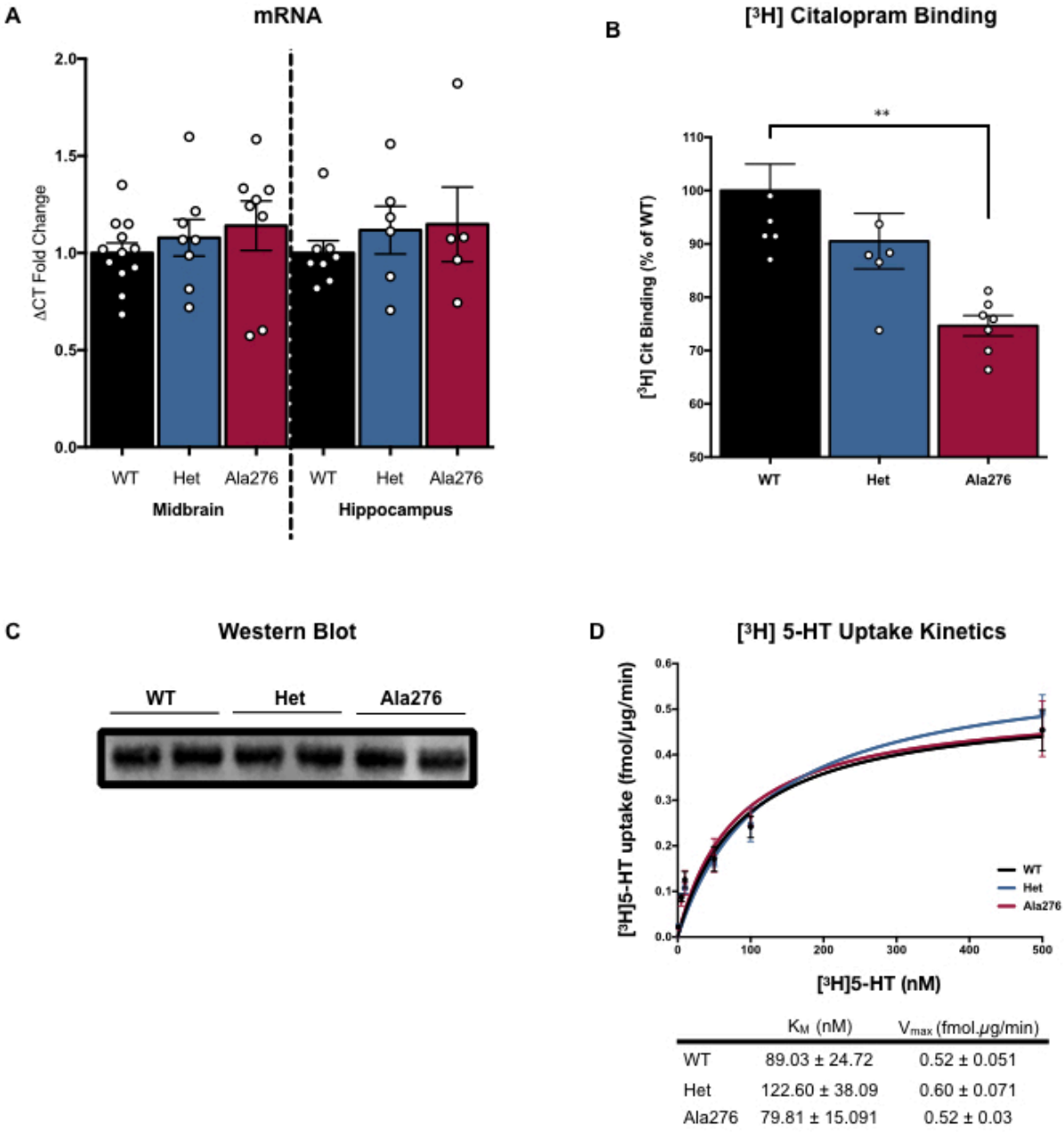

	K_M (nM)	V_{max} (fmol.µg/min)
WT	89.03 ± 24.72	0.52 ± 0.051
Het	122.60 ± 38.09	0.60 ± 0.071
Ala276	79.81 ± 15.091	0.52 ± 0.03

Figure 19. Midbrain mRNA and protein levels of SERT Ala276 mice

(A) qPCR analysis revels no significant difference in mRNA levels between genotypes in both the midbrain and hippocampus (One-way ANOVA, n.s.; n= 7-10) **(B)** Midbrain membranes from SERT Ala276 has decreased [^{3}H]citalopram binding compared to membranes prepared from WT mice (Ordinary one-way ANOVA, ** $P < 0.01$) **(C)** Western blot analysis of whole midbrain lysed in RIPA reveals no difference in protein levels across genotypes. **(D)** [^{3}H]5-HT uptake kinetic analysis shows no difference in SERT mediated uptake between genotypes as assessed by both Vmax and K_M (Ordinary one-way ANOVA, n.s, ±SEM, n=5)

SERT mRNA, Protein Levels, and Uptake Kinetics in SERT Glu276

Unlike SERT Ala276, [^{3}H]5-HT uptake from midbrain synaptosomes was completely abolished in the SERT Glu276 mouse (**Figure 20A**). Western blot of SERT from RIPA-lysed midbrain synaptosomes reveals a loss of SERT protein (**Figure 20B**). In another assay, [^{3}H]citalopram binding from both midbrain and hippocampal membrane preparations (**Figure 20C&D)** confirmed a loss of SERT protein expression in the SERT Glu276 mice. This loss in protein expression is explained by the loss of SERT mRNA expression in SERT Glu276 KI mice as assessed by qPRC analysis (**Figure 20E**). For this reason, we have not pursued further analysis of the SERT Glu276 mouse model until a mechanism for this loss of SERT mRNA and protein are determined.

No Gross Abnormalities Observed with SERT Ala276 Mice

An extensive Irwin screen (Irwin, 1968) of SERT Ala276 mice and their littermates revealed no gross abnormalities. Briefly, we measured several physical factors and gross appearances, including whisker length, fur, piloerection and wounds. Additionally, we observed behavior in a novel environment and noticed no differences between genotypes (**Table 9)**. Importantly, SERT Ala276 exhibit normal locomotion as measured in open field travel distance (data not shown), indicating that further tests that use locomotor activity as a variable will not be confounded by locomotor ability. Reflex and reactions to simple stimuli such as touch were also found to be equivalent comparing WT to SERT Ala276 mice. Finally, multiple measures were collected when mice were subject to supine restraint, and SERT Ala276 exhibited were found to exhibit behavior and physiological changes comparable to WT littermates **(Table 9**).

Anxiety- and Expression-like Behaviors in SERT Ala276 are Not Different from WT Animals

Since both 5-HT and SERT have been extensively studied for their role in depression and anxiety-linked behaviors, we sought to assess if the expression of SERT Ala276 affected measures often used to

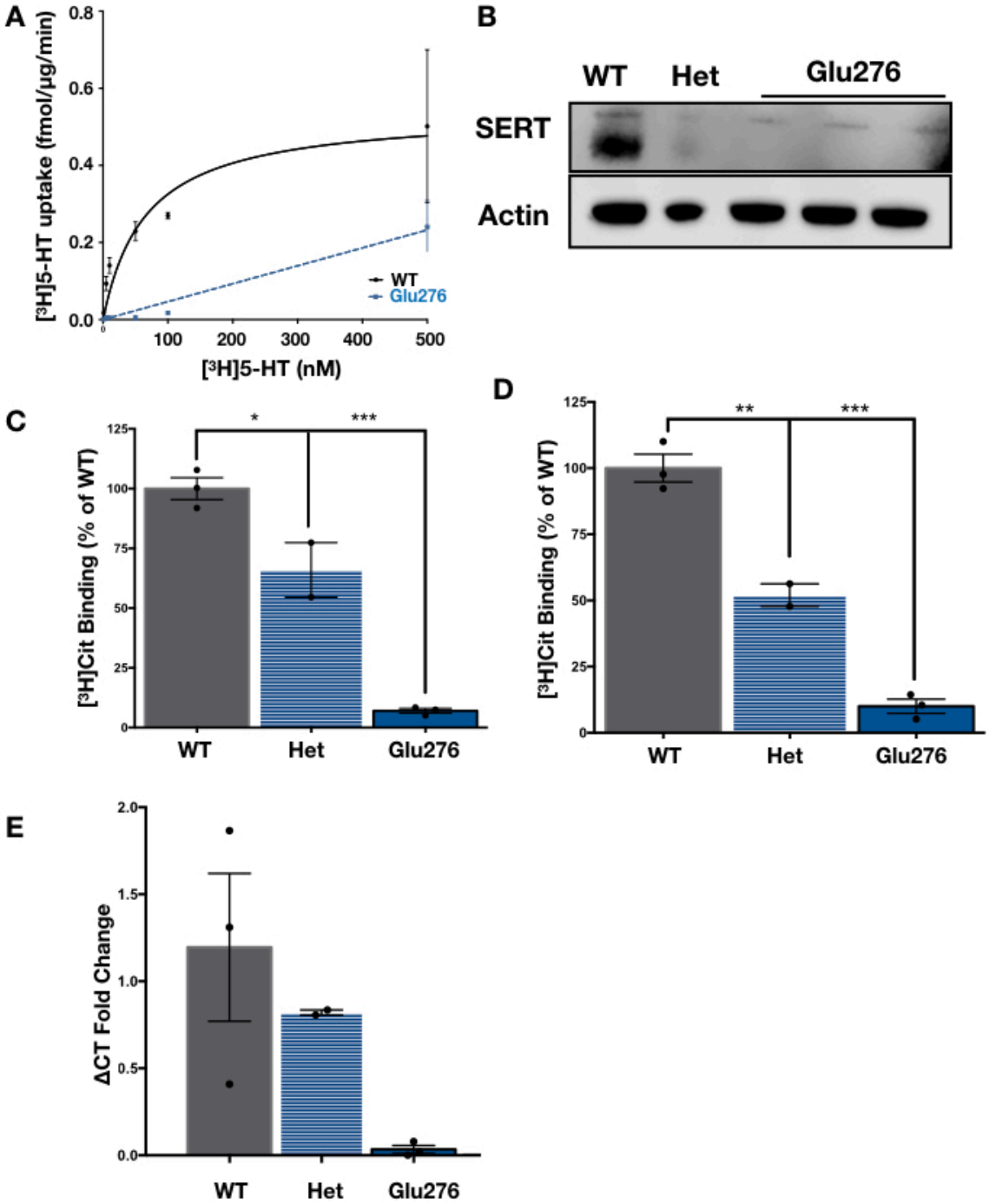

Figure 20. Loss of SERT Glu276 5-HT uptake, protein and mRNA

(A) [^{3}H]5-HT uptake kinetic analysis shows SERT Glu276 loses substrate mediated uptake (n=3-5) **(B)** Western blot analysis of midbrain lysed synaptosomes reveals loss of SERT protein in both HET and SERT Glu276, supported by loss of [^{3}H]citalopram binding in both **(C)** midbrain and **(D)** hippocampus membrane (One-way ANOVA, * $P < 0.05$, ** $P < 0.01$, *** $P < 0.001$.; n= 3) **(E)** qPCR analysis revels loss of SERT mRNA (n=2-3).

		WT		HET		Ala276	
		Male	Female	Male	Female	Male	Female
	Sample Size (n)	14	11	6	7	9	6
Physical Factors and Gross Appearance	Body Weight (g)	24.56 ± 0.89	19.05 ± 0.38	24.58 ± 1.63	18.74 ± 0.64	22.97 ± 0.97	17.37 ± 0.92
	Presence of Whiskers	Score: 3 14/14	Score: 3 11/11	Score: 3 6/6	Score: 3 7/7	Score: 3 9/9	Score: 3 6/6
	Appearance of fur	Score: 2 14/14	Score: 2 11/11	Score: 2 6/6	Score: 2 7/7	Score: 2 9/9	Score: 2 6/6
	Piloerection	Score:1 7/14	Score:1 5/11	Score:1 5/6	Score:1 3/7	Score:1 5/9	Score:1 5/6
	Fur missing on face	Score: 2 0/14	Score 2: 1/11	Score 2: 0/6	Score 2: 0/7	Score 2: 0/9	Score 2: 0/6
	Fur missing on body	Score 2: 0/14	Score 2: 0/11	Score 2: 0/6	Score 2: 0/7	Score 2: 0/9	Score 2: 0/6
	Wounds	Score: 0 14/14	Score: 0 0/11	Score: 0 0/6	Score: 0 0/7	Score: 0 0/9	Score: 0 0/6
Observation of Behavior in Novel Environment	Transfer Behavior	Score: 5 14/14	Score: 5 11/11	Score: 5 6/6	Score: 5 7/7	Score: 5 9/9	Score: 5 6/6
	Body position	Score 4: 14/14	Score 4: 11/11	Score 4: 6/6	Score 4: 7/7	Score 4: 9/9	Score 4: 6/6
	Spontaneous activity	Score 2: 3/14 Score 3: 11/14	Score 3: 11/11	Score 2:1/6 Score 2.5: 2/6 Score 3: 3/6	Score 3: 7/7	Score 2.5: 1/9 Score 3: 8/9	Score 3: 6/6
	Respiration Rate	Score 2: 14/14	Score 2: 11/11	Score 2: 6/6	Score 2: 7/7	Score 2: 9/9	Score 2: 6/6
	Tremor	Score 0: 14/14	Score 0: 11/11	Score 0: 6/6	Score 0: 7/7	Score 0: 9/9	Score 0: 6/6
	Palpebral closure	Score 0: 14/14	Score 0: 11/11	Score 0: 6/6	Score 0: 7/7	Score 0: 9/9	Score 0: 6/6
	Piloerection	Score 0: 14/14	Score 0: 11/11	Score 0: 6/6	Score 0: 7/7	Score 0: 9/9	Score 0: 6/6
	Gait	Score 0: 14/14	Score 0: 11/11	Score 0: 6/6	Score 0: 7/7	Score 0: 9/9	Score 0: 6/6
	Pelvic elevation	Score 2: 14/14	Score 2: 11/11	Score 2: 6/6	Score 2: 7/7	Score 2: 9/9	Score 2: 6/6
	Tail elevation	Score 1: 14/14	Score 1: 11/11	Score 1: 6/6	Score 1: 7/7	Score 1: 9/9	Score 1: 6/6
	Urination	Score 1: 14/14	Score 1: 11/11	Score 1: 6/6	Score 1: 7/7	Score 1: 9/9	Score 1: 6/6
	Defecation	3	3	2	2	3	4

Reflexes & Reactions to Simple Stimuli	Touch escape	Score 2: 14/14	Score 2: 11/11	Score 2: 6/6	Score 2: 7/7	Score 2: 9/9	Score 2: 6/6
	Positional Passivity	Score 0: 14/14	Score 0: 11/11	Score 0: 6/6	Score 0: 7/7	Score 0: 9/9	Score 0: 6/6
	Trunk curl	Score 1: 14/14	Score 1: 11/11	Score 1: 6/6	Score 1: 7/7	Score 1: 9/9	Score 1: 6/6
	Body tone	Score 1: 14/14	Score 1: 11/11	Score 1: 6/6	Score 1: 7/7	Score 1: 9/9	Score 1: 6/6
	Pinna reflex	Score 1: 14/14	Score 1: 11/11	Score 1: 6/6	Score 1: 7/7	Score 1: 9/9	Score 1: 6/6
Behavior Recorded During Supine Restraint	Skin color	Score 1: 14/14	Score 1: 11/11	Score 1: 6/6	Score 1: 7/7	Score 1: 9/9	Score 1: 6/6
	Heart rate	Score 1: 14/14	Score 1: 11/11	Score 1: 6/6	Score 1: 7/7	Score 1: 9/9	Score 1: 6/6
	Abdominal tone	Score 1: 14/14	Score 1: 11/11	Score 1: 6/6	Score 1: 7/7	Score 1: 9/9	Score 1: 6/6
	Provoked biting	Score 1: 8/14	Score 1: 5/11	Score 1: 1/6	Score 1: 2/5	Score 1: 4/6	Score 1: 0/6

Table 9. Irwin Screen of SERT Ala276 Mice

Mice showed no deficiencies in the following tests: physical and gross appearance, behaviors in a novel environment, reflexes and reaction to simple stimuli, and behavior recorded during supine restraint. Score numbers for each test are defined in the method section. Each test was analyzed by ordinary one-way ANOVA, $P < 0.05$, n.s. (n= 6-14).

examine these traits. To assess anxiety-like behavior, we measured both the time spent in the periphery of an open field arena and time spent in the open arms of the elevated zero maze.

Expression of the SERT Ala276 allele does not affect the total distance travel in the open field (data not shown), nor does it affect the time spent in the outer edges of the open field area (thigmotaxis) (**Figure 21A),** a measure often interpreted as an indication of anxiety. In the elevated zero maze test, another measure of anxiety behavior, all mice, regardless of sex or genotype, spent the same percentage of time in the open arms (**Figure 21B**), indicating no effect of Ala276 on anxiety behavior.

To assess depressive-like behaviors, we measured the time immobile in the tail suspension test and the forced swim test. For both male and females, all mice displayed similar times spent immobile in the forced swim test (**Figure 21C**). To avoid any forced swim-induced stress that may carry over to the tail suspension test, a separate cohort of mice was used for the tail suspension test. Due to the allocation of animals to other studies, only male WT and SERT Ala276 KI mice were assessed. Male SERT Ala276 mice showed no difference in the time spend immobile compared to their wildtype (WT) littermates during the tail suspension (**Figure 21D**).

Sex-dependent Deficits in SERT Ala276

Interestingly, SERT Ala276 mice exhibited sex-dependent behavioral changes in a few assays. In the inverted screen, males but not females demonstrated a decreased latency to fall from hanging on a wire screen (**Figure 22A**). In the tube test of social dominance, in which two mice of the same sex meet in the middle of the tube to determine which mouse will back out first, male SERT Ala276, but not females, won significantly less compared to WT littermates (**Figure 22B**). Female SERT Ala276 mice, however, appear to show deficits in marble burying (**Figure 22C**), whereas male SERT Ala276 mice bury a similar amount of marbles as male WT animals during a 20-minute session.

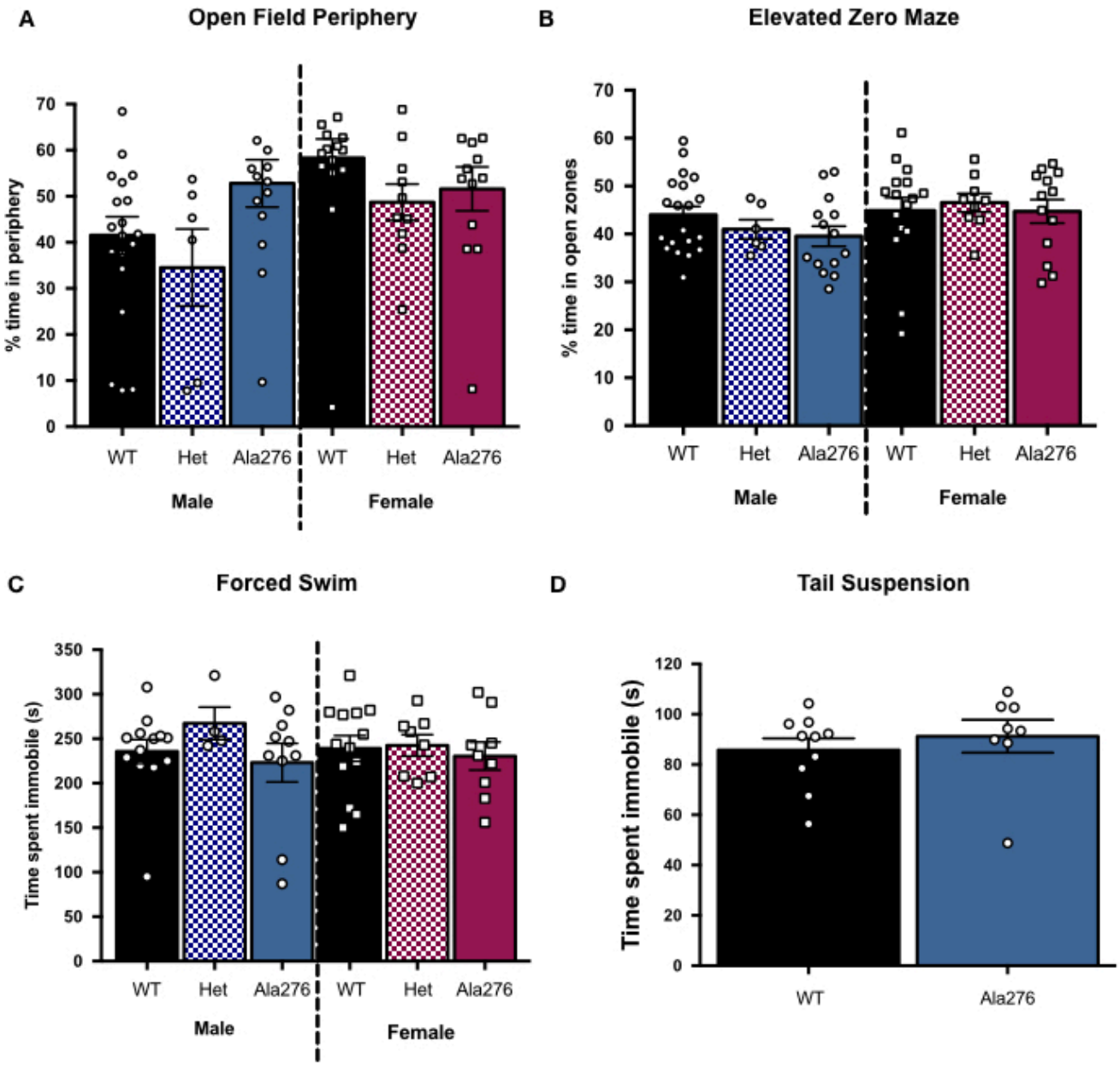

Figure 21. Normal anxiety and depressive like behaviors in SERT Ala276 mice

(A) SERT Ala276 mice spend similar percent of time in the periphery of the open field chamber (One-way ANOVA n.s.; n=6-20). **(B)** There is no difference in time SERT Ala276 mice spend in the open arms of the elevated zero maze compared to WT littermate (One-way ANOVA n.s.; n=6-20) **(C&D)** Time spend immobile in both the FST and TST was not different between genotypes for both males and females(One-way ANOVA n.s.; n=7-13).

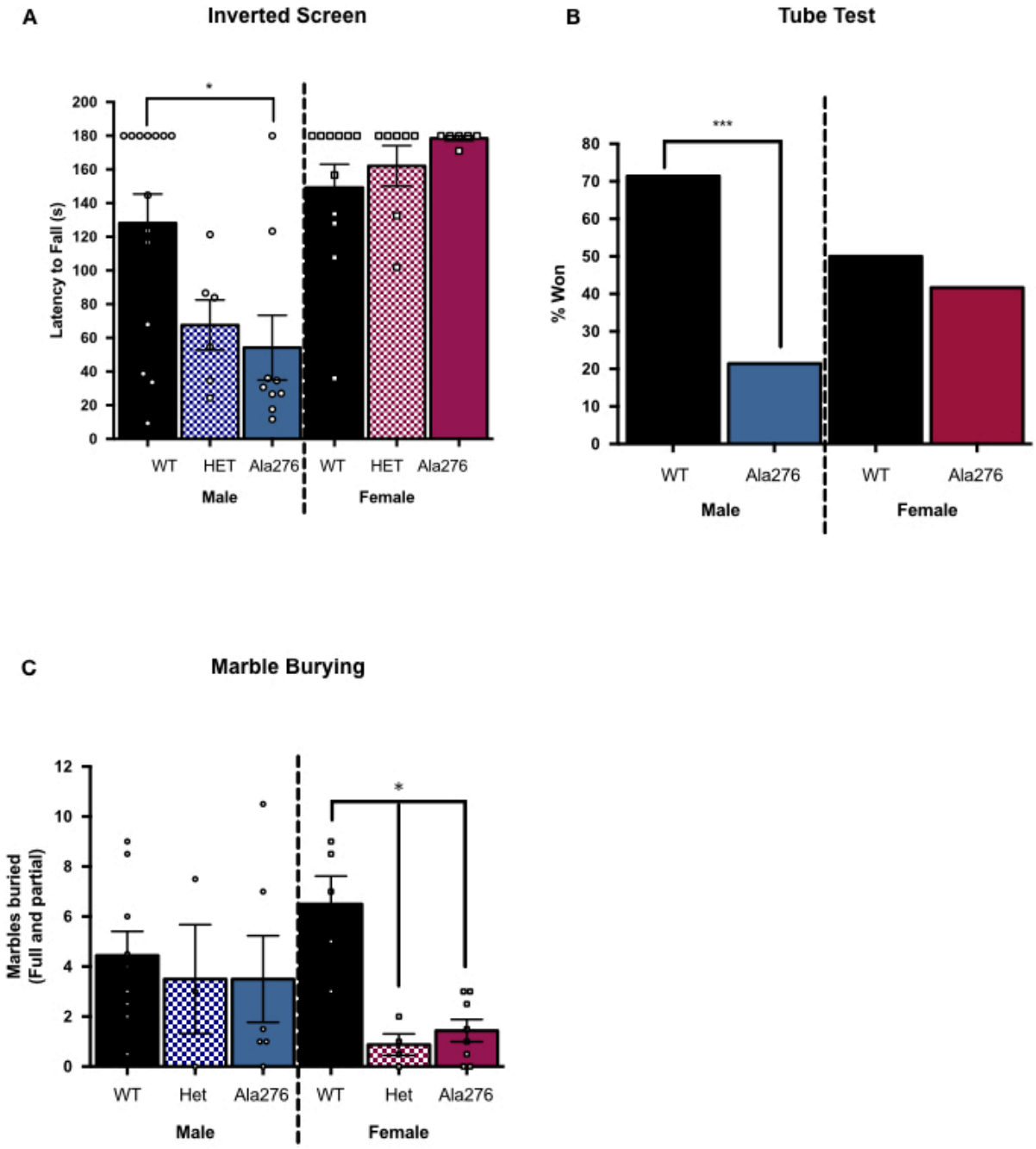

Figure 22. Sex dependent deficits in SERT Ala276 mice

(A) Male SERT Ala276 have a decreased latency to fall from an inverted wire screen compared to WT male mice, with no difference between genotypes in females (Ordinary One-way ANOVA followed by Tukey's multiple comparison test, **P* <0.05. (n=6-14) **B)** In an assessment of social interaction, male SERT Ala276 win less in the tube test compared to WT littermate (28 bouts, n=4-5; Chi square test ***p<0.001). **(C)** Female SERT Ala276 heterozygous and homozygous mice bury less marbles in 20 minutes compared to WT female mice. (Ordinary one-way ANOVA followed by Sidak's multiple comparisons test, **P* < 0.05, n= 3-9)

Discussion

SERT amino acid Thr276 has been identified as phosphorylation site that participates in transporter conformational dynamics (Zhang et al., 2016), as well as PKG-dependent regulation of the transporter (Ramamoorthy et al., 2007). However, up until this point, the role of this phosphorylation site *in vivo* has gone unexplored. The generation of a SERT Ala276 knock-in mouse model via CRISPR/Cas 9 technology, provides a platform to address the function of SERT Thr276 phosphorylation with respect to transporter function, 5-HT signaling, physiology and circuit-dependent effects *in vivo*, including actions on behavior The data presented here provides an initial characterization of the SERT Ala276 mouse model from which further investigations can be based to determine the functional aspects of SERT phosphorylation at amino acid Thr276.

While most characteristics of the SERT Ala276 model proved equivalent to WT animals, such as growth (as assessed by gross inspection and body weight) and transmission of the Ala276 allele met Mendelian expectations, there was an interesting sex bias towards females in animals tabulated at weening, however each sex showed equivalent allele distribution, thus we do not believe that the sex-genotype interaction occurs at the level of pup genotype, but rather reflects a deficit in male viability, either *in utero* or after birth. While we do not currently know the reason for this sex bias, there a recent publication attributed exposure of the dam and sire to the selective SSRI paroxetine, skewing litters toward a female bias (Gaukler et al., 2016). We also must take into consideration the possibility the SERT genotype of the mother (in this case Het) could bias the sex distribution of the offspring. SERT is expressed in the placenta (Balkovetzs et al., 1989) and a recent paper showed that maternal genotype of another SERT coding variant, SERT Ala56, impacts 5-HT levels in the developing pup forebrain and the organization of thalamocortical projections (Muller et al., 2017). This effect could be due to maternal behavior or the role of SERT in the placenta that results in death selectively of males. This potentially suggests that changes to SERT function and activity may influence either sex determination or pup survival.

In parallel to the generation of the SERT Ala276 mouse, the phosphomimetic SERT Glu276 mouse was also created via CRISPR/Cas9 technology. Surprisingly, expression of SERT Glu276 leads to a loss of

both SERT mRNA and protein expression, though a currently unknown mechanism. One possible explanation is during the CRISPR/Cas9 process another mutation was introduced, shutting down the promoter or damaging coding or noncoding sequences that by some mechanism causes the shutdown of SERT RNA production. On the other hand, there is the possibility that the point mutation from Thr to Glu destabilized the RNA that leads to nonsense-mediated RNA decay.

As expected, we detected no differences in biogenic amine levels across genotypes in four different brain regions, midbrain, hippocampus, frontal cortex, and cerebellum. While other brain regions should be assessed, the absence of changes in biogenic amine levels across these regions suggests that expression of the SERT Ala276 mutation does not disrupt the density of serotonergic projections and their neurotransmitter synthetic and storage machinery.

We also found no discrepancies in mRNA and protein levels as assessed by qPCR and Western blot analysis, respectively. Surprisingly, we found that SERT Ala276 midbrain membranes displayed a decrease in [^{3}H]citalopram binding with statistical significance reached in Homo animals and a trend evident in Het mice. This may be an indication that SERT Ala276 alters citalopram binding or it may be indicative of a decrease in SERT surface expression of the SERT Ala276. This finding has possible translational relevance, as many individuals diagnosed with depression do not find relief after treatment with SSRIs (Warden et al., 2007). If this mutation is indeed causing an altered binding of citalopram to SERT, and not simply changing its surface expression levels, it will be essential for future studies to further define the structural changes that Ala276 may be having on SERT in relation to SSRI interactions, with more SSRIs tested, and the potency assessed for SSRIs in suppressing SERT-dependent behaviors, such as behavior in the tail suspension and forced swim test.

Interestingly, we found sex-dependent differences in specific behaviors comparing WT and Ala276 mice. Although more work is needed to define the exact cause(s) of these sex differences, it has become increasingly clear that 5-HT has opposing actions in males and females in social behaviors (Terranova et al., 2016). SERT Ala276 male mice showed a deficit in the inverted screen, in which the mouse hangs upside from a wire mesh screen and the time to fall is recorded. This may be an indication of decreased

grip strength in the SERT Ala276 mice. There is a substantial amount of literature addressing the link between 5-HT, SERT, and spinal motor reflex (Machacek et al., 2001; Sibille et al., 2007; Horvath et al., 2011, 2017; Enjin et al., 2012; Gourab et al., 2015; Gurel et al., 2015), which may explain the deficit in this task.

Although we have focused most of our efforts on understanding the role of SERT phosphorylation in the brain, we must recognize that SERT is more widely expressed with important functions in blood platelets (Mercado and Kilic, 2010), in the gastrointestinal tract (Wade et al., 1996), in the adrenal gland (Brindley et al., 2018), and in the immune system (Baganz and Blakely, 2013). The regulation and role of SERT phosphorylation may have distinct functions in the periphery compared to the central nervous system. The SERT Ala276 mouse model affords us the opportunity to assess the role of SERT phosphorylation in these non-CNS tissues and systems.

Future studies aim to further characterize the impact of the Ala276 mutation *in vivo* and *ex vivo* on SERT phosphorylation states, SERT membrane surface levels and response to drug perturbations. Importantly, we would also like to assess the effect of SERT Ala276 on PKG-dependent regulation of the transporter. Another area of interest is assessing the role of phosphorylation on biasing structural conformational dynamics of the transporter. We will also assess the altered regulation of the SERT Ala276 in more complex behavior and drug responses. These studies offer opportunities to assess the contribution of SERT conformational modulation *in vivo* and its physiological significance.

Methods

Generation of SERT Ala276/Glu276 Mice and Animal Usage

All experiments using animal subjects were conducted according to the National Institutes of Health Guide for the Care and Use of Laboratory Animals and were pre-approved by the Vanderbilt University and Florida Atlantic University Institutional Animal Care and Use Committees. To generate the SERT Ala276 and Glu275 KI mouse model, we utilized CRISPR/Cas9 technology. Briefly, by using the online

CRISPR design software developed in the Zhang laboratory (Massachusetts Institute of Technology, http://crispr.mit.edu) we identified and generated oligos to insert our guide RNA (Sense RB5167: CACCGAGGAGTCAAAACGTCTGGCA; Antisense RB5216: AAACTGCCAGACGTTTTGACTCCTC) into the pX330 plasmid, a generous gift from Feng Zhang (Addgene plasmid #42230) that also encodes CAS9. Donor oligos were also generated to knock-in a non-synonymous SNP from threonine (ACG) to alanine (GCG) at amino acid 276 (bolded and underlined below; RB5192: GCATCATGCTCATCTTCACCATTA TCTACTTCAGCATCTGGAAAGGAGTCAAA**GCG**TCTGGCAAGTTGAGGACTCTGCAGCTTGTCCT GAACTGCCCAGGGCCCCGCAG). The plasmid and donor oligo were injected into C57BL6/J embryos by the Vanderbilt ES/Transgenic Mouse Core. The founder heterozygous male mouse labeled #9 (**Figure 18B**) was breed with a C57Bl/6J female to produce pups. Pups that were verified to contain the mutation via sequencing were then backcrossed for 10 generations on a C57Bl/6J background to remove off target CRISPR events. For all experiments, SERT Ala276 and WT littermate males and females (C57BL/6J) 8-12 weeks old were generated from heterozygous breeding. Mouse genotyping was conducted by Transnetyx, Inc. using real-time PCR (Slc6a4-10 MUT; Forward Primer: TGCAGATCCATCAGTCAAAGG; Reverse Primer: CCCTTGAACCTTCTAACAGATGTG).

Assessment of Mendelian Genetics and Growth of SERT Ala276

To determine genotype and gender distribution, we compared the expectation derived from Hardy–Weinberg equilibrium to the observed outcome using χ^2 tests set to $P < .05$ as an indication of statistical significance. To compare the growth of the animals from development to adulthood, both male and female mice of all three genotypes were weighed weekly from 3 to 12 weeks of age. One-way ANOVA was used to determine statistical significance across genotypes.

HPLC of Monoamine and Amino Acid Levels

Following rapid decapitation, the midbrain, hippocampus, frontal cortex and cerebellum were dissected and flash frozen in liquid nitrogen. Biogenic amine levels were detected utilizing HPLC through the Vanderbilt Molecular Neuroscience core facility as previously described (Veenstra-VanderWeele et al., 2012). Biogenic amines were eluted with a mobile phase consisting of 89.5% 0.1M TCA, 10^{-2} M sodium acetate, 10^{-4} M EDTA, and 10.5% (vol/vol) methanol (pH 3.8). Concentrations were determined using comparisons to injections with known standards.

Quantitative Real-Time PRC Analysis of SERT mRNA expression

Quantitative PCR (qPCR) was utilized to determine Slc6a4 mRNA expression in wild type (WT) and SERT Ala276 heterozygous and homozygous animals. Midbrain and hippocampus samples were collected from both male and female mice that were sacrificed by rapid decapitation, with tissues immediately frozen on dry ice, prior to storage at -80°C. RNA isolations were conducted from tissue samples using Trizol reagent (Thermo Fisher, Catalog no. 15596018) according to the manufacturer's instructions. The total RNA concentration for each sample was quantified by spectrophotometry using the LVis plate (BMG LabTech, FLUOstar Omega Plate Reader, Omega Software Version 5.11), with the purity of samples checked to confirm that the 260/280 ratio was in the range of 1.8–2.1. Reverse Transcription PCR was conducted on 1µg of RNA using a High Capacity cDNA Reverse Transcription Kit according to the manufacturer's instructions (Applied Biosystems, Catalog no. 4368814). qPCR was conducted on the cDNA using a TaqMan Gene Expression assay consisting of the TaqMan Gene Expression Master Mix, and appropriate TaqMan probes (Master Max: Thermo Fisher Scientific, Applied Biosystems, Catalog no. 4369016, TaqMan probes: Slc6a4 Mm00439391_m1, Catalog no. 4331182; 18S HS99999901, Catalog no. 4331182). All experiments were conducted using a Bio-Rad qPCR machine (Bio-Rad CFX96 Real-Time System, C1000 Touch Thermal Cycler). Sample mRNA levels from qPCR assays were calculated using the ΔΔCt method (Schmittgen and Livak, 2008) and normalized compared to WT littermates and the threshold cycle (Ct value) of each gene was then normalized to 18S rRNA expression.

Western Blot Analysis

Detection of SERT protein by western blot was performed as previously described(Brindley et al., 2018) with minor revisions. Briefly, freshly dissected midbrain samples were homogenized in 50 mM Tris pH 7.4 and then centrifuged at 15,000 X g for 20 minutes. The resulting pellet was resuspended RIPA buffer (50 mM Tris-HCl, pH 8.0, 150 mM NaCl, 1% NP-40, 0.5% sodium deoxycholate and 0.1% sodium dodecyl sulfate (SDS); Sigma-Aldrich, St Louis, MO) containing protease inhibitor cocktail (Sigma-Aldrich, St Louis, MO, USA). Homogenates were nutated for 1 hour at 4 °C and the resulting protein lysates were cleared of any insoluble material by centrifuging for 20 min at 15,000 × *g* and 4 °C. Protein concentrations of the resulting supernatant were determined by the bicinchoninic acid (BCA) assay (Thermo Fisher Scientific, Waltham, MA). 2X Laemmli loading buffer (Bio-Rad Laboratories, Hercules, CA) was added to 50 µg of protein and then incubated at 37 °C for 12 minutes. The protein was separated by a NuPAGE 10% Bis-Tris protein gel (Invitrogen, Carlsbad, CA) and then transfer to Immobilon-FL PVDF membrane (Millipore Sigma, Burlington, MA). Membranes were blocked for 1 hour at room temperature in 5% non-fat milk in Tris-buffered saline, 0.1% Tween 20 (TBST). Primary SERT antibody (1:1000 dilution, Guinea pig anti-5HTT, Cat # HTT-GP-Af1400, RRID: AB2571777 Frontier Institute, Japan) was incubated overnight at 4°C with constant agitation. The next day, membranes were subjected to 4, 5 min washes, in TBST and then probed with IRDye 800RD Donkey anti Guinea Pig secondary antibody (LI-COR Biosciences, Lincoln, NE). Immunoreactivity was detected using the Odyssey Fc (LI-COR Biosciences, Lincoln, NE) followed by densitometry analysis using was using Image Studio software (LI-COR Biosciences, Lincoln, NE).

Synaptosomes [^{3}H]5-HT Uptake

Radioactive 5-HT uptake in midbrain synaptosomes was conducted as previously described (Thompson et al., 2011). Briefly, mice were rapidly decapitated followed by dissection of the midbrain into 3 mL of ice-cold 0.32 M sucrose and homogenized. Samples were then centrifuged at 800 X g for 10 minutes at 4°C. The resulting supernatant was then centrifuged at 15,000 X g for 20 minutes at 4°C. Pellets

were resuspended in Krebs-Ringers-HEPES (KRH) assay buffer (130 mM NaCl, 1.3 mM KCl, 2.2 mM $CaCl_2$, 1.2 mM $MgSO_4$, 1.2 mM KH_2PO_4, 10 mM HEPES, 10 mM glucose, 100 μM pargyline, 100 μM ascorbic acid, pH 7.4). Protein concentrations were then determined by the BCA method (Thermo Fisher, Waltham, MA). Radiolabeled [^{3}H]5-HT (Perkin Elmer, Waltham, Ma) at 1, 5, 10, 50, 100, and 500 nM (100 and 500 nM was 10% hot and 90% cold 5-HT) uptake into synaptosomes (50 μg) was conducted for 10 min at 37°C and terminated by rapid washing with ice-cold PBS onto Whatman filters (coated with 0.3% PEI) using a Brandel Cell Harvester (Brandel). Non-specific uptake was calculated by subtracting the counts from samples incubated in parallel with 10 μM paroxetine for 10 minutes at 37°C prior to the addition of [^{3}H]5-HT, from total counts without paroxetine to yield specific uptake activity. Michaelis-Menten curve fit in Prism 7.0 was used to calculate K_M and V_{max} values.

Membrane [^{3}H]Citalopram Binding

Membrane [^{3}H]citalopram binding was conducted as previously described (Veenstra-VanderWeele et al., 2012). Briefly, after rapid decapitation, the midbrain was dissected and homogenized in 3 mL of 50 mM Tris-HCl, pH 7.4 using a glass Teflon homogenizer (Wheaton Science Products, Millville, NJ). Tissue samples were then centrifuged at 17,000 X g for 15 minutes at 4°C. The pellet was washed by resuspending in 50 mM Tris-HCl and centrifuged again. The resulting pellet was resuspended in 50 mM Tris + 150 mM NaCl. Protein concentration was determined by the BCA method as described above. In a 250 μL final volume, 200 μg of membranes were added to 5 nM [^{3}H]citalopram (Perkin Elmer, Waltham, MA) for 1 hour at room temperature. Binding was terminated by rapid washing with ice-cold Phosphate buffer saline (137 mM NaCl, 2.7 mM KCl, 1.8 mM KH_2PO_4, 10 mM Na_2HPO_4; PBS) onto Whatman filters (coated with 0.3% polyethylenimine) using a Brandel Cell Harvester (Brandel). Non-specific binding was calculated by subtracting the counts determined from samples incubated in parallel with 10 μM paroxetine, from total counts without paroxetine.

Irwin Behavioral Screen

Irwin behavioral screen, as previously described (Irwin, 1968), was conducted by the Vanderbilt Murine Neurobehavioral core. First, physical factors and gross appearance were recorded by: coat color, body weight, presence of whiskers (0-3 with 3 is a full set), appearance of fur (0-2 with 2 being well groomed, normal), piloerection (0 = none, 1 = most hair standing on end); patches of missing fur on face and body (2 = extensive), wounds (0 = none). Next, the mice were monitored and scored in a novel environment (3 minutes in a clean tub cage) by: transfer behavior (5 = no freeze, immediate movement), body position (4 = rearing on hind legs), spontaneous activity (0 = none, resting); respiration rate (2 = normal), tremor (0 = none), palpebral closure (0 = eyes wide open), piloerection (0 = none), gait (0 = normal), pelvic elevation (2 = normal, 3mm elevation), tail elevation during forward motion (1 = horizontal extended), urination (1 = little), and defecation (number of fecal boli emitted during 3 minute period). Then, reflexes and reactions to simple stimuli were observed and scored by: touch escape (finger stroke from light to firm; 2 = moderate rapid response to light stroke), positional passivity (struggle response to sequential handling; 0 = struggles when restrained by tail), trunk curl (grip tail and lift about 30 cm; 1 = present), body tone (compress both sides of the mouse between thumb and index finger; 1 = slight resistance), and pinna reflex (while the mouse is gently restrained, the auditory meatus is lightly touched with the tip of a 31 gauge stainless-steel wire probe and ear retraction or head movement was recorded; 1 = active retraction, moderately brisk flick). Finally, during supine restraint, the following was scored: skin color (color gradations of plantar surface and digits of forelimbs, 1 = pink), heart rate (felt by palpation below sternum; 1 = normal), abdominal tone (palpation of abdomen, 1 = slightly resistance), and proved biting (gently inserted dowel between the teeth at the side of the mouse, 1 = present).

Open Field

To determine locomotor activity, mice were placed in an open field locomotor chamber (11.0 x 11.0 inches, MedAssociates OFA-510, St. Albans, VT) containing 16 infrared photobeam detectors for 1 hour. Activity was assessed by the Med Associated software.

Elevated Zero Maze

A mouse is placed on an open zone of the zero maze (Stoelting, Wood Dale, IL) and permitted to explore freely while being videotaped from above. At the end of the trial, the mouse is removed from the maze and returned to their home cage. Maze 'arms' are approximately 5-cm wide, with a 0.5 cm lip in the open zones to prevent the mouse from falling. The closed 'arms' of the maze are 20-30 cm tall. The maze is elevated approx. 2 feet from the floor. The maze is cleaned before and after each animal with either 10% ethanol solution. AnyMaze was used to detect and analyze the mouse position during the 5-min trail.

Forced Swim Test

Mice are placed in a large beaker, filled with 25-27° C water such that they cannot escape from the beaker and cannot touch the bottom. On each of two consecutive days, the mouse is placed in the beaker for 5-15 min. Latency to float and the amount of time spent struggling are measured. The experimenter monitors the mouse during the task, either by being within the same room or in an adjacent room with a live video feed. If there is any indication that the mouse is struggling to keep its mouth above water or is in danger of drowning, it is removed from the beaker immediately and excluded from the study. At the completion of the test, the animal is removed from the beaker, towel dried and recovered for 10-20 min in a warm cage (~35-37°C) sitting on a heating pad. Experimenters were blind to genotype during the test.

Tail Suspension Test

The tail of a mouse is taped to a vertical aluminum bar connected to a strain gauge inside a commercial tail suspension test chamber (Med Associates, Fairfax, VT). Mice are hung directly vertically to minimize chances of injury and to decrease the propensity for mice to climb their tail during the test. Mice were monitored by two independent researchers for a total of 6 minutes to measures time spent struggling. Experimenters were blind to genotype during the test.

Inverted Screen

Mice are placed on a hardware wire cloth screen measuring approximately 15 cm x 15 cm. To ensure the mice grip onto the wires, the screen is waved gently in the air three times. The screen is then turned upside down, approximately 60 cm above a tub cage containing soft bedding material, and latency to fall into the cage is measured. Maximal trial length is 60 seconds. If a mouse is observed to be abnormally fatigued, distressed, or injured, it is immediately removed from the apparatus. Mice are given 3 trials per session with an inter-trial interval of at least 5-mins between trials.

Tube Test

The tube test was conducted as previously described (Veenstra-VanderWeele et al., 2012; Robson et al., 2018). For two consecutive days prior to testing, mice are introduced and allowed to enter and exit the tube apparatus, a 30 cm long, 3.5 cm-diameter clear acrylic tube with small, acrylic funnels attached to each end to aid in entry into the tube. On testing day, pairings were run in both directions as previously described to avoid positional bias and were paired off against all counterparts present in opposing home cage (Veenstra-VanderWeele et al., 2012). For each testing bout, randomized mice from the same sex and age cohorts but separate and distinct home cages were placed at the opposite ends of the tube and released. Each subject was declared a "winner" when their respective opponent backed out of the tube. If neither animal backed out of the tube after a period of 2 minutes, a draw was declared. Draws were excluded from analysis. All wins and losses were included in the analysis of tube test data.

Marble Burying

Mice are placed in individual cages containing ~5 cm of beta chip sawdust bedding or similar (including Harlan, diamond soft bedding) for 15 minutes to acclimate to the test conditions. After 15 minutes each mouse is briefly removed from its cage, the bedding is smoothed and slightly compacted, and up to twenty-five marbles (~1.5 cm) are placed in the cage in 5 rows. The mice are returned to the cage and

allowed 20-60 minutes (most typically 30 minutes) to investigate the marbles. At the end of the study, the mice are returned to their home cages and the number of marbles buried at least two-thirds of the way in the bedding is recorded.

Statistical and Graphical Analysis

Data from experiments were analyzed and graphed using Prism 7.0 (GraphPad Software, Inc., La Jolla, CA, USA). For all analyses, a $P < 0.05$ was taken to infer statistical significance. Specific details of statistical tests are given in Figure Legends.

CHAPTER 5

CONCLUSIONS AND FUTURE DIRECTIONS

While the work complied herein has added to the current knowledge of the role of SERT variants in regulation of 5-HT uptake, several new questions have now arisen that need to be addressed to fully understand the role of disease-associated variants in altering the regulation of SERT structure-function.

Structure-function relationship of ASD-associated SERT variants

The structure-function relationship is the basis of understanding how alterations in one aspect have the ability to impact change in the other. One of the main hypotheses overarching in the field is that disruptions in the structural conformation of a protein, either through genetic variation of the protein itself or variation of another protein that acts on and/or with the protein of interest, will in turn affect the function and/or regulation of the protein. This is evident of the ASD-associated SERT coding variants, SERT Ala56 and SERT Asn605, as described in Chapter 2 in which we demonstrated these variants exhibited conformational equilibrium to a more outward-facing conformation and in Chapter 3 where we showed SERT Ala56 affected protein complexes. Full understanding of the relationship between SERT protein structure and function and its role in a larger signaling network can have much broader implications in providing clues for potential targets for therapeutics that may be beneficial in disorders linked to 5-HT disruption.

p38 MAPK Effect on SERT Conformational Equilibrium

As discussed in Chapter 2, the ASD-associated SERT variants insensitive to p38 MAPK dependent upregulation of 5-HT uptake show altered conformational states (Quinlan et al., 2019). One question that

remains, is if the stabilization of these variants is dependent on p38 MAPK signaling and does p38 MAPK activation exhibit similar changes in SERT conformational states (**Figure 23**).

In light of the ability of a p38α MAPK inhibitor, MW150 and MW108, to reverse SERT Ala56 increase in 5-HT clearance in vivo (Robson et al., 2018) it is hypothesized that inhibition of p38 MAPK will also reverse the stabilization of SERT Ala56 in an outward facing conformation. However, it is important to keep in mind, that only chronic one-week treatment of MW150 showed normalization of 5-HT uptake as this was the treatment paradigm required for reversal of the ASD-like behavioral phenotypes (Robson et al., 2018). It would be necessary to test the ability of local administration of MW150 to reduce the enhanced 5-HT clearance in vivo as in vitro studies show that inhibition of p38 MAPK with SB203580 had no effect on SERT Ala56 transport (Prasad et al., 2009). However, the elevated SERT phosphorylation seen in vivo in SERT Ala56 mice was rapidly (10 minutes) reversed by inhibition of p38 MAPK with the compound PD169316 directly to synaptosomes (Veenstra-VanderWeele et al., 2012). Elucidation of this time dependent reversal of uptake and phosphorylation by p38 MAPK inhibition is necessary to understand the potential effects on SERT conformational states

It is currently unknown how p38 MAPK activation affects the conformational equilibrium of SERT. If the hypothesis that SERT Ala56 mimics the SERT* state (trafficking independent enhanced 5-HT affinity state) induced by p38 MAPK activation (Zhu et al., 2005, 2007), one would expect that p38 MAPK activation would show similar changes in the SERT conformational equilibrium as seen for SERT Ala56. Preliminary data from out lab shows that activation of p38 MAPK with 10 μM anisomysin in hippocampal brain slices decreases fenfluramine mediated [^{3}H]5-HT efflux (**Figure 24)**, mimicking what seen in SERT Ala56 mice (**Figure 6**). One past study has linked p38 MAPK to amphetamine mediated efflux showing that amphetamine increases SERT phosphorylation in a p38 MAPK dependent manner (Samuvel et al., 2005). So, while this effect on p38 MAPK on efflux capacity does show that p38 MAPK has the capability to mediated SERT conformational equilibrium. Repeating the MTS, FRET, and tryptic digestion experiments as described in Chapter 2 in the presence of p38 MAPK activators and inhibitors would shed light onto the role of p38 MAPK on regulating SERT structural conformation.

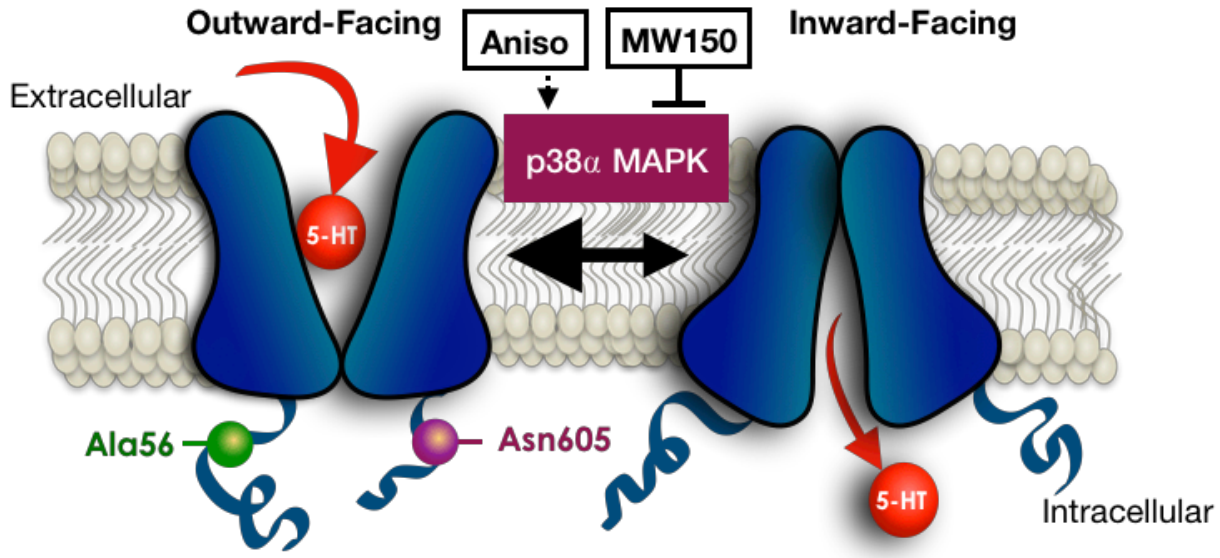

Figure 23. Hypothesized model of p38 MAPK effect on SERT conformational equilibrium

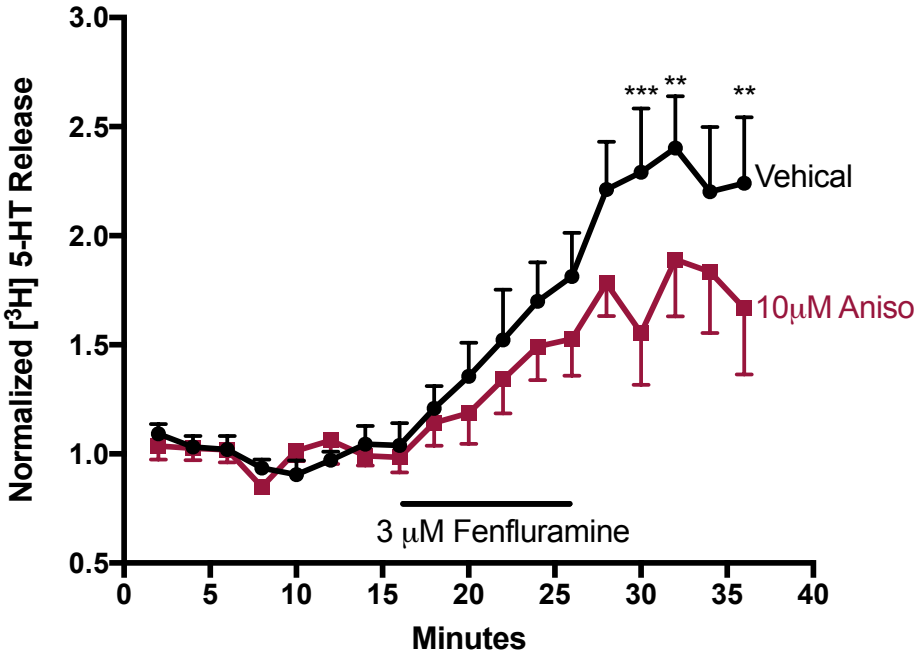

Figure 24. Anisomycin decreases D-Fenfluramine mediated [^{3}H]5-HT efflux from hippocampal slices

Hippocampal slices from WT mice were pre-incubated with 10 μM anisomycin or vehicle 30 minutes prior to D-fenfluramine mediated [^{3}H]5-HT efflux assay. Slices were loaded with 400 nM [^{3}H]5-HT for 30 minutes and then perfused with KRB buffer for 15 min to establish baseline followed by 15 min 3 μM D-fenfluramine pulse and then a 15 min wash out with KRB. Slices pre-treated with anisomycin showed a blunted D-fenfluramine mediated [^{3}H]5-HT efflux compared vehicle treated slices (two-way repeated-measures ANOVA; Bonferroni post-hoc test of genotype differences, *$P \leq 0.05$, **$P \leq 0.01$, ***$P \leq 0.001$; n=5).

Another question that also remains to be unanswered is if SERT Ala56 is in a conformation that allows for basal p38 MAPK activity to act on the transporter or if SERT Ala56, through a currently unknown mechanism, constitutively activates p38 MAPK, which then in a feedforward loop sustains the enhanced uptake. If this hypothesis were true, it would be expected that the SERT Ala56 KI mice and cells expressing SERT Ala56 would show enhanced p38 MAPK activation and phosphorylation. It would further have to be shown that 5-HT uptake through SERT could activate p38 MAPK, which can be done comparing cells transfected or not transfected with SERT and measuring p38 MAPK activation. This paradigm is analogous to SERT mediated activation of nNOS, which was shown to interact and modulate SERT function (Chanrion et al., 2007).

Turnover rate of SERT Ala56 uptake

Under basal conditions, it is thought that SERT takes up 5-HT at a rate of one 5-HT per second (Talvenheimo et al., 1979; Ross and Hall, 1983; Qian et al., 1997). This rate is dependent on several factors including the rate of 5-HT and ion binding as well as the rate of transition from the outward-facing to inward facing conformation. It is possible that SERT Ala56 increase in 5-HT uptake is either through affecting substrate binding affinities (discussed below) and/or though accelerating the rate of transition. One way to test this hypothesis is through a 5-HT pair-pulsed assay as described by Kern and colleagues (Kern et al., 2017). In this assay, the time it takes to recover 5-HT induced current after the initial addition of 5-HT is measured from patched cells expressing SERT Ala56 or WT SERT. If SERT Ala56 does increase the rate of transport, it would be expected that the recovery of 5-HT induced second current would be shorter compared to WT. Interestingly, this assay would also provide evidence to test the hypothesis that SERT Ala56 increase in 5-HT uptake is due to a shift in the SERT population to a more outward-facing conformation. It is reasoned that if more of the transporters are in an outward facing conformation, the current induced by the first pulse of 5-HT would also be greater (Hasenhuetl et al., 2018), therefore it would be expected if that SERT Ala56 would have a significantly increased current compared to WT SERT in response to 5-HT. A major caveat to these electrophysiological experiments, however, is the requirement

of high expression of SERT to generate a detectable signal, and therefore often use preparations of overexpressed SERT such as in transfected HEK-293T cells or oocytes. The Blakley lab has found that kinase-dependent regulation of SERT is lost in systems that overexpress SERT likely due to the improper stoichiometric ratio of SERT to kinase (Ramamoorthy et al., 1998).

Another proxy to measure the rate of 5-HT uptake would be a measurement of the N- and C-terminus proximity utilizing FRET-based assay as described in Chapter 2. As it is thought that as SERT moves through the transport cycle, the distance between the N-and C- termini change (Fenollar-Ferrer et al., 2014), one may expect the rate change may be different between SERT Ala56 and WT expressing cells depending on the addition of substrate and activation/inhibition of key regulatory kinases, like p38 MAPK and PKG. In this assay, using the C-SERT-Y and C-Ala56-Y construct transfected into CHO cells, one could track FRET intensity over time in the presence and absence of SERT substrates, such as 5-HT, noribogaine, or fenfluramine.

SERT Ala56 Affinity for 5-HT and Ion Dependency

Since SERT Ala56 is stabilized in an outward-facing conformation (Quinlan et al., 2019), one may expect 5-HT and/or Na^+/Cl^- affinity may also be affected as the outward-facing conformation is required for these substrates to bind under basal conditions. To test 5-HT affinity of SERT Ala56 one could perform a radioactive displacement a SERT substrate, such as the cocaine analog RTI-55, in the presence of various concentrations of 5-HT. This assay demonstrated that activation of p38 MAPK increased 5-HT affinity for SERT (Zhu et al., 2005) and therefore it is hypothesized that SERT Ala56 would show a similar decreased 5-HT K_i, which may explain the decreased 5-HT K_M in SERT uptake assay(Prasad et al., 2009). However, it should be noted midbrain synaptosomal preparation from SERT Ala56 mice showed no difference in Na^+ uptake when Na^+ was replaced with either Li^+ or NMDG (**Figure 25**). That being said, SERT Ala56 does not show an increase in [^{3}H]5-HT uptake in synaptosomes (data not shown), suggesting that the reduced preparation of synaptosomes does not contain the necessary machinery to sustain elevated SERT Ala56 uptake.

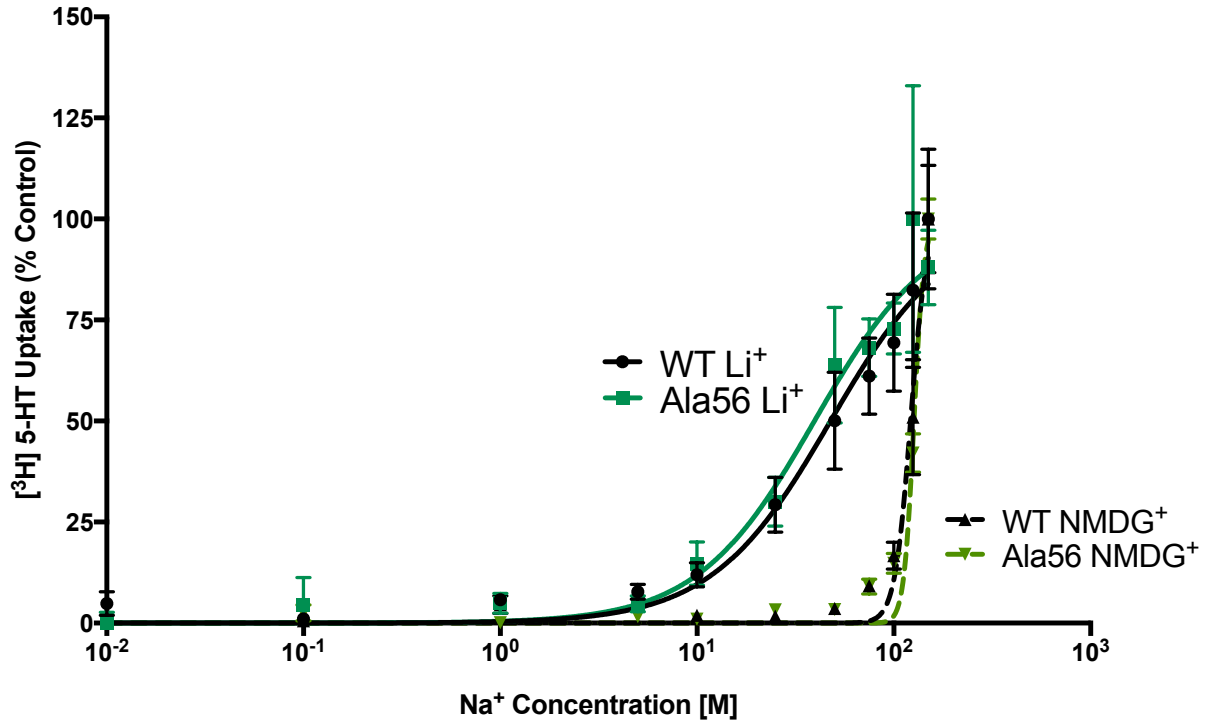

Figure 25. Na^+ dependent 5-HT uptake in SERT Ala56 midbrain synaptosomes

Midbrain synaptosomal [^{3}H]5-HT uptake with various concentrations of NaCl replace with either $NMDG^+$ or LiCl to maintain ionic concentration. WT and SERT Ala56 show no difference in the concentration of Na^+ required for 5-HT uptake.

Another possibility to explore is SERT Ala56 sensitivity to K^+. K^+ binding to the inward facing conformation is required for SERT reorientation to the outward facing conformation, a requirement not found for other monoamine transporters. Considering the N terminus shows the most sequences divergence between the monoamine transporters, potentially the N-terminus plays a role in K^+ binding to the inward facing conformation. Since the N-terminal SERT Ala56 variant is stabilized in an outward facing conformation, this may be caused by an enhanced affinity of K^+ to the transporter and then reorientation to the outward facing conformation. A difference between SERT Ala56 and WT on K^+ loading may provide a clue to understanding the role of the N-terminus and K+ in SERT mediated transport.

Surface Expression of SERT Ala56 In Vivo

Another important unexplained molecular mechanism of SERT Ala56 is the enhanced sensitivity to PKC mediated downregulation of 5-HT uptake as well as SERT Ala56 unexpected PKG mediated decrease in surface expression with no congruent change in SERT uptake activity (Prasad et al., 2009). In transfected cells under basal conditions SERT Ala56 does not affect SERT surface expression; however, in SERT Ala56 KI mice, SERT biotinylating studies have not been done. Based on the *in vitro* data, it would be expected that SERT Ala56 *in vivo* also shows no difference in surface expression. However, there are many instances where *in vitro* data do not match *in vivo* data, such as with the ADHD-associated DAT variant, Val559, which showed no difference in DAT uptake and surface level *in vitro* (Mazei-Robison et al., 2008), but *in vivo,* DAT Val559 mice showed decreased DA uptake and paradoxical increase in DAT surface expression (Gowrishankar et al., 2018). Utilizing a surface biotinylation assay from brain slices of different regions, as described in Gowrishankar et al. 2018, of SERT Ala56 mice compared to WT mice may determine if SERT surface levels vary across brain regions in a genotype-dependent manner, which may provide insight into region-specific modulation of SERT.

SERT Ala56 Lateral Mobility within the Plasma Membrane

The lateral mobility of transporters within lipid rafts of the plasma membrane has been extensively studied utilizing quantum dots conjugated to a cognate substrate that allows the tracking of single transporters under physiologic conditions (Chang and Rosenthal, 2013). It has been shown that activation of p38 MAPK and PKG pathways increases SERT mobility in plasma membranes (Chang et al., 2012). Considering these kinase pathways increase SERT uptake it is hypothesized that the hyperactive SERT Ala56 may also have enhanced lateral mobility. Interestingly, a C-terminal peptide against the C-terminus of SERT that disrupts C-terminal interacting proteins, also increases SERT mobility within the membrane. It is thought that the increased mobility is due to an untethering of SERT from scaffolding proteins, increasing SERT motility (Chang et al., 2012). Proteomic analysis of SERT Ala56 also shows a decrease in SIPs compared to WT, which may support the increased motility. Another means to increase SERT lateral mobility is by changing the lipid composition of the plasma membrane, as Bailey and colleagues found that depletion of cholesterol also increased SERT lateral diffusion within the membrane and increased phosphorylation at Thr276 (Bailey et al., 2018). Interestingly, cholesterol has been shown to play a role in regulating SERT conformational dynamics and SERT phosphorylation state (Scanlon et al., 2001; Magnani et al., 2004).

Interacting proteins of ASD-associated SERT variants

SERT is part of a dynamic network of proteins connected to a number of scaffolding proteins that mediate SERT's location within the membrane as well as signaling cascades that affect the SERT PTM and regulation of SERT activity. To identify proteins that interact with SERT in a state-dependent manner, our lab employed a proteomic analysis from SERT affinity purified midbrain synaptosomes from WT, SERT Ala 56 and SERT KO mice (**Chapter 3**). Several novel SIPs were identified as well as several previously described SIPs. Below I discuss some of the interesting novel SIPs identified from our proteomic analysis as well as some preliminary data on candidate proteins, either identified in the proteomic screen or proteins that were of interest due to their link to p38 MAPK and PKG pathways.

Novel SERT Interacting Proteins

One novel family of proteins identified from our proteomic analysis of SIPs is the septin (Sept) family, Sept5, Sept8, Sept 10, Sept11. Sept 7 and Sept11 were also found in Haase et al. analysis of SIPs, shown to interact with GST-SERT C-terminal fusion proteins (Haase et al., 2017). Septins are a cytoskeletal GTPases that regulate vesicle trafficking and compartmentalization of the plasma membrane (Tokhtaeva et al., 2015). Accumulating evidence suggests that septins impact the exocytosis process (Tokhtaeva et al., 2015). Interestingly Sept5 (also referred to as CDCrel-1) has been shown to bind to syntaxin 1A, a previously identified SIP (Quick, 2002a), and inhibit exocytosis (Beites et al., 1999). Sept5 is located on human chromosome 22q11.2, a region with copy number variation (CNV) that has been associated with increased risk to develop ASD. Mouse models that knock-out Sept5 gene show reduced social interaction compared to WT mice (Harper et al., 2012; Hiroi et al., 2012). Our proteomic analysis reveals that Sept5 has an increased interaction with SERT Ala56, a mouse model that also shows deficits in social interactions paradigms (Veenstra-VanderWeele et al., 2012). Future studies need to verify septin:SERT interaction and determine if septins regulate SERT function.

Protein Phosphatase 2A

Two proteins linked to PKG and p38 MAPK regulation of SERT are PP2A and syntaxin 1A, and thus are of interest in regards to SERT Ala56 variant. It is known that inhibition of PP2A decreases SERT uptake in transfected HeLa; however, this effect is lost with SERT Ala56 (as well as I435L) (Prasad et al., 2009). Surprisingly though, preliminary data from the Ramamoorthy lab shows that SERT Ala56 increases interaction with PP2A compared to SERT (**Figure 26**), which is in contrast to the proteomic analysis (Chapter 3) which shows that SERT Ala56 decreases interactions with PP2Ac. However, it was also found from the same proteomic analysis that SERT Ala56 increases interaction with PP2A regulatory subunit B compared to WT (Chapter 3), potentially explaining Ramamoorthy's data. Being that PP2A is a phosphatase and considering that SERT Ala56 is hyperphosphorylated in a p38 MAPK dependent manner

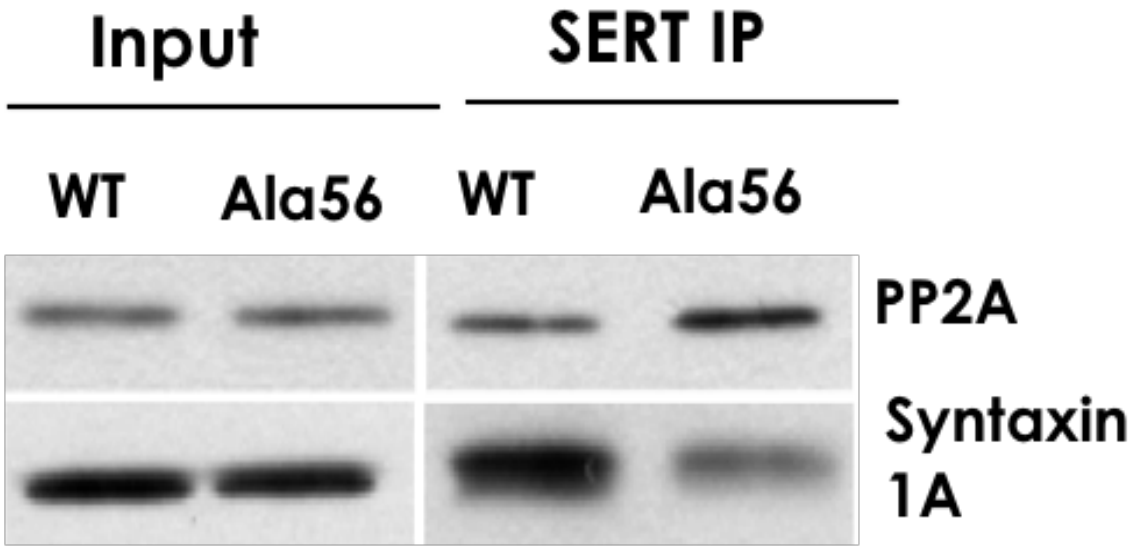

Figure 26. SERT Ala56 interaction with PP2A and syntaxin 1A

Figure courtesy of Sammanda Ramamoorthy Ph.D. Preliminary data shows previously described SIPs, PP2A and syntaxin 1A differentially interact with SERT Ala56 compared to WT from mouse midbrain lysates.

(Veenstra-VanderWeele et al., 2012) and the PP2A has been shown to be activated by p38 MAPK (Westermarck et al., 2001) it might be expected that SERT Ala56 would show less interaction with PP2A. However, it has been shown that inhibition of p38 MAPK disrupts SERT:PP2A interaction (Samuvel et al., 2005), potentially suggesting that activation of p38 MAPK enhances and/or stabilizes the interaction and thus explains the increased interaction seen with SERT Ala56. Interestingly, SERT Ala56 is insensitive to PP2A mediated downregulation by calyculin A and fostriecin (PP2A inhibitors) (Prasad et al., 2009), potentially suggesting a loss of PP2Ac:SERT Ala56 interaction. Most likely, PP2A interacts with SERT in a large signaling complex and plays a complicated role in regulating SERT kinetics that still needs further analysis.

Syntaxin 1A

Another protein of interest, syntaxin 1A, showed disrupted interaction with SERT Ala56 compared to WT SERT (**Figure 26).** This is somewhat surprising in the context that a protein that interacts with syntaxin 1A, Sep5 (Beites et al., 1999), showed enhanced association with SERT Ala56 compared to WT in proteomic analysis of SIPs (Chapter 3). Disruptions of syntaxin 1A interaction with SERT have also been shown to decrease SERT Vmax (Quick, 2002a), which does not align with the decreased K_M exhibited by SERT Ala56. Also, it was previously found that inhibition of p38 MAPK disrupts syntaxin 1A:SERT interaction (Samuvel et al., 2005), suggesting that p38 MAPK activity stabilizes syntaxin 1A:SERT interaction and therefore it might be expected that if SERT Ala56 would have an enhanced interaction with syntaxin 1A if SERT Ala56 is hyperactive and hyperphosphorylated in a p38 MAPK manner (Veenstra-VanderWeele et al., 2012; Robson et al., 2018). However, uncoupling of syntaxin 1A from SERT has also been shown to induce a Na^+ conducting state of SERT independent of substrate (Quick, 2003), which has yet to be examined in SERT Ala56.

Flotillin-1

A previous study has shown that FLOT1, a membrane-raft protein, interacts with SERT in a state-dependent manner (Reisinger et al., 2018). FLOT1 has been linked to DAT localization to membrane microdomains (Sakrikar et al., 2012); however, the role of FLOT1 on SERT compartmentalization within the membrane has not been explored. On the same note, it is not known if SERT Ala56 or other SERT variants co-localize to membrane microdomains and/or certain biosynthetic compartments. Proteomic analysis of SIPs shows that SERT Ala56 decreases interaction with FLOT1 (Chapter 3). This is somewhat analogous to the ADHD-associated DAT variant (R615C), which also showed impaired regulation by amphetamine and decreased interaction with FLOT1. Also of interesting note, FLOT1 depletion has been shown to enhance diffusion of DAT within the plasma membrane (Sorkina et al., 2012). Therefore, it may be expected untethering of SERT from FLOT1 would also increase SERT lateral diffusion within the membrane, a hypothesis suggested above.

Post-translational modifications of SERT

It was shown that SERT from Ala56 KI mice is hyperphosphorylated in a p38 MAPK dependent manner (Veenstra-VanderWeele et al., 2012), and shows insensitivity to further stimulation by PKG and p38 MAPK. However, which specific residues are phosphorylated in the presence of Ala56 substitution are currently unknown. One possibility is that SERT Ala56 places the transporter in a conformation to be more accessible for phosphorylation at Thr276 considering it has been shown to be mediated by both PKG (Ramamoorthy et al., 2007) and p38 MAPK pathways (unpublished data). Thr276 is located in a conformationally sensitive alpha helical loop (ICL2) that unwinds as the transporter transitions from the outward-facing conformation to inward-facing conformation (Zhang et al., 2016). Thr276 becomes accessible for modification as the transporter transitions into the inward-facing state. One hypothesis is that the bulky phosphate group at Thr276 forms electrostatic interactions or repulsions with key residues, perhaps on the N-terminus, that ultimately impact the ability of the ILC2 from completing the entire

winding and unwinding process as the transporter completes the transporter cycle and essentially shorting the transition time from outward to inward facing conformation, thus leading to increase uptake.

Another post-translational modification that may affect SERT function and has been understudied is ubiquitination. While ubiquitination is most commonly thought of labeling a protein for degradation, there are several ubiquitination patterns that affect protein function independent from degradation. Several ubiquitin ligases were shown to interact with SERT in the proteomic analysis (see chapter 3). In the appendix, I highlight an E3 ubiquitin ligase (melanoma antigen E1; MAGE-E1) as a SERT interacting protein, showing increased interaction with Ala56 expression. One hypothesis is the SERT Ala56 is differentially ubiquitinated in a MAGE-E1 dependent manner, which can be tested utilizing a Ub-pull-down method from SERT Ala56 expressing tissue or cells followed by immunoblot for SERT. Three putative lysine residues in the SERT N-terminus were identified, K10, K29, K37 via the UbPred website. Examining the effects of mutating these lysine residues to alanine on SERT protein expression and 5-HT uptake on both the WT and Ala56 background would elucidate a potential role of ubiquitination on SERT regulation.

SERT Ala276 KI mouse model

Amino acid Thr276 of SERT is a conformationally sensitive phosphorylation site (Zhang et al., 2016), implicated in PKG (Ramamoorthy et al., 2007) and p38 MAPK (unpublished data) dependent regulation of the transporter. To explore the role of this phosphorylation site *in vivo* we generated a phospho-insensitive SERT Ala276 KI mouse via CRISPR/Cas 9 technology. The data presented in Chapter 4 establishes a baseline characterization of the SERT Ala276 mouse model that allows for these further investigations to determine the functional aspects of SERT phosphorylation at amino acid Thr276.

There are no gross abnormalities exhibited by the SERT Ala276 mice. These mice show normal locomotor activity, body weights, neurochemical levels, SERT mRNA and protein levels, and uptake kinetics. Interestingly, SERT Ala276 showed significantly less [^{3}H]citalopram binding from midbrain membrane samples compared to WT. It is currently not known if this is due to decrease in the surface level

expression of SERT Ala276 or if the affinity for citalopram is affected by the Ala276 mutation. In order to address this, we need to perform a surface biotinylation assay from SERT Ala56 and WT littermates. *In vitro* evidence of SERT Ala276 (Ramamoorthy et al., 2007) and the lack of SERT Vmax effect suggests that SERT Ala276 does not affect surface levels. However, if there is a difference in surface expression, this may point to PKG pathway as past studies have shown that activation of PKG increases SERT surface expression (Miller and Hoffman, 1994; Zhu et al., 2004). The other possibility explaining the difference in [^{3}H]citalopram binding is a difference in citalopram affinity. To determine the equilibrium dissociation constant (K_D) of citalopram requires saturation binding assay with [^{3}H]citalopram.

Behaviorally, these mice under baseline conditions did not show any depressive- and anxiety-like behavior. Considering the difference in the [^{3}H]citalopram binding assay as mentioned above, there is the possibility that there is an altered sensitivity of SSRI to decrease immobility time in the TST and FST in the SERT Ala276 mice compared to WT.

Future studies aim to probe the effect of SERT Ala276 mutation on the ability to respond to stimuli that act on p38 MAPK and PKG pathways identified in past studies to regulate transporter activity *in vivo* and *ex vivo* and its effect on relevant behaviors. First and foremost is to assess the sensitivity of SERT Ala276 compared to WT mice to p38 MAPK and PKG mediated simulation of SERT activity, assessed by synaptosomal [^{3}H]5-HT uptake assays and *in vivo* chronoamperometry based studies. If phosphorylation at Thr276 is critical for SERT activation stimulated by activation of these pathways, it is expected, as seen *in vitro,* that SERT Ala276 mice will be insensitive to p38 MAPK- and PKG-dependent increase in 5-HT uptake.

Several studies have shown environmental and physiological relevance of these pathways acting on SERT activity. Of particular interest to our lab is the effect of SERT Ala276 on SERT uptake and depressive-like behaviors in response to low dose peripheral immune activation by LPS. Previous studies from our lab have shown that 0.2 mg/kg I.P. injection of LPS rapidly (1-hr post injection) increases SERT activity and induces depressive-like phenotypes (Zhu et al., 2010), which is dependent on p38α MAPK expression within serotonergic neurons (Baganz et al., 2015). Unpublished data from our lab indicate that

p38 MAPK dependent increase in 5-HT uptake *in vitro* is dependent on the expression of Thr276 within SERT, suggesting Thr276 as a critical phosphorylation site for p38 MAPK dependent effects. Therefore, we hypothesize that SERT Ala276 mice will be insensitive to or blunts LPS dependent increase in 5-HT uptake and depressive-like phenotypes. If SERT Ala276 shows no difference between WT on LPS mediated changes there is the possibility that p38 MAPK signaling cascade activated by LPS affects SERT through a yet unknown mechanism. SERT has multiple phosphorylation sites, including Thr616 which has been shown to be phosphorylated in the presence of p38 MAPK (Sørensen et al., 2014) and a number of other kinase and proteins act on the transporter which may be also affected by LPS.

Other pathways of interest involve KOR (Sundaramurthy et al., 2017) and A3AR (Zhu et al., 2004), which have both been linked to p38 MAPK- and PKG-dependent regulation of SERT (see Chapter 1). The availability of the first SERT Ala276 KI mouse provides for the first time the opportunity to assess the contribution of SERT phosphorylation modulation *in vivo* and its physiological significance.

Conclusion

Overall, we hypothesize that SERT exists in distinct conformational states that dictate the transporters activity and that SIPs and post-translational modifications can shift the population of SERT to a hyperactive state (SERT*). Environmental factors and/or genetic variations can either directly or indirectly impact SIPs and PTMs ultimately affecting SERT conformational dynamics and function. In this dissertation, we provided evidence that two ASD-associated SERT variants, SERT Ala56 and SERT Asn605, that are insensitive to p38 MAPK- and PKG-dependent upregulation, stabilized SERT in an outward-facing conformation. We also generated a functional network analysis of SIPs that differentially interact with SERT Ala56. In addition, we characterized a new KI mouse model, SERT Ala276, to study the effect of the conformationally sensitive PKG/p38α MAPK dependent phosphorylation site Thr276. The goal of this dissertation was to explore the structural and functional dynamics of previously identified SERT variants. Of great scope, the work presented here demonstrates that remarkably minor coding variation can have profound effects on structural and functional regulation of a protein and understanding how these

genetic variations function in a complex network of proteins has the potential to identify novel targets for pharmacotherapies that can be beneficial in the treatment of diseases.

APPENDIX

Interaction between SERT and MAGE-E1

The N-terminus of SERT has become increasingly appreciated for its important role in modulating SERT activity and is of particular interest to our lab, as a hyperfunctional and regulationally insensitive variant associated with ASD was identified in this region, SERT Ala56 (Sutcliffe et al., 2005; Prasad et al., 2009). To identify novel proteins that differentially interacted between WT and SERT Ala56 N-terminus, I performed a GST pull-down with the fusion protein containing the N-terminus of rSERT that possesses either Gly56 (WT) or Ala56 using mouse midbrain detergent extracts followed by LC-MS/MS analysis. This study identified a number of novel proteins that interacted with N-terminus; however, one protein that we decided to pursue further was the melanoma antigen E1 (MAGE-E1) as this protein showed enhanced interaction with GST-SERT N-terminus expressing Ala56 compared to Gly56. Interestingly, MAGE-E1 was also identified in two separate LC-MS/MS experiment directed at characterizing the SERT interactome from affinity purified (AP) full-length SERT from mouse midbrain samples as previously described (Ye et al., 2016). Verification of this interaction by western blot analysis reveals that MAGE-E1 interacts with N-terminal tail expressing both Ala56 and Gly56 as well as the C-terminal tail (**Figure 27A).** Subsequently, I verified the enriched nature of SERT Ala56:MAGE-E1 interactions by co-IP followed by western-blot analysis (**Figure 27B**). These results provide strong evidence that SERT forms a complex with MAGE-E1, potentially in an activity-dependent manner.

MAGE-E1 is of particular interest as a novel SIP for a number of reasons. For one, other MAGE family members have been implicated in neuropsychiatric disorders linked to altered 5-HT signaling. MAGE-E1 is a member of the melanoma antigen family, which all share a common ~170 amino acid long MAGE homology domain (MHD; MAGE-E1 contains two MHDs), originally identified as a cell surface antigen in melanoma cancer cells (Barker and Salehi, 2002). However, MAGE-E1, along with most other MAGE family members, are classified as Type II ubiquitous MAGE proteins, which are expressed in

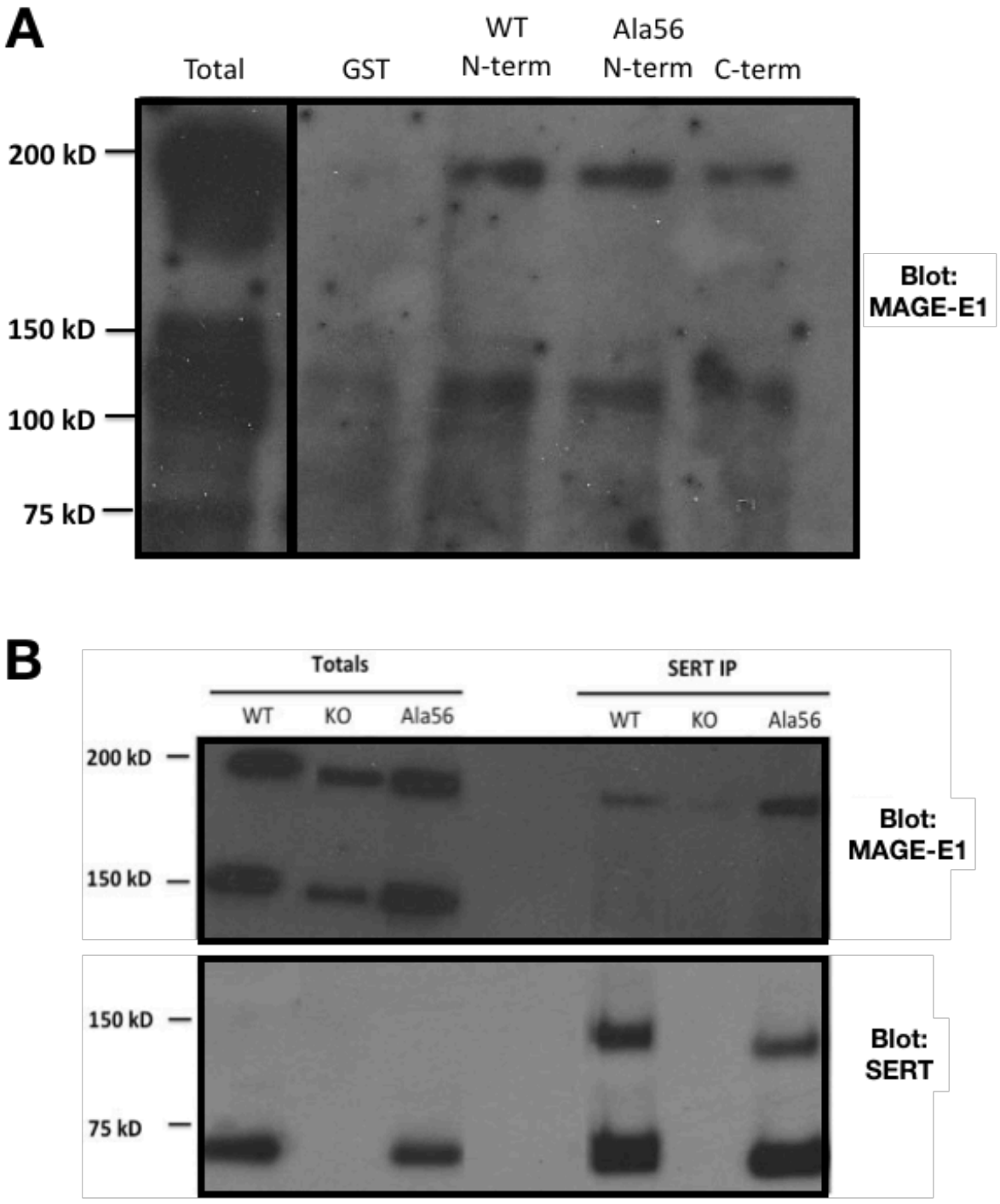

Figure 27. SERT:MAGE-E1 complex verified by Western blot
(A) MAGE-E1 from midbrain lysate of WT mice interacts with N- (both WT and Ala56) and C-terminus of SERT as demonstrated by GST-pull down. (B) SERT co-IP (as described in Chapter 3) shows SERT Ala56 and WT SERT interact with MAGE-E1 but not SERT KO (negative control).

normal somatic cells. Other members of the MAGE Type II family include MAGE-L2, -D1, and Necidin, have been implicated in neurodevelopmental disorders associated with 5-HT dysfunction, such as Prader-Willi Syndrome and autism (Barker and Salehi, 2002; Lee et al., 2005; Zanella et al., 2008; Dombret et al., 2012; Schaaf et al., 2013). Importantly for our studies, MAGE-E1 has also been found to be highly expressed in the brain (Albrecht and Froehner, 2004). Specifically, MAGE-E1 was found to be enriched in microarray profiled embryonic 5-HT neurons (Wylie et al., 2010) (**Figure 28**) and is expressed in adult MB 5-HT neurons (**Figure 29**). Also, MAGE-E1 is part of a complex that contains proteins previously described to interact with SERT. While the functional role of MAGE-E1 in this complex is still not clearly defined, it has been shown to directly interact with α-dystrobrevin, giving MAGE-E1 its cognate name, DAMAGE (α-dystrobrevin-associated MAGE protein) (Albrecht and Froehner, 2004). Alpha-dystrobrevin associates with dysbindin (Benson et al., 2001), a protein that has also been implicated in 5-HT-linked neuropsychiatric disorders, including schizophrenia and depression (Numakawa et al., 2004; Owen et al., 2004; Zill et al., 2004; Domschke et al., 2011). In addition, α-dystrobrevin, MAGE-E1, and dysbindin are members of the dystrophin-associated protein complex (DPC), which also includes nitric oxide synthase (NOS), a previously described SERT partner (Chanrion et al., 2007). The DPC functions to anchor the cytoskeleton to the extracellular matrix (ECM) (Michalak and Opas, 1997). Many other scaffolding proteins have been shown to interact with SERT, including integrin βIII, HIC-5, and NLGN2 (Carneiro and Blakely, 2006; Carneiro et al., 2008; Ye et al., 2016).

Another MAGE family protein, MAGE-D1, also forms a functional interaction with SERT. MAGE-D1 KO mice exhibit increases SERT expression and exhibit depressive-like behaviors, which are reversed by SSRI administration. Conversely, MAGE-D1 overexpression increases SERT ubiquitylation and 26S-proteasome-dependent degradation of SERT (Mouri et al., 2012). MAGE-D1 interacts with SERT via the MHD (Mouri et al., 2012), which shares 46% sequence homology with the MHDs of MAGE-E1 (Doyle et al., 2010).

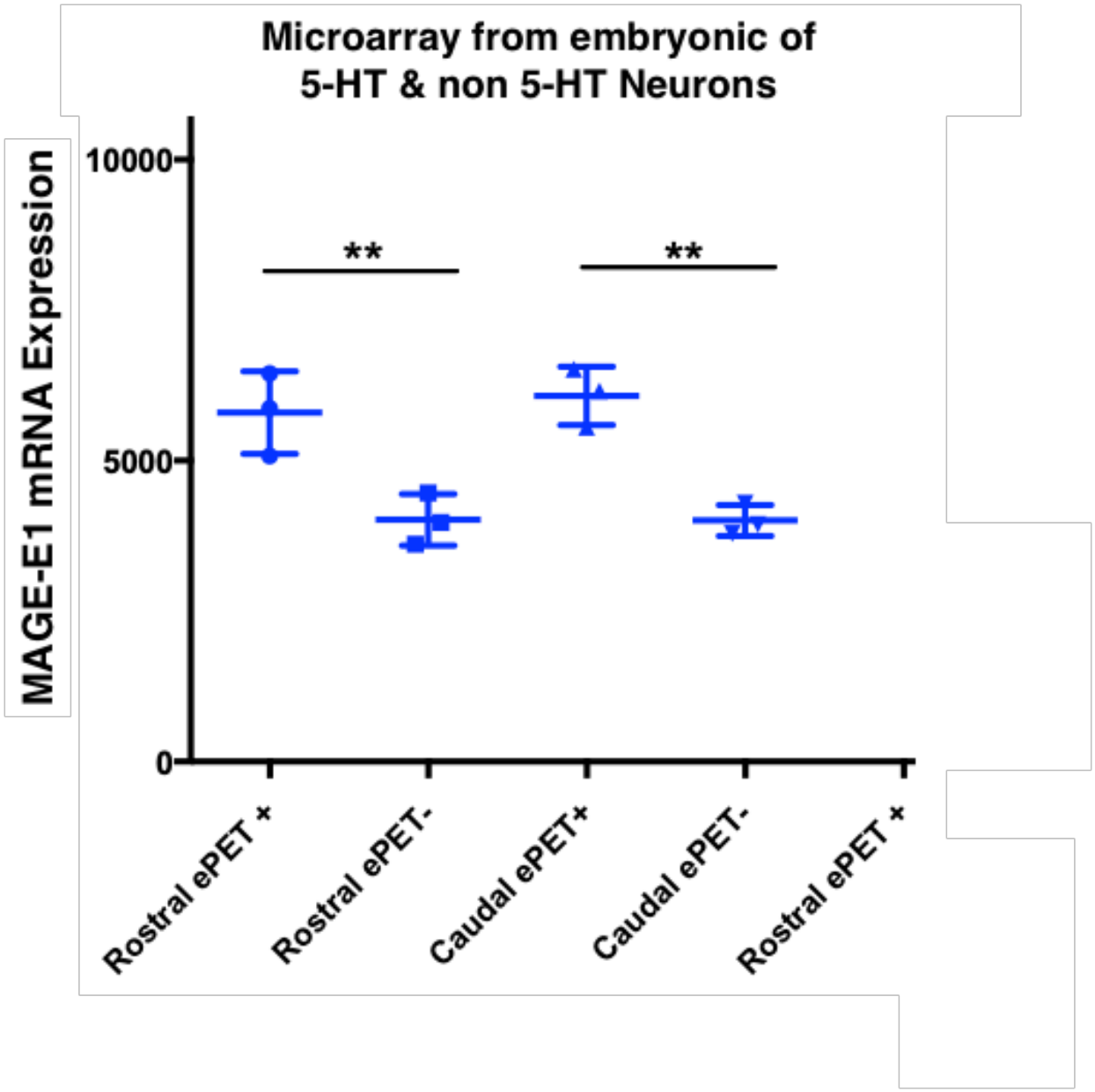

Figure 28. MAGE-E1 mRNA expression is enriched in ePET1 positive neurons
Microarray profiled from flow sorted ePET+ neurons (transcription factor of 5-HT neurons) and ePET- neurons from embryonic mice as described in Wylie et al. 2010. MAGE-E1 mRNA expression is enriched in serotonergic neurons in both the rostral and caudal brain.

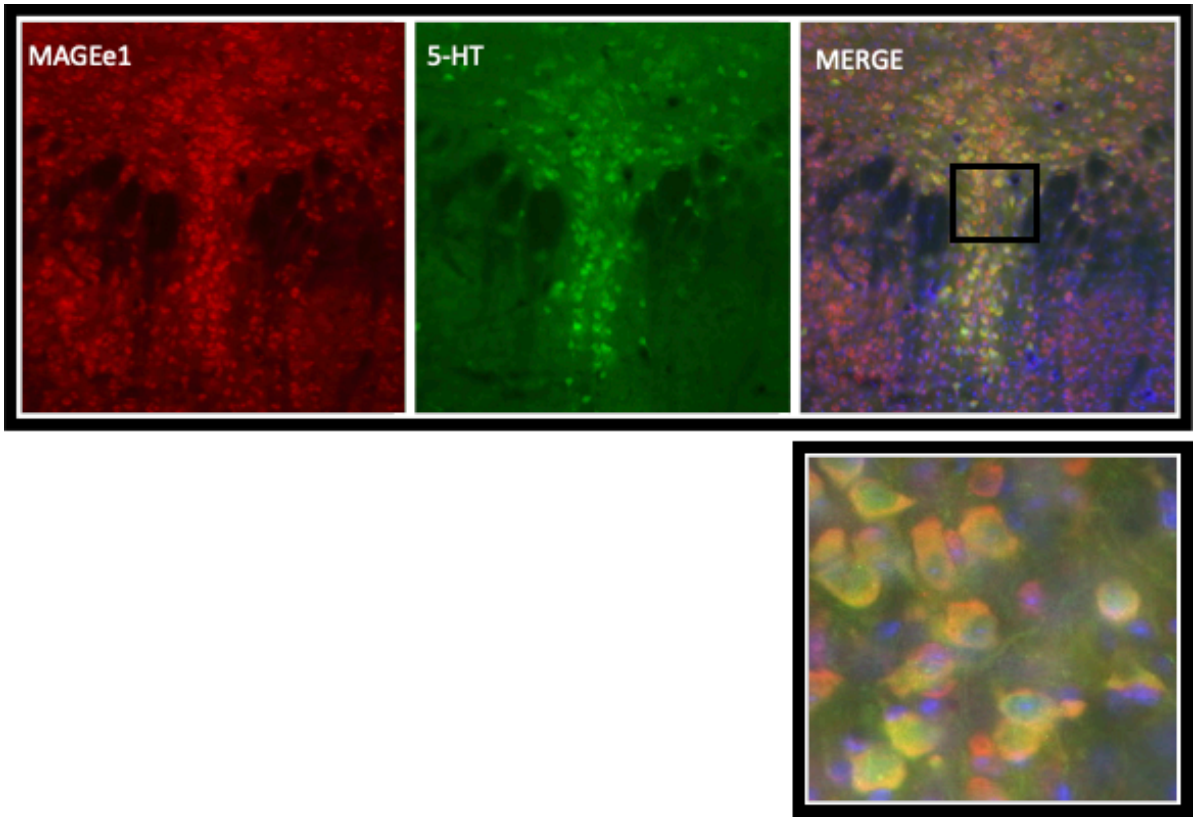

Figure 29. MAGE-E1 is localize in serotonergic midbrain neurons
Immunohistochemistry of midbrain slices from WT mice stained with antibody against MAGE-E1 and 5-HT shows that some MAGE-E1 positive cells are co-labeled with 5-HT.

One hypothesis is that MAGE-D1 reduces SERT activity by facilitating endocytosis and degradation, whereas MAGE-E1 stabilizes SERT*, ensuring surface retention and/or a shift in 5-HT recognition, for efficient 5-HT clearance. Clearly, future studies are needed to parcel out the MAGE-D1/E1 interaction with SERT and SERT Ala56.

Novel SERT phosphorylation Ser8 identified by LC-MS/MS

Contained within all mass spectra generated from the AP-MS/MS experiments utilized to characterize SERT interactome, is a rich data set that allows for the identification of PTMs, such as phosphorylation and ubiquitination A few programs have been developed to search for shifts in MS2 spectra that account for the PTM of interest. For example, X! Tandem refinement search within Scaffold can be performed (Kertész-Farkas et al., 2014). In this method, only proteins that have been previously defined by Sequest (or Mascot) are utilized to generate the reference database of spectra to match onto the experimental spectra and now allow for variable modification of phosphorylation (+79.97 of Ser, Thr, or Tyr) and ubiquitination (+144.04293 of K). Unfortunately, X! Tandem refinement search from the proteomic analysis described in Chapter 3 did not identify any modified peptides in SERT. However, in a preliminary study to optimize the conditions for the SERT co-IP for LC-MS/MS analysis, this refinement search identified an N-terminal peptide within SERT phosphorylated at Ser8 (**Figure 30**). Future studies need to verify Ser8 as a phosphorylation site and determine its role in the regulation of SERT function.

D-fenfluramine mediated prolactin release, hypothermia, and FLOT1:SERT interaction

SERT Ala56 mice show blunted 5-HT mediated efflux to D-fenfluramine both *in vitro* and *in vivo* (Quinlan et al., 2019). D-fenfluramine has long been used as a means to assess the overall serotonergic tone of a system, both in humans and rodents, as D-fenfluramine challenge results in a number of easily measured physiological responses, such as prolactin release (Quattrone et al., 1983) and hypothermia (Cryan et al., 2000).

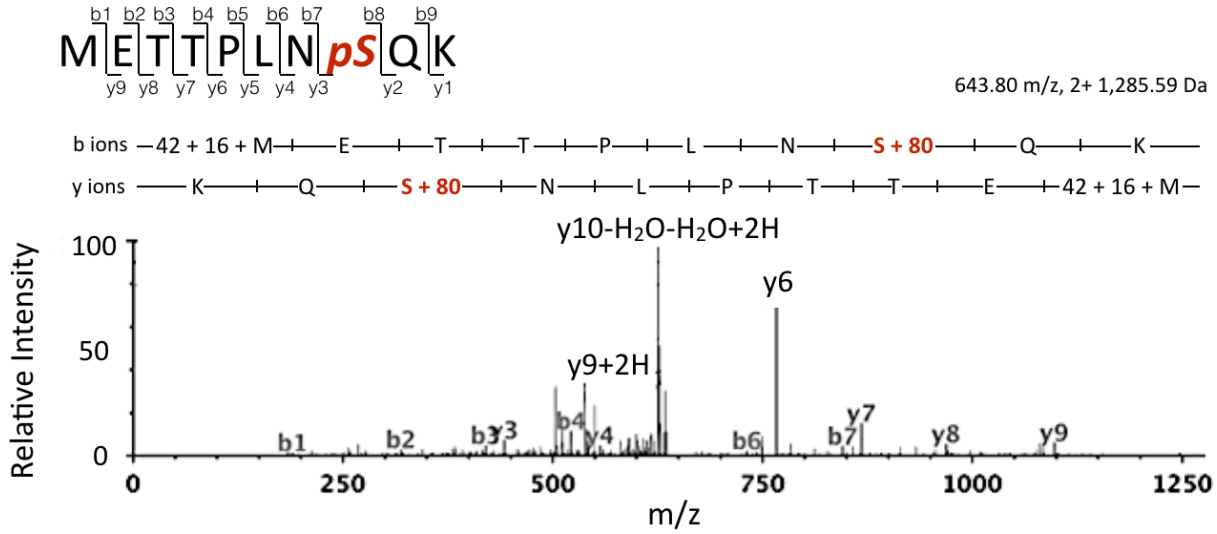

Figure 30. Identification of p-Ser8 in SERT from AP-MS/MS data
Immunoprecipitated SERT from mouse midbrain synaptosomes was subjected to MS/MS analysis. MS/MS spectra were first matched against the SEQUEST database to identify peptide and then the MS/MS spectra were reanalyzed against the X! Tandem database containing only proteins previously defined by SEQUEST to query for a shift in mass of 80 Da (the mass of a phospho group) at serine, threonine, and tyrosine residues. Fragmentation patterns defined Ser8 in the peptide METTPLN**S**QK as phosphorylated.

Therefore, we decided to evaluate SERT Ala56 mice response to D-fenfluramine challenge. SERT Ala56 mice show increased serum prolactin levels 30 minutes post IP injection at 3 mg/kg D-fenfluramine compared to WT mice; however, there was no difference between genotypes at the 10 mg/kg dose (**Figure 31A**). On the other hand, at the 10 mg/kg dose, SERT Ala56 exhibit a trend for enhanced response to D-fenfluramine-induced hypothermia, while it appears the 3 mg/kg dose was too low to induced hypothermia (**Figure 31B**). Even though our previous report shows that SERT Ala56 bunts D-fenfluramine mediated 5-HT efflux, this elevated response to D-fenfluramine prolactin release and hyperthermia is most likely due to the hypersensitivity of 5-HT receptors in these mice. Prolactin release stems from stimulation of $5HT_{2A/C}$ receptors expressed in the paraventricular nucleus of the hypothalamus through (Quattrone et al., 1983; Emiliano and Fudge, 2004), while hyperthermia is driven in part by $5HT_{1A}$ receptor activation (Cryan et al., 2000). Previous studies have shown that SERT Ala56 mice are also hypersensitive to 8-OH-DPAT ($5HT_{1A}$ agonist) induced hyperthermia and DOI ($5HT2_{A/C}$ agonist) induced head twitch (Veenstra-VanderWeele et al., 2012). This hypersensitivity of 5-HT receptors is thought to be due to a chronic decrease in extracellular 5-HT levels due to the enhance 5-HT uptake.

In a parallel study, we identified by proteomic analysis that SERT Ala56 has decreased interaction with FLOT1 compared to WT SERT (Chapter 3). Previous studies have shown that DAT:FLOT1 interaction is linked to amphetamine action (Sakrikar et al., 2012). Therefore, we decided to assess the association of SERT:FLOT1 in response to 10 mg/kg challenge of D-fenfluramine or saline injection. Interestingly, saline-treated animals showed no difference between genotype for SERT:Flot-1 interaction (**Figure 32**). This may be due to the stress of saline injection, as SERT:FLOT1 interaction was shown to critical in response to corticosterone stress paradigm (Reisinger et al., 2018). D-fenfluramine injection significantly enhances SERT:FLOT1 interaction in SERT Ala56 mice compared to WT mice (**Figure 32**). This may suggest that SERT Ala56 under normal conditions does not interact with FLOT1, however, SERT Ala56 is located or more easily relocates into a FLOT1 containing raft compartment in response to certain environmental demands which increases its probability to interact with FLOT1.

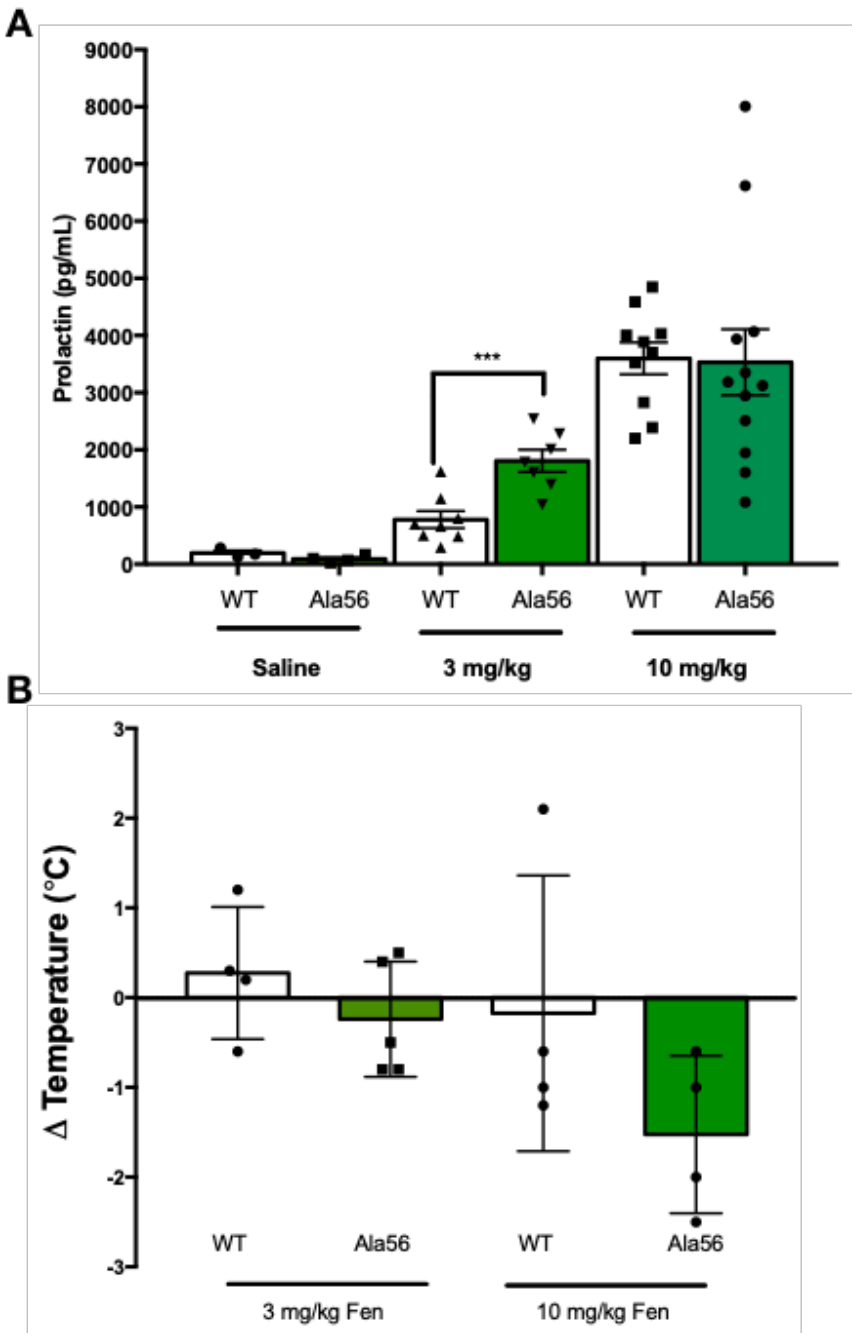

Figure 31. Fenfluramine mediated prolactin release and hypothermia in SERT Ala56 KI Mice

(A) WT and SERT Ala56 treated IP with 3 mg/kg or 10 mg/kg with fenfluramine 30 minutes prior to dissection. Prolactin levels from blood serum in SERT Ala56 mice injected with 3 mg/kg of fenfluramine is increased compared to WT mice (n=7, unpaired t test, $P \leq 0.001$), but no difference between genotypes at 10 mg/kg fenfluramine. (B) 30 minutes post injection of fenfluramine body temperature was measures. Preliminary data shows SERT Ala56 mice injected with 10 mg/kg fenfluramine trends toward enhanced hypothermia compared to WT mice (n = 3).

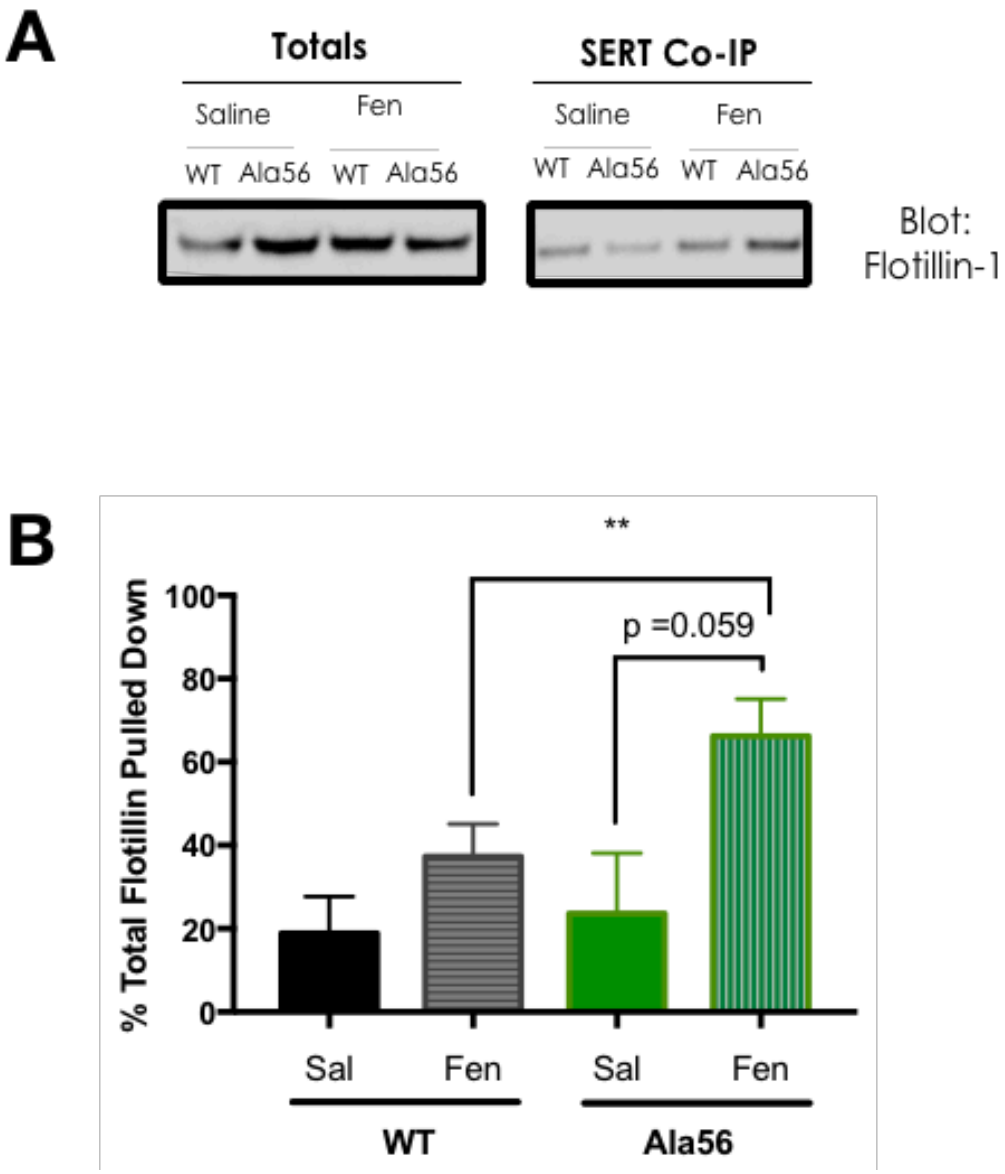

Figure 32. SERT:FLOT1 interaction increases in response to fenfluramine in vivo

WT and SERT Ala56 mice were I.P. injected with 10 mg/kg fenfluramine or saline. After 30 minutes midbrain synaptosomes were immunoprecipitated for SERT (n=3). Western blot shows SERT:FLOT1 interaction increases in the presence of fenfluramine.

SERT Ala56 vesicular release

Parallel studies in our lab identified that the ADHD-associated DAT Val559 variant impaired vesicular [^{3}H]DA release from striatal slices (Mergy et al., 2014). With the enhanced uptake exhibited by SERT Ala56, it was hypothesized the loading of vesicles may be altered, leading to changes in 5-HT release. To determine if SERT Ala56 mice affected vesicular release, midbrain slices preloaded with [^{3}H]5-HT were challenged with the 50 μM 4-aminopyridine (4-AP) to block voltage-gated K+ channels. However, no difference between genotypes in 4-AP stimulated vesicular release of 5-HT was detected in the midbrain (**Figure 33**). Future studies will need to determine if other brain regions, such as the hippocampus and prefrontal cortex, also show no difference in vesicular release between WT and SERT Ala56 mice.

Effects of LPS on SERT interacting proteins and SERT phosphorylation

There are many similarities between LPS mediated increase in 5-HT uptake and SERT Ala56 hyperfunction. The main link being p38α MAPK, as both LPS and SERT Ala56 enhanced 5-HT is dependent on p38α MAPK signaling (Baganz et al., 2015; Robson et al., 2018), a state we have labeled as SERT*. SERT Ala56 was also shown to be hyperphosphorylated in a p38 MAPK dependent manner (Veenstra-VanderWeele et al., 2012); however, it was not known if p38 MAPK also induced hyperphosphorylation of SERT in response to the low dose LPS challenge. In collaboration with the Ramamoorthy lab, we assessed in LPS or saline-treated mice (0.2 mg/kg, 1 hr post-I.P. injection) ^{32}P labeling of SERT in hippocampal synaptosomes in the presence and absence of a p38 MAPK inhibitor, PD169316. Preliminary data shows a trend that LPS treatment increases SERT phosphorylation levels which can be prevented through the inhibition of p38 MAPK (**Figure 34**), mimicking the results found for SERT Ala56.

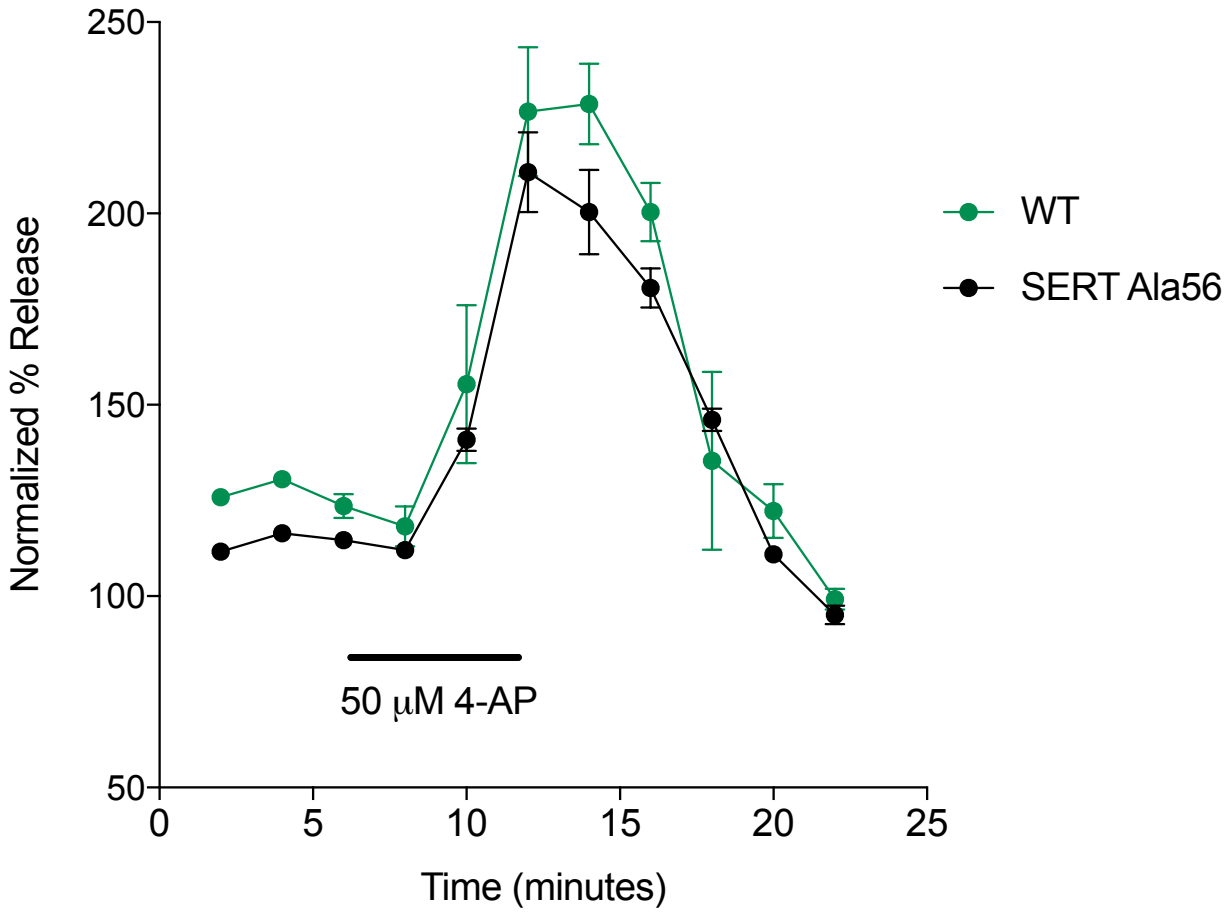

Figure 33. 4-AP mediated vesicular release of [^{3}H]5-HT from SERT Ala56 mice

Midbrain slices from WT and SERT Ala56 mice were (n=3) show no difference in 4-AP stimulated vesicular release of [^{3}H]5-HT.

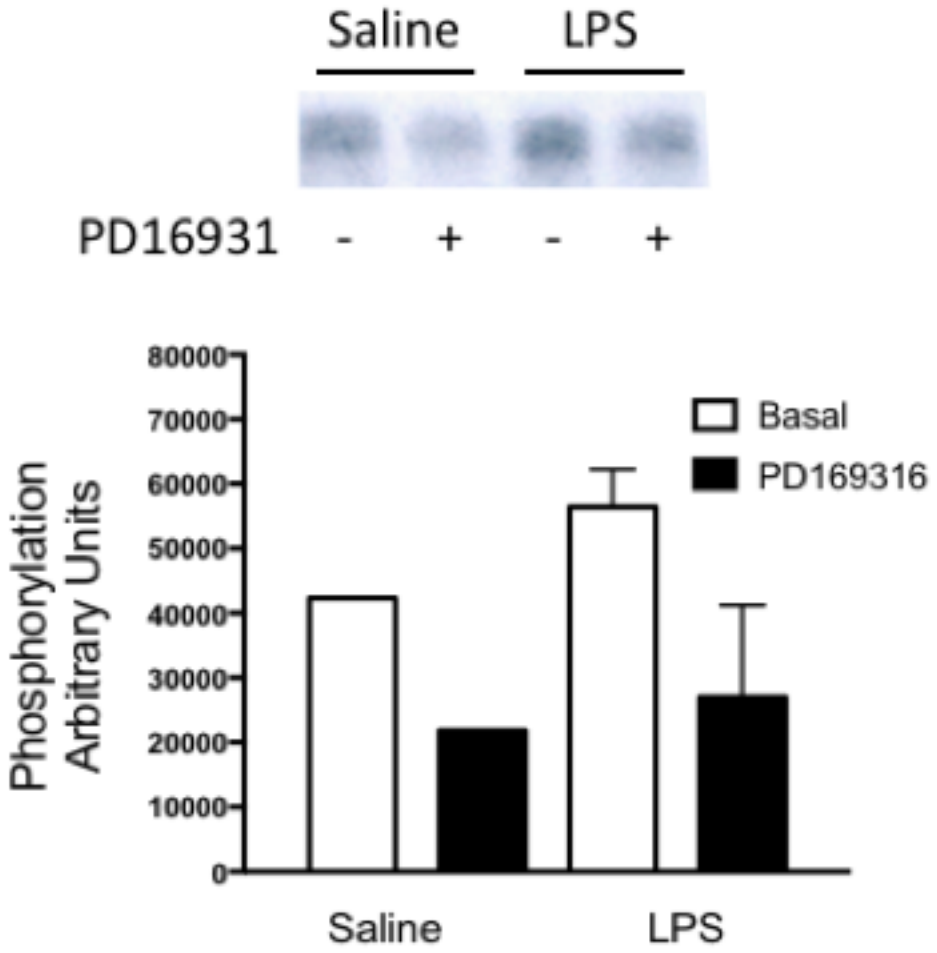

Figure 34. LPS induced SERT phosphorylation dependent on p38 MAPK
Autoradiogram immunoprecipitated SERT from hippocampal synaptosomes metabolically labeled with orthophosphate ^{32}P from mice pretreated one hour before dissection with 200 ng/kg LPS or saline. Synaptosomes were pretreated 10 minutes before ^{32}P labeling with p38 MAPK inhibitor PD166931. Preliminary data (n=1-2) shows under basal conditions SERT is hyperphosphorylated in a p38 MAPK dependent manner in LPS treated animals compared to saline treated mice.

We also aimed to identify SIPs that may modulate both SERT Ala56 and LPS treated animals. To address this, we injected WT and SERT Ala56 mice with 0.2 mg/kg dose of LPS (or saline vehicle) and then 1 hour later harvest midbrain synaptosomes followed by a co-IP with SERT antibody #48 (as described in Chapter 3). Interestingly, WT SERT only interacted with nNOS in the LPS condition, while SERT Ala56 was shown to interact with nNOS, independent of drug treatment (**Figure 35**). This might suggest that nNOS preferentially interacts with SERT* state. Future studies need to determine if this interaction is dependent on p38 MAPK signaling.

Identification of de novo missense variation SERT Ile576Val Variant in ASD cohort

Recently, a collaborator, Jim Sutcliffe at Vanderbilt University, who identified the original five ASD-associated SERT coding variants, found deposited in a database of ASD sequences, a novel de novo missense variant, SERT Ile576Val. Interestingly, de novo mutations in gene coding sequences are rare and are thought if functional, that the gene targeted is a relevant one for the clinical features exhibited in the carrier (Alonso-Gonzalez et al., 2018). SERT Iso576 is found at the extracellular facing side of TM12. This is of interest as Iso576 in hSERT aligns with the ADHD/ASD associated variant Val559 in hDAT. DAT Val559 has been shown to exhibit anomalous domain efflux, DA uptake capacity and altered behavioral phenotypes *in vivo* (Mazei-Robison et al., 2008; Mergy et al., 2014; Gowrishankar et al., 2018). Future studies aim to determine if this variant, SERT Val576 confers a similar or distinct phenotype from DAT Val559 and might open a new line of investigation, or complement our ongoing work on understanding the role of SERT variants in regulating 5-HT uptake and homeostasis.

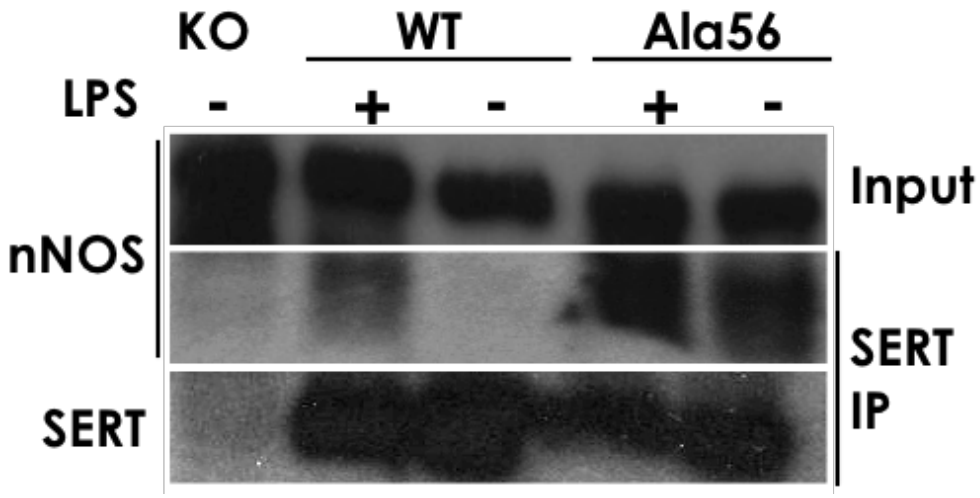

Figure 35. State dependent nNOS interaction with SERT
SERT Ala56 and WT mice were treated one hour before dissection with 200 ng/kg LPS or saline. Midbrain synaptosomes from WT and SERT Ala56 treated mic and SERT KO (negative control) were then subjected to SERT IP.

REFERENCES

Adams S V, DeFelice LJ (2003) Ionic Currents in the Human Serotonin Transporter Reveal Inconsistencies in the Alternating Access Hypothesis. Biophys J 85:1548–1559.

Adhikary S, Deredge DJ, Nagarajan A, Forrest LR, Wintrode PL, Singh SK (2017) Conformational Dynamics of a Neurotransmitter:Sodium Symporter in a Lipid Bilayer. Proc Natl Acad Sci 114:1786–1795.

Aitken A, Baxter H, Dubois T, Clokie S, Mackie S, Mitchell K, Peden A, Zemlickova E (2004) Specificity of 14-3-3 Isoform Dimer Interactions and Phosphorylation. Biochem Soc Trans 30:351–360.

Albrecht DE, Froehner SC (2004) DAMAGE, a Novel α-Dystrobrevin-associated MAGE Protein in Dystrophin Complexes. J Biol Chem 279:7014–7023.

Alonso-Gonzalez A, Rodriguez-Fontenal C, Carracedo A (2018) De novo Mutations (DNMs) in Autism Spectrum Disorder (ASD): Pathway and Network Analysis. Front Genet 9:406.

Anderson GM, Feibel FC, Cohen DJ (1987) Determination of Serotonin in Whole Blood, Platelet-Rich Plasma, Platelet-Poor Plasma and Plasma Ultrafiltrate. Life Sci 40:1063–1070.

Annamalai B, Mannangatti P, Arapulisamy O, Shippenberg TS, Jayanthi LD, Ramamoorthy S (2012) Tyrosine Phosphorylation of the Human Serotonin Transporter: A Role in the Transporter Stability and Function. Mol Pharmacol 81:73–85.

Ansah T-A, Ramamoorthy S, Montañez S, Daws LC, Blakely RD (2003) Calcium-Dependent Inhibition of Synaptosomal Serotonin Transport by the Alpha 2-Adrenoceptor Agonist 5-Bromo-N-[4,5-dihydro-1H-imidazol-2-yl]-6-quinoxalinamine (UK14304). J Pharmacol Exp Ther 305:956–965.

Arons MH, Thynne CJ, Grabrucker AM, Li D, Schoen M, Cheyne JE, Boeckers TM, Montgomery JM, Garner CC (2012) Autism-associated Mutations in ProSAP2/Shank3 Impair Synaptic Transmission and Neurexin-Neuroligin-Mediated Transsynaptic Signaling. J Neurosci 32:14966–14978.

Artigas F (1993) 5-HT and Antidepressants: New Views from Microdialysis Studies. Trends Pharmacol Sci 14:262.

Azmitia EC, Gannon PJ, Kheck NM, Whitaker-Azmitia PM (1996) Cellular Localization of the 5-HT $_{1A}$ Receptor in Primate Brain Neurons and Glial Cells. Neuropsychopharmacology 14:35–46.

Baganz NL, Blakely RD (2013) A Dialogue Between the Immune System and Brain, Spoken in the Language of Serotonin. ACS Chem Neurosci 4:48–63.

Baganz NL, Lindler KM, Zhu CB, Smith JT, Robson MJ, Iwamoto H, Deneris ES, Hewlett WA, Blakely RD (2015) A Requirement of Serotonergic p38α Mitogen-Activated Protein Kinase for Peripheral Immune System Activation of CNS Serotonin Uptake and Serotonin-Linked Behaviors. Transl Psychiatry 5:e671.

Bailey DM, Catron MA, Kovtun O, Macdonald RL, Zhang Q, Rosenthal SJ (2018) Single Quantum Dot Tracking Reveals Serotonin Transporter Diffusion Dynamics are Correlated with Cholesterol-Sensitive Threonine 276 Phosphorylation Status in Primary Midbrain Neurons. ACS Chem Neurosci 9:2534–2541.

Baio J et al. (2018) Prevalence of Autism Spectrum Disorder Among Children Aged 8 Years — Autism and Developmental Disabilities Monitoring Network, 11 Sites, United States, 2014. MMWR Surveill Summ 67:1–23.

Balcioglu A, Wurtman RJ (1998) Effects of Fenfluramine and Phentermine (Fen-Phen) on Dopamine and Serotonin Release in Rat Striatum: In Vivo Microdialysis Study in Conscious Animals. Brain Res 813:67–72.

Balkovetzs DF, Tiruppathis C, Leibachs FH, Maheshe VB, Ganapathyst V (1989) Evidence for an Imipramine-Sensitive Serotonin Transporter in Human Placental Brush-border Membranes. J Biol Chem 264:2195–2198.

Ballesteros J, Callado LF (2004) Effectiveness of Pindolol Plus Serotonin Uptake Inhibitors in Depression: A Meta-Analysis of Early and Late Outcomes from Randomised Controlled Trials. J Affect Disord 79:137–147.

Barker PA, Salehi A (2002) The MAGE Proteins: Emerging Roles in Cell Cycle Progression, Apoptosis, and Neurogenetic Disease. J Neurosci Res 67:705–712.

Bauman AL, Apparsundaram S, Ramamoorthy S, Wadzinski BE, Vaughan RA, Blakely RD (2000) Cocaine and Antidepressant-Sensitive Biogenic Amine Transporters Exist in Regulated Complexes with Protein Phosphatase 2A. J Neurosci 20:7571–7578.

Bear MF, Huber KM, Warren ST (2004) The mGluR Theory of Fragile X Mental Retardation. Trends Neurosci 27:370–377.

Beites CL, Xie H, Bowser R, Trimble WS (1999) The Septin CDCrel-1 Binds Syntaxin and Inhibits Exocytosis. Nat Neurosci 2:434–439.

Belmer A, Klenowski PM, Patkar OL, Bartlett SE (2017) Mapping the Connectivity of Serotonin Transporter Immunoreactive Axons to Excitatory and Inhibitory Neurochemical Synapses in the Mouse Limbic Brain. Brain Struct Funct 222:1297–1314.

Belmonte MK, Bourgeron T (2006) Fragile X Syndrome and Autism at the Intersection of Genetic and Neural Networks. Nat Neurosci 9:1221–1225.

Benmansour S, Deltheil T, Piotrowski J, Nicolas L, Reperant C, Gardier AM, Frazer A, David DJ (2008) Influence of Brain-Derived Neurotrophic Factor (BDNF) on Serotonin Neurotransmission in the Hippocampus of Adult Rodents. Eur J Pharmacol 587:90–98.

Benmansour S, Privratsky AA, Adeniji OS, Frazer A (2014) Signaling Mechanisms Involved in the Acute Effects of Estradiol on 5-HT Clearance. Int J Neuropsychopharmacol 17:765–777.

Bennett MK, Garcia-Arrarás JE, Elferink LA, Peterson K, Fleming AM, Hazuka CD, Scheller RH (1993) The Syntaxin Family of Vesicular Transport Receptors. Cell 74:863–873.

Benson MA, Newey SE, Martin-Rendon E, Hawkes R, Blake DJ (2001) Dysbindin, a Novel Coiled-coil-containing Protein that Interacts with the Dystrobrevins in Muscle and Brain. J Biol Chem 276:24232–24241.

Berger B, Rothmaier AK, Wedekind F, Zentner J, Feuerstein TJ, Jackisch R (2006) Presynaptic Opioid Receptors on Noradrenergic and Serotonergic Neurons in the Human as Compared to the Rat Neocortex. Br J Pharmacol 148:795–806.

Bermingham DP, Blakely RD (2016) Kinase-Dependent Regulation of Monamine Neurotransmitter

Transporters. Pharmacol Rev 68:888–953.

Berney C, Danuser G (2003) FRET or No FRET: A Quantitative Comparison. Biophys J 84:3992–4010.

Binda F, Dipace C, Bowton E, Robertson SD, Lute BJ, Fog JU, Zhang M, Sen N, Colbran RJ, Gnegy ME, Gether U, Javitch JA, Erreger K, Galli A (2008) Syntaxin 1A Interaction with the Dopamine Transporter Promotes Amphetamine-induced Dopamine Efflux. Mol Pharmacol 74:1101–1108.

Blakely RD, Bauman AL (2000) Biogenic Amine Transporters: Regulation in Flux. Curr Opin Neurobiol 10:328–336.

Blakely RD, Berson HE, Fremeau RT, Carson MG, Peek MM, Prince HK, Bradley CC (1991) Cloning and Expression of Functional Serotonin Transporter from Rat Brain. Nature 354:66–70.

Blakely RD, Ramamoorthy S, Schroeter S, Qian Y, Apparsundaram S, Galli A, DeFelice LJ (1998) Regulated Phosphorylation and Trafficking of Antidepressant-Sensitive Serotonin Transporter Proteins. Biol Psychiatry 44:169–178.

Bläser S, Röseler S, Rempp H, Bartsch I, Bauer H, Lieber M, Lessmann E, Weingarten L, Busse A, Huber M, Zieger B (2010) Human Endothelial Cell Septins: SEPT11 is an Interaction Partner of SEPT5. J Pathol 220:114–125.

Blelch A, Brown S-L, Kahm R, van Praag HM (1988) The Role of Serotonin in Schizophrenia. Schizophr Bull 14:297.

Bolan EA, Kivell B, Jaligam V, Oz M, Jayanthi LD, Han Y, Sen N, Urizar E, Gomes I, Devi LA, Ramamoorthy S, Javitch J, Zapata A, Shippenberg TS (2007) D2 Receptors Regulate Dopamine Transporter Function via an Extracellular Signal-regulated Kinases 1 and 2-Dependent and Phosphoinositide 3 Kinase-independent Mechanism. Mol Pharmacol 71:1222–1232.

Boschert U, Aït. Amara D, Segu L, Hen R (1994) The Mouse 5-Hydroxytryptamine$_{1B}$ Receptor is Localized Predominantly on Axon Terminals. Neuroscience 58:167–182.

Brindley RL, Bauer MB, Walker LA, Quinlan MA, Carneiro AMD, Sze JY, Blakely RD, Currie KPM (2018) Adrenal Serotonin Derives from Accumulation by the Antidepressant-Sensitive Serotonin Transporter. Pharmacol Res 140:56–66.

Bruchas MR, Schindler AG, Shankar H, Messinger DI, Miyatake M, Land BB, Lemos JC, Hagan CE, Neumaier JF, Quintana A, Palmiter RD, Chavkin C (2011) Selective p38α MAPK Deletion in Serotonergic Neurons Produces Stress Resilience in Models of Depression and Addiction. Neuron 71:498–511.

Brzostowski JA, Meckel T, Hong J, Chen A, Jin T (2009) Imaging Protein-Protein Interactions by Förster Resonance Energy Transfer (FRET) Microscopy in Live Cells. Curr Protoc Protein Sci.

Buchmayer F, Schicker K, Steinkellner T, Geier P, Stubiger G, Hamilton PJ, Jurik A, Stockner T, Yang J-W, Montgomery T, Holy M, Hofmaier T, Kudlacek O, Matthies HJG, Ecker GF, Bochkov V, Galli A, Boehm S, Sitte HH (2013) Amphetamine Actions at the Serotonin Transporter Rely on the Availability of Phosphatidylinositol-4,5-bisphosphate. Proc Natl Acad Sci 110:11642–11647.

Budnik V (1996) Synapse Maturation and Structural Plasticity at Drosophila Neuromuscular Junctions. Curr Opin Neurobiol 6:858–867.

Bulling S, Schicker K, Zhang Y-W, Steinkellner T, Stockner T, Gruber CW, Boehm S, Freissmuth M, Rudnick G, Sitte HH, Sandtner W (2012) The Mechanistic Basis for Noncompetitive Ibogaine Inhibition of Serotonin and Dopamine Transporters. J Biol Chem 287:18524–18534.

Campbell NG, Zhu C-B, Lindler KM, Yaspan BL, Kistner-Griffin E, Hewlett WA, Tate CG, Blakely RD, Sutcliffe JS (2013) Rare Coding Variants of the Adenosine A3 Receptor are Increased in Autism: On the Trail of the Serotonin Transporter Regulome. Mol Autism 4:28.

Cantor RM, Kono N, Duvall JA, Alvarez-Retuerto A, Stone JL, Alarcón M, Nelson SF, Geschwind DH (2005) Replication of Autism Linkage: Fine-Mapping Peak at 17q21. Am J Hum Genet 76:1050–1056.

Carneiro AMD, Blakely RD (2006) Serotonin-, Protein Kinase C-, and Hic-5-associated Redistribution of the Platelet Serotonin Transporter. J Biol Chem 281:24769–24780.

Carneiro AMD, Cook EH, Murphy DL, Blakely RD (2008) Interactions Between Integrin αIIbβ3 and the Serotonin Transporter Regulate Serotonin Transport and Platelet Aggregation in Mice and Humans. J Clin Invest 118:1544–1552.

Carrasco JL, Sandner C (2005) Clinical Effects of Pharmacological Variations in Selective Serotonin Reuptake Inhibitors: An Overview. Int J Clin Pract 59:1428–1434.

Carvelli L, Blakely RD, DeFelice LJ (2008) Dopamine Transporter/Syntaxin 1A Interactions Regulate Transporter Channel Activity and Dopaminergic Synaptic Transmission. Proc Natl Acad Sci 105:14192–14197.

Caspi A, Sugden K, Moffitt TE, Taylor A, Craig IW, Harrington H, McClay J, Mill J, Martin J, Braithwaite, Poulton R (2003) Influence of Life Stress on Depression: Moderation by a Polymorphism in the 5-HTT Gene. Science (80-) 301:386–389.

Castagné V, Moser P, Roux S, Porsolt RD (2011) Rodent Models of Depression: Forced Swim and Tail Suspension Behavioral Despair Tests in Rats and Mice. Curr Protoc Neurosci 55:8.10A.1-8.10A.14.

Cervinski MA, Foster JD, Vaughan RA (2010) Syntaxin 1A Regulates Dopamine Transporter Activity, Phosphorylation and Surface Expression. Neuroscience 170:408–416.

Challasivakanaka S, Zhen J, Smith ME, Reith ME, Foster JD, Vaughan RA (2017) Dopamine Transporter Phosphorylation Site Threonine 53 is Stimulated by Amphetamines and Regulates Dopamine Transport, Efflux, and Cocaine Analog Binding. J Biol Chem 292:19066–19075.

Chang JC, Rosenthal SJ (2013) A Bright Light to Reveal Mobility: Single Quantum Dot Tracking Reveals Membrane Dynamics and Cellular Mechanisms. J Phys Chem Lett 4:2858–2866.

Chang JC, Tomlinson ID, Warnement MR, Ustione A, Carneiro AMD, Piston DW, Blakely RD, Rosenthal SJ (2012) Single Molecule Analysis of Serotonin Transporter Regulation Using Antagonist-Conjugated Quantum Dots Reveals Restricted, p38 MAPK-Dependent Mobilization Underlying Uptake Activation. J Neurosci 32:8919–8929.

Chanrion B, Mannoury la Cour C, Bertaso F, Lerner-Natoli M, Freissmuth M, Millan MJ, Bockaert J, Marin P (2007) Physical Interaction Between the Serotonin Transporter and Neuronal Nitric Oxide Synthase Underlies Reciprocal Modulation of their Activity. Proc Natl Acad Sci 104:8119–8124.

Charlton BG (2000) The Malaise Theory of Depression: Major Depressive Disorder is Sickness Behavior and Antidepressants are Analgesic. Med Hypotheses 54:126–130.

Charnay Y, Léger L (2010) Pharmacological Aspects: Brain Serotonergic Circuitries. Dialogues Clin Neurosci 12:471–487.

Chen J-G, Liu-Chen S, Rudnick G (1997) External Cysteine Residues in the Serotonin Transporter. Biochemistry 36:1479–1486.

Chen J-G, Rudnick G (2000) Permeation and Gating Residues in Serotonin Transporter. Proc Natl Acad Sci 97:1044–1049.

Cheng Y-C, Prusoff WH (1973) Relationship Between the Inhibition Constant and the Concentration of Inhibitor which Causes 50 per cent Inhibition of an Enzymatic Reaction. Biochem Pharmacol 22:3099–3108.

Chou F-S, Wang P-S (2016) The Arp2/3 Complex is Essential at Multiple Stages of Neural Development. Neurogenesis 3:e1261653.

Chugani DC, Muzik O, Rothermel R, Behen M, Chakraborty P, Mangner T, Da Silva EA, Chugani HT (1997) Altered Serotonin Synthesis in the Dentatothalamocortical Pathway in Autistic Boys. Ann Neurol 42:666–669.

Ciccone MA, Timmons M, Phillips A, Quick MW (2008) Calcium/calmodulin-dependent Kinase II Regulates the Interaction Between the Serotonin Transporter and Syntaxin 1A. Neuropharmacology 55:763–770.

Clerk A, Harriosn, Joanne G, Long CS, Sugden PH (1999) Pro-Inflammatory Cytokines Stimulate Mitogen-activated Protein Kinase Subfamilies, Increase Phosphorylation of c-Jun and ATF2 and Upregulate c-Jun Protein in Neonatal Rat Ventricular Myocytes. J Mol Cell Cardiol 2099:2087–2099.

Coba MP, Ramaker MJ, Ho E V., Thompson SL, Komiyama NH, Grant SGN, Knowles JA, Dulawa SC (2018) Dlgap1 Knockout Mice Exhibit Alterations of the Postsynaptic Density and Selective Reductions in Sociability. Sci Rep 8:2281.

Coleman JA, Green EM, Gouaux E (2016) X-ray Structures and Mechanism of the Human Serotonin Transporter. Nature 532:334–339.

Colgan LA, Cavolo SL, Commons KG, Levitan ES (2012) Action Potential-Independent and

Pharmacologically Unique Vesicular Serotonin Release from Dendrites. J Neurosci 32:15737–15746.

Cook EH, Arora RC, Anderson GM, Berry-Kravis EM, Yan S, Yeoh HC, Sklena PJ, Charak DA, Leventhal BL (1993) Platelet Serotonin Studies in Hyperserotonemic Relatives of Children with Autistic Disorder. Life Sci 52:2005–2015.

Cook EH, Courchesne R, Lord C, Cox NJ, Yan S, Lincoln A, Haas R, Courchesne E, Leventhal BL (1997) Evidence of Linkage Between the Serotonin Transporter and Autistic Disorder. Mol Psychiatry 2:247–250.

Cool DR, Leibach FH, Bhalla VK, Mahesh VB, Ganapathy V (1991) Expression and Cyclic AMP-Dependent Regulation of a High Affinity Serotonin Transporter in the Human Placental Choriocarcinoma Cell Line (JAR). J Biol Chem 266:15750–15757.

Corbett C, Armstrong MJ, Parker R, Webb K, Neuberger JM (2013) Mental Health Disorders and Solid-Organ Transplant Recipients. Transplantation 96:593–600.

Couroussé T, Gautron S (2015) Role of Organic Cation Transporters (OCTs) in the Brain. Pharmacol Ther 146:94–103.

Cremona ML, Matthies HJG, Pau K, Bowton E, Speed N, Lute BJ, Anderson M, Sen N, Robertson SD, Vaughan RA, Rothman JE, Galli A, Javitch JA, Yamamoto A (2011) Flotillin-1 is essential for PKC-triggered endocytosis and membrane microdomain localization of DAT. Nat Neurosci 14:469–477.

Crozatier C, Farley S, Mansuy IM, Dumas S, Giros B, Tzavara ET (2007) Calcineurin (Protein Phosphatase 2B) is Involved in the Mechanisms of Action of Antidepressants. Neuroscience 144:1470–1476.

Cryan JF, Harkin A, Naughton M, Kelly JP, Leonard BE (2000) Characterization of D-fenfluramine-Induced Hypothermia: Evidence for Multiple Sites of Action. Eur J Pharmacol 390:275–285.

Datta D, Arion D, Roman KM, Volk DW, Lewis DA (2017) Altered Expression of ARP2/3 Complex Signaling Pathway Genes in Prefrontal Layer 3 Pyramidal Cells in Schizophrenia. Am J Psychiatry 174:163–171.

Daws LC, Gould GG, Teicher SD, Gerhardt GA, Frazer A (2000) 5-HT_{1B} Receptor-mediated Regulation of Serotonin Clearance in Rat Hippocampus In Vivo. J Neurochem 75:2113–2122.

Delorme R et al. (2005) Support for the Association Between the Rare Functional Variant I425V of the Serotonin Transporter Gene and Susceptibility to Obsessive Compulsive Disorder. Mol Psychiatry 10:1059–1061.

Dimri S, Basu S, De A (2016) Use of BRET to Study Protein-Protein Interactions In Vitro and In Vivo. In: Methods in Molecular Biology, pp 57–78. Humana Press, New York, NY.

Dipace C, Sung U, Binda F, Blakely RD, Galli A (2007) Amphetamine Induces a Calcium/Calmodulin-Dependent Protein Kinase II-Dependent Reduction in Norepinephrine Transporter Surface Expression Linked to Changes in Syntaxin 1A/Transporter Complexes. Mol Pharmacol 71:230–239.

Dockendorff TC, Labrador M (2019) The Fragile X Protein and Genome Function. Mol Neurobiol 56:711–721.

Dombret C, Nguyen T, Schakman O, Michaud JL, Hardin-Pouzet H, Bertrand MJM, De Backer O (2012) Loss of *Maged1* Results in Obesity, Deficits of Social Interactions, Impaired Sexual Behavior and Severe Alteration of Mature Oxytocin Production in the Hypothalamus. Hum Mol Genet 21:4703–4717.

Domschke K, Lawford B, Young R, Voisey J, Morris CP, Roehrs T, Hohoff C, Birosova E, Arolt V, Baune BT (2011) Dysbindin (DTNBP1) – A Role in Psychotic Depression? J Psychiatr Res 45:588–595.

Doyle JM, Gao J, Wang J, Yang M, Potts PR (2010) MAGE-RING Protein Complexes Comprise a Family of E3 Ubiquitin Ligases. Mol Cell 39:963–974.

Drago A, Ronchi D De, Serretti A (2008) 5-HT_{1A} Gene Variants and Psychiatric Disorders: A Review of Current Literature and Selection of SNPs for Future Studies. Int J Neuropsychopharmacol 11:701–721.

Duke AA, Bègue L, Bell R, Eisenlohr-Moul T (2013) Revisiting the Serotonin-Aggression Relation in Humans: A Meta-Analysis. Psychol Bull 139:1148–1172.

Egana LA, Cuevas RA, Baust TB, Parra LA, Leak RK, Hochendoner S, Pena K, Quiroz M, Hong WC, Dorostkar MM, Janz R, Sitte HH, Torres GE (2009) Physical and Functional Interactions Between the Dopamine Transporter and the Synaptic Vesicle Protein Synaptogyrin-3. J Neurosci 29:4592–

4604.

Eiden LE, Weihe E (2011) VMAT2: A Dynamic Regulator of Brain Monoaminergic Neuronal Function Interacting with Drugs of Abuse. Ann N Y Acad Sci 1216:86–98.

Emiliano ABF, Fudge JL (2004) From Galactorrhea to Osteopenia: Rethinking Serotonin-Prolactin Interactions. Neuropsychopharmacology 29:833–846.

Enjin A, Leão KE, Mikulovic S, Le Merre P, Tourtellotte WG, Kullander K (2012) Sensorimotor Function is Modulated by the Serotonin Receptor 1D, a Novel Marker for Gamma Motor Neurons. Mol Cell Neurosci 49:322–332.

Evard A, Laporte AM, Chastanet M, Hen R, Hamon M, Adrien J (1999) 5-HT_{1A} and 5-HT_{1B} Receptors Control the Firing of Serotoninergic Neurons in the Dorsal Raphe Nucleus of the Mouse: Studies in 5-HT_{1B} Knock-out Mice. Eur J Neurosci 11:3823–3831.

Faraj BA, Olkowski ZL, Jackson RT (1994) Expression of a High-affinity Serotonin Transporter in Human Lymphocytes. Int J Immunopharmacol 16:561–567.

Felts B, Pramod AB, Sandtner W, Burbach N, Bulling S, Sitte HH, Henry LK (2014) The Two Na^{2+} Sites in the Human Serotonin Transporter Play Distinct Roles in the Ion Coupling and Electrogenicity of Transport. J Biol Chem 289:1825–1840.

Fenollar-Ferrer C, Stockner T, Schwarz TC, Pal A, Gotovina J, Hofmaier T, Jayaraman K, Adhikary S, Kudlacek O, Mehdipour AR, Tavoulari S, Rudnick G, Singh SK, Konrat R, Sitte HH, Forrest LR (2014) Structure and Regulatory Interactions of the Cytoplasmic Terminal Domains of Serotonin Transporter. Biochemistry 53:5444–5460.

Fischer JF, Cho AK (1979) Chemical Release of Dopamine from Striatal Homogenates: Evidence for an Exchange Diffusion Model. J Pharmacol Exp Ther 208:203–209.

Fog JU, Khoshbouei H, Holy M, Owens WA, Vaegter CB, Sen N, Nikandrova Y, Bowton E, McMahon DG, Colbran RJ, Daws LC, Sitte HH, Javitch JA, Galli A, Gether U (2006) Calmodulin Kinase II Interacts with the Dopamine Transporter C Terminus to Regulate Amphetamine-Induced Reverse Transport. Neuron 51:417–429.

Fontana A, De Laureto PP, Spolaore B, Frare E, Picotti P, Zambonin M (2004) Probing Protein Structure by Limited Proteolysis. In: Acta Biochimica Polonica, pp 299–321.

Forrest LR, Rudnick G (2009) The Rocking Bundle: A Mechanism for Ion-coupled Solute Flux by Symmetrical Transporters. Physiology 24:377–386.

Forrest LR, Tavoulari S, Zhang Y-W, Rudnick G, Honig B (2007) Identification of a Chloride Ion Binding Site in Na^+/Cl^- Dependent Transporter. Proc Natl Acad Sci 104:12761–12766.

Forrest LR, Zhang Y-W, Jacobs MT, Gesmonde J, Xie L, Honig BH, Rudnick G (2008) Mechanism for Alternating Access in Neurotransmitter Transporters. Proc Natl Acad Sci 105:10338–10343.

Foster JD, Yang JW, Moritz AE, ChallaSivaKanaka S, Smith MA, Holy M, Wilebski K, Sitte HH, Vaughan RA (2012) Dopamine Transporter Phosphorylation Site Threonine 53 Regulates Substrate Reuptake and Amphetamine-Stimulated Efflux. J Biol Chem 287:29702–29712.

Francesco Ferrari P, Palanza P, Parmigiani S, De Almeida RMM, Miczek KA (2005) Serotonin and Aggressive Behavior in Rodents and Nonhuman Primates: Predispositions and Plasticity. Eur J Pharmacol 526:259–273.

Frazer A, Hensler JG (1999) Serotonin Involvement in Physiological Function and Behavior Basic Neurochemistry: Molecular, Cellular and Medical Aspects. (Siegel G, Agranoff B, Albers R, eds). Philadelphia: Lippincott-Raven.

Gabriel LR, Wu S, Kearney P, Bellve KD, Standley C, Fogarty KE, Melikian HE (2013) Dopamine Transporter Endocytic Trafficking in Striatal Dopaminergic Neurons: Differential Dependence on Dynamin and the Actin Cytoskeleton. J Neurosci 33:17836–17846.

Garner CC, Nash J, Huganir RL (2000) PDZ Domains in Synapse Assembly and Signalling. Trends Cell Biol 10:274–280.

Garthwaite J (2007) Neuronal Nitric Oxide Synthase and the Serotonin Transporter Get Harmonious. Proc Natl Acad Sci 104:7739–7740.

Gaukler SM, Ruff JS, Potts WK (2016) Paroxetine Exposure Skews Litter Sex Ratios in Mice Suggesting a Trivers-Willard Process. Behav Ecol 27:1113–1121.

Gershon MD, Tack J (2007) The Serotonin Signaling System: From Basic Understanding To Drug Development for Functional GI Disorders. Gastroenterology 132:397–414.

Gill RK, Pant N, Saksena S, Singla A, Nazir TM, Vohwinkel L, Turner JR, Goldstein J, Alrefai WA, Dudeja PK (2007) Function, Expression, and Characterization of the Serotonin Transporter in the Native Human Intestine. AJP Gastrointest Liver Physiol 294:G254–G262.

Glennon RA, Titeler M, McKenney JD (1984) Evidence for 5-HT_2 Involvement in the Mechanism of Action of Hallucinogenic Agents. Life Sci 35:2505–2511.

Gobbi M, Frittoli E, Uslenghi A, Mennini T (1993) Evidence of an Exocytotic-Like Release of [^{3}H]5-Hydroxytryptamine Induced by d-Fenfluramine in Rat Hippocampal Synaptosomes. Eur J Pharmacol 238:9–17.

González MI, Robinson MB (2004) Neurotransmitter Transporters: Why Dance with So Many Partners? Curr Opin Pharmacol 4:30–35.

Goodnick PJ, Goldstein BJ (1998) Selective Serotonin Reuptake Inhibitors in Affective Disorders: Basic Pharmacology. J Psychopharmacol 12:5-S20.

Gourab K, Schmit BD, Hornby TG (2015) Increased Lower Limb Spasticity but Not Strength or Function Following a Single-Dose Serotonin Reuptake Inhibitor in Chronic Stroke. Arch Phys Med Rehabil 96:2112–2119.

Gowrishankar R, Gresch PJ, Davis GL, Katamish RM, Riele JR, Stewart AM, Vaughan RA, Hahn MK, Blakely RD (2018) Region-specific Regulation of Presynaptic Dopamine Homeostasis by D2 Autoreceptors Shapes the In Vivo Impact of the Neuropsychiatric Disease-associated DAT Variant Val559. J Neurosci 38:0055-18.

Green AR, Mechan AO, Elliott JM, O'Shea E, Colado MI (2003) The Pharmacology and Clinical Pharmacology of 3,4-Methylenedioxymethamphetamine (MDMA, "Ecstasy"). Pharmacol Rev 55:463–508.

Guptaroy B, Zhang M, Bowton E, Binda F, Shi L, Weinstein H, Galli A, Javitch JA, Neubig RR, Gnegy ME (2009) A Juxtamembrane Mutation in the N-Terminus of the Dopamine Transporter Induces

Preference for an Inward-Facing Conformation. Mol Pharmacol 75:514–524.

Gurel V, Lins J, Lambert K, Lazauski J, Spaulding J, McMichael J (2015) Serotonin and Histamine Therapy Increases Tetanic Forces of Myoblasts, Reduces Muscle Injury, and Improves Grip Strength Performance of Dmd^{mdx} Mice. Dose-Response 13:1–8.

Haase J, Grudzinska-Goebel J, Müller HK, Münster-Wandowski A, Chow E, Wynne K, Farsi Z, Zander JF, Ahnert-Hilger G (2017) Serotonin Transporter Associated Protein Complexes Are Enriched in Synaptic Vesicle Proteins and Proteins Involved in Energy Metabolism and Ion Homeostasis. ACS Chem Neurosci 8:1101–1116.

Haase J, Killian a M, Magnani F, Williams C (2001) Regulation of the Serotonin Transporter by Interacting Proteins. Biochem Soc Trans 29:722–728.

Hagan CE, Mcdevitt RA, Liu Y, Furay AR, Neumaier JF (2012) 5-HT_{1B} Autoreceptor Regulation of Serotonin Transporter Activity in Synaptosomes. Synapse 66:1024–1034.

Hanley HG, Stahl SM, Freedman DX (1977) Hyperserotonemia and Amine Metabolites in Autistic and Retarded Children. Arch Gen Psychiatry 34:521–531.

Hanson AC, Hagerman RJ (2015) Serotonin Dysregulation in Fragile X Syndrome: Implications for Treatment. Intractable Rare Dis Res 3:110–117.

Harper KM, Hiramoto T, Tanigaki K, Kang G, Suzuki G, Trimble W, Hiroi N (2012) Alterations of Social Interaction Through Genetic and Environmental Manipulation of the 22q11.2 Gene Sept5 in the Mouse Brain. Hum Mol Genet 21:3489–3499.

Hasenhuetl PS, Bhat S, Mayer FP, Sitte HH, Freissmuth M, Sandtner W (2018) A Kinetic Account for Amphetamine-Induced Monoamine Release. J Gen Physiol 150:431–451.

Hasenhuetl PS, Freissmuth M, Sandtner W (2016) Electrogenic Binding of Intracellular Cations Defines a Kinetic Decision Point in the Transport Cycle of the Human Serotonin Transporter. J Biol Chem 291:25864–25876.

Heal DJ, Smith SL, Gosden J, Nutt DJ (2013) Amphetamine, Past and Present - A Pharmacological and Clinical Perspective. J Psychopharmacol 27:479–496.

Heils A, Teufel A, Petri S, Stöber G, Riederer P, Bengel D, Lesch KP (2002) Allelic Variation of Human Serotonin Transporter Gene Expression. J Neurochem 66:2621–2624.

Henry LK, Field JR, Adkins EM, Parnas ML, Vaughan RA, Zou M-F, Newman AH, Blakely RD (2006) Tyr-95 and Ile-172 in Transmembrane Segments 1 and 3 of Human Serotonin Transporters Interact to Establish High Affinity Recognition of Antidepressants. J Biol Chem 281:2012–2023.

Henry LK, Iwamoto H, Field JR, Kaufmann K, Dawson ES, Jacobs MT, Adams C, Felts B, Zdravkovic I, Armstrong V, Combs S, Solis E, Rudnick G, Noskov SY, DeFelice LJ, Meiler J, Blakelya RD (2011) A Conserved Asparagine Residue in Transmembrane Segment 1 (TM1) of Serotonin Transporter Dictates Chloride-Coupled Neurotransmitter Transport. J Biol Chem 286:30823–30836.

Hensler JG, Ferry RC, Kovachich GB, Frazer A (1994) Quantitative Autoradiography of the Serotonin Transporter to Assess the Distribution of Serotonergic Projections from the Dorsal Raphe Nucleus. Synapse 17:1–15.

Hilber B, Scholze P, Dorostkar MM, Sandtner W, Holy M, Boehm S, Singer EA, Sitte HH (2005) Serotonin-Transporter Mediated Efflux: A Pharmacological Analysis of Amphetamines and Non-Amphetamines. Neuropharmacology 49:811–819.

Hiroi N, Hiramoto T, Harper KM, Suzuki G, Boku S (2012) Mouse Models of 22q11.2-Associated Autism Spectrum Disorder. Autism Open Access Suppl 1.

Hirschfeld RMA (2000) Hisotry and Evolution of the Monoamine Hypotheis of Depression. J Clin Psychiatry 61:4–6.

Hoffman BJ, Mezey E, Brownstein MJ (1991) Cloning of a Serotonin Transporter Affected by Antidepressants. Science (80-) 254:579–580.

Hollander E, Soorya L, Chaplin W, Anagnostou E, Taylor BP, Ferretti CJ, Wasserman S, Swanson E, Settipani C (2012) A Double-blind Placebo-controlled Trial of Fluoxetine for Repetitive Behaviors and Global Severity in Adult Autism Spectrum Disorders. Am J Psychiatry 169:292–299.

Holmes A, Murphy DL, Crawley JN (2003) Abnormal Behavioral Phenotypes of Serotonin Transporter Knockout mice: Parallels with Human Anxiety and Depression. Biol Psychiatry 54:953–959.

Horvath GA, Meisner L, Selby K, Stowe R, Carleton B (2017) Improved Strength on 5-Hydroxytryptophan and Carbidopa in Spinal Cord Atrophy. J Neurol Sci 378:59–62.

Horvath GA, Selby K, Poskitt K, Hyland K, Waters PJ, Coulter-Mackie M, Stockler-Ipsiroglu SG (2011) Hemiplegic Migraine, Seizures, Progressive Spastic Paraparesis, Mood Disorder, and Coma in Siblings with Low Systemic Serotonin. Cephalalgia 31:1580–1586.

Huang DW, Sherman BT, Lempicki RA (2009a) Systematic and Integrative Analysis of Large Gene Lists using DAVID Bioinformatics Resources. Nat Protoc 4:44–57.

Huang G, Shi LZ, Chi H (2009b) Regulation of JNK and p38 MAPK in the Immune System: Signal Integration, Propagation and Termination. Cytokine 48:161–169.

Hulbert SW, Jiang YH (2016) Monogenic Mouse Models of Autism Spectrum Disorders: Common Mechanisms and Missing Links. Neuroscience 321:3–23.

Inazu M, Takeda H, Ikoshi H, Sugisawa M, Uchida Y, Matsumiya T (2001) Pharmacological Characterization and Visualization of the Glial Serotonin Transporter. Neurochem Int 39:39–49.

Irwin S (1968) Comprehensive Observational Assessment: A Systematic, Quantitative Procedure for Assessing the Behavioral and Physiologic State of the Mouse. Psychopharmacologia 13:222–257.

Iversen SD (1984) 5-HT and Anxiety. Neuropharmacology 23:1553–1560.

Jacobs BL, Azmitia EC (1992) Structure and Function of the Brain Serotonin System. Physiol Rev 72:165–229.

Jacobs MT, Zhang YW, Campbell SD, Rudnick G (2007) Ibogaine, a Noncompetitive Inhibitor of Serotonin Transport, Acts by Stabilizing the Cytoplasm-Facing State of the Transporter. J Biol Chem 282:29441–29447.

Jahn R, Scheller RH (2006) SNAREs - Engines for Membrane Fusion. Nat Rev Mol Cell Biol 7:631–643.

Jayanthi LD, Samuvel DJ, Blakely RD, Ramamoorthy S (2005) Evidence for Biphasic Effects of Protein Kinase C on Serotonin Transporter Function, Endocytosis, and Phosphorylation. Mol Pharmacol 67:2077–2087.

Ji NY, Findling RL (2015) An Update on Pharmacotherapy of Autism Spectrum Disorder in Children and

Adolescents. Curr Opin Psychiatry 28:91–101.

Johnson LA, Guptaroy B, Lund D, Shamban S, Gnegy ME (2005) Regulation of Amphetamine-Stimulated Dopamine Efflux by Protein Kinase C β. J Biol Chem 280:10914–10919.

Kalueff AV, Olivier JDA, Nonkes LJP, Homberg JR (2010) Conserved Role for the Serotonin Transporter Gene in Rat and Mouse Neurobehavioral Endophenotypes. Neurosci Biobehav Rev 34:373–386.

Kalyuzhny AE, Wessendorf MW (1999) Serotonergic and GABAergic Neurons in the Medial Rostral Ventral Medulla Express κ-Opioid Receptor Immunoreactivity. Neuroscience 90:229–234.

Karlin A, Akabas MH, Karl A, Akabas MH (1998) Substituted-Cysteine Accessibility Method. Academic Press.

Kellner M (2010) Drug Treatment of Obesssive-Compulsive Disorder. Dialogues Clin Neurosci 12:187–197.

Kern C, Erdem FA, El-Kasaby A, Sandtner W, Freissmuth M, Sucic S (2017) The N-Terminus Specifies the Switch between Transport Modes of the Human Serotonin Transporter. J Biol Chem 292:3603–3613.

Kerr TM, Muller CL, Miah M, Jetter CS, Pfeiffer R, Shah C, Baganz N, Anderson GM, Crawley JN, Sutcliffe JS, Blakely RD, Veenstra-Vanderweele J (2013) Genetic Background Modulates Phenotypes of Serotonin Transporter Ala56 Knock-in Mice. Mol Autism 4:1–11.

Kertész-Farkas A, Reiz B, Vera R, Myers MP, Pongor S (2014) PTMTreeSearch: A Novel Two-Stage Tree-Search Algorithm with Pruning Rules for the Identification of Post-Translational Modification of Proteins in MS/MS Spectra. Bioinformatics 30:234–241.

Khelashvili G, Stanley N, Sahai MA, Medina J, LeVine M V., Shi L, De Fabritiis G, Weinstein H (2015) Spontaneous Inward Opening of the Dopamine Transporter Is Triggered by PIP2-Regulated Dynamics of the N-Terminus. ACS Chem Neurosci 6:1825–1837.

Khoshbouei H, Sen N, Guptaroy B, Johnson L, Lund D, Gnegy ME, Galli A, Javitch JA (2004) N-Terminal Phosphorylation of the Dopamine Transporter is Required for Amphetamine-Induced Efflux. PLoS Biol 2:387–393.

Kilic F, Murphy DL, Rudnick G (2003) A Human Serotonin Transporter Mutation Causes Constitutive Activation of Transport Activity. Mol Pharmacol 64:440–446.

Kimelberg HK, Katz DM (1985) High-Affinity Uptake of Serotonin into Immunocytochemically Identified Astrocytes. Science (80-) 228:889–891.

Koban F, El-Kasaby A, Häusler C, Stockner T, Simbrunner BM, Sitte HH, Freissmuth M, Sucic S (2015) A Salt Bridge Linking the First Intracellular Loop with the C Terminus Facilitates the Folding of the Serotonin Transporter. J Biol Chem 290:13263–13278.

Koldsø H, Autzen HE, Grouleff J, Schiøtt B (2013) Ligand Induced Conformational Changes of the Human Serotonin Transporter Revealed by Molecular Dynamics Simulations Cavalli A, ed. PLoS One 8:63635.

Kolevzon A, Newcorn JH, Kryzak L, Chaplin W, Watner D, Hollander E, Smith CJ, Cook EH, Silverman JM (2010) Relationship Between Whole Blood Serotonin and Repetitive Behaviors in Autism. Psychiatry Res 175:274–276.

Korobova F, Kvitkina T (2010) Molecular Architecture of Synaptic Actin Cytoskeleton in Hippocampal Neurons Reveals a Mechanism of Dendritic Sping Morphogesis. Mol Biol Cell 21:165–177.

Kremmer E, Ohst K, Kiefer J, Brewis N, Walter G (2015) Separation of PP2A Core Enzyme and Holoenzyme with Monoclonal Antibodies Against the Regulatory A Subunit: Abundant Expression of Both Forms in Cells. Mol Cell Biol 17:1692–1701.

Krishnamurthy H, Gouaux E (2012) X-ray Structures of LeuT in Substrate-free Outward-open and Apo Inward-open States. Nature 481:469–474.

Kristensen AS, Andersen J, Jorgensen TN, Sorensen L, Eriksen J, Loland CJ, Stromgaard K, Gether U (2011) SLC6 Neurotransmitter Transporters: Structure, Function, and Regulation. Pharmacol Rev 63:585–640.

Kubota N, Kiuchi Y, Nemoto M, Oyamada H, Ohno M, Funahashi H, Shioda S, Oguchi K (2001) Regulation of Serotonin Transporter Gene Expression in Human Glial Cells by Growth Factors. Eur J Pharmacol 417:69–76.

Kurochkina N, Guha U (2013) SH3 Domains: Modules of Protein-Protein Interactions. Biophys Rev 5:29–39.

Larsen MB, Fjorback AW, Wiborg O (2006) The C-Terminus is Critical for the Functional Expression of the Human Serotonin Transporter. Biochemistry 45:1331–1337.

Lau T, Schneidt T, Heimann F, Gundelfinger ED, Schloss P (2010) Somatodendritic Serotonin Release and Re-uptake in Mouse Embryonic Stem Cell-Derived Serotonergic Neurons. Neurochem Int 57:969–978.

Launay J-M, Bondoux D, Oset-Gasque M-J, Emami S, Mutel V, Haimart M, Gespach C, Cedex P, Oset-gasque J (1994) Increase of Human Platelet Serotonin by Atypical Histamine Receptors Uptake. Am J Physiol 266:526–536.

Launay J-M, Schneider B, Loric S, Prada M Da, Kellermann O (2006) Serotonin Transporter and Serotonin Transporter-Mediated Antidepressant Recognition are Controlled by 5-HT_{2B} Receptor Signaling in Serotonergic Neuronal Cells. FASEB J 20:1843–1854.

Laursen L, Severinsen K, Kristensen KB, Periole X, Overby M, Müller HK, Schiøtt B, Sinning S (2018) Cholesterol Binding to a Conserved Site Modulates the Conformation, Pharmacology, and Transport Kinetics of the Human Serotonin Transporter. J Biol Chem 293:3510–3523.

Lee KH, Kim MY, Kim DH, Lee YS (2004) Syntaxin 1A and Receptor for Activated C Kinase Interact with the N-terminal Region of Human Dopamine Transporter. Neurochem Res 29:1405–1409.

Lee S, Walker CL, Karten B, Kuny SL, Tennese AA, O'Neill MA, Wevrick R (2005) Essential Role for the Prader-Willi Syndrome Protein Necdin in Axonal Outgrowth. Hum Mol Genet 14:627–637.

Leo Kanner (1943) Autistic Disturbances of Affective Contact. Nerv Child 2:217–250.

Lesch K-P, Bengel D, Heils A, Sabol SZ, Greenberg BD, Petri S, Benjamin J, Muller CR, Hamer DH, Murphy D (1996) Gene Regulatory Region Association of Anxiety-Related Traits with a Polymorphism in the Serotonin Transporter Gene Regulatory Region. Science (80-) 274:1527–1531.

Lesch K, Wolozin BL, Murphy DL, Riederer P (1993) Primary Structure of the Human Platelet Serotonin Uptake Site : Identity with the Brain Serotonin Transporter. J Neurochem 60:2319–2322.

Li J, Shi M, Ma Z, Zhao S, Euskirchen G, Ziskin J, Urban A, Hallmayer J, Snyder M (2014) Integrated Systems Analysis Reveals a Molecular Network Underlying Autism Spectrum Disorders. Mol Syst Biol 10:774–774.

Lin F, Lester HA, Mager S (1996) Single-channel Currents Produced by the Serotonin Transporter and Analysis of a Mutation Affecting Ion Permeation. Biophys J 71:3126–3135.

Lin Y-C, Frei JA, Kilander MBC, Shen W, Blatt GJ (2016) A Subset of Autism-Associated Genes Regulate the Structural Stability of Neurons. Front Cell Neurosci 10:263.

Liu X, Yamashita T, Chen Q, Belevych N, Mckim DB, Tarr AJ, Coppola V, Nath N, Nemeth DP, Syed ZW, Sheridan JF, Godbout JP, Zuo J, Quan N (2015) Interleukin 1 Type 1 Receptor Restore: A Genetic Mouse Model for Studying Interleukin 1 Receptor-Mediated Effects in Specific Cell Types. J Neurosci 35:2860–2870.

Machacek DW, Garraway SM, Shay BL, Hochman S (2001) Serotonin 5-HT_2 Receptor Activation Induces a Long-Lasting Amplification of Spinal Reflex Actions in the Rat. J Physiol 537:201–207.

Maes M (1999) Major Depression and Activation of the Inflammatory Response System. Cytokines, Stress Depress 95:233–243.

Mager S, Min C, Henry, Douglas J, Chavkin C, Hoffman BJ, Davidson N, Lester HA (1994) Conducting States of a Mammalian Serotonin Transporter. Neuron 12:845–859.

Magnani F, Tatell CG, Wynne S, Williams C, Haase J (2004) Partitioning of the Serotonin Transporter into Lipid Microdomains Modulates Transport of Serotonin. J Biol Chem 279:38770–38778.

Malynn S, Campos-Torres A, Moynagh P, Haase J (2013) The Pro-inflammatory Cytokine TNF-α Regulates the Activity and Expression of the Serotonin Transporter (SERT) in Astrocytes. Neurochem Res 38:694–704.

Mann JJ, Arango V, Underwood MD (1990) Serotonin and Suicidal Behavior. Ann N Y Acad Sci 600:476–484.

Margolis KG, Li Z, Stevanovic K, Saurman V, Israelyan N, Anderson GM, Snyder I, Veenstra-VanderWeele J, Blakely RD, Gershon MD (2016) Serotonin Transporter Variant Drives Preventable

Gastrointestinal Abnormalities in Development and Function. J Clin Invest 126:2221–2235.

Martin KF, Phillips I, Hearson M, Prow MR, Heal DJ (1992) Characterization of 8-OH-DPAT-Induced Hypothermia in Mice as a 5-HT_{1A} Autoreceptor Response and its Evaluation as a Model to Selectively Identify Antidepressants. Br J Pharmacol 107:15–21.

Martínez-Cerdeño V (2017) Dendrite and Spine Modifications in Autism and Related Neurodevelopmental Disorders in Patients and Animal Models. Dev Neurobiol 77:393–404.

Mayser W, Betz H, Schloss P (1991) Isolation of cDNAs Encoding a Novel Member of the Neurotransmitter Transporter Gene Family. Fed Eur Biochem Socieities 295:203–206.

Mazei-Robison MS, Bowton E, Holy M, Schmudermaier M, Freissmuth M, Sitte HH, Galli A, Blakely RD (2008) Anomalous Dopamine Release Associated with a Human Dopamine Transporter Coding Variant. J Neurosci 28:7040–7046.

McDougle CJ, Naylor ST, Cohen DJ, Aghajanian GK, Heninger GR, Price LH (1996a) Effects of Tryptophan Depletion in Drug-free Adults with Autistic Disorder. Arch Gen Psychiatry 53:993–1000.

McDougle CJ, Naylor ST, Cohen DJ, Volkmar FR, Heninger GR, Price LH (1996b) A Double-blind, Placebo-controlled Study of Fluvoxamine in Adults with Autistic Disorder. Arch Gen Psychiatry 53:1001–1008.

Meltzer HY (1990) Role of Serotonin in Depression. Ann N Y Acad Sci 600:486–499.

Meltzer HY (1999) The Role of Serotonin in Antipsychotic Drug Action. Neuropsychopharmacology 21:106–115.

Mercado CP, Kilic F (2010) Molecular Mechanisms of SERT in Platelets: Regulation of Plasma Serotonin Levels. Mol Interv 10:231–241.

Mergy MA, Gowrishankar R, Gresch PJ, Gantz SC, Williams J, Davis GL, Wheeler CA, Stanwood GD, Hahn MK, Blakely RD (2014) The Rare DAT Coding Variant Val559 Perturbs DA Neuron Function, Changes Behavior, and Alters In Vivo Responses to Psychostimulants. Proc Natl Acad Sci 111:E4779–E4788.

Michalak M, Opas M (1997) Functions of Dystrophin and Dystrophin Associated Proteins. Curr Opin

Neurol 10:436–442.

Miller KJ, Hoffman BJ (1994) Adenosine A3 Receptors Regulate Serotonin Transport via Nitric Oxide and cGMP. J Biol Chem 269:27351–27356.

Miranda M, Dionne KR, Sorkina T, Sorkin A (2007) Three ubiquitin conjugation sites in the amino terminus of the dopamine transporter mediate protein kinase C-dependent endocytosis of the transporter. Mol Biol Cell 18:313–323.

Miranda M, Wu CC, Sorkina T, Korstjens DR, Sorkin A (2005) Enhanced ubiquitylation and accelerated degradation of the dopamine transporter mediated by protein kinase C. J Biol Chem 280:35617–35624.

Miteva Y V., Budayeva HG, Cristea IM (2013) Proteomics-based Methods for Discovery, Quantification, and Validation of Protein-Protein Interactions. Anal Chem 85:749–768.

Moessner R, Marshall CR, Sutcliffe JS, Skaug J, Pinto D, Vincent J, Zwaigenbaum L, Fernandez B, Roberts W, Szatmari P, Scherer SW (2007) Contribution of SHANK3 Mutations to Autism Spectrum Disorder. Am J Hum Genet 81:1289–1297.

Montgomery T, Sucic S, Steinkellner T, Freissmuth M, Sitte H (2011) Differential Regulation of Amphetamine-induced Serotonergic and Dopaminergic Efflux by Syntaxin 1A. In: BMC Pharmacology, pp A38.

Moron JA, Zakharova I, Ferrer J V, Merrill GA, Hope B, Lafer EM, Lin ZC, Wang JB, Javitch JA, Galli A, Shippenberg TS, Morón JA (2003) Mitogen-Activated Protein Kinase Regulates Dopamine Transporter Surface Expression and Dopamine Transport Capacity. J Neurosci 23:8480–8488.

Mouri A, Ikeda M, Koseki T, Iwata N, Nabeshima T (2016) The Ubiquitination of Serotonin Transporter in Lymphoblasts Derived from Fluvoxamine-Resistant Depression Patients. Neurosci Lett 617:22–26.

Mouri A, Sasaki A, Watanabe K, Sogawa C, Kitayama S, Mamiya T, Miyamoto Y, Yamada K, Noda Y, Nabeshima T (2012) MAGE-D1 Regulates Expression of Depression-Like Behavior through Serotonin Transporter Ubiquitylation. J Neurosci 32:4562–4580.

Mukhopadhyay D, Riezman H (2007) Proteasome-independent Functions of Ubiquitin in Endocytosis and Signaling. Science (80-) 315:201–205.

Mulder EJ, Anderson GM, Kema IP, De Bildt A, Van Lang NDJ, Den Boer JA, Minderaa RB (2004) Platelet Serotonin Levels in Pervasive Developmental Disorders and Mental Retardation: Diagnostic Group Differences, Within-group Distribution, and Behavioral Correlates. J Am Acad Child Adolesc Psychiatry 43:491–499.

Muller CL, Anacker AM, Rogers TD, Goeden N, Keller EH, Forsberg CG, Kerr TM, Wender C La, Anderson GM, Stanwood GD, Blakely RD, Bonnin A, Veenstra-Vanderweele J (2017) Impact of Maternal Serotonin Transporter Genotype on Placental Serotonin, Fetal Forebrain Serotonin, and Neurodevelopment. Neuropsychopharmacology 42:427–436.

Muller CL, Anacker AMJ, Veenstra-VanderWeele J (2016) The Serotonin System in Autism Spectrum Disorder: From Biomarker to Animal Models. Neuroscience 321:24–41.

Nackenoff AG, Moussa-Tooks AB, McMeekin AM, Veenstra-VanderWeele J, Blakely RD (2016) Essential Contributions of Serotonin Transporter Inhibition to the Acute and Chronic Actions of Fluoxetine and Citalopram in the SERT Met172 Mouse. Neuropsychopharmacology 41:1733–1741.

Nackenoff AG, Simmler LD, Baganz NL, Pehrson AL, Sánchez C, Blakely RD (2017) Serotonin Transporter-independent Actions of the Antidepressant Vortioxetine As Revealed Using the SERT Met172 Mouse. ACS Chem Neurosci 8:1092–1100.

Namkung J, Kim H, Park S (2015) Peripheral Serotonin: A New Player in Systemic Energy Homeostasis. Mol Cells 38:1023–1028.

Nelson PJ, Rudnick G (1979) Coupling Between Platelet 5-Hydroxytryptamine and Potassium Transport. J Biol Chem 254:10084–10089.

Nesvizhskii AI, Keller A, Kolker E, Aebersold R (2003) A Statistical Model for Identifying Proteins by Tandem Mass Spectrometry. Anal Chem 75:4646–4658.

Newman AH (2017) A Novel PKC Inhibitor Shows Promise for Amphetamine Use Disorders. Neuropsychopharmacology 42:1929–1930.

Nichols C, Sanders-Bush E (2001) Serotonin Receptor Signaling and Hallucinogenic Drug Action. Heffter Rev Psychedelic Res 2:73–79.

Nichols DE, Nichols C (2008) Serotoin Receptors. Chem Rev 108:1614–1641.

Nobukuni M, Mochizuki H, Okada S, Kameyama N, Tanaka A, Yamamoto H, Amano T, Seki T, Sakai N (2009) The C-terminal Region of Serotonin Transporter is Important for its Trafficking and Glycosylation. J Pharmacol Sci 111:392–404.

Nourry C, Grant SGN, Borg J-P (2003) PDZ Domain Proteins: Plug and Play! Sci STKE 2003:re7.

Numakawa T, Yagasaki Y, Ishimoto T, Okada T, Suzuki T, Iwata N, Ozaki N, Taguchi T, Tatsumi M, Kamijima K, Straub RE, Weinberger DR, Kunugi H, Hashimoto R (2004) Evidence of Novel Neuronal Functions of Dysbindin, a Susceptibility Gene for Schizophrenia. Hum Mol Genet 13:2699–2708.

Owen MJ, Williams NM, O'Donovan MC (2004) Dysbindin-1 and Schizophrenia: From Genetics to Neuropathology. J Clin Invest 113:1255–1257.

Owens WA, Williams JM, Daws LC, Saunders C, Galli A, Avison MJ (2012) Rescue of Dopamine Transporter Function in Hypoinsulinemic Rats by a D2 Receptor-ERK-dependent Mechanism. J Neurosci 32:2637–2647.

Ozaki N, Goldman D, Kaye WH, Plotnicov K, Greenberg BD, Lappalainen J, Rudnick G, Murphy DL (2003) Serotonin Transporter Missense Mutation Associated with a Complex Neuropsychiatric Phenotype. Mol Psychiatry 8:933–936.

Ozaslan D, Wang S, Ahmed BA, Kocabas AM, McCastlain JC, Bene A, Kilic F (2003) Glycosyl Modification Facilitates Homo- and Hetero-oligomerization of the Serotonin Transporter. A Specific Role for Sialic Acid Residues. J Biol Chem 278:43991–44000.

Pagan C, Delorme R, Callebert J, Goubran-Botros H, Amsellem F, Drouot X, Boudebesse C, Le Dudal K, Ngo-Nguyen N, Laouamri H, Gillberg C, Leboyer M, Bourgeron T, Launay J-M (2014) The Serotonin-N-acetylserotonin-Melatonin Pathway as a Biomarker for Autism Spectrum Disorders. Transl Psychiatry 4:e479.

Pantouli E, Boehm MM, Koka S (2005) Inflammatory Cytokines Activate p38 MAPK to Induce Osteoprotegerin Synthesis by MG-63 Cells. Biochem Biophys Res Commun 329:224–229.

Paoletti AC, Parmely TJ, Tomomori-Sato C, Stao S, Zhu D, Conaway RC, Conaway JW, Florens L, Washbrun MP (2006) Quantitative Proteomic Analysis of Distinct Mammalian Mediator Complexes using Normalized Spectral Abundance Factors. Proc Natl Acad Sci 103:18928–18933.

Pavanetto M, Zarpellon A, Borgo C, Donella-Deana A, Deana R (2011) Regulation of Serotonin Transporter in Human Platelets by Tryosine Kinase Syk. Cell Physiol Biochem 27:139–148.

Pezawas L, Meyer-Lindenberg A, Drabant EM, Verchinski BA, Munoz KE, Kolachana BS, Egan MF, Mattay VS, Hariri AR, Weinberger DR (2005) 5-HTTLPR Polymorphism Impacts Human Cingulate-amygdala Interactions: A Genetic Susceptibility Mechanism for Depression. Nat Neurosci 8:828–834.

Piston DW, Kremers GJ (2007) Fluorescent Protein FRET: The Good, the Bad and the Ugly. Trends Biochem Sci 32:407–414.

Pizzo AB, Karam CS, Zhang Y, Yano H, Freyberg RJ, Karam DS, Freyberg Z, Yamamoto A, McCabe BD, Javitch JA (2013) The Membrane Raft Protein Flotillin-1 is Essential in Dopamine Neurons for Amphetamine-Induced Behavior in Drosophila. Mol Psychiatry 18:824–833.

Plaznik A, Kostowski W, Archer T (1989) Serotonin and Depression: Old Problems and New Data. Prog Neuropsychopharmacol Biol Psychiatry 13:623–633.

Prasad HC, Steiner JA, Sutcliffe JS, Blakely RD (2009) Enhanced Activity of Human Serotonin Transporter Variants Associated with Autism. Philos Trans R Soc Lond B Biol Sci 364:163–173.

Prasad HC, Zhu C-B, McCauley JL, Samuvel DJ, Ramamoorthy S, Shelton RC, Hewlett WA, Sutcliffe JS, Blakely RD (2005) Human Serotonin Transporter Variants Display Altered Sensitivity to Protein Kinase G and p38 Mitogen-Activated Protein Kinase. Proc Natl Acad Sci 102:11545–11550.

Prast H, Philippu A (2001) Nitric Oxide as Modulator of Synaptic Function. Prog Neurobiol 64:51–68.

Qian Y, Galli A, Ramamoorthy S, Risso S, Defelice LJ, Blakely RD (1997) Protein Kinase C Activation Regulates Human Serotonin Transporters in HEK-293 Cells via Altered Cell Surface Expression. J Neurosci 17:45–57.

Qian Y, Melikian HE, Moore KR, Duke B, Blakely RD (1995a) Phosphoyrlation of Serotonin Transporter Domains and thier Role in Phosphorylation in Acute Transporter Regulation. In: Society for Neuroscience, pp 344. 347. Sand Diego, CA.

Qian Y, Melikian HE, Rye DB, Levey AI, Blakely RD (1995b) Identification and Characterization of Antidepressant-Sensitive Serotonin Transporter Proteins Using Site-Specific Antibodies. J Neurosci 15:1261–1274.

Quattrone A, Tedeschi G, Aguglia U, Scopacasa F, Direnzo G, Annunziato L (1983) Prolactin Secretion in Man: A Useful Tool to Evaluate the Activity of Drugs on Central 5-Hydroxytryptaminergic Neurones. Studies with Fenfluramine. Br J Clin Pharmacol 16:471–475.

Quick MW (2002a) Role of Syntaxin 1A on Serotonin Transporter Expression in Developing Thalamocortical Neurons. Int J Dev Neurosci 20:219–224.

Quick MW (2002b) Substrates Regulate Gamma-Aminobutyric Acid Transporters in a Syntaxin 1A-Dependent Manner. Proc Natl Acad Sci U S A 99:5686–5691.

Quick MW (2003) Regulating the Conducting States of a Mammalian Serotonin Transporter. Neuron 40:537–549.

Quinlan MA, Krout D, Katamish R, Robson MJ, Nettesheim C, Gresch PJ, Mash D, Henry K, Blakely RD (2019) Human Serotonin Transporter Coding Variation Establishes Conformational Bias with Functional Consequences. ACS Chem Neurosci 14:acschemneuro.8b00689.

Radivojac P, Vacic V, Haynes C, Cocklin RR, Mohan A, Heyen JW, Goebl MG, Iakoucheva LM (2010) Identification, Analysis, and Prediction of Protein Ubiquitination Sites. Proteins Struct Funct Bioinforma 78:365–380.

Rajamanickam J, Annamalai B, Rahbek-Clemmensen T, Sundaramurthy S, Gether U, Jayanthi LD, Ramamoorthy S (2015) Akt-Mediated Regulation of Antidepressant-Sensitive Serotonin Transporter Function, Cell-Surface Expression and Phosphorylation. Biochem J 468:177–190.

Ramamoorthy S, Bauman AL, Moore KR, Han H, Yang-Feng T, Chang AS, Ganapathy V, Blakely RD (1993) Antidepressant-and Cocaine-Sensitive Human Serotonin Transporter: Molecular Cloning,

Expression, and Chromosomal Localization. Proc Natl Acad Sci 90:2542–2546.

Ramamoorthy S, Blakely RD (1999) Phosphorylation and Sequestration of Serotonin Transporters Differentially Modulated by Psychostimulants. Science 285:763–766.

Ramamoorthy S, Giovanetti E, Qian Y, Blakely RD (1998) Phosphorylation and Regulation of Antidepressant-Sensitive Serotonin Transporters. J Biol Chem 273:2458–2466.

Ramamoorthy S, Samuvel DJ, Buck ER, Rudnick G, Jayanthi LD (2007) Phosphorylation of Threonine Residue 276 is Required for Acute Regulation of Serotonin Transporter by Cyclic GMP. J Biol Chem 282:11639–11647.

Ramamoorthy S, Shippenberg TS, Jayanthi LD (2011) Regulation of Monoamine Transporters: Role of Transporter Phosphorylation. Pharmacol Ther 129:220–238.

Rapport MM, Green AA, Page IH (1948) Crystalline Serotonin. Science (80-) 108:329–330.

Rausch JL (2005) Initial Conditions of Psychotropic Drug Response: Studies of Serotonin Transporter Long Promoter Region (5-HTTLPR), Serotonin Transporter Efficiency, Cytokine and Kinase Gene Expression Relevant to Depression and Antidepressant Outcome. Prog Neuro-Psychopharmacology Biol Psychiatry 29:1046–1051.

Razavi AM, Khelashvili G, Weinstein H (2018) How Structural Elements Evolving from Bacterial to Human SLC6 Transporters Enabled New Functional Properties. BMC Biol 16.

Reisinger SN, Kong E, Molz B, Humberg T, Sideromenos S, Cicvaric A, Steinkellner T, Yang JW, Cabatic M, Monje FJ, Sitte HH, Nichols BJ, Pollak DD (2018) Flotillin-1 Interacts with the Serotonin Transporter and Modulates Chronic Corticosterone Response. Genes, Brain Behav e12482:1–11.

Robson MJ, Quinlan MA, Margolis KG, Gajewski-Kurdziel PA, Veenstra-VanderWeele J, Gershon MD, Watterson DM, Blakely RD (2018) p38α MAPK Signaling Drives Pharmacologically Reversible Brain and Gastrointestinal Phenotypes in the SERT Ala56 Mouse. Proc Natl Acad Sci 115:E10245–E10254.

Robson MJ, Zhu C-B, Quinlan MA, Botschner DA, Baganz NL, Lindler KM, Thome JG, Hewlett WA, Blakely RD (2016) Generation and Characterization of Mice Expressing a Conditional Allele of the

Interleukin-1 Receptor Type 1 Graca L, ed. PLoS One 11:e0150068.

Rocher C, Jacquot C, Gardier AM (1999) Simultaneous Effects of Local Dexfenfluramine Application on Extracellular Glutamate and Serotonin Levels in Rat Frontal Cortex: A Reverse Microdialysis Study. Neuropharmacology 38:513–523.

Rojas DC (2014) The Role of Glutamate and its Receptors in Autism and the Use of Glutamate Receptor Antagonists in Treatment. J Neural Transm 121:891–905.

Ross SB, Hall H (1983) Maximal Turnover Number of the Membranal Serotonin Carrier in Rat Brain Synaptosomes In Vitro. Acta Physiol Scand 118:185–187.

Roth BL (2011) 5-HT2A Serotonin Receptor Biology: Interacting Proteins, Kinases and Paradoxical Regulation. Neuropharmacology 61:348–354.

Rothman RB, Baumann MH, Dersch CM, Romero D V, Rice KC, Carroll FI, Partilla JS (2001) Amphetamine-Type Central Nervous System Stimulants Release Norepinephrine More Potently Than They Release Dopamine and Serotonin. Synapse 39:32–41.

Ruan Y, Miyagi A, Wang X, Chami M, Boudker O, Scheuring S (2017) Direct Visualization of Glutamate Transporter Elevator Mechanism by High-Speed AFM. Proc Natl Acad Sci 114:1584–1588.

Rudnick G (1977) Active Transport of 5-Hydroxytryotamine by Plasma Membrane Vesicles Isolated from Human Blood Platelets. J Biol Chem 252:2170–2174.

Rudnick G (2006) Structure/Function Relationships in Serotonin Transporter: New Insights from the Structure of a Bacterial Transporter. Handb Exp Pharmacol 175:59–73.

Rudnick G (2011) Cytoplasmic Permeation Pathway of Neurotransmitter Transporters. Biochemistry 50:7462–7475.

Rudnick G, Nelson PJ (1978) Platelet 5-Hydroxytryptamine Transport, an Electroneutral Mechanism Coupled to Potassium. Biochemistry 17.

Rudnick G, Wall SC (1992) p-Chloroamphetamine Induces Serotonin Release through Serotonin Transporters. Biochemistry 31:6710–6718.

Sager JJ, Torres GE (2011) Proteins Interacting with Monoamine Transporters: Current State and Future

Challenges. Biochemistry 50:7295–7310.

Sakrikar D, Mazei-Robison MS, Mergy MA, Richtand NW, Han Q, Hamilton PJ, Bowton E, Galli A, Veenstra-Vanderweele J, Gill M, Blakely RD (2012) Attention Deficit/Hyperactivity Disorder-Derived Coding Variation in the Dopamine Transporter Disrupts Microdomain Targeting and Trafficking Regulation. J Neurosci 32:5385–5397.

Samuvel DJ, Jayanthi LD, Bhat NR, Ramamoorthy S (2005) A Role for p38 Mitogen-activated Protein Kinase in the Regulation of the Serotonin Transporter: Evidence for Distinct Cellular Mechanisms Involved in Transporter Surface Expression. J Neurosci 25:29–41.

Sari Y (2004) Serotonin 1B Receptors: From Protein to Physiological Function and Behavior. Neurosci Biobehav Rev 28:565–582.

Sato Y, Zhang YW, Androutsellis-Theotokis A, Rudnick G (2004) Analysis of Transmembrane Domain 2 of Rat Serotonin Transporter by Cysteine Scanning Mutagenesis. J Biol Chem 279:22926–22933.

Savelieva K V, Zhao S, Pogorelov VM, Rajan I, Yang Q, Cullinan E, Lanthorn TH (2008) Genetic Disruption of Both Tryptophan Hydroxylase Genes Dramatically Reduces Serotonin and Affects Behavior in Models Sensitive to Antidepressants. PLoS One 3:3301.

Scanlon SM, Williams DC, Schloss P (2001) Membrane Cholesterol Modulates Serotonin Transporter Activity. Biochemistry 40:10507–10513.

Schaaf CP, Gonzalez-Garay ML, Xia F, Potocki L, Gripp KW, Zhang B, Peters BA, McElwain M a, Drmanac R, Beaudet AL, Caskey CT, Yang Y (2013) Truncating Mutations of *MAGEL2* Cause Prader-Willi Phenotypes and Autism. Nat Genet 45:1405–1408.

Schain RJ, Freedman DX (1961) Studies on 5-Hydroxyindole Metabolism in Autistic and Other Mentally Retarded Children. J Pediatr 58:315–320.

Schicker K, Uzelac Z, Gesmonde J, Bulling S, Stockner T, Freissmuth M, Boehm S, Rudnick G, Sitte HH, Sandtner W (2012) Unifying Concept of Serotonin Transporter-Associated Currents. J Biol Chem 287:438–445.

Schindler AG, Messinger DI, Smith JS, Shankar H, Gustin RM, Schattauer SS, Lemos JC, Chavkin NW,

Hagan CE, Neumaier JF, Chavkin C (2012) Stress Produces Aversion and Potentiates Cocaine Reward by Releasing Endogenous Dynorphins in the Ventral Striatum to Locally Stimulate Serotonin Reuptake. J Neurosci 32:17582–17596.

Schmittgen TD, Livak KJ (2008) Analyzing Real-Time PCR Data by the Comparative CT Method. Nat Protoc 3:1101–1108.

Schneider C, Newman RA, Sutherland DR, Asser U, Greaves MF (1982) A One-Step Purification of Membrane Proteins Using a High Efficiency Immunomatrix. J Biol Chem 257:10766–10769.

Schnell JD, Hicke L (2003) Non-Traditional Functions of Ubiquitin and Ubiquitin-Binding Proteins. J Biol Chem 278:35857–35860.

Schroeter S, Blakely RD (1996) Drug Targets in the Embryo. Studies on the Cocaine- and Antidepressant-Sensitive Serotonin Transporter. Ann N Y Acad Sci 801:239–255.

Seidel S, Singer EA, Just H, Farhan H, Scholze P, Kudlacek O, Holy M, Koppatz K, Krivanek P, Freissmuth M, Sitte HH (2005) Amphetamines Take Two to Tango: an Oligomer-based Counter-transport Model of Neurotransmitter Transport Explores the Amphetamine Action. Mol Pharmacol 67:140–151.

Seimandi M, Seyer P, Park CS, Vandermoere F, Chanrion B, Bockaert J, Mansuy IM, Marin P (2013) Calcineurin Interacts with the Serotonin Transporter C-Terminus to Modulate Its Plasma Membrane Expression and Serotonin Uptake. J Neurosci 33:16189–16199.

Shih JC, Chen K, Ridd MJ (1999) Monoamine Oxidase: From Genes to Behavior. Annu Rev Neurosci 22:197–217.

Sibille E, Su J, Leman S, Le Guisquet AM, Ibarguen-Vargas Y, Joeyen-Waldorf J, Glorioso C, Tseng GC, Pezzone M, Hen R, Belzung C (2007) Lack of Serotonin$_{1B}$ Receptor Expression Leads to Age-related Motor Dysfunction, Early Onset of Brain Molecular Aging and Reduced Longevity. Mol Psychiatry 12:1042–1056.

Siemann JK, Muller CL, Forsberg CG, Blakely RD, Veenstra-VanderWeele J, Wallace T (2017) An Autism-associated Serotonin Transporter Variant Disrupts Multisensory Processing. Transl Psychiatry 7:1067.

Simmler LD, Anacker AMJ, Levin MH, Vaswani NM, Gresch PJ, Nackenoff AG, Anastasio NC, Stutz SJ, Cunningham KA, Wang J, Zhang B, Henry LK, Stewart A, Veenstra-VanderWeele J, Blakely RD (2017) Blockade of the 5-HT Transporter Contributes to the Behavioural, Neuronal and Molecular Effects of Cocaine. Br J Pharmacol 174:2716–2738.

Singh SK, Eroglu C (2013) Neuroligins Provide Molecular Links Between Syndromic and Nonsyndromic Autism. Sci Signal 6.

Sinopoli VM, Burton CL, Kronenberg S, Arnold PD (2017) A Review of the Role of Serotonin System Genes in Obsessive-compulsive Disorder. Neurosci Biobehav Rev 80:372–381.

Sitte HH, Hiptmair B, Zwach J, Pifl C, Singer EA, Scholze P (2001) Quantitative Analysis of Inward and Outward Transport Rates in Cells Stably Expressing the Cloned Human Serotonin Transporter: Inconsistencies with the Hypothesis of Facilitated Exchange Diffusion. Mol Pharmacol 59:1129–1137.

Sneddon JM (1969) Sodium-dependent Accumulation of 5-Hydroxytryptamine by Rat Blood Platelets. Br J Pharmacol 37:680–688.

Sørensen L, Strømgaard K, Kristensen AS (2014) Characterization of Intracellular Regions in the Human Serotonin Transporter for Phosphorylation Sites. ACS Chem Biol 9:935–944.

Sorkina T, Caltagarone J, Sorkin A (2012) Flotillins Regulate Membrane Mobility of the Dopamine Transporter but are Not Required for its Protein Kinase C Dependent Endocytosis. Traffic 14:709–724.

Staley JK, Ouyang Q, Pablo J, Hearn WL, Flynn DD, Rothman RB, Rice KC, Mash DC (1996) Pharmacological Screen for Activities of 12-Hydroxyibogamine: A Primary Metabolite of the Indole Alkaloid Ibogaine. Psychopharmacology (Berl) 127:10–18.

Steiner JA, Carneiro AMD, Blakely RD (2008) Going with the Flow: Trafficking-Dependent and -Independent Regulation of Serotonin Transport. Traffic 9:1393–1402.

Steiner JA, Carneiro AMD, Wright J, Matthies HJG, Prasad HC, Nicki CK, Dostmann WR, Buchanan CC, Corbin JD, Francis SH, Blakely RD (2009) cGMP-Dependent Protein Kinase Iα Associates with the

Antidepressant-Sensitive Serotonin Transporter and Dictates Rapid Modulation of Serotonin Uptake. Mol Brain 2:26.

Steinkellner T, Montgomery TR, Hofmaier T, Kudlacek O, Yang J-W, Rickhag M, Jung G, Lubec G, Gether U, Freissmuth M, Sitte HH (2015) Amphetamine Action at the Cocaine- and Antidepressant-Sensitive Serotonin Transporter Is Modulated by CaMKII. J Neurosci 35:8258–8271.

Steinkellner T, Mus L, Eisenrauch B, Constantinescu A, Leo D, Konrad L, Rickhag M, Sørensen G, Efimova E V, Kong E, Willeit M, Sotnikova TD, Kudlacek O, Gether U, Freissmuth M, Pollak DD, Gainetdinov RR, Sitte HH (2014) *In Vivo* Amphetamine Action is Contingent on αCaMKII. Neuropsychopharmacology 39:2681–2693.

Stone JL, Merriman B, Cantor RM, Yonan AL, Gilliam TC, Geschwind DH, Nelson SF (2004) Evidence for Sex-Specific Risk Alleles in Autism Spectrum Disorder. Am J Hum Genet 75:1117–1123.

Strum JM, Junod AF (1972) Radioautographic Demonstration 5-Hydroxytryptamine-^{3}H Uptake by Pulmonary Endothelial Cells. J Cell Biol 54:456–467.

Sucic S, Dallinger S, Zdrazil B, Weissensteiner R, Jørgensen TN, Holy M, Kudlacek O, Seidel S, Cha JH, Gether U, Newman AH, Ecker GF, Freissmuth M, Sitte HH (2010) The N-Terminus of Monoamine Transporters is a Lever Required for the Action of Amphetamines. J Biol Chem 285:10924–10938.

Sucic S, El-Kasaby A, Kudlacek O, Sarker S, Sitte HH, Marin P, Freissmuth M (2011) The Serotonin Transporter is an Exclusive Client of the Coat Protein Complex II (COPII) Component SEC24C. J Biol Chem 286:16482–16490.

Sulzer D, Sonders MS, Poulsen NW, Galli A (2005) Mechanisms of Neurotransmitter Release by Amphetamines: A Review. Prog Neurobiol 75:406–433.

Sundaramurthy S, Annamalai B, Samuvel DJ, Shippenberg TS, Jayanthi LD, Ramamoorthy S (2017) Modulation of Serotonin Transporter Function by Kappa-opioid Receptor Ligands. Neuropharmacology 113:281–292.

Sung U, Apparsundaram S, Galli A, Kahlig KM, Savchenko V, Schroeter S, Quick MW, Blakely RD (2003) A Regulated Interaction of Syntaxin 1A with the Antidepressant-Sensitive Norepinephrine

Transporter Establishes Catecholamine Clearance Capacity. J Neurosci 23:1697–1709.

Sung U, Jennings JL, Link AJ, Blakely RD (2005) Proteomic Analysis of Human Norepinephrine Transporter Complexes Reveals Associations with Protein Phosphatase 2A Anchoring Subunit and 14-3-3 Proteins. Biochem Biophys Res Commun 333:671–678.

Sutcliffe JS, Delahanty RJ, Prasad HC, McCauley JL, Han Q, Jiang L, Li C, Folstein SE, Blakely RD (2005) Allelic Heterogeneity at the Serotonin Transporter Locus (SLC6A4) Confers Susceptibility to Autism and Rigid-Compulsive Behaviors. Am J Hum Genet 77:265–279.

Sweeney CG, Tremblay BP, Stockner T, Sitte HH, Melikian HE (2017) Dopamine Transporter Amino and Carboxyl Termini Synergistically Contribute to Substrate and Inhibitor Affinities. J Biol Chem 292:1302–1309.

Szklarczyk D, Morris JH, Cook H, Kuhn M, Wyder S, Simonovic M, Santos A, Doncheva NT, Roth A, Bork P, Jensen LJ, Von Mering C (2017) The STRING Database in 2017: Quality-Controlled Protein-protein Association Networks, Made Broadly Accessible. Nucleic Acids Res 45:D362–D368.

Takeuchi K, Roehrl MHA, Sun ZYJ, Wagner G (2007) Structure of the Calcineurin-NFAT Complex: Defining a T Cell Activation Switch Using Solution NMR and Crystal Coordinates. Structure 15:587–597.

Talvenheimo J, Nelson PJ, Rudnick G (1979) Mechanism of Imipramine Inhibition of Platelet 5-Hydroxytryptamine Transport. J Biol Chem 254:4631–4635.

Tate CG, Blakely RD (1994) The Effect of N-linked Glycosylation on Activity of the Na^+- and Cl^--dependent Serotonin Transporter Expressed Using Recombinant Baculovirus in Insect Cells. J Biol Chem 269:26303–26310.

Tavoulari S, Forrest LR, Rudnick G (2009) Fluoxetine (Prozac) Binding to Serotonin Transporter Is Modulated by Chloride and Conformational Changes. J Neurosci 29:9635–9643.

Tavoulari S, Margheritis E, Nagarajan A, DeWitt DC, Zhang YW, Rosado E, Ravera S, Rhoades E, Forrest LR, Rudnick G (2016) Two Na^+ Sites Control Conformational Change in a Neurotransmitter Transporter Homolog. J Biol Chem 291:1456–1471.

Terranova JI, Song Z, Larkin TE, Hardcastle N, Norvelle A, Riaz A, Albers HE (2016) Serotonin and Arginine–vasopressin Mediate Sex Differences in the Regulation of Dominance and Aggression by the Social Brain. Proc Natl Acad Sci 113:13233–13238.

Thompson BJ, Jessen T, Henry LK, Field JR, Gamble KL, Gresch PJ, Carneiro AM, Horton RE, Chisnell PJ, Belova Y, McMahon DG, Daws LC, Blakely RD (2011) Transgenic Elimination of High-Affinity Antidepressant and Cocaine Sensitivity in the Presynaptic Serotonin Transporter. Proc Natl Acad Sci 108:3785–3790.

Tokhtaeva E, Capri J, Marcus EA, Whitelegge JP, Khuzakhmetova V, Bukharaeva E, Deiss-Yehiely N, Dada LA, Sachs G, Fernandez-Salas E, Vagin O (2015) Septin Dynamics are Essential for Exocytosis. J Biol Chem 290:5280–5297.

Tsai Y-C, Miteva Y, Boonmee A, Cristea IM, Greco TM (2012) Functional Proteomics Establishes the Interaction of SIRT7 with Chromatin Remodeling Complexes and Expands its Role in Regulation of RNA Polymerase I Transcription. Mol Cell Proteomics 11:60–76.

Underhill SM, Wheeler DS, Li M, Watts SD, Ingram SL, Amara SG (2014) Amphetamine Modulates Excitatory Neurotransmission through Endocytosis of the Glutamate Transporter EAAT3 in Dopamine Neurons. Neuron 83:404–416.

Uzunova G, Hollander E, Shepherd J (2014) The Role of Ionotropic Glutamate Receptors in Childhood Neurodevelopmental Disorders: Autism Spectrum Disorders and Fragile X Syndrome. Curr Neuropharmacol 12:71–98.

Vaughan RA, Foster JD (2013) Mechanisms of Dopamine Transporter Regulation in Normal and Disease States. Trends Pharmacol Sci 34:489–496.

Veenstra-VanderWeele J et al. (2012) Autism Gene Variant Causes Hyperserotonemia, Serotonin Receptor Hypersensitivity, Social Impairment and Repetitive Behavior. Proc Natl Acad Sci 109:5469–5474.

Veenstra-VanderWeele J, Jessen TN, Thompson BJ, Carter M, Prasad HC, Steiner JA, Sutcliffe JS, Blakely RD (2009) Modeling Rare Gene Variation to Gain Insight into the Oldest Biomarker in Autism: Construction of the Serotonin Transporter Gly56Ala Knock-in Mouse. J Neurodev Disord 1:158–171.

Wade PR, Chen J, Blakely RD, Gershonl MD (1996) Localization and Function of a 5-HT Transporter of the Gastrointestinal Tract in Crypt Epithelia. J Neurosci 76:2352–2364.

Walsh JJ, Christoffel DJ, Heifets BD, Ben-Dor GA, Selimbeyoglu A, Hung LW, Deisseroth K, Malenka RC (2018) 5-HT Release in Nucleus Accumbens Rescues Social Deficits in Mouse Autism Model. Nature 560:589–594.

Walther DJ, Peter JU, Bashammakh S, Hörtnagl H, Voits M, Fink H, Bader M (2003) Synthesis of Serotonin by a Second Tryptophan Hydroxylase Isoform. Science (80-) 299:76.

Warden D, Rush AJ, Trivedi MH, Fava M, Wisniewski SR (2007) The STAR*D Project Results: A Comprehensive Review of Findings. Curr Psychiatry Rep 9:449–459.

Waye MMY, Cheng HY (2018) Genetics and Epigenetics of Autism: A Review. Psychiatry Clin Neurosci 72:228–244.

Westermarck J, Li SP, Kallunki T, Han J, Kahari VM (2001) p38 Mitogen-Activated Protein Kinase-Dependent Activation of Protein Phosphatases 1 and 2A Inhibits MEK1 and MEK2 Activity and Collagenase 1 (MMP-1) Gene Expression. MolCell Biol 21:2373–2383.

Williams K, Brignell A, Randall M, Silove N, Hazell P (2013) Selective Serotonin Reuptake Inhibitors (SSRIs) for Autism Spectrum Disorders (ASD). Cochrane Database Syst Rev 2013.

Wolters DA, Washburn MP, Yates JR (2001) An Automated Multidimensional Protein Identification Technology for Shotgun Proteomics. Anal Chem 73:5683–5690.

Wong A, Zhang YW, Jeschke GR, Turk BE, Rudnick G (2012) Cyclic GMP-dependent Stimulation of Serotonin Transport Does Not Involve Direct Transporter Phosphorylation by cGMP-dependent Protein Kinase. J Biol Chem 287:36051–36058.

Wong JWH, Cagney G (2009) An Overview of Label-Free Quantitation Methods in Proteomics by Mass Spectrometry.

Wong ML, Licinio J (2001) Research and Treatment Approaches to Depression. Nat Rev Neurosci 2:343–351.

Wylie CJ, Hendricks TJ, Zhang B, Wang L, Lu P, Leahy P, Fox S, Maeno H, Deneris ES (2010) Distinct

Transcriptomes Define Rostral and Caudal Serotonin Neurons. J Neurosci 30:670–684.

Yaffe D, Forrest LR, Schuldiner S (2018) The Ins and Outs of Vesicular Monoamine Transporters. J Gen Physiol:1–12.

Yamashita A, Singh SK, Kawate T, Jin Y, Gouaux E (2005) Ctrystal Structure of a Bacterial Homologue of Na^+/Cl^--Dependent Neurotransmitter Transporters. Nature 437:215–223.

Yammamoto H, Tanaka S, Tanaka A, Hide I, Seki T, Sakai N (2013) Long-Term Exposure of RN46A Cells Expressing Serotonin Transporter (SERT) to a cAMP Analog Up-regulates SERT Activity and is Accompanied by Neural Differentiation of the Cells. J Pharmacol Sci 121:25–38.

Yan Z, Kim E, Datta D, Lewis DA, Soderling SH (2016) Synaptic Actin Dysregulation, a Convergent Mechanism of Mental Disorders? J Neurosci 36:11411–11417.

Ye R, Carneiro AMD, Han Q, Airey D, Sanders-Bush E, Zhang B, Lu L, Williams R, Blakely RD (2014) Quantitative Trait Loci Mapping and Gene Network Analysis Implicate Protocadherin-15 as a Determinant of Brain Serotonin Transporter Expression. Genes, Brain Behav 13:261–275.

Ye R, Quinlan MA, Iwamoto H, Wu H-H, Green NH, Jetter CS, McMahon DG, Veestra-VanderWeele J, Levitt P, Blakely RD (2016) Physical Interactions and Functional Relationships of Neuroligin 2 and Midbrain Serotonin Transporters. Front Synaptic Neurosci 7:1–17.

Yirmiya R, Pollak Y, Morgag M, Reicheberg A, Barak O, Avitsur R, Shavit Y, Ovadia H, Weidenfeld J, Morag A, Newman ME, Pollmacher T (2000) Illness, Cytokines, and Depression. Ann N Y Acad Sci 917:478–487.

Zanella S, Watrin F, Mebarek S, Marly F, Roussel M, Gire C, Diene G, Tauber M, Muscatelli F, Hilaire G (2008) Necdin Plays a Role in the Serotonergic Modulation of the Mouse Respiratory Network: Implication for Prader-Willi Syndrome. J Neurosci 28:1745–1755.

Zhang Y-W, Turk BE, Rudnick G (2016) Control of Serotonin Transporter Phosphorylation by Conformational State. Proc Natl Acad Sci 113:E2776–E2783.

Zhang Y-WW, Rudnick G (2005a) Serotonin Transporter Mutations Associated with Obsessive-compulsive Disorder and Phosphorylation Alter Binding Affinity for Inhibitors. Neuropharmacology

49:791–797.

Zhang YW, Rudnick G (2005b) Cysteine-Scanning Mutagenesis of Serotonin Transporter Intracellular Loop 2 Suggests an Alpha-Helical Conformation. J Biol Chem 280:30807–30813.

Zhang YW, Rudnick G (2006) The Cytoplasmic Substrate Permeation Pathway of Serotonin Transporter. J Biol Chem 281:36213–36220.

Zhang YW, Rudnick G (2011) Myristoylation of cGMP-Dependent Protein Kinase Dictates Isoform Specificity for Serotonin Transporter Regulation. J Biol Chem 286:2461–2468.

Zhao R, Wang S, Huang Z, Zhang L, Yang X, Bai X, Zhou D, Qin Z, Du G (2015) Lipopolysaccharide-induced Serotonin Transporter Up-regulation Involves PKG-I and p38MAPK Activation Partially Through A3 Adenosine Receptor. Biosci Trends 9:367–376.

Zhong H, Sánchez C, Caron MG (2012) Consideration of Allosterism and Interacting Proteins in the Physiological Functions of the Serotonin Transporter. Biochem Pharmacol 83:435–442.

Zhong J, Li S, Zeng W, Li X, Gu C, Liu J, Luo X-J (2019) Integration of GWAS and Brain eQTL Identifies FLOT1 as a Risk Gene for Major Depressive Disorder. Neuropsychopharmacology 0:1–10.

Zhu C Bin, Blakely RD, Hewlett WA (2006) The Proinflammatory Cytokines Interleukin-1beta and Tumor Necrosis Factor-Alpha Activate Serotonin Transporters. Neuropsychopharmacology 31:2121–2131.

Zhu C-B, Carneiro AM, Dostmann WR, Hewlett WA, Blakely RD (2005) p38 MAPK Activation Elevates Serotonin Transport Activity via a Trafficking-Independent, Protein Phosphatase 2A-Dependent Process. J Biol Chem 280:15649–15658.

Zhu C-B, Hewlett WA, Feoktistov I, Biaggioni I, Blakely RD (2004) Adenosine Receptor, Protein Kinase G, and p38 Mitogen-Activated Protein Kinase-Dependent Up-Regulation of Serotonin Transporters Involves Both Transporter Trafficking and Activation. Mol Pharmacol 5:1462–1474.

Zhu C-B, Lindler KM, Campbell NG, Sutcliffe JS, Hewlett WA, Blakely RD (2011) Colocalization and Regulated Physical Association of Presynaptic Serotonin Transporters with A_3 Adenosine. Mol Pharmacol 80:458–465.

Zhu C-B, Lindler KM, Owens AW, Daws LC, Blakely RD, Hewlett W a (2010) Interleukin-1 Receptor

Activation by Systemic Lipopolysaccharide Induces Behavioral Despair Linked to MAPK Regulation of CNS Serotonin Transporters. Neuropsychopharmacology 35:2510–2520.

Zhu C-B, Steiner JA, Munn JL, Daws LC, Hewlett WA, Blakely RD (2007) Rapid Stimulation of Presynaptic Serotonin Transport by A_3 Adenosine Receptors. J Pharmacol Exp Ther 322:332–340.

Zill P, Baghai TC, Engel R, Zwanzger P, Schüle C, Eser D, Behrens S, Rupprecht R, Möller HJ, Ackenheil M, Bondy B (2004) The Dysbindin Gene in Major Depression: An Association Study. Am J Med Genet Genet 129B:55–58.